Vibration Suppression using Orthogonal Eigenstructure Control

Mohammad Rastgaar-Aagaah

Dissertation submitted to the faculty of the
Virginia Polytechnic Institute and State University
in partial fulfillment of the requirements for the degree of

Doctor of Philosophy
in
Mechanical Engineering

Mehdi Ahmadian, Chairman
Steve C. Southward, Co-chairman
Daniel J. Inman
Corina Sandu
John B. Ferris
Adrian Sandu

July 23, 2008
Blacksburg, Virginia

Keywords: Orthogonal eigenstructure control,
eigenstructure assignment, active vibration cancellation,

Vibration Suppression using Orthogonal Eigenstructure Control

Mohammad Rastgaar-Aagaah

ABSTRACT

A novel control method called orthogonal eigenstructure control is developed for active vibration cancellation in structures. Orthogonal eigenstructure control is a feedback control method applicable to multi-input multi-output linear systems. While the available control design methodologies offer a large and complex design space of options that can often overwhelm a designer, this control method offers a significant simplification of the design task while still allowing some experience-based design freedom. For example, eigenstructure assignment methods need definition of a desired eigenvector for the closed-loop system. The controller designer may also be required to do pole placement. Considering the fact that there are no one-to-one relationships between the elements of the closed-loop eigenvectors of a model and the states of the system, this effort could be inefficient for many practical systems. Moreover, for large-scale systems, defining or shaping the eigenstructures become a relatively difficult task. Orthogonal eigenstructure control is a state feedback-like control law that is relatively easy to design and implement to multiple-input multiple-output systems. It allows control engineers to achieve good performing designs even with little design experience, while the existing methods are highly dependent on designer experience.

The control method developed in this study, uses the fact that each open-loop eigenvector lies within the achievable closed-loop eigenvector set, since it is associated with the zero output feedback control gain matrix. By defining the achievable eigenvector set for each open-loop eigenvalue, a class of the vectors orthogonal to the open-loop eigenvectors can be considered to be substituted as the associated eigenvector, eliminating the need for any guesswork by the controller designer.

The proposed concept eliminates the error due to differences between the achievable and desirable eigenvectors, since the open-loop eigenvectors are replaced by the vectors orthogonal to them that are already within the achievable eigenvector set. When the open-loop model of the system is available, some of the target eigenvalues can be determined and their respective eigenvectors are orthogonalized. If the first orthogonal vector does not lead to a satisfactory performance, the method uses another orthogonal vector to be substituted. It has been shown that the dynamic modes of a system with eigenvectors that are orthogonal to each other are decoupled and there is less spillover of energy from one mode to another, leading to a system with better performance.

Orthogonal eigenstructure control is introduced and extended to be applicable to linear systems regardless of the number and location of the actuators and sensors. Also, the concept of progressive application of the proposed control method for increasing robustness is described. Finally, the result of application of the control method for vibration cancellation of a test plate is investigated through experiments for tonal and wideband disturbances. The results show a significant reduction of vibrations using the orthogonal eigenstructure control with relative ease in finding the control gain matrix.

Acknowledgements

I am deeply indebted to my advisor Mehdi Ahmadian for the incomparable opportunity that provided me. I am grateful for his encouraging guidance, for his close attention to our manuscripts, and for his mentorship. Our discussions on different topics taught me to broaden my research horizon.

I sincerely thank my co-advisor Steve Southward. I highly appreciate his help and guidance throughout my Ph.D. program. I have been inspired by his practical knowledge of controls.

I would like to thank the members of my committee Daniel Inman, Corina Sandu, John Ferris, and Adrian Sandu for reviewing my dissertation and providing me with their comments, which greatly helped me to improve the quality of this dissertation.

CVeSS is like a home for me. I loved the time that I spent working there. I will definitely miss all friendly colleagues and all the good times that I had. I appreciate the help of two wonderful work-mates and great friends, Brian Templeton and Florin Marcu.

I cannot express how invaluable has been the unconditional and loving support of my wife Nina. It has been a real joy to take classes together, discuss our research, and plan for the future. I dedicate this dissertation to her.

Mohammad Rastgaar

July 2008
Blacksburg, Virginia

To Nina

Contents

List of Figures

List of Tables

Chapter 1

Introduction

1.1. Motivation

This study is motivated by the need for more advanced control methods for active vibration cancellation that is relatively easy to design and implement, and allows control engineers to achieve good performing designs even with little design experience. It has been shown that eigenstructure assignment methods are effective for active vibration cancellation in structures. The methods currently available, however, depend on the experience of the controller designer, based on the geometry and dynamics of the structures. In general, there are no unified methods for the application of eigenstructure assignment with the purpose of vibration cancellation in structures. Existing methods require apriori definition of the desired eigenstructure [1]. Identifying the desirable locations for the closed-loop eigenvalues and defining the desirable closed-loop eigenvectors are not a straightforward task [2]. For large scale systems it becomes impractical to define a desired closed-loop eigenstructure. Therefore, the existing methods are not able to be applied to such systems or many other similar practical engineering structures. Considering that there are no one-to-one relationship between the elements of closed-loop eigenvectors and the states of the system, one may define a desirable eigenvector that does not satisfy a given design criterion. This may lead to excessive actuation forces because of improper location of the associated closed-loop poles. Additionally, the desirable eigenvectors do not necessarily lie within the space of achievable eigenvectors. The missing piece of this puzzle is a control method that can automatically lead to a set of desirable closed-loop eigenvectors that result in mode decoupling and disturbance rejection.

1.2. Objectives of the proposed research

The primary aim of the proposed research is to provide a novel active vibration control method that is relatively easy to design and implement and can automatically determine the feedback control law with minimal design experience by the controller designer. Specifically, this study intends to:

1. develop a novel structural vibration control method that can perform robustly in the presence of a wide variety of disturbances, beyond any of the existing design methods;
2. significantly reduce the controller development cycle through a mathematically sound approach that can easily be implemented to a broad range of structures in practice, while it gives insight to the controller designer how to efficiently use the design freedom;
3. examine the applicability of the developed methods to cases that commonly arise in practice, such as the effect of actuator and sensor failure on the performance of the control loop system that requires developing the method to be applicable to systems with non-collocated actuators and sensors. (This enables the vibration control method to be used as a general control method);

1.3. Research approach

This study has adopted a multi-step approach to reach the above goals. The outcome of this research is a novel control method that is widely applicable to linear multi-input multi-output systems. The main research elements are detailed below.

1.3.1. Developing a novel eigenstructure orthogonalization structural control method

To achieve the first research objective a thorough exploration of the mathematics of eigenstructure orthogonalization is needed. The method seeks to find an effective procedure for orthogonalizing the proper eigenvectors. The foremost approach is to identify the modes where the products of their eigenvectors with the remaining system's

eigenvectors are the largest. Since the focus is not on eigenvalue placement, the associated eigenvalues will be consistent with the new orthogonalized eigenvectors. If the orthogonalized eigenvectors are parallel to any of the unchanged eigenvectors of the system, then they generate a deficient closed-loop state matrix. The deficient state matrix would have poles in the right half of the *S* plane, resulting in system instability.

The goal for orthogonalizing the eigenvectors is to find a system with decoupled modes. Decoupled modes require that the eigenvectors of the system become orthogonal to each other to the extent feasible, thereby minimizing the spillover of energy from one mode to another. This approach is based on finding the vectors orthogonal to the eigenvectors of a system within the achievable eigenvectors set, and replacing the eigenvectors with those orthogonal vectors. The orthogonal vectors are a subset of the achievable eigenvector set.

1.3.2. Reducing controller development cycle by developing a relatively easy to design and implementing control methodology

While the available control design methodologies offer a large and complex design space of options that can often overwhelm a designer, a control method is needed to provide a significant simplification of the design task while still allowing some experience-based design freedom. For example, eigenstructure assignment methods need definition of a desired eigenvector for the closed-loop system. The controller designer may also be required to do pole placement. Considering the fact that there are no one-to-one relationships between the elements of the closed-loop eigenvectors of a model and the states of the system, this effort could be inefficient for many practical systems. Moreover, for large-scale systems, defining or shaping the eigenstructures become a relatively difficult task that may result in a desirable eigenvector that does not satisfy a given design criterion. Also, the desirable eigenvectors may not necessarily lie within the space of achievable eigenvectors set. This may lead to excessive actuation forces because of improper use of design freedom. This study is to develop a state feedback-like control law that is relatively easy to design and implement to multiple-input multiple-output systems. It would allow control engineers to achieve good performing designs even with little design experience, while the existing methods are highly dependent on designer experience on how to use the design freedom.

This study seeks to develop a control method that reduces those design freedoms that are not guarantied to help the disturbance rejection purposes. It limits the design freedom to use of vectors orthogonal to the eigenvectors of the system and lets the controller designer to substitute the eigenvectors with vectors that are almost orthogonal to them. Even though the design freedom is limited, but the control method gives an infinite design freedom in more efficient direction.

1.3.3. Effect of practical issues such as sensors and actuator failures result in systems with non-collocated sensors and actuators

A reality of practical application of control systems is the failure of sensors and actuators. The ability of the closed-loop system to continue to perform satisfactorily in the event of a failure is critical to the practical value of the controller. Another important practical aspect of the control method is the robustness of the controller in the case of actuator or sensor failure. In this task, the knowledge about the overlap between achievable eigenvector sets associated with different number of actuators needs to be developed. Therefore, to design a fail-safe control law, we need to be able to design the control for non-collocated actuators and sensors, or control systems with different number of actuators and sensors. This part of the proposed study addresses the need for a method that is independent of the placement or numbers of actuators and sensors and continues to perform robustly in the presence of sensor or actuator failure.

1.3.4. Demonstrate the utility of the proposed method

The utility of the proposed study will be tested through a series of experiments. The vibration isolation of a plate will be tested. The test setup will consist of a plate with actuators and sensors and control hardware. The signals from the sensors are collected using a data acquisition system and transferred to a real time processor that generates appropriate commands for the control actuators. The output signals from the sensors will be used to identify the system using a system identification method. The developed mode orthogonalizing method will be applied in order to determine the proper output feedback control gain matrix.

The size of the identified system depends on the number of sensors and actuators. Since there are limitations on the number of sensors that can be placed on the plate, a finite element model of the system will be developed in order to give an insight to the behavior of the plate and the proper locations for the control actuators. By increasing the number of elements in the model and comparing the results with the results of the experiment, the applicability of the method to a large system will be evaluated.

1.4. Outline

Chapter 2 provides background information of eigenstructure assignment methods and their application to active vibration cancellation of structures.

Chapter 3 focuses on the mathematical explanation of orthogonal eigenstructure control. The relationship between open-loop eigenvectors and closed-loop eigenvectors, the achievable eigenvector set and the method of finding the orthogonal vectors to the open-loop eigenvectors that lie within the achievable eigenvector set is described.

Chapter 4 explains the method further for systems with collocated actuators and sensors, utilizing lump-mass systems. In addition, the concept of progressive application of orthogonal eigenstructure control has been explained.

Chapter 5 presents the further development of orthogonal eigenstructure control to be applicable to systems with non-collocated actuators and sensors, and systems with different number of actuators and sensors to address the robustness of controller in case of components fail.

Chapter 6 discusses the application of orthogonal eigenstructure control to the systems with large degrees of freedom utilizing the finite element model of a plate. The effect of operating eigenvalues and number of pairs of actuators and sensors for systems with collocated actuator and sensors will be discussed. The problems of the number and location of actuators and the robustness of the control are investigated using a finite element model of a plate.

Chapter 7 presents the test setup for validation of the proposed control method. In this chapter the hardware used in setup has been described. The test setup consists of a steel plate. The control actuators are piezoelectric bimorphs. Orthogonal eigenstructure control has been used to find the control gain matrix for cancellation of vibrations induced by disturbances. The disturbances are different tonal signals as well as a wideband signal in form of a constant amplitude chirp (sine sweep) signal within the frequency range of 200-300 Hz. Also, the system identification method that has been used is described.

Chapter 8 presents the conclusion and suggestions regarding the future work on the research conducted on this study on active vibration cancellation in structures using orthogonal eigenstructure control.

Chapter 2

Literature Review

Eigenstructure assignment, whether state feedback or output feedback, has an important role in active control of the transient responses in Multi-Input Multi-Output systems (MIMO) to either improve the performance of the closed-loop system, or minimize the required control effort. For example, when a system has uncontrollable modes, state feedback control cannot change the associated eigenvalues, but the associated eigenvectors can be shaped in order to have a more smooth response [1]. The idea of eigenstructure assignment is given by Moore [2]. Moore characterized the class of entire eigenvector sets related to a distinct set of closed-loop eigenvalues using state feedback. Therefore, a control problem of eigenvalue placement for a MIMO system which had been introduced earlier by Wonham [3], was redefined to both placement of eigenvalues in desired locations, and choosing a set of related eigenvectors from a class of possible eigenvectors. This gives a considerable freedom to the control design which Moore had presented as a design scheme. He explained that the speed of response is determined by the assigned closed-loop eigenvalues, while the shape of the response is related to the assigned eigenvectors. Klein and Moore also presented an algorithm for non-distinct closed-loop eigenvalues and their related eigenvectors [4].

Chapter 1 Srinathkumar used a parametric output feedback scheme and derived sufficient conditions to assign a set of arbitrary distinct eigenvalues [5]. Fahmy introduced a parametric approach using the differentiation of the determinant of the combined system matrices. This method identifies the class of achievable eigenvectors and describes explicitly the generalized eigenvectors associated with the assigned eigenvalues. It also includes the entire closed-loop eigenstructure of the linear MIMO system [6, 7]. Andry et al. studied constrained output feedback to reduce the controller complexity by setting

some of the elements of the feedback gain matrix to zero [8]. Calvo-Ramon solved the eigenstructure assignment by determining a minimum distance, considering the fact that the desired eigenvectors will not usually lie in the corresponding achievable subspaces [9].

It was Cunningham who first used Singular Value Decomposition (SVD) to find the basis of the null space for achievable eigenvector sub-space. In his output feedback control method, the basis vectors were optimally combined to minimize the error between achievable and desirable eigenvectors. This method was the first practical method of eigenstructure assignment in order to have a desirable transient response behavior [10]. Utilizing SVD, a finite number of actuators are needed to shape the eigenvectors of the system[11].

Normal mode localization is a phenomenon that a structure divides into two areas of small and large amplitude of vibration. It happens when one or more global modes of vibration become confined to a local region of the structure. Some disorders in the periodicity of a structure, such as material discontinuity, create mode localization. It means that the energy of vibration coming to the structure is not able to propagate far through the structure and will be confined to the areas close to the source of vibration [12, 13]. Material discontinuity, in classical periodic isolator structures, creates stop bands that suppress the wave propagation of external disturbances within a particular frequency range. Hodges showed that the normal mode localization mostly occurs in the structures with large number of weakly coupled substructures. The steady-state responses of these structures decay exponentially away from the vibration source. In other words, disruption of the periodicity causes the attenuation of vibrational waves in all frequency bands irrespective of dissipations in the system. In mode localization, eigenvectors have the major influence in distributing vibrational energy. Localization occurs when the eigenvalues are clustered in a small band. The localization degree depends on the ratio of disorder to coupling, with a stronger localization when this ratio increases. Localized modes in disordered structures can be useful or harmful. For example, localization can be harmful if it results in fatigue as it happens in turbine blades. Displacements are relatively

large in the area of localization, with localized amplitudes frequently ten times that of the isolated areas of the structure [14]. Also, localization can affect the robustness and stability of active control systems for large space structures if the control law is designed assuming a large numbers of modes of the structure. For the class of large space structures; however, localization can be used as a method of vibration confinement at the areas close to the source of disturbance [15]. Vibration confinement is a method of manipulating the structural vibrational modes in order to reduce the amplitude of vibrations in the concerned areas of the system. The energy of vibration is confined to the remaining parts of the system which are less important or their isolation is much easier in practical sense than the isolated areas. It has been shown that methods based on vibration confinement reduce the amplitude of vibration much more effectively than other methods of vibration suppression [16, 17]. Most of the active control methods emphasize on damping or cancellation of disturbance; therefore, they have to be designed for specific disturbances or inputs. The actuators provide sufficient damping for energy dissipation to reduce vibration in all parts of the structure almost in the same amount. In other words, those algorithms decay the vibration at both the isolated and the confined part at the same rate which does not necessarily comply with the performance specifications [11]. The conventional methods are considered to have global objectives in comparison to eigenstructure assignment that has local effects on the structural response [16]. Using the concept of the normal mode localization phenomenon in periodic structures, Song et al. proposed an algorithm for choosing a linearly independent set of mode shapes in order to reduce the relative vibrational amplitude at certain areas by redistributing the vibrational energy [17]. This algorithm could be applied to any system that shows an oscillatory behavior.

Kwon and Youn generalized a simple eigenstructure assignment via output feedback in linear multivariable systems using the left and right eigenvectors. Their method does not need the assumptions that eigenvalues of the closed-loop system are distinct or different from eigenvalues of the open-loop system [18]. Mudge and Patton [19] presented the procedures for both modal decoupling and robust eigenstructure assignment when the allowable subspaces have been determined using SVD. They presented a modally shaped

design application when the desired modal structure of the closed-loop system response is known. For the cases when the desired forms are not achievable, since they do not lie in the allowable subspace, they may be projected in a least-squares sense into the required subspace. Also, they proposed a robust eigenstructure design when no prior knowledge of the modal coupling is available and there are no criteria to choose desirable eigenvectors.

Robustness in eigenstructure assignment is the degree of insensitivity of the closed-loop eigenvalues to the uncertainties and perturbations in the system. Satisfying different stability robustness criteria as well as performance robustness criteria are the main subjects of robust control. Among different methods, eigenstructure assignment is the simplest one that is fairly successful; hence, a lot of research has been performed on this subject [20]. Near orthogonality is a very desirable condition to have insensitive eigenvalue placement to modeling uncertainty. This means that corresponding modal matrix has the minimum condition number. A minimum condition number in turn means spillover suppression [21]. Juang et al. proposed a non-iterative algorithm based on QR or SVD methods, applicable to both state and output feedback, while the design freedom is used for minimizing the gain. This method is basically uses a projection of closed-loop eigenvectors onto the achievable eigenvector subspace. Closed-loop eigenvectors are close to the desired one in a least square sense. Since arbitrary selection of acceptable eigenvectors may cause an ill-condition eigenvector modal matrix, closeness of the closed-loop eigenvectors to the achievable ones becomes important. If the closed-loop and the achievable eigenvectors are not close, the associated gain matrix cannot be accurately calculated and the closed-loop system may be highly sensitive [22]. In the latter reference, a modified algorithm has been presented. This algorithm determines the closed-loop eigenvectors close to both desired and open-loop ones in a least square sense. A high-gain state feedback system eigenstructure assignment which is insensitive to the perturbations, has been reported by Sen et al. [23]. The perturbations are the parameter perturbations in both the plant and the gain matrices [24].Liu et al. also proposed an explicit parametric expression for gain matrix of a state feedback control for applying an eigenstructure assignment to a system [25]. One problem that occurs in large flexible structures (especially space structures) is that they have a large number of lightly damped

modes that are very close together. Use of a high authority controller can cause spillover-induced instabilities. Low-authority controllers in conjunction with high authority ones makes the stability of the system robust. This class of controllers uses collocated sensors and actuators and is called static dissipative controllers. This method is a sequential method to calculate velocity and position gain matrices to assign an arbitrary number of closed-loop eigenvalues to their specific locations and has been studied and applied by Maghami et al. [26] and has been applied by Maghami et al. in [27].

To describe the dynamic of a structural system, usually a second-order differential equation is used, with structural matrices that are symmetric and sparse. On the other hand, control theory and estimation techniques are established for first order realization of the systems. Therefore, a large effort is made to transfer second order equations to first order configuration. The first order system of equations increases the dimension of the equations and loses the symmetry and sparsity of the structural matrices. Thus, a model reduction is needed before applying a controller or an estimator to the system in order to reduce the difficulty of the numerical computations. An output feedback method based on SVD or QR has been proposed by Maghami et al. [28]. The coefficients corresponding to the bases of the null space are computed using an algorithm based on subspace intersections, after finding the orthogonal null space. Another method is proposed by Juang et al. for solving the second order system. This approach preserves the second order dynamic equations and designs an estimator and a controller for the system [29]. Also, a controller design without estimator is reported by Juang et al. in [30]. This algorithm can be applied to both state and output feedback control. Because the system is second order, displacement and velocity or velocity and acceleration can be used to assign the eigenvalues. This is interesting because of the practical implementation and frequent use of accelerometer in practice. The closeness of the closed-loop eigenvectors to both open-loop and desired one is the objective of this algorithm which is the result of the intersection of the feasible and target eigenvectors. The importance of this method is to keep the computational features of a second order system, such as symmetry and sparsity of the mass and stiffness matrices. SVD is used to find the feasible eigenvector

subspace in this method. Chan et al. solved a similar problem by combined derivative and proportional state feedback for almost arbitrary eigenvalue assignment.

Datta et al. developed an algorithm for the partial eigenstructure assignment of quadratic matrix pencil. Their scheme directly determines the control gain for second order mechanical systems with no need to transform them to the state-space form [31]. Another algorithm by Keel et al. determines a robust state feedback to restrict the closed-loop eigenvalues' location within an arbitrary neighborhood around their desired locations [32]. The bounded parameter perturbations of the open-loop matrix will not move the closed-loop eigenvalues too far from their desired locations. Another technique for eigenstructure assignment to an actively controlled second order system is presented by Schulz et al. [33]. This method is a parametric method and optimizes the controller and structural parameters. The feedback gains are explicitly parameterized in terms of the eigensystem and structural matrices. The closed-loop system is optimized by minimizing the norms related to the feedback gains.

Shelly et al. studied the absolute displacement in the first and second order systems, because the existing eigenstructure assignment would not have a control on them. In fact it is not possible to tell if the absolute displacements in a system is increased, decreased or remained intact just by changing the system's eigenvectors [14]. Furthermore, they introduced a mode localization technique called eigenvector scaling while studying the time domain response of the system. This method adjusts specific parts of each eigenvector to uniformly increase the relative displacement of the corresponding areas in the system [34]. They showed analytically that absolute displacements in isolated areas can be reduced by eigenvector shaping, regardless of the type of the disturbance. The experimental result has been shown in [35]. The test rig is a simply-supported beam subjected to an impulse disturbance. Eigenstructure Realization Algorithm (ERA) was used to study the problem. In other studies by the same group of researchers, a numerical simulation of vibration confinement in a pinned-pinned beam was shown in [36, 37]. Two piezoelectric actuators and sensors were used to confine the vibrations within a simply supported beam. Both passive and active control methods were used. The passive

control reduces the number of required actuators and also reduces their operating power which leads to a lower application cost.

Eigenstructure shaping method that has been used for active control of the beams is also called eigenvector shaping. This method is an active control method and is basically regenerating the behavior of the system when passive mode localization happens, by scaling and reforming the system mode shapes partly or entirely. Since all the shape modes are scaled in the same way, vibration confinement of the system is not affected by the type of disturbance. An application of this method is reported in [16]. This work experimentally investigates a feedback control of vibration propagation based on the eigenvector scaling. It is shown that the scaling matrix magnifies the coupling force applied by the isolated area and reduces the coupling force applied by the localized area. Therefore, the feedback control makes simultaneous stiffening and softening of the coupling between the isolated and localized regions. The consistent scaling of the eigenvectors makes the relative displacement of isolated and localized areas constant over the entire range of the eigenvalues. On the contrary, passive localization, as occurs in some structures due to irregularities, makes confined areas move with excitation frequency change. As a result, for any disturbances applied to the isolated area, the absolute displacement in localized area will increase but the displacement in the isolated area will remain almost intact. On the other hand, if a disturbance applies to the localized area, the absolute displacement in the isolated areas will decrease but the localized area will remain the same [16]. One of the drawbacks of the uniform scaling is that the number of needed pairs of actuators and sensors has to be equivalent to the number of coupled modes of the system. It means that the action between neighboring systems has the key role in the number of pairs of actuators and sensors that are needed. For example, when adjacent masses interconnected with spring and damper the maximum and also optimum number of the pairs of actuators and sensors is two. The number of masses is not a parameter for the number of pairs of actuators and sensors. Therefore, not only the number of required pairs of actuators and sensors for continuous systems is infinite but also a large number of actuators and sensors are needed for their linearly discretized models. A modification of this method has been reported in [38]. SVD-eigenvector

shaping has been introduced and used as a solution to the problem of limited pairs of actuators and sensors. This method is a combination of authors' earlier method and Cunningham [10] approach. SVD-eigenvector shaping uses Moore-Penrose generalized left inverse and produces the closest eigenvector in least square sense to the desired ones, since it minimizes Euclidean 2-norm error. The result of applying this method to a simply supported beam test rig, as a distributed parameter system, is presented in [38].

An active-passive hybrid vibration confinement system using a network of piezoelectric actuators has been proposed by Tang et al. Instead of the mechanical parts, the passive elements of the systems are the circuit inductors and resistors. The goal of this study is to find optimal eigenvectors using a Rayleigh principle. Therefore, the need for pre-selecting the closed-loop eigenvectors is eliminated. After finding the subspace for the eigenvectors, the optimal achievable eigenvectors that have the minimal vector 2-norm in concerned regions can be achieved, thereby eliminating the problem of closeness of the desired and achievable eigenvectors. On the other hand, a perfect match between the desired eigenvectors and the achievable one is not necessary, because the vibration suppression is concerned in certain degrees of freedom. Pre-determination of the desired eigenvector components can cause unsatisfactory performance if a match between components of the desired and achievable eigenvectors in the unimportant degrees of freedom happens. This makes a trade-off on the closeness of the important degrees of freedom. Using the passive circuitry elements as extra design variables, the system can be introduced a larger dimension. Also the passive electrical elements can be assigned to be the confined part of the hybrid system. Obviously, the change in electrical elements is much easier than changing the mechanical structure or elements [39, 40]. A case study of this method is presented in [41]

A different method of vibration confinement, based on applying a distributed feedback for one and two dimensional structures such as uniform strings and beams, has been proposed by Choura and Yigit [42, 43]. In this method feedback control alters the mode shapes to exponentially decaying functions of space. The feedback makes the settling time of some parts of the system to be faster while makes the rate of settling of other

parts slower. This method is basically an inverse eigenvalue problem that the designer finds the best geometry and material properties to confine the energy. As a result, the mass, damping, and stiffness matrices for closed-loop system are highly populated and the number of actuators/sensors is equal to the number of states. To address the problem of limited actuators, a new method by partitioning the system in two subsystems has been introduced by Choura and Yigit in [11]. This method requires full state and acceleration feedback. Therefore, the states that are not being measured need to be estimated by a dynamic observer in order to meet practical issues. This method is strongly depends on decoupling the system into two parts. All the sensitive parts and the neighboring areas assigned to be controlled by actuators based on the altering the eigenvectors. The rest of the insensitive parts of the system are stabilized by different actuators. Even though both parts are controlled, more attention is paid to the sensitive areas which are located in the first subsystem such that settling time for this subsystem is faster. This way, the original vibratory modes are converted into modes that let the vibrational energy remains in the insensitive parts. A case study of this subject on the axial vibration confinement of the rods is presented in [44]. A similar method for linear time varying systems is reported in [45].

An eigenstructure method for constrained state or output feedback has been presented by Slater et al. considering the problem of movement of neighborhood of the closed-loop eigenvalues [46]. They showed that when the eigenvectors are the only parameters that are required to be changed, the control efforts are not necessarily minimized if the closed-loop eigenvalues are forced to be close to the open-loop eigenvalues. In fact, a large change in eigenvectors may need a large movement of the eigenvalues to minimize the feedback gains. They also showed that closed-loop eigenvalues and eigenvectors have to be consistent in order to avoid the large control efforts. Moreover, since there is no method to have closed-loop eigenvectors and eigenvalues consistent, the minimum number of constraints should be imposed to the eigenvectors' elements in order to have a reasonable control effort. Also, a sufficient condition is presented by Sobel et al. for the structural uncertainties [47]. The result is the condition for stability robustness of linear systems with time-varying norm bounded state-space uncertainty. It shows that the

nominal eigenvalues have to lie to the left of a vertical line in the complex plane that is determined by a norm involving the structure of the uncertainty and the nominal closed-loop eigenvector matrix. Using this result, a robust eigenstructure assignment design method has been proposed by Yu et al. [48]. This approach optimizes either the performance robustness or sufficient condition for stability and constrains the dominant eigenvalues to lie within chosen regions in the complex plane. Pre-specified eigenvalues have a restrictive effect on the eigenvectors and diminish the domain in which eigenvectors can reside. On the other hand, pre-specified eigenvectors have restrictive effect on the pole placement. It is known that the closed-loop poles have to lie in certain areas in order to have a stable system. Based on this assumption, a robust feedback control eigenstructure assignment based on the constrained minimization of the difference between the actual and desired eigenvectors and the closed-loop Lyapunov Equation are presented by Wilson et al. [49, 50].

A parametric robust control design of descriptor systems using eigenstructure assignment is presented by Patton [51]. Both the desired closed-loop pole placement in the time domain and the minimization of a robustness index in the frequency domain are considered, so that the controller uses both time and frequency domains specifications. Triller et al. applied eigenstructure assignment in a new control coordinate system based on the substructure representation of the system. They were a reduced-order model-based controller that yields a good accuracy. This coordinated system is able to accurately predict the actuators' forces while a model reduction has been applied [52]. It has been known that partial eigensystem assignment with output feedback can make a closed-loop system unstable. On the other hand, output feedback for passive linear time-invariant systems, such as flexible space structures, always leads to stable system if the controller is dissipative. Dissipative output feedback gain matrices for assigning a selected number of closed-loop poles is presented by Maghami [53]. The method is a sequential procedure which assigns one self-conjugate pair of closed-loop eigenvalues at each step using dissipative output feedback gain matrices. The algorithm checks the eigenvalues assigned in the previous steps not to be disturbing the system. But it may happen that the previously assigned eigenvalues become unstable. A control algorithm combining the

time-domain performance by eigenstructure assignment and frequency domain robust performance with H_∞ specifications for a descriptor system has been proposed by Liu et al. [54]. This method is a parametric state feedback control and is a joint optimal robust control design in both time and frequency domains. Based on the same optimization method, a robust eigenstructure assignment control using genetic algorithms and gradient-based approach has been proposed by Liu et al. [55, 56]. The constraint of being different from zero on the closed-loop eigenvalues has been removed for state feedback control of the descriptor system in [57]. This work uses the parametric solution of generalized Sylvester matrix equation to apply an output feedback to a descriptor system [57].

The problem of robust eigenvalue assignment in descriptor linear systems via proportional plus partial derivative state feedback control has been studied by Duan [58]. A perturbation analysis of a multi-input eigenstructure assignment problem is studied by Cawood and upper bounds for perturbations on the eigenvector matrix are derived [59]. Another method of eigenstructure assignment for multi-variable linear systems using state feedback control is proposed by Duan [60, 61]. In this method the set of achievable eigenvectors has been calculated by SVD, and then they are parameterized to provide the entire design degrees of freedom. The same method has been applied to a second order linear system using a proportional plus derivative feedback controller by Duan [62, 63]. A similar approach for high-order descriptor linear systems via proportional plus derivative feedback by solving a high-order Sylvester matrix equation is also studied by Duan [64]. He also applied a similar eigenstructure assignment algorithm for high-order linear systems via proportional plus derivative feedback [65] as well as a second order system [66]. A general parametric solution of the general high order Sylvester Equation has been given by Duan in [67]. An output feedback control with a reduced orthogonality condition has been developed by Clarke et al. [68]. This method relaxes the requirements on the number of eigenvectors that must be specified to assign a set of eigenvalues. It consists of two-stages for assignment of eigenvectors, and allows a subset of eigenvectors to be assigned before assigning the rest of the degrees of freedom to the eigenvectors in next stage.

Duan has presented parametric approaches for eigenstructure assignment in multi-variable linear systems using parametric design of dynamical compensators. This method treats the problem of robust dynamical compensator design, in the sense that the closed-loop eigenvalues are insensitive to small partial variations in the open-loop system matrices [69]. Also, state feedback controller [70] and descriptor system [71] has been proposed using similar approach. The problem of eigenstructure assignment by decentralized output feedback is studied by Duan [72]. In this method, a parametric solution of a generalized Sylvester matrix equation, parametric representations of both the left and right closed-loop eigenvectors and feedback gains are established. Duan proposed a complete parametric approach to eigenstructure assignment in continuous descriptor systems via output feedback based on the parametric solution of the generalized Sylvester matrix equation [73]. A solution of the Sylvester equation is given in [71, 74]. A thorough study and a complete parametric algorithm for linear descriptive system has been done by Duan and Patton [75]. Another independent output feedback algorithm is proposed using the solutions of two coupled Sylvester equations [76]. A numerical approach for solving the descriptive systems has been given by Mimins [20]. This method is a state feedback multi-input eigenstructure assignment. A new methodology based on the parallel hybrid genetic algorithm and parallel solutions of the LQR problems is developed in [77, 78]. This method is used for an aircraft controller and has been able to find the weighting matrices Q and R in algebraic Riccati equation in order to determine the control gain.

The right eigenstructure assignment is the methods that assign eigenvalues and right eigenvectors of the system, while the left eigenstructure assignment is the method of assigning eigenvalues and left eigenvectors of the system. Even though the eigenstructure assignment techniques for vibration cancellation had started with using the right eigenvectors, but there are some authors who used left eigenvector assignment. Choi et al. have presented a general left eigenstructure assignment method, based on the bi-orthogonality condition between the right and left modal matrices of a system [79]. This method considers both the modal disturbance suppressibility and modal controllability in control systems design. A more general work has been presented in [80].

Chapter 3

Theory

Vibration cancellation in structures using a novel eigenstructure method is introduced. This method is based on finding the gain matrix such that the closed-loop eigenvectors are almost orthogonal to the open-loop ones. Also, this method does not need to define desired eigenvectors beforehand. Therefore, the complicated task of defining desirable eigenvectors that is a trial and error procedure is eliminated. Instead, the designer has a set of achievable closed-loop eigenvectors that are orthogonal to the open-loop eigenvectors. As a result, the task of defining a desirable eigenvector by shaping, or finding the control gains that result in the required characteristics of closed-loop system, are taken place by simply choosing the most appropriate solution and associated feedback gains. The closed-loop eigenvalues are not defined by the designer, and are left free to be consistent with the orthogonal eigenvectors of the closed-loop system. This is an advantage of this method; the only needed information is merely the information about the open-loop system.

3.1. Introduction

The proposed orthogonal eigenstructure control is an output feedback control for structural vibration cancellation. This method is based on finding the closed-loop eigenstructures that their eigenvectors are orthogonal to the open-loop eigenvectors. Most of the eigenstructure assignment methods require a pre-determination of the eigenstructure or at least eigenvectors. A prediction of the proper closed-loop system in terms of the elements of the eigenvectors is not an easy task and usually from a practical point of view is almost impossible. The proposed method does not need a pre-determination of the closed-loop eigenstructure; thus, a prior knowledge of the closed-loop system is not required.

Orthogonal eigenstructure control does not need specifying the value or range of the closed-loop eigenvalues. The closed-loop system has eigenvalues that are different from the open-loop eigenvalues. They are consistent with the closed-loop eigenvectors when the closed-loop eigenvectors are lying in the achievable eigenvectors space.

Orthogonal eigenstructure control utilizes an interesting property of the null space of the closed-loop system generated by Singular Value Decomposition (SVD). The upper part of the null space is the basis that spans the eigenvectors of the closed-loop system. The eigenvectors of the combined closed-loop system are a linear combination of the columns of this sub-matrix.

Proper use of design freedom is depended on the experience controller designer. Improper use of this design freedom may cause excessive actuation forces. Orthogonal eigenstructure control reduces those design freedoms that are depended on the designer experience. It limits the design freedom to use of vectors orthogonal to the eigenvectors of the system and lets the controller designer to substitute the eigenvectors with vectors that are almost orthogonal to them. Even though the design freedom is limited, progressive orthogonal eigenstructure control gives an infinite design freedom in more efficient directions.

3.2. Problem statement and null space

To define the problem, a second order system of equations in matrix notation is considered;

$$M\ddot{q} + C_d\dot{q} + K_s q = F_i u_i + F_d u_d \qquad (3.1)$$

where M , C_d , and K_s are $n \times n$ mass, damping and stiffness matrices of the system respectively. F_i and F_d are the respective control input and the disturbance input matrices while q , $\dot{q}$, and $\ddot{q}$ are the displacement, velocity, and acceleration. u_i and u_d are the

external control and the external disturbance vectors. The equation of the motion of this system in the state space form can be written as

$$\dot{x} = Ax + Bu + Ef \tag{3.2}$$

where A is the $2n \times 2n$ state matrix, B is the $2n \times m$ input matrix, E is the disturbance input matrix with $2n$ rows, u is the input vector of dimension m, and f is the disturbance vector. x is the $2n \times 1$ state vector and $\dot{x}$ is the time derivative of the state vector.

Matrix A in terms of the physical properties of the system can be written as

$$A = \begin{bmatrix} 0 & I \\ -M^{-1}K_s & -M^{-1}C_d \end{bmatrix} \tag{3.3}$$

The input matrix is

$$B = \begin{bmatrix} 0 \\ -M^{-1}F_i \end{bmatrix} \tag{3.4}$$

The disturbance input matrix can be written as

$$E = \begin{bmatrix} 0 \\ -M^{-1}F_d \end{bmatrix} \tag{3.5}$$

The state vector is

$$x = \begin{Bmatrix} q \\ \dot{q} \end{Bmatrix} \tag{3.6}$$

Also, the output equation for the system can be written as

$$y = Cx \tag{3.7}$$

where C is the $m \times 2n$ output matrix and y is the $m \times 1$ output vector. For this control method, the effect of feedthrough in output measurement is not considered. Also, since the control method in this chapter is for systems with collocated actuators and sensors, the output vector y, and output matrix C have the same number of rows as the control input matrix B does. The eigenvalues of the second order and the first order systems are related by

$$\hat{\lambda}_i = \lambda_{2i-1}\lambda_{2i} = \bar{\lambda}_{2i}\lambda_{2i} \qquad i = 1, 2, \cdots n \tag{3.8}$$

where $\hat{\lambda}_i$ are the eigenvalues of the second order system, λ_i are the eigenvalues of the first order system, and $\bar{\lambda}_{2i}$ is the complex conjugate of λ_{2i}, all in $rad/\sec$. For the first order system, the eigenvalues related to the same eigenvalues of the second order system are complex conjugates. Eigenvalues of the second order system and its first order realization are related as

$$\left|\sqrt{\hat{\lambda}_i}\right| = \left|\lambda_{2i}\right| = \left|\bar{\lambda}_{2i}\right| = \left|\lambda_{2i-1}\right| \qquad i = 1, 2 \cdots n \tag{3.9}$$

In order to have an output feedback control, the input control force can be written as

$$u = Ky \tag{3.10}$$

where K is $m \times m$ feedback gain matrix. Therefore the closed-loop equation of the motion can be written as

$$\dot{x} = (A + BKC)x + Ef \tag{3.11}$$

Assuming that the actuators and sensors are collocated, the eigenstructure assignment problem in general seeks to find control gain matrix K in order to cancel the effect of the disturbance f in the areas that need to be isolated. For this reason, the eigenvalues and eigenvectors of the closed-loop system need to be determined simultaneously while the gain matrix K is determined. Therefore, the following eigenvalue problem has to be solved:

$$(A+BKC)\phi_i = \lambda_i \phi_i \qquad i = 1,...,2n \tag{3.12}$$

for K, λ_i, and ϕ_i, where λ_i and ϕ_i are the closed-loop eigenvalues and associated eigenvectors of the system. The latter equation can be written in the matrix form as

$$[A-\lambda_i I \quad | B]\begin{Bmatrix} \phi_i \\ KC\phi_i \end{Bmatrix} = 0 \qquad i = 1,...,2n \tag{3.13}$$

where I is a $2n \times 2n$ identity matrix. It can be seen that the vector $\begin{Bmatrix} \phi_i \\ KC\phi_i \end{Bmatrix}$ spans the null space of the matrix $S_{\lambda i} = [A-\lambda_i I \quad | B]$. Applying singular value decomposition to $S_{\lambda i}$, we can write

$$\begin{aligned} S_{\lambda i} &= [A-\lambda_i I \quad | B]_{2n\times(2n+m)} \\ &= [U_i]_{2n\times 2n}[\Sigma_i \,|\, 0_{2n\times m}]_{2n\times(2n+m)}[V_i^*]_{(2n+m)\times(2n+m)} \end{aligned} \tag{3.14}$$

We call λ_i in Equation (3.14) the operating eigenvalues. The number of operating eigenvalues is the same as the number of the required pairs of actuators and sensors m. The first m open-loop eigenvalues with negative real parts farthest from the origin are chosen to be the operating eigenvalues. U_i and V_i are the left and right orthonormal matrices, respectively. V_i^* is the conjugate transpose of the complex matrix V_i. Index i is to specify the equation for the ith closed-loop eigenvalue. Using the orthonormal property, one can write

$$U_i^* U_i = I_{2n\times 2n} \tag{3.15}$$

and

$$V_i^* V_i = I_{(2n+m)\times(2n+m)} \tag{3.16}$$

V_i can be partitioned as

$$[V_i]_{(2n+m)\times(2n+m)} = \begin{bmatrix} [V_{11}^i]_{2n\times 2n} & [V_{12}^i]_{2n\times m} \\ [V_{21}^i]_{m\times 2n} & [V_{22}^i]_{m\times m} \end{bmatrix} \tag{3.17}$$

Using the orthonormal property Equation (3.16), it is seen that

$$\begin{bmatrix} [V_{11}^i]_{2n\times 2n}^* & [V_{21}^i]_{m\times 2n}^* \\ [V_{12}^i]_{2n\times m}^* & [V_{22}^i]_{m\times m}^* \end{bmatrix} \begin{bmatrix} [V_{11}^i]_{2n\times 2n} & [V_{12}^i]_{2n\times m} \\ [V_{21}^i]_{m\times 2n} & [V_{22}^i]_{m\times m} \end{bmatrix} = \begin{bmatrix} I_{2n\times 2n} & 0 \\ 0 & I_{m\times m} \end{bmatrix} \tag{3.18}$$

More particularly, it can be seen that the product of the first row block of the V_i^* to the second column block of the V_i is equal to zero.

$$[V_{11}^i]_{2n\times 2n}^* [V_{12}^i]_{2n\times m} + [V_{21}^i]_{m\times 2n}^* [V_{22}^i]_{m\times m} = 0 \tag{3.19}$$

The second column block of the V_i is indeed the null space of $S_{\lambda i}$. It is easy to show that

$$S_{\lambda i} \begin{Bmatrix} [V_{12}^i]_{2n\times m} \\ [V_{22}^i]_{m\times m} \end{Bmatrix} = [A - \lambda_i I \quad | B] \begin{Bmatrix} [V_{12}^i]_{2n\times m} \\ [V_{22}^i]_{m\times m} \end{Bmatrix}$$

$$= U_i [\Sigma_i \,|\, 0] V_i^* \begin{Bmatrix} [V_{12}^i]_{2n\times m} \\ [V_{22}^i]_{m\times m} \end{Bmatrix}$$

$$= U_i[\Sigma_i]\left\{[V_{11}^i]_{2n\times 2n}^* \quad [V_{21}^i]_{m\times 2n}^*\right\}\begin{Bmatrix}[V_{12}^i]_{2n\times m}\\ [V_{22}^i]_{m\times m}\end{Bmatrix} = 0 \tag{3.20}$$

Equation (3.20) holds because V_i is orthonormal. The eigenvalue problem (3.13) can be rewritten as

$$[A-\lambda_i I \quad | B]\begin{Bmatrix}\phi_i\\ KC\phi_i\end{Bmatrix} = [A-\lambda_i I \quad | B]\begin{Bmatrix}[V_{12}^i]\\ [V_{22}^i]\end{Bmatrix} r^i = 0 \quad i = 1,...,2n \tag{3.21}$$

where r^i is an arbitrary coefficient vector, which its dimension is equal to m. Any linear combination of m columns of V_{12}^i is an achievable eigenvector of the closed-loop system. The problem of eigenstructure assignment can be reduced to the problem of finding coefficient vector r^i that makes the eigenvectors of the system desirable.

If the desirable eigenvectors of the system due to a particular vector r^i is

$$\phi_i^a = V_{12}^i r^i \tag{3.22}$$

then the corresponding control gain matrix K can be found using the following equation

$$KC\phi_i^a = V_{22}^i r^i \tag{3.23}$$

Available methods define a desired eigenvector for the system ϕ_i^d using different approaches such as eigenvector shaping. Reference [81] uses a Moore-Penrose inverse (pseudo inverse) of V_{12}^i, to find the required r^i. As a limitation of the method; however, the controlled eigenvectors are not identical to the desired eigenvectors, because the Moore-Penrose inverse of a vector gives the closest possible vector in sense of the least square or Euclidean 2-norm. Therefore, in general, there is always a distance between the desired and controlled eigenvectors as shown in Figure 3.1 [81]. Another method

proposed in [40] minimizes the ratio of the energy at the concerned locations to the total energy of the system. This method uses Rayleigh Principle to find the optimal controlled eigenvector. The need for defining the achievable eigenvectors still exists.

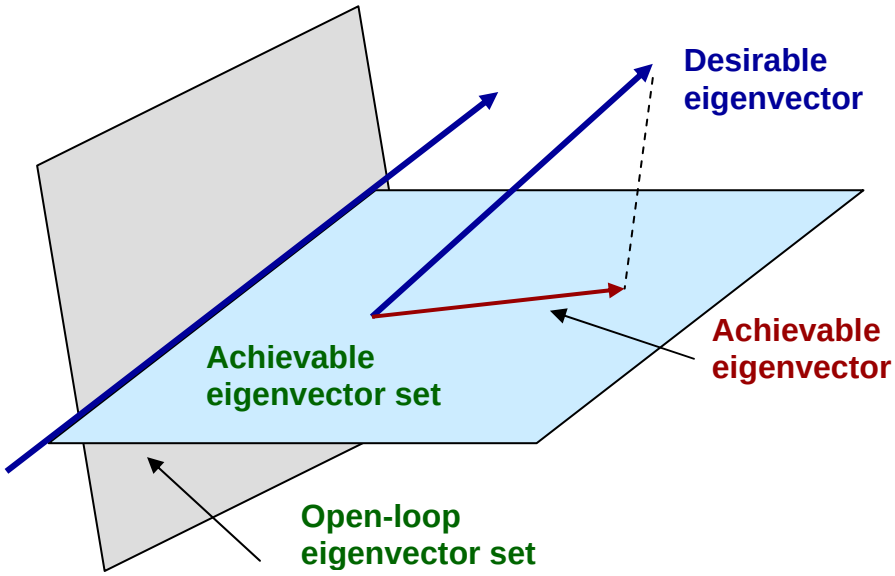

Figure 3.1. The difference between an achievable and a desirable eigenvector

The orthogonal eigenstructure control regenerates the open-loop system by finding the open-loop eigenvectors and their orthogonal vectors for the operating modes. In other words, the open-loop eigenvectors of the operating modes are defined by the intersections of the open-loop eigenvectors set and the achievable eigenvectors sets, as illustrated in Figure 3.2.

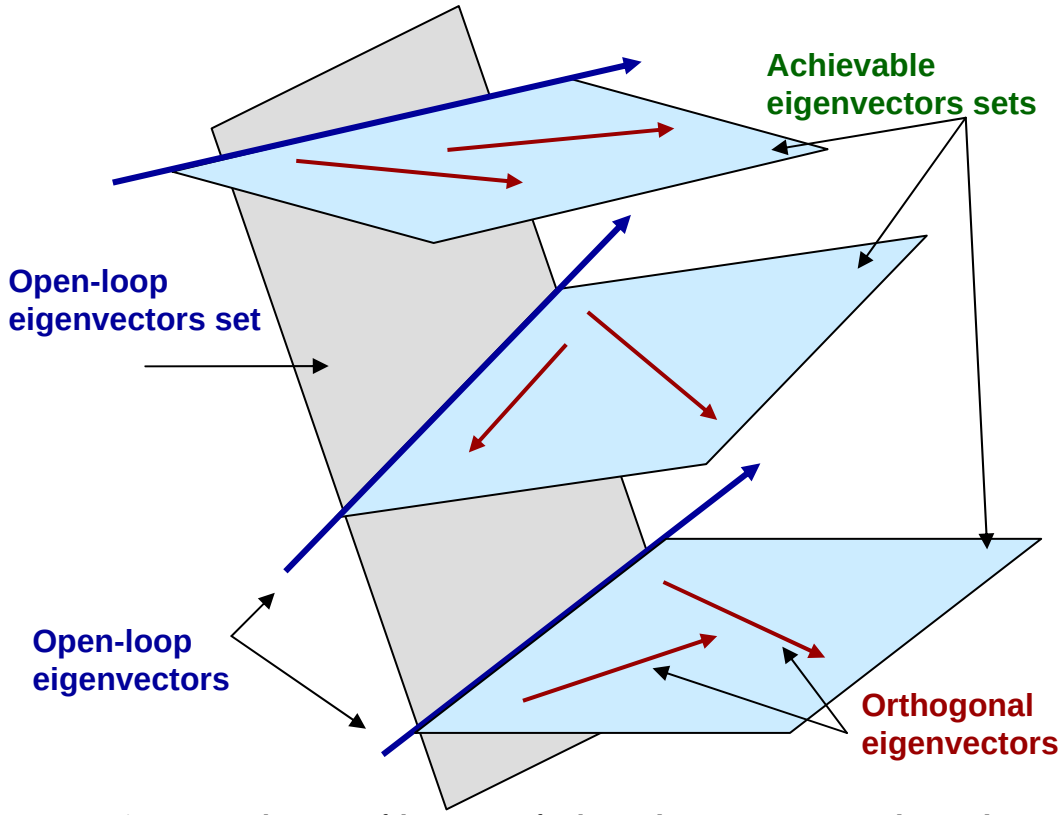

Figure 3.2. Schematics of the process of orthogonal eigenstructure control. Open-loop eigenvectors are the intersections of the open-loop eigenvectors set and the achievable eigenvectors set. The orthogonal eigenvectors within the achievable eigenvectors set are substituted as the open-loop ones

3.3. Orthogonal eigenstructure control

The normalized modal norm of the system corresponding to the ith eigenvalue of the closed-loop system can be written as

$$E_i = r^{i*} V_{12}^{i*} V_{12}^{i} r^{i} \tag{3.24}$$

The above is the pre-multiplication of an achievable eigenvector $\phi_i^a = V_{12}^i r^i$ by its conjugate transpose.

Consider the matrix of null space basis N^i associated with the operating eigenvalue λ_i

$$\mathrm{N}^i = \begin{Bmatrix} V_{12}^i \\ V_{22}^i \end{Bmatrix} \tag{3.25}$$

The norm of N^i is equal to one since the columns of N^i are the basis of the null space.

$$\left\| \mathrm{N}^i \right\|_2 = 1 \tag{3.26}$$

Therefore, any row block of N^i has a norm of less or equal than 1, and the magnitudes of their singular values belong to the interval $[0 \;\; 1]$ [82].

$$\left\| [V_{12}^i] \right\| \leq 1 \tag{3.27}$$

Applying SVD to the $[V_{12}^i]$,

$$V_{12}^i = \bar{V}^i \bar{S}^i \bar{U}^{i*} \tag{3.28}$$

while singular values of $\bar{S}^i$ lie in the $[0 \;\; 1]$ interval. Also

$$V_{12}^{i\,*} = \bar{U}^i \bar{S}^{i*} \bar{V}^{i*} \tag{3.29}$$

Multiplying Equation (3.29) by Equation (3.28) yields

$$V_{12}^{i\,*} V_{12}^i = \bar{U}^i \bar{S}^{i*} \bar{V}^{i*} \bar{V}^i \bar{S}^i \bar{U}^{i*} \tag{3.30}$$

Since $\bar{V}^i$ is an orthonormal matrix, it can be seen

$$\bar{V}^{i*} \bar{V}^i = I \tag{3.31}$$

Therefore,

$$V_{12}^{i\,*}V_{12}^{i}=\bar{U}^{i}\bar{S}^{i*}\bar{S}^{i}\bar{U}^{i*}=\bar{U}^{i}\left|\bar{S}^{i}\right|^{2}\bar{U}^{i*}=\bar{U}^{i}\Lambda^{i}\bar{U}^{i*} \tag{3.32}$$

where $\bar{\Lambda}_i$ is the matrix of eigenvalues and $\bar{U}^i$ is the matrix of eigenvectors of $V_{12}^{i\,*}V_{12}^{i}$. Equation (3.32) is clearly showing that the eigenvalues of the Hermitian product $V_{12}^{i\,*}V_{12}^{i}$ belong to the $[0\ \ 1]$ interval, since the absolute values of the singular values of $\bar{S}^i$ belong to this interval.

Interestingly, $V_{22}^{i\,*}V_{22}^{i}$ has the same eigenvectors as $V_{12}^{i\,*}V_{12}^{i}$ but its eigenvalues are different. More precisely, the summation of the eigenvalues of $V_{12}^{i\,*}V_{12}^{i}$ and $V_{22}^{i\,*}V_{22}^{i}$ associated with similar eigenvectors are unity.

Theorem:

Consider a $2n\times m$ non-square matrix $S_{\lambda i}$, $2n\geq m$. The null space of this matrix is spanned by the columns of a $(2n+m)\times m$ matrix N^i. V_{12}^{i} is the upper $2n\times m$ sub-matrix of the null space basis and V_{22}^{i} is the lower $m\times m$ sub-matrix of the null space basis. $V_{12}^{i*}V_{12}^{i}$ and $V_{22}^{i*}V_{22}^{i}$ have identical $m\times m$ eigenvector matrices and the summation of their ordered eigenvalue matrices is an $m\times m$ identity matrix.

Proof:

As the result of Equation (3.18), we have

$$[V_{12}^{i}]_{2n\times 2n}^{*}[V_{12}^{i}]_{2n\times 2n}+[V_{22}^{i}]_{m\times m}^{*}[V_{22}^{i}]_{m\times m}=I \tag{3.33}$$

Equation (3.33) can be re-written using an eigenvalue decomposition of the left hand side Hermitian matrices.

$$\bar{U}^i \bar{\Lambda}^i \bar{U}^{i*} + \bar{U}_w^i \bar{\Lambda}_w^i \bar{U}_w^{i*} = I \tag{3.34}$$

where $\bar{\Lambda}_w^i$ and $\bar{U}_w^i$ are the eigenvalue and eigenvector matrices of $V_{22}^{i\,*} V_{22}^i$. Pre-multiplying the aforementioned equation by $\bar{U}^{i*}$ and post multiplying by $\bar{U}^i$ gives

$$\bar{\Lambda}^i + \bar{U}^{i*} \bar{U}_w^i \bar{\Lambda}_w^i \bar{U}_w^{i*} \bar{U}^i = \bar{U}^{i*} I \bar{U}^i = I \tag{3.35}$$

or

$$(\bar{U}^{i*} \bar{U}_w^i)(\bar{\Lambda}_w^i)(\bar{U}^{i*} \bar{U}_w^i)^* = I - \bar{\Lambda}^i \tag{3.36}$$

The left hand side of the equation is an eigenvalue decomposition of the diagonal matrix $I - \bar{\Lambda}^i$. Since the eigenvalue matrix of a diagonal matrix is the matrix itself, therefore,

$$\bar{\Lambda}_w^i = I - \bar{\Lambda}^i \tag{3.37}$$

or

$$\bar{\Lambda}_w^i + \bar{\Lambda}^i = I \tag{3.38}$$

Also Equation (3.35) holds if

$$\bar{U}^{i*} \bar{U}_w^i = I \tag{3.39}$$

which concludes

$$\bar{U}^i = \bar{U}_w^i \tag{3.40}$$

□

If the eigenvector $\bar{U}_J^i$ associated with a unity eigenvalue of $V_{12}^{i\,*}V_{12}^i$ is substituted as r^i in Equation (3.24), then $E^i = 1$. The selected r^i generates the open-loop eigenvectors since it requires the control gain to be zero.

The eigenvalue decomposition of $V_{12}^{i\,*}V_{12}^i$ can be written as

$$V_{12}^{i\,*}V_{12}^i = \bar{U}^i \bar{\Lambda}^i \bar{U}^{i*} \tag{3.41}$$

that can be re-arranged as

$$\bar{U}^{i*} V_{12}^{i\,*} V_{12}^i \bar{U}^i = \bar{\Lambda}^i \tag{3.42}$$

For eigenvalue equal to unity and its corresponding eigenvector $\bar{U}_J^i$, it yields

$$\bar{U}_J^{i*} V_{12}^{i\,*} V_{12}^i \bar{U}_J^i = 1 \tag{3.43}$$

This implies that $V_{12}^i \bar{U}_J^i$ is identical to the eigenvector corresponding to the open-loop eigenvalue, since the gain associated with this eigenvector is zero. If we write the eigenvalue equation for $V_{22}^{i\,*}V_{22}^i$, the eigenvector $\bar{U}_J^i$ is corresponding to a zero eigenvalue of $V_{22}^{i\,*}V_{22}^i$.

$$\bar{U}_J^{i*} (V_{22}^{i\,*} V_{22}^i) \bar{U}_J^i = 0 \tag{3.44}$$

or

$$(V_{22}^i \bar{U}_J^i)^* (V_{22}^i \bar{U}_J^i) = 0 \tag{3.45}$$

which holds if and only if $V_{22}^i \bar{U}_J^i = 0$. Therefore

$$KC\phi_i^a = V_{22}^i r^i = V_{22}^i \bar{U}_J^i = 0 \tag{3.46}$$

The above holds if $K = 0$. Since there is no control gain, the open-loop system has been regenerated.

Knowing that other eigenvectors associated with non-unity eigenvalues of $V_{12}^{i\,*} V_{12}^i$ are orthogonal to the eigenvectors of the unity eigenvalue of $V_{12}^{i\,*} V_{12}^i$, one can find the closed-loop eigenvectors that are orthogonal to the open-loop ones.

Usually the j th non-unity eigenvalue of $V_{12}^{i\,*} V_{12}^i$ is much smaller than unity. Substituting their eigenvectors $\bar{U}_j^i$ - the j th column of eigenvector matrix $\bar{U}^i$ - as r^i, we may write

$$r^{i*} V_{12}^{i\,*} V_{12}^i r^i = \bar{\lambda}_j^i = 0 \tag{3.47}$$

Appending all of the calculated closed-loop eigenvectors for the entire modes that have been calculated gives

$$V = \left[V_{12}^1 r^1 \cdots V_{12}^m r^m \right] \tag{3.48}$$

$$W = \left[V_{22}^1 r^1 \cdots V_{22}^m r^m \right] \tag{3.49}$$

Feedback gain matrix K can be found from Equations (3.22) and (3.23).

$$K = W(CV)^{-1} \tag{3.50}$$

The state matrix for the closed-loop system is defined as

$$A_c = A + BKC \tag{3.51}$$

It has to be noted that it is possible to have a closed-loop system that has $m-1$ of the coefficient vectors r^i equal to the eigenvectors associated with unity eigenvalues of $V_{12}^{i\,*}V_{12}^{i}$. It implies that the algorithm is not orthogonalizing those particular modes. It leads to the zero columns in W; therefore, K does not have a full rank.

The trace of a square matrix is the summation of its eigenvalues. Since the matrix BKC has zero elements on its diagonal its trace is zero. As a result, the summations as well as the average of the eigenvalues for the open-loop and closed-loop systems are equal. Equation (3.42) can be re-written in an expanded form as,

$$\bar{U}^{i*}V_{12}^{i\,*}V_{12}^{i}\bar{U}^{i}=\begin{bmatrix}\bar{\lambda}_1^i & & & \\ & \bar{\lambda}_2^i & & 0 \\ & & \ddots & \\ & 0 & & \bar{\lambda}_{m-1}^i \\ & & & & \bar{\lambda}_m^i\end{bmatrix} \tag{3.52}$$

Among the eigenvalues $\bar{\lambda}_j^i$, $j=1,2,\cdots m$, there is one eigenvalue equal to unity and the rest are zero. If the eigenvector associated with those unity eigenvalues are selected as the coefficient vectors, the open-loop system is just regenerated. There are m options for choosing which eigenvector of $V_{12}^{i\,*}V_{12}^{i}$ should be chosen as r^i. When there are m inputs to the system, the number of eigenvectors that have to be orthogonalized is m. Also there are m choices for each eigenvector. After excluding the regenerated open-loop system, there are m^m-1 options for closed-loop system as the result of orthogonal eigenstructure control.

The possible answers for one set of the closed-loop eigenstructure can be found using

$$\bar{U}_j^{i*}V_{12}^{i\,*}V_{12}^{i}\bar{U}_j^{i}=\bar{\lambda}_j^i \qquad j=1,2,\cdots m-1 \tag{3.53}$$

that holds for all the non-unity eigenvalues and their corresponding eigenvectors. The most desirable closed-loop system is the one which has the smallest phase plane of isolated states.

3.4. Procedure for orthogonal eigenstructure control with collocated actuators and sensors

This procedure defines the proposed output feedback control of orthogonal eigenstructure control

1. Define state space realization of the system similar to Equations (3.2-3.7)

2. Determine the first m eigenvalues of the open-loop system with negative real parts farthest from the origin, where m is the number of the pairs of actuators and sensors.

3. Using the i th λ_i, define non-square matrix $S_{\lambda i}$ as Equation (3.14)

4. Apply SVD to $S_{\lambda i}$ generated from step 3

5. Partition the right unitary matrix V_i and define V_{12}^i and V_{22}^i as described in Equation (3.17)

6. Calculate $V_{12}^{i*}V_{12}^i$

7. Find the eigenvalue matrix $\bar{\Lambda}^i$ and eigenvector matrix $\bar{U}^i$ for Hermitian matrix $V_{12}^{i*}V_{12}^i$, using Equation (3.32)

8. Pick the j th eigenvector $\bar{U}_j^i$ associated with the j th eigenvalue λ_j^i. Define $r^i = \bar{U}_j^i$ similar to Equation (3.46)

9. Calculate $v^i = V_{12}^i r^i$ and $w^i = V_{22}^i r^i$

10. Repeat Step 3 to Step 9, m times and find v_i and w_i for all the operating eigenvalues

11. Define matrices V and W by appending v^i and w^i resulting from step 9 and 10 as defined in Equations (3.48) and (3.49)

12. Find the gain matrix K using Equation (3.50)

13. Go to step 8, change the index j. Repeat the algorithm m^m times. Exclude the case that open-loop system has been regenerated

14. Choose gain matrix K from $m^m - 1$ closed-loop systems that produce the smallest phase plane for one of the isolated states of the system.

Chapter 4

Finite Dimensional Systems: Collocated Actuators and Sensors

In this chapter, the application of orthogonal eigenstructure control to finite dimensional systems is investigated. First a simple model of interconnected masses has been considered and the control method is applied to control the vibrations at different masses. Different models with various numbers of collocated actuators and sensors are considered and the responses of the systems to different disturbances are studied and the procedure of application of orthogonal eigenstructure control is described in detail. To keep the design freedom space unbounded, the concept of progressive application of orthogonal eigenstructure control is introduced and implemented.

4.1 System with collocated actuators and sensors

A simple lumped longitudinal vibration system is considered and the orthogonal eigenstructure control is applied to isolate the left side of the system from the vibration. The system consists of 10 masses which are interconnected by springs and dampers as indicated in Figure 4.1.

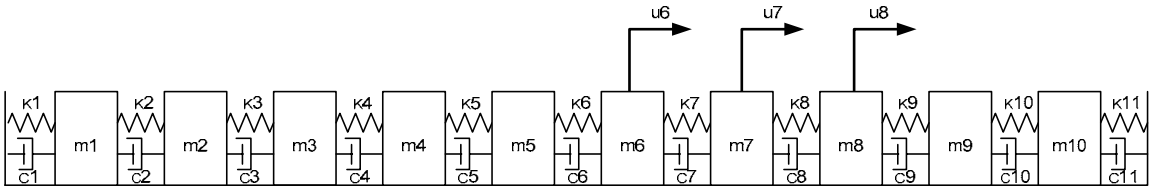

Figure 4.1. The system of 10 masses with interconnecting springs and dampers

Recalling Equation (3.1)

$$M\ddot{q} + C_d\dot{q} + K_s q = F_i u_i + F_d u_d \tag{4.1}$$

the mass, damping and stiffness matrices for this system are

$$M = \begin{bmatrix} m_1 & & & \cdots & 0 \\ & m_2 & & & \vdots \\ & & \ddots & & \\ \vdots & & & m_9 & \\ 0 & \cdots & & & m_{10} \end{bmatrix} \tag{4.2}$$

$$C_d = \begin{bmatrix} c_1 + c_2 & -c_2 & & \cdots & 0 \\ -c_2 & c_2 + c_3 & -c_3 & & \vdots \\ & -c_3 & \ddots & -c_9 & \\ \vdots & & -c_9 & c_9 + c_{10} & -c_{10} \\ 0 & \cdots & & -c_{10} & c_{10} + c_{11} \end{bmatrix} \tag{4.3}$$

$$K_s = \begin{bmatrix} k_1 + k_2 & -k_2 & & \cdots & 0 \\ -k_2 & k_2 + k_3 & -k_3 & & \vdots \\ & -k_3 & \ddots & -k_9 & \\ \vdots & & -k_9 & k_9 + k_{10} & -k_{10} \\ 0 & \cdots & & -k_{10} & k_{10} + k_{11} \end{bmatrix} \tag{4.4}$$

It is assumed that all the masses are equal to $50\,kg$. Also, all the spring coefficients are identical and are equal to $1000\,N/m$. Damping coefficients are assumed to be $10\,N.s/m$.

Finally, the second order system has to be transferred to state space form. The Equations (3.3) and (3.4) are used for this transformation. Since there are 10 masses in the system, the state space realization of the system has the dimension of 20. The state space form equation of the system is

$$\dot{x} = Ax + Bu + Ef \tag{4.5}$$

$$y = Cx \tag{4.6}$$

Matrix A is a 20×20 matrix. Using Equation (3.3), A is defined as

$$A = \begin{bmatrix} \begin{vmatrix} 0 & \cdots & 0 \\ \vdots & \ddots & \vdots \\ 0 & \cdots & 0 \end{vmatrix} & \begin{vmatrix} 1 & & & \cdots & 0 \\ & 1 & & & \vdots \\ & & \ddots & & \\ \vdots & & & 1 & \\ 0 & \cdots & & & 1 \end{vmatrix} \\ \begin{vmatrix} -40 & 20 & & \cdots & 0 \\ 20 & -40 & 20 & & \vdots \\ & 20 & \ddots & 20 & \\ \vdots & & 20 & -40 & 20 \\ 0 & \cdots & & 20 & -40 \end{vmatrix} & \begin{vmatrix} -0.4 & 0.2 & & \cdots & 0 \\ 0.2 & -0.4 & 0.2 & & \vdots \\ & 0.2 & \ddots & 0.2 & \\ \vdots & & 0.2 & -0.4 & 0.2 \\ 0 & \cdots & & 0.2 & -0.4 \end{vmatrix} \end{bmatrix} \tag{4.7}$$

Next, we will study this system with two and three pairs of sensors and actuators. The pairs of sensors and actuators are assumed to be collocated.

4.2 System with two pairs of sensors and actuators

For this case study, the pairs of sensors/actuators are assumed to be located on the 7th and 8th masses. Therefore, F_i and C in Equations (3.2) and (3.7) are defined as

$$F_i^T = C = \begin{Bmatrix} 0 & 0 & 0 & 0 & 0 & 0 & 1 & 0 & 0 & 0 \\ 0 & 0 & 0 & 0 & 0 & 0 & 0 & 1 & 0 & 0 \end{Bmatrix} \tag{4.8}$$

Using Equation (3.4), B is also defined as

$$B = \begin{Bmatrix} 0 & 0 & 0 & 0 & 0 & 0 & -0.02 & 0 & 0 & 0 \\ 0 & 0 & 0 & 0 & 0 & 0 & 0 & -0.02 & 0 & 0 \end{Bmatrix}^T \tag{4.9}$$

4.2.1 Response to impulse input

An impulse input of magnitude 1 m/s is applied to m_{10} .The first and the third eigenvalues of the open-loop system with negative real parts farthest from the origin are considered as the operating eigenvalues, as described in Equation (3.14). The second open-loop eigenvalue is the complex conjugate of the first eigenvalue, therefore it is not considered as the operating eigenvalue.

Open-loop eigenvalues λ_1 and λ_3 are considered and SVD is applied to Equation (3.14). Based on Equation (3.21), the basis of the null spaces of the eigenvectors associated with the chosen eigenvalues can be determined. Basis of the null spaces N^1 and N^3 are presented in Tables 4.1 and 4.2.

Table 4.1. Basis of null space associated with the first eigenvalue λ_1

	N^1	
1	-0.0102 - 0.0022i	0.0084 + 0.0018i
2	0.0195 + 0.0042i	-0.0161 - 0.0035i
3	-0.0273 - 0.0058i	0.0225 + 0.0048i
4	0.0329 + 0.0070i	-0.0271 - 0.0058i
5	-0.0358 - 0.0076i	0.0294 + 0.0063i
6	0.0358 + 0.0076i	-0.0294 - 0.0063i
7	-0.0329 - 0.0070i	0.0271 + 0.0058i
8	0.0269 + 0.0059i	-0.0230 - 0.0048i
9	-0.0192 - 0.0042i	0.0164 + 0.0034i
10	0.0100 + 0.0022i	-0.0086 - 0.0018i
11	0.0232 - 0.0892i	-0.0193 + 0.0734i
12	-0.0446 + 0.1711i	0.0370 - 0.1409i
13	0.0623 - 0.2392i	-0.0517 + 0.1970i
14	-0.0750 + 0.2879i	0.0622 - 0.2371i
15	0.0816 - 0.3132i	-0.0677 + 0.2580i
16	-0.0816 + 0.3132i	0.0677 - 0.2580i
17	0.0750 - 0.2879i	-0.0622 + 0.2371i
18	-0.0624 + 0.2356i	0.0515 - 0.2013i
19	0.0447 - 0.1685i	-0.0368 + 0.1440i
20	-0.0233 + 0.0878i	0.0192 - 0.0750i
21	0.4078 + 0.0000i	0.4920 - 0.0000i
22	0.4908 + 0.0000i	0.5922 - 0.0000i

The first 20 rows of N^1 and N^3 are V_{12}^1 and V_{12}^3 , respectively. Applying eigenvalue decomposition to $V_{12}^{1*}V_{12}^1$, one can write

$$V_{12}^{1*}V_{12}^1 = \begin{bmatrix} 0.5928 & -0.4913 \\ -0.4913 & 0.4072 \end{bmatrix} = \begin{bmatrix} -0.6381 & 0.7699 \\ -0.7699 & -0.6381 \end{bmatrix} \begin{bmatrix} 0.00004433 & 0 \\ 0 & 1 \end{bmatrix} \begin{bmatrix} -0.6381 & -0.7699 \\ 0.7699 & -0.6381 \end{bmatrix}$$

Therefore

$$\begin{bmatrix} -0.6381 & -0.7699 \\ 0.7699 & -0.6381 \end{bmatrix} \left(V_{12}^{1*}V_{12}^1 \right) \begin{bmatrix} -0.6381 & 0.7699 \\ -0.7699 & -0.6381 \end{bmatrix} = \begin{bmatrix} 0.00004433 & 0 \\ 0 & 1 \end{bmatrix}$$

Table 4.2. Basis of null space associated with the first eigenvalue λ_3

	N^3	
1	0.0141 + 0.0081i	-0.0183 - 0.0106i
2	-0.0237 - 0.0136i	0.0308 + 0.0179i
3	0.0258 + 0.0148i	-0.0335 - 0.0195i
4	-0.0197 - 0.0113i	0.0256 + 0.0149i
5	0.0074 + 0.0042i	-0.0095 - 0.0055i
6	0.0074 + 0.0042i	-0.0095 - 0.0055i
7	-0.0197 - 0.0113i	0.0256 + 0.0149i
8	0.0252 + 0.0148i	-0.0340 - 0.0194i
9	-0.0232 - 0.0136i	0.0312 + 0.0179i
10	0.0138 + 0.0081i	-0.0186 - 0.0106i
11	-0.0744 + 0.1180i	0.0980 - 0.1529i
12	0.1252 - 0.1986i	-0.1648 + 0.2572i
13	-0.1362 + 0.2161i	0.1793 - 0.2799i
14	0.1040 - 0.1650i	-0.1369 + 0.2137i
15	-0.0388 + 0.0615i	0.0510 - 0.0797i
16	-0.0388 + 0.0615i	0.0510 - 0.0797i
17	0.1040 - 0.1650i	-0.1369 + 0.2137i
18	-0.1364 + 0.2107i	0.1792 - 0.2840i
19	0.1254 - 0.1936i	-0.1646 + 0.2610i
20	-0.0745 + 0.1151i	0.0979 - 0.1551i
21	0.6327 - 0.0000i	0.4810 + 0.0000i
22	0.4831 - 0.0000i	0.3673 + 0.0000i

Hence, the normalized scalar coefficient vector associated with the first eigenvalue is

$$r^1 = \begin{bmatrix} -0.6381 \\ -0.7699 \end{bmatrix}.$$

Similarly, for $V_{12}^{3*}V_{12}^{3}$ we can write

$$V_{12}^{3*}V_{12}^{3} = \begin{bmatrix} 0.3663 & -0.4818 \\ -0.4818 & 0.6337 \end{bmatrix} = \begin{bmatrix} 0.7960 & -0.6052 \\ 0.6052 & 0.7960 \end{bmatrix} \begin{bmatrix} 0.00006247 & 0 \\ 0 & 1 \end{bmatrix} \begin{bmatrix} 0.7960 & 0.6052 \\ -0.6052 & 0.7960 \end{bmatrix}$$

and

$$\begin{bmatrix} 0.7960 & 0.6052 \\ -0.6052 & 0.7960 \end{bmatrix} \left(V_{12}^{3*}V_{12}^{3} \right) \begin{bmatrix} 0.7960 & -0.6052 \\ 0.6052 & 0.7960 \end{bmatrix} = \begin{bmatrix} 0.00006247 & 0 \\ 0 & 1 \end{bmatrix}$$

Therefore, $\bar{U}_1^3 = \begin{bmatrix} 0.7960 \\ 0.6052 \end{bmatrix}$ and the normalized scalar coefficient associated with the third eigenvalue is

$$r^3 = \bar{U}_1^3 = \begin{bmatrix} 0.7960 \\ 0.6052 \end{bmatrix}.$$

Eigenvalues and natural frequencies of the open and closed-loop systems are presented in Tables 4.3 and 4.4. The poles of the open-loop and closed-loop systems are presented in Figure 4.2. The average of the eigenvalues remains intact when the orthogonal eigenstructure control is applied.

Table 4.3. Natural frequencies of the open-loop and closed-loop systems, (in $rad/\sec$)

Mode number	Natural frequencies, open-loop system	Natural frequencies closed-loop system
1	8.8532	9.8609
2	8.5820	8.8217
3	8.1360	8.5914
4	7.5244	7.8821
5	6.7596	7.2053
6	5.8573	6.7247
7	4.8356	1.8904
8	3.7156	5.3466
9	2.5199	3.682
10	1.2729	4.0119

Table 4.4. Eigenvalues of the open-loop and closed-loop systems, (in $rad/\sec$)

Mode number	Eigenvalues of the open-loop system	Eigenvalues of the closed-loop system
1	-0.3919 + 8.8446i	-0.4092 + 9.8524i
2	-0.3919 - 8.8446i	-0.4092 - 9.8524i
3	-0.3683 + 8.5741i	-0.3097 + 8.8163i
4	-0.3683 - 8.5741i	-0.3097 - 8.8163i
5	-0.3310 + 8.1293i	-0.3076 + 8.5859i
6	-0.3310 - 8.1293i	-0.3076 - 8.5859i
7	-0.2831 + 7.5191i	-0.2923 + 7.8767i
8	-0.2831 - 7.5191i	-0.2923 - 7.8767i
9	-0.2285 + 6.7558i	-0.2156 + 7.2021i
10	-0.2285 - 6.7558i	-0.2156 - 7.2021i
11	-0.1715 + 5.8547i	-0.1926 + 6.7219i
12	-0.1715 - 5.8547i	-0.1926 - 6.7219i
13	-0.1169 + 4.8342i	-0.0162 + 1.8904i
14	-0.1169 - 4.8342i	-0.0162 - 1.8904i
15	-0.0690 + 3.7149i	-0.1308 + 5.3450i
16	-0.0690 - 3.7149i	-0.1308 - 5.3450i
17	-0.0317 + 2.5197i	-0.0581 + 3.6816i
18	-0.0317 - 2.5197i	-0.0581 - 3.6816i
19	-0.0081 + 1.2729i	-0.0679 + 4.0113i
20	-0.0081 - 1.2729i	-0.0679 - 4.0113i

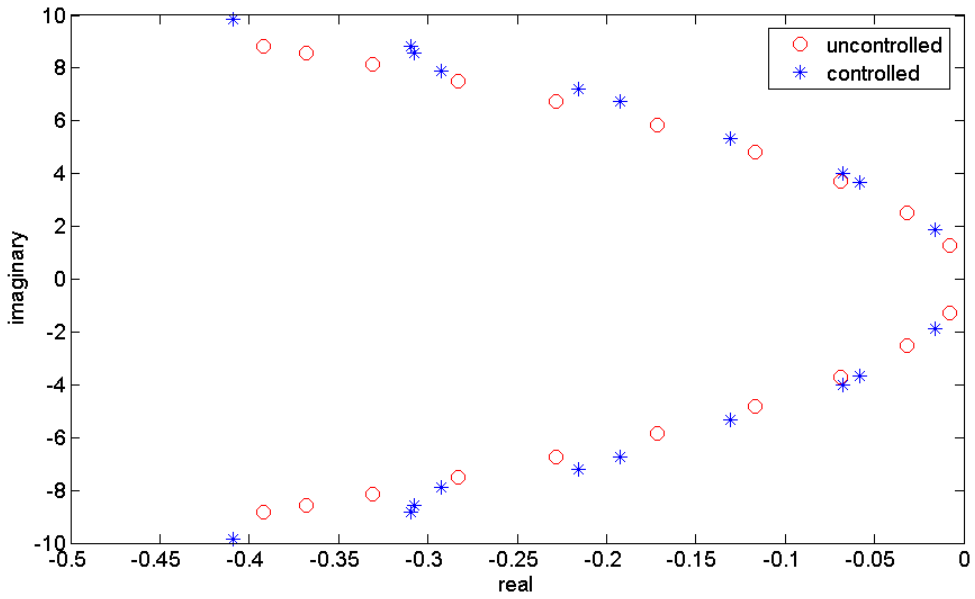

Figure 4.2. Open-loop and closed-loop poles

Displacements and velocities of the open-loop and closed-loop systems in response to the impulse input applied to m_{10} are presented in Figures 4.3 and 4.4. Vibration cancellation has occurred within area that includes m_1 to m_6. In fact, the actuators located on m_7 and m_8 prevent the vibrational energy generated by the impulse input to proceed beyond them. Both the displacement and the velocity of the masses in the isolated area of the closed-loop system have lower amplitude than those of the open-loop system. This is true about m_7, located in the transition area in between isolated and confined areas. The confined area that includes m_8, m_9, and m_{10} experiences higher amplitude of vibration in the closed-loop system than the open-loop system. The vibrations; however, die out when the vibrational energy of the impulse input diminishes due to damping in structure.

Figure 4.5 shows the actuation forces applied to the system. The first actuator is located on m_7 and the second actuator on m_8. The maximum force applied by the first and the second actuators are 125 N and 96 N, respectively. The actuation forces decay smoothly in time.

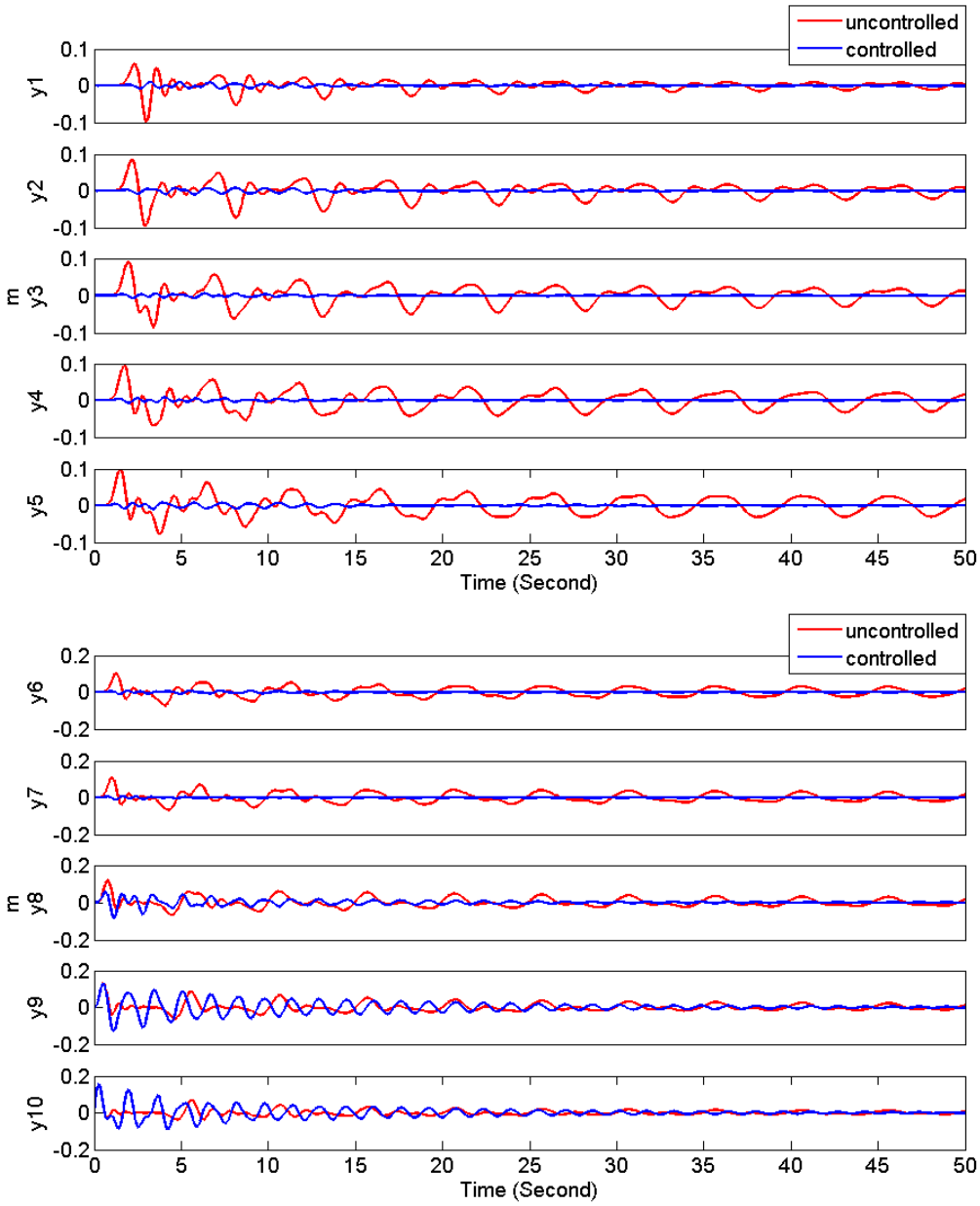

Figure 4.3. Open-loop and closed-loop system displacement response to the impulse input applied at mass 10

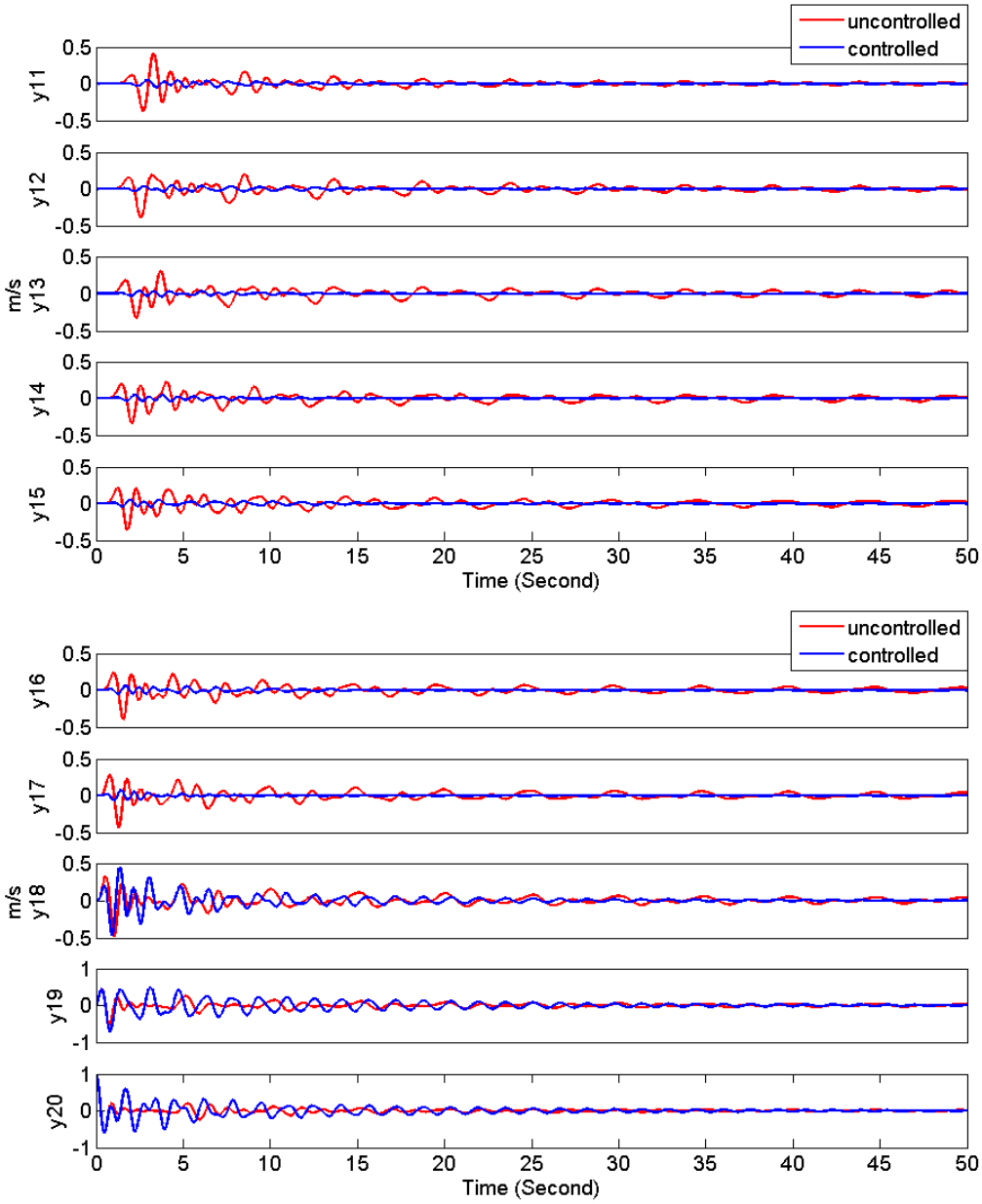

Figure 4.4. Open-loop and closed-loop system velocity response to the impulse input applied at mass 10

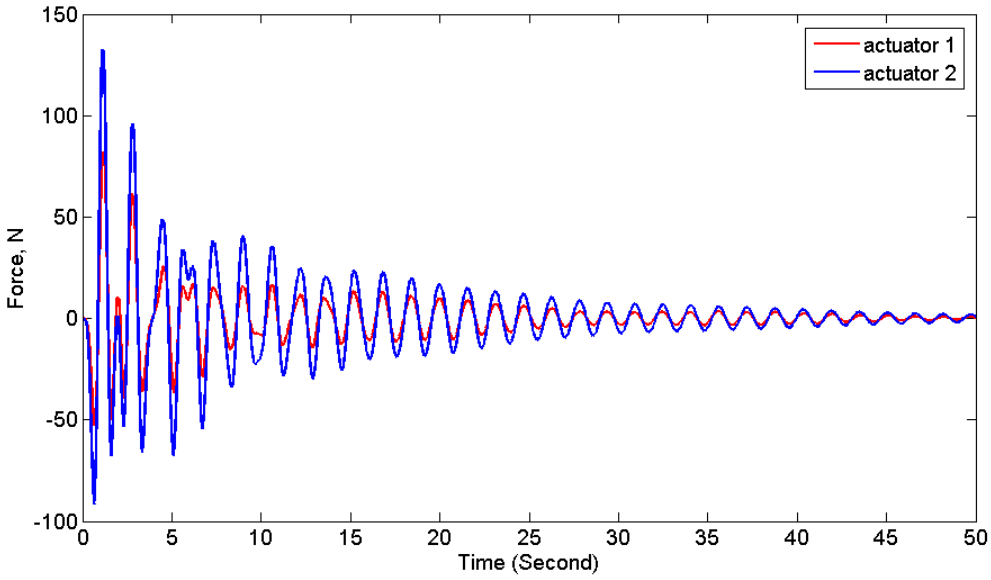

Figure 4.5. Actuation forces for isolating the system due to the impulse input at mass 10

4.2.2 Response to sinusoidal input with frequency equal to natural frequency

For this problem, sinusoidal input applied to m_9 and m_{10}, while the control actuators are mounted to m_7 and m_8. Inputs have the amplitude of $10\,N$ and frequency of 1.2729 rad/s equal to the first natural frequency of the open-loop system. The two largest open-loop eigenvalues -0.3919 + 8.8446i and -0.3683 + 8.5741i are chosen as the operating eigenvalues as defined in Equation (3.14). Figures 4.6 and 4.7 present the displacement and velocity of the masses of the system due to the sinusoidal input. The results are similar to the results of the impulse input in terms of lower displacement and velocity in the isolated area that includes m_1 to m_6. Behavior of mass m_7 is similar to the isolated area. In the confined area, which includes m_8, m_9, and m_{10}, we observe a higher displacement and velocity than the open-loop system.

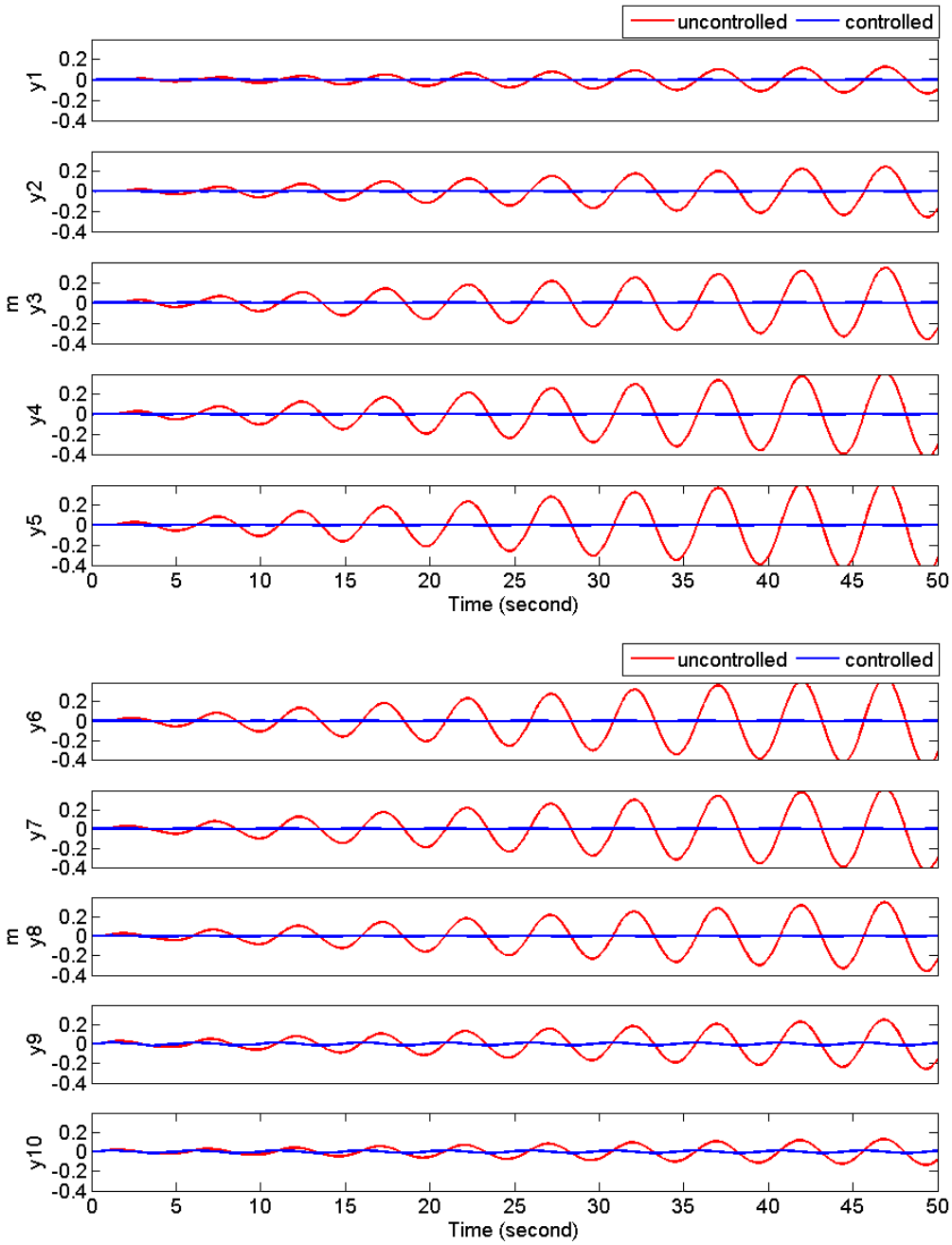

Figure 4.6. Open-loop and closed-loop system displacement response to the sinusoidal input with frequency equal to the first natural frequency applied to m_9 and m_{10}

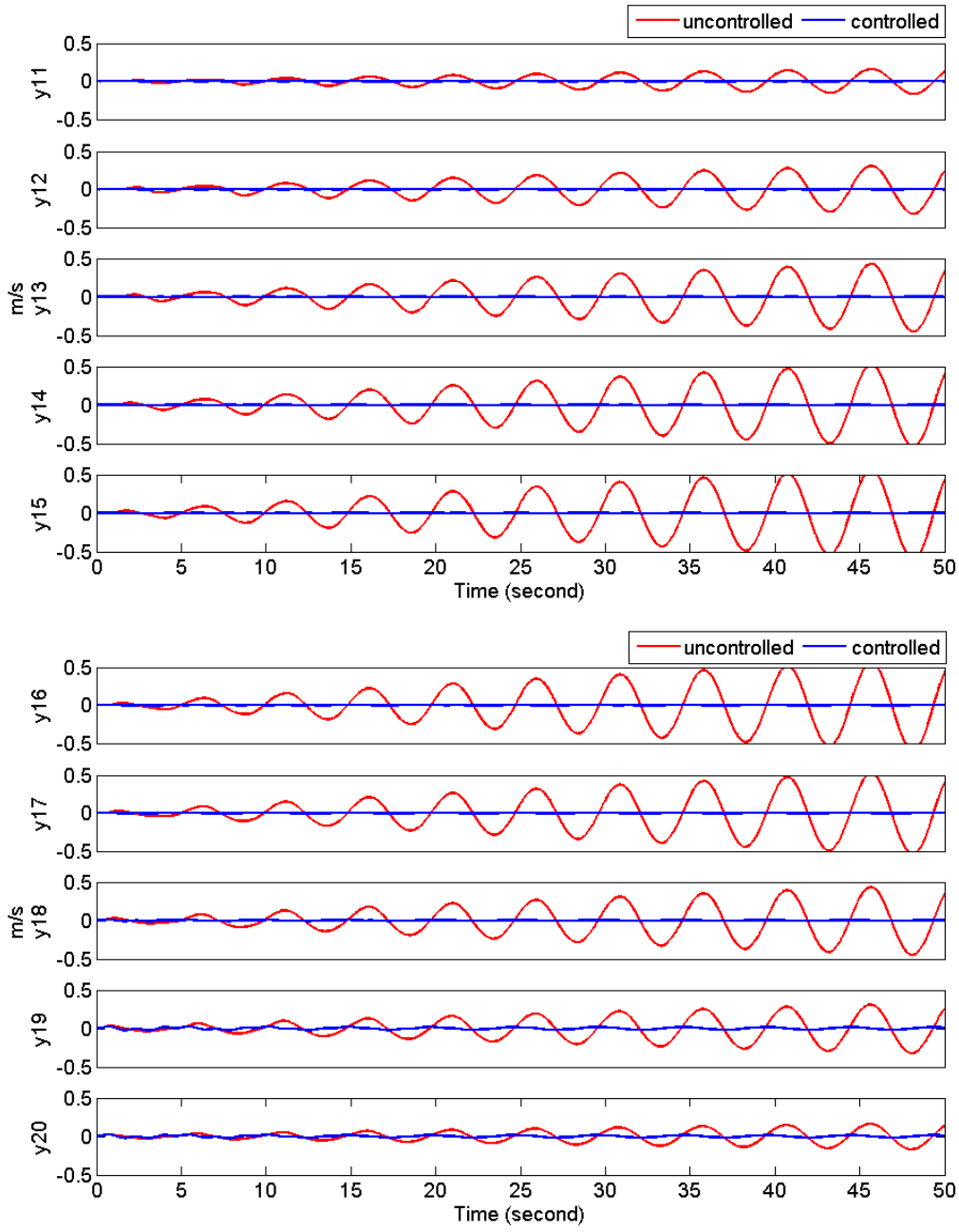

Figure 4.7. Open-loop and closed-loop system velocity response to the sinusoidal input with frequency equal to the first natural frequency applied to m_9 and m_{10}

Figure 4.8 shows the actuation force applied to the system. The first actuator is located on m_7 and the second actuator on m_8 mass. The maximum forces applying by the first and the second actuators are 5.11 N and 8.83 N , respectively.

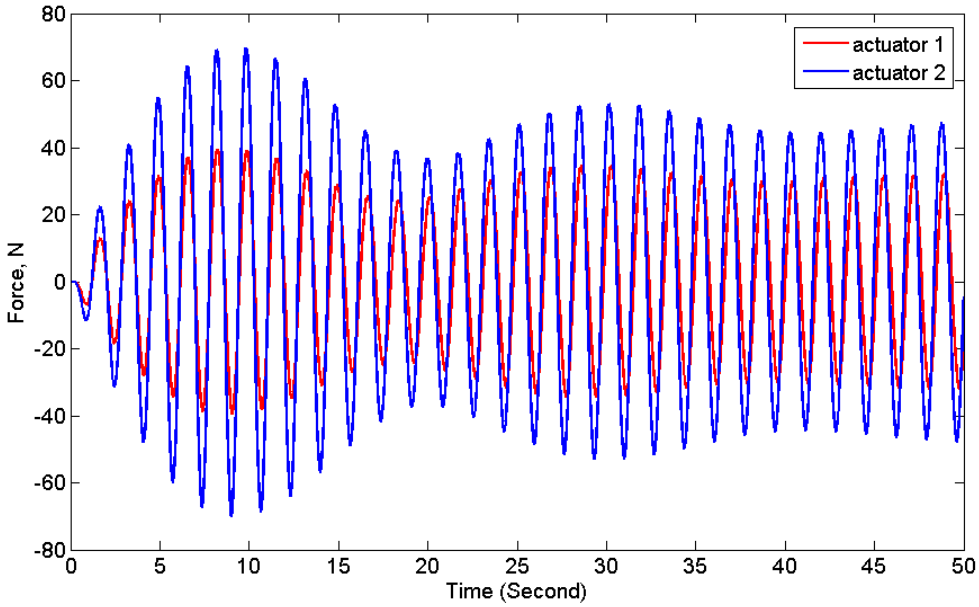

Figure 4.8. Actuator forces for isolating the system due to the sinusoidal input with frequency equal to the first natural frequency

4.2.3 Response to sinusoidal input with frequency of non-operating natural frequencies

When the disturbance frequency is equal to one of the natural frequencies of the system, then the question to be asked which open-loop eigenvalue has to be chosen as the operating eigenvalue. To answer this, we sort the open-loop eigenvalues in ascending order of their real parts and keep the frequency of disturbance equal to the natural frequency corresponding to the 9th open-loop eigenvalue $\lambda_9 = -0.2285 + 6.7558\mathrm{i}$. A comparison is made between selecting (λ_1, λ_3) and (λ_1, λ_9) as the operating eigenvalues, ($\lambda_1 = -0.3919 + 8.8446\mathrm{i}$ and $\lambda_3 = -0.3683 + 8.5741\mathrm{i}$). Figures 4.9 and 4.10 depict the comparison between the displacement and velocity of the two models. It is seen that using (λ_1, λ_3) as the operating eigenvalues generates slightly better results on the isolated areas both for displacement and velocity. The results for the confined area show that both methods result in almost similar responses.

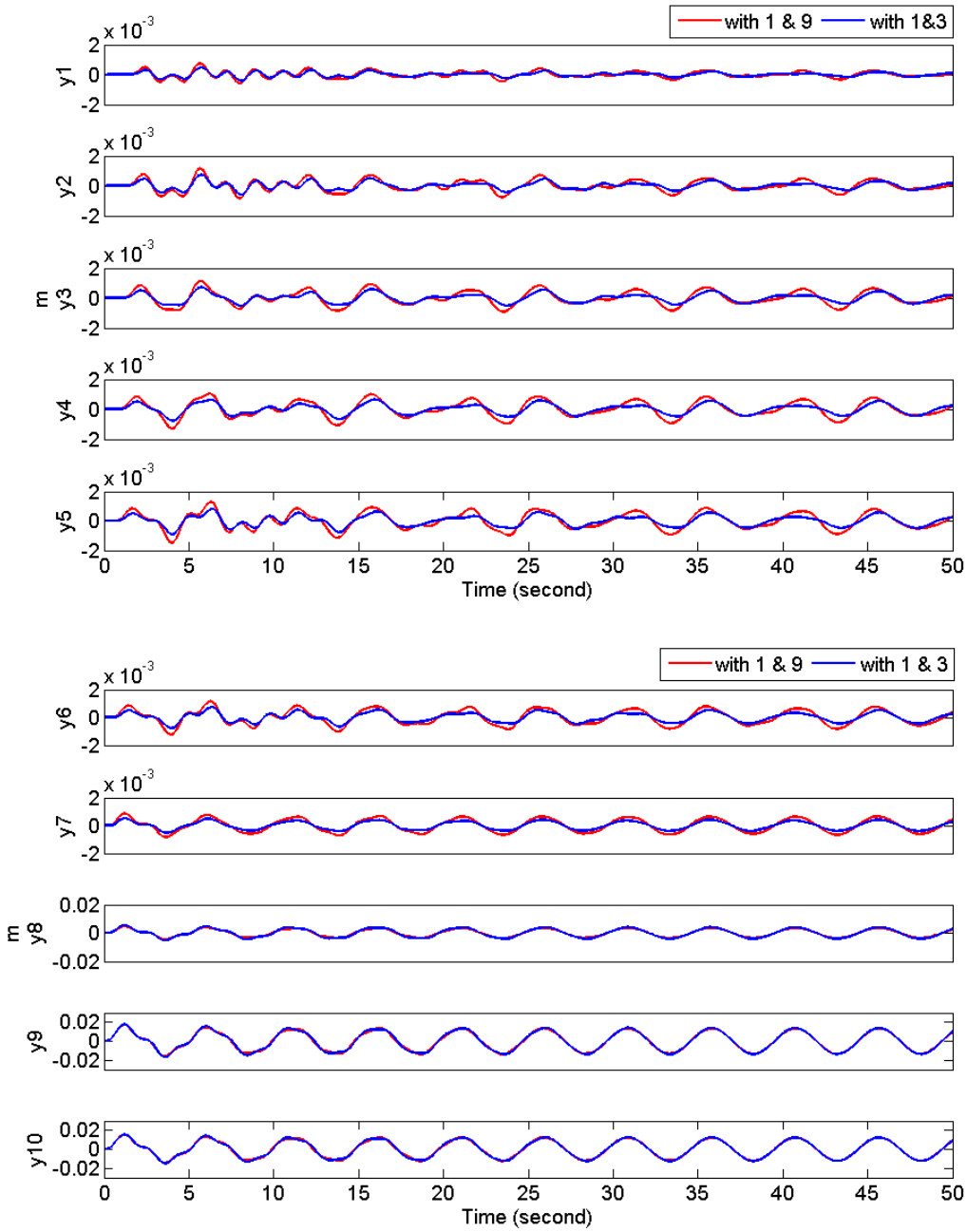

Figure 4.9. Comparison of displacements due to sinusoidal input with frequency of λ_9
With operating eigenvalues (λ_1, λ_3) and (λ_1, λ_9)

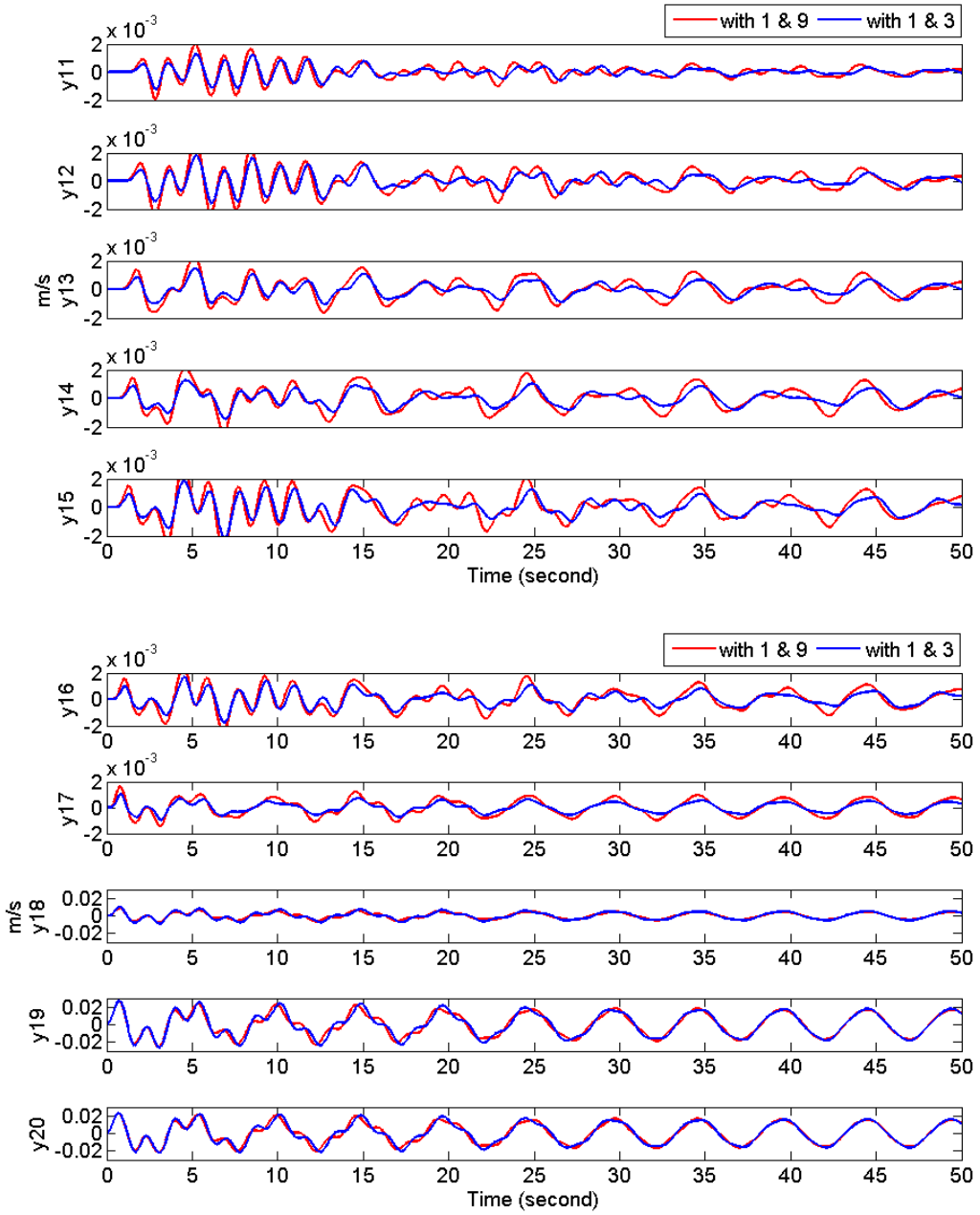

Figure 4.10. Comparison of velocities due to sinusoidal input with frequency of λ_9
With operating eigenvalues (λ_1, λ_3) and (λ_1, λ_9)

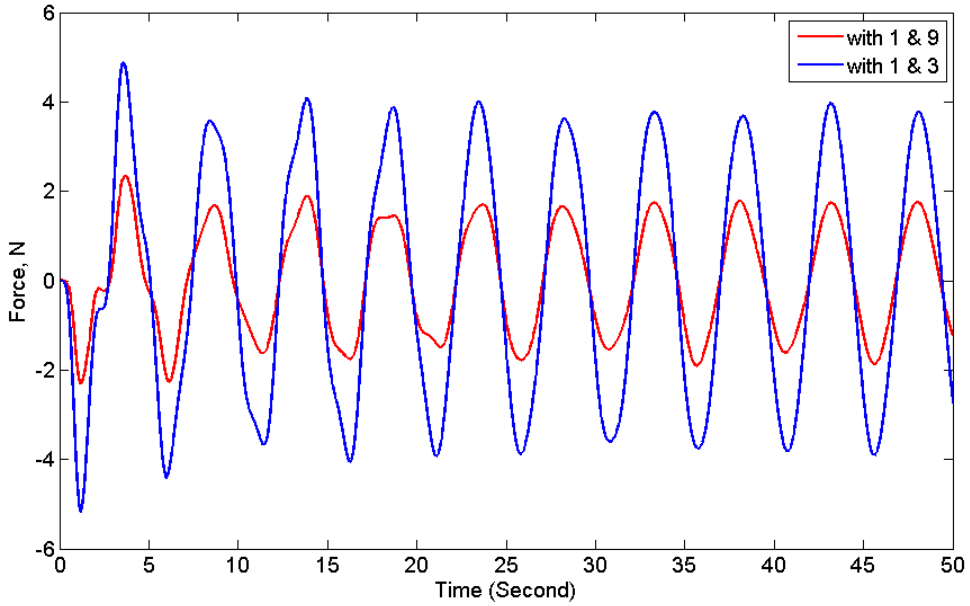

Figure 4.11. Comparison of the first actuator force mounted to m_7 due to sinusoidal input with frequency of λ_9 with operating eigenvalues (λ_1 , λ_3) and (λ_1 , λ_9)

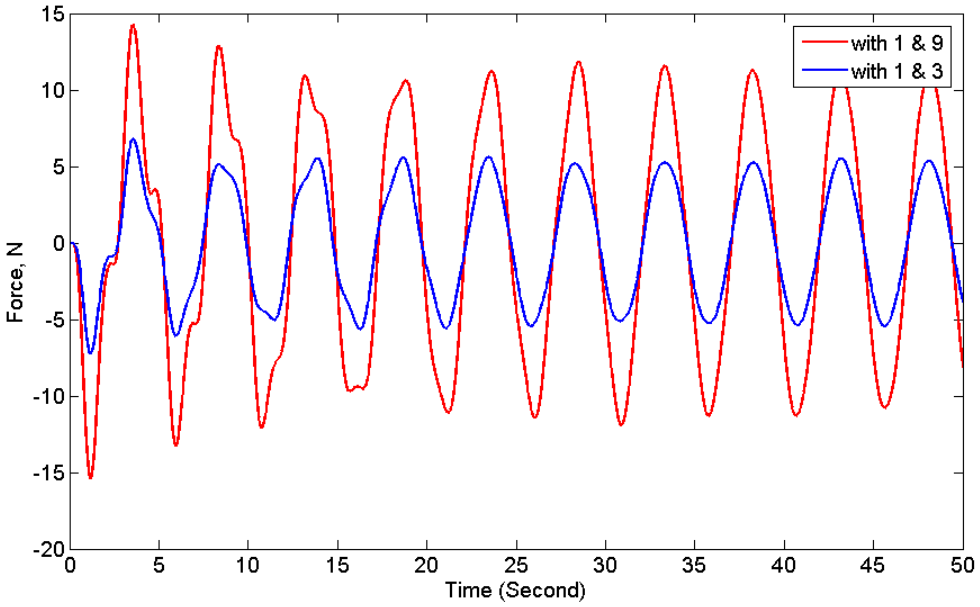

Figure 4.12. Comparison of the first actuator force mounted to m_8 due to sinusoidal input with frequency of λ_9 with operating eigenvalues (λ_1 , λ_3) and (λ_1 , λ_9)

Figures 4.11 and 4.12 show the comparison between actuator forces, indicating that the actuation force of the first actuator located on m_7 for the case (λ_1, λ_3) is 5.16 N, which is greater than the case when the operational eigenvalues are (λ_1, λ_9). In the latter case the maximum force of the actuator is 2.34 N. For the second actuator force mounted to m_8 the peak force of the actuators are 7.27 N and 15.41 N, respectively for the cases where (λ_1, λ_3) and (λ_1, λ_9) used as the operating eigenvalues. It is seen that choosing the operating eigenvalues can effect significantly on the actuation forces, but does not show the same effects on the response of the system. If operating eigenvalues with negative real parts farthest from the origin are used, it leads to lower actuation forces.

4.3 System with three pairs of actuators and sensors and detail explanation of the method

The core of the orthogonal eigenstructure control is the control of the system in such a way that the closed-loop eigenvectors become near orthogonal to the open-loop ones. The mechanism is explained using a few examples.

Considering the previous system with three pairs of actuators and sensors on m_6, m_7, and m_8 with the operating eigenvalues λ_1, λ_3, and λ_5, we intend to find the appropriate r^1, r^2, and r^3 for $V_{12}^1 r^1$, $V_{12}^2 r^2$, and $V_{12}^3 r^3$, respectively. The disturbance is an impulse input to m_{10}.

The orthogonal eigenstructure control method suggests that if r^i is one of the eigenvectors associated with the non-unity eigenvalues of $V_{12}^{i*} V_{12}^i$, an almost orthogonal closed-loop eigenvector can be generated. Interestingly, if r^i is the eigenvector associated with the unity eigenvalues of $V_{12}^{i*} V_{12}^i$, the closed-loop and open-loop systems are identical since the control gains become zero. The reason is that $V_{22}^{i*} V_{22}^i$ has exactly the same eigenvectors as $V_{12}^{i*} V_{12}^i$ but their eigenvalues are different. Eigenvectors associated with unity eigenvalue of $V_{12}^{i*} V_{12}^i$ is identical to the eigenvector associated with

zero eigenvalue of $V_{22}^{i*}V_{22}^{i}$. Therefore, W in Equation (3.51) becomes zero, which means gain matrix K in Equation (3.52) is zero. Even though each r^i associated with non-unity eigenvalues generates orthogonal closed-loop eigenvectors; it does not mean that they can be chosen arbitrarily. Since new closed-loop eigenvectors have to be orthogonal to the open-loop ones as well as to the other closed-loop eigenvectors, the appropriate eigenvectors of $V_{12}^{i*}V_{12}^{i}$ have to be chosen carefully in order to achieve a desirable solution. Determining all the possible closed-loop systems and monitoring their stability and behavior especially monitoring their phase portrait may stand out the most desirable solution with a phase portrait with minimum area. To elaborate, three different cases with different values for r^i are considered.

Case 1:

$r^1 = \bar{U}_3^1$, $r^2 = \bar{U}_3^2$, and $r^3 = \bar{U}_3^3$, which gives the zero gain matrix. The open-loop and closed-loop systems are identical.

Case 2:

$r^1 = \bar{U}_2^1$, $r^2 = \bar{U}_1^2$, and $r^3 = \bar{U}_1^3$, which generates the best vibration confinement.

Case 3:

$r^1 = \bar{U}_1^1$, $r^2 = \bar{U}_2^2$, and $r^3 = \bar{U}_1^3$, which generates an unstable closed-loop system.

The time histories of the displacement of m_1 are presented in Figure 4.13 for different cases. It is seen that the closed-loop response of y_1 is the same as the open-loop response in case 1. In case 2, vibration is isolated and in case 3, instability can be seen in the time response of y_1.

For case 1, with the first operating eigenvalue, λ_1, the following equations can be written

$$V_{12}^{1*}V_{12}^{1}=\begin{bmatrix}0.4137 & -0.3793 & 0.3140\\ -0.3793 & 0.3479 & -0.2881\\ 0.3140 & -0.2881 & 0.2387\end{bmatrix}$$

$$V_{12}^{1*}V_{12}^{1}=\bar{U}^{1}\bar{\Lambda}^{1}\bar{U}^{1*}=\begin{bmatrix}0.3723 & -0.6692 & 0.6431\\ 0.7982 & -0.1228 & -0.5898\\ 0.4737 & 0.7329 & 0.4884\end{bmatrix}\begin{bmatrix}0 & \cdots & 0\\ \vdots & 0.0002 & \vdots\\ 0 & \cdots & 1\end{bmatrix}\begin{bmatrix}0.3723 & 0.7982 & 0.4737\\ -0.6692 & -0.1228 & 0.7329\\ 0.6431 & -0.5898 & 0.4884\end{bmatrix}$$

Also

$$V_{22}^{1*}V_{22}^{1}=\begin{bmatrix}0.5863 & 0.3793 & -0.3140\\ 0.3793 & 0.6521 & 0.2881\\ -0.3140 & 0.2881 & 0.7613\end{bmatrix}$$

$$V_{22}^{1*}V_{22}^{1}=\bar{U}^{1}\bar{\Lambda}_{w}{}^{1}\bar{U}^{1*}=\begin{bmatrix}0.3723 & -0.6692 & 0.6431\\ 0.7982 & -0.1228 & -0.5898\\ 0.4737 & 0.7329 & 0.4884\end{bmatrix}\begin{bmatrix}1 & \cdots & 0\\ \vdots & 0.9998 & \vdots\\ 0 & \cdots & 0\end{bmatrix}\begin{bmatrix}0.3723 & 0.7982 & 0.4737\\ -0.6692 & -0.1228 & 0.7329\\ 0.6431 & -0.5898 & 0.4884\end{bmatrix}$$

It is observe that

$$V_{12}^{1*}V_{12}^{1}+V_{22}^{1*}V_{22}^{1}=\begin{bmatrix}0.4137 & -0.3793 & 0.3140\\ -0.3793 & 0.3479 & -0.2881\\ 0.3140 & -0.2881 & 0.2387\end{bmatrix}+\begin{bmatrix}0.5863 & 0.3793 & -0.3140\\ 0.3793 & 0.6521 & 0.2881\\ -0.3140 & 0.2881 & 0.7613\end{bmatrix}=\begin{bmatrix}1 & 0 & 0\\ 0 & 1 & 0\\ 0 & 0 & 1\end{bmatrix}$$

In addition, $V_{12}^{1*}V_{12}^{1}$ and $V_{22}^{1*}V_{22}^{1}$ have the same eigenvectors and their eigenvalues satisfies the Equation (3.39).

$$\bar{\Lambda}_{w}^{1}+\bar{\Lambda}^{1}=\begin{bmatrix}1 & \cdots & 0\\ \vdots & 0.9998 & \vdots\\ 0 & \cdots & 0\end{bmatrix}+\begin{bmatrix}0 & \cdots & 0\\ \vdots & 0.0002 & \vdots\\ 0 & \cdots & 1\end{bmatrix}=\begin{bmatrix}1 & \cdots & 0\\ \vdots & 1 & \vdots\\ 0 & \cdots & 1\end{bmatrix}$$

$$V_{22}^{1} r^{1} = V_{22}^{1} \bar{U}_{3}^{1} = \begin{bmatrix} 0.5872 & 0.3793 & -0.3151 \\ 0.3785 & 0.6521 & 0.2890 \\ -0.3135 & 0.2881 & 0.7606 \end{bmatrix} \begin{bmatrix} 0.6431 \\ -0.5898 \\ 0.4884 \end{bmatrix} = \begin{bmatrix} 0 \\ 0 \\ 0 \end{bmatrix}$$

For the second operating eigenvalue, λ_3, the following equations can be written

$$V_{12}^{2*} V_{12}^{2} = \begin{bmatrix} 0.0445 & -0.1245 & 0.1636 \\ -0.1245 & 0.3501 & -0.4604 \\ 0.1636 & -0.4604 & 0.6058 \end{bmatrix}$$

$$V_{12}^{2*} V_{12}^{2} = \bar{U}^{2} \bar{\Lambda}^{2} \bar{U}^{2*} = \begin{bmatrix} -0.4115 & -0.8868 & 0.2103 \\ -0.7757 & 0.2196 & -0.5917 \\ -0.4785 & 0.4066 & 0.7783 \end{bmatrix} \begin{bmatrix} 0 & \cdots & 0 \\ \vdots & 0.0003 & \vdots \\ 0 & \cdots & 1 \end{bmatrix} \begin{bmatrix} -0.4115 & -0.7757 & -0.4785 \\ -0.8868 & 0.2196 & 0.4066 \\ 0.2103 & -0.5917 & 0.7783 \end{bmatrix}$$

Also

$$V_{22}^{2*} V_{22}^{2} = \begin{bmatrix} 0.9555 & 0.1245 & -0.1636 \\ 0.1245 & 0.6499 & 0.4604 \\ -0.1636 & 0.4604 & 0.3942 \end{bmatrix}$$

$$V_{22}^{2*} V_{22}^{2} = \bar{U}^{2} \bar{\Lambda}_{w}^{2} \bar{U}^{2*} = \begin{bmatrix} -0.4115 & -0.8868 & 0.2103 \\ -0.7757 & 0.2196 & -0.5917 \\ -0.4785 & 0.4066 & 0.7783 \end{bmatrix} \begin{bmatrix} 1 & \cdots & 0 \\ \vdots & 0.9997 & \vdots \\ 0 & \cdots & 0 \end{bmatrix} \begin{bmatrix} -0.4115 & -0.7757 & -0.4785 \\ -0.8868 & 0.2196 & 0.4066 \\ 0.2103 & -0.5917 & 0.7783 \end{bmatrix}$$

It is seen that

$$V_{12}^{2*} V_{12}^{2} + V_{22}^{2*} V_{22}^{2} = \begin{bmatrix} 0.0445 & -0.1245 & 0.1636 \\ -0.1245 & 0.3501 & -0.4604 \\ 0.1636 & -0.4604 & 0.6058 \end{bmatrix} + \begin{bmatrix} 0.9555 & 0.1245 & -0.1636 \\ 0.1245 & 0.6499 & 0.4604 \\ -0.1636 & 0.4604 & 0.3942 \end{bmatrix} = \begin{bmatrix} 1 & 0 & 0 \\ 0 & 1 & 0 \\ 0 & 0 & 1 \end{bmatrix}$$

Note that $V_{12}^{2*} V_{12}^{2}$ and $V_{22}^{2*} V_{22}^{2}$ have the same eigenvectors and their eigenvalues satisfies the Equation (3.39).

$$\bar{\Lambda}_w^2 + \bar{\Lambda}^2 = \begin{bmatrix} 1 & \cdots & 0 \\ \vdots & 0.9997 & \vdots \\ 0 & \cdots & 0 \end{bmatrix} + \begin{bmatrix} 0 & \cdots & 0 \\ \vdots & 0.0003 & \vdots \\ 0 & \cdots & 1 \end{bmatrix} = \begin{bmatrix} 1 & \cdots & 0 \\ \vdots & 1 & \vdots \\ 0 & \cdots & 1 \end{bmatrix}$$

$$V_{22}^2 r^2 = V_{22}^2 \bar{U}_3^2 = \begin{bmatrix} 0.9555 & 0.1245 & -0.1636 \\ 0.1245 & 0.6499 & 0.4604 \\ -0.1636 & 0.4604 & 0.3942 \end{bmatrix} \begin{bmatrix} 0.2103 \\ -0.5917 \\ 0.7783 \end{bmatrix} = \begin{bmatrix} 0 \\ 0 \\ 0 \end{bmatrix}$$

For the third operating eigenvalue, λ_5, the following equations can be written

$$V_{12}^{3*} V_{12}^3 = \begin{bmatrix} 0.6954 & -0.2180 & -0.4053 \\ -0.2180 & 0.0684 & 0.1269 \\ -0.4053 & 0.1269 & 0.2364 \end{bmatrix}$$

$$V_{12}^{3*} V_{12}^3 = \bar{U}^3 \bar{\Lambda}^3 \bar{U}^{3*} = \begin{bmatrix} -0.8339 & -0.2216 & 0.5054 \\ 0.2614 & 0.6480 & 0.7154 \\ 0.4861 & -0.7287 & 0.4825 \end{bmatrix} \begin{bmatrix} 0 & \cdots & 0 \\ \vdots & 0.0003 & \vdots \\ 0 & \cdots & 1 \end{bmatrix} \begin{bmatrix} -0.8339 & 0.2614 & 0.4861 \\ -0.2216 & 0.6480 & -0.7287 \\ 0.5054 & 0.7154 & 0.4825 \end{bmatrix}$$

Also

$$V_{22}^{3*} V_{22}^3 = \begin{bmatrix} 0.3046 & 0.2180 & 0.4053 \\ 0.2180 & 0.9316 & -0.1269 \\ 0.4053 & -0.1269 & 0.7636 \end{bmatrix}$$

$$V_{22}^{3*} V_{22}^3 = \bar{U}^3 \bar{\Lambda}_w^3 \bar{U}^{3*} = \begin{bmatrix} -0.8339 & -0.2216 & 0.5054 \\ 0.2614 & 0.6480 & 0.7154 \\ 0.4861 & -0.7287 & 0.4825 \end{bmatrix} \begin{bmatrix} 1 & \cdots & 0 \\ \vdots & 0.9997 & \vdots \\ 0 & \cdots & 0 \end{bmatrix} \begin{bmatrix} -0.8339 & 0.2614 & 0.4861 \\ -0.2216 & 0.6480 & -0.7287 \\ 0.5054 & 0.7154 & 0.4825 \end{bmatrix}$$

It is noted that

$$V_{12}^{3*}V_{12}^{3}+V_{22}^{3*}V_{22}^{3}=\begin{bmatrix}0.6954 & -0.2180 & -0.4053\\ -0.2180 & 0.0684 & 0.1269\\ -0.4053 & 0.1269 & 0.2364\end{bmatrix}+\begin{bmatrix}0.3046 & 0.2180 & 0.4053\\ 0.2180 & 0.9316 & -0.1269\\ 0.4053 & -0.1269 & 0.7636\end{bmatrix}=\begin{bmatrix}1 & 0 & 0\\ 0 & 1 & 0\\ 0 & 0 & 1\end{bmatrix}$$

Similar to the previous cases, $V_{12}^{3*}V_{12}^{3}$ and $V_{22}^{3*}V_{22}^{3}$ have the same eigenvectors but their eigenvalues satisfy Equation (3.39).

$$\bar{\Lambda}_{w}^{3}+\bar{\Lambda}^{3}=\begin{bmatrix}1 & \cdots & 0\\ \vdots & 0.9997 & \vdots\\ 0 & \cdots & 0\end{bmatrix}+\begin{bmatrix}0 & \cdots & 0\\ \vdots & 0.0003 & \vdots\\ 0 & \cdots & 1\end{bmatrix}=\begin{bmatrix}1 & \cdots & 0\\ \vdots & 1 & \vdots\\ 0 & \cdots & 1\end{bmatrix}$$

$$V_{22}^{3}r^{3}=V_{22}^{3}\bar{U}_{3}^{3}=\begin{bmatrix}0.3046 & 0.2180 & 0.4053\\ 0.2180 & 0.9316 & -0.1269\\ 0.4053 & -0.1269 & 0.7636\end{bmatrix}\begin{bmatrix}0.5054\\ 0.7154\\ 0.4825\end{bmatrix}=\begin{bmatrix}0\\ 0\\ 0\end{bmatrix}$$

Similar results are found for $V_{22}^{2}r^{2}$ and $V_{22}^{3}r^{3}$, if r^{2} and r^{3} are the eigenvectors associated with unity eigenvalue of $V_{12}^{2*}V_{12}^{2}$ and $V_{12}^{3*}V_{12}^{3}$ (eigenvalue 0 of $V_{22}^{2*}V_{22}^{2}$ and $V_{22}^{3*}V_{22}^{3}$) respectively. As a result, according to Equations (3.51) and (3.52), the gain matrix becomes zero, and the open-loop and closed-loop systems are identical, as it seen in Figure 4.13.

For case 2, the following equations can be written

$$V_{22}^{1}r^{1}=V_{22}^{1}\bar{U}_{2}^{1}=\begin{bmatrix}0.5872 & 0.3793 & -0.3151\\ 0.3785 & 0.6521 & 0.2890\\ -0.3135 & 0.2881 & 0.7606\end{bmatrix}\begin{bmatrix}-0.6692\\ -0.1228\\ 0.7329\end{bmatrix}=\begin{bmatrix}-0.6705\\ -0.1216\\ 0.7318\end{bmatrix}$$

$$V_{22}^2 r^2 = V_{22}^2 \bar{U}_1^2 = \begin{bmatrix} 0.9555 & 0.1245 & -0.1636 \\ 0.1245 & 0.6499 & 0.4604 \\ -0.1636 & 0.4604 & 0.3942 \end{bmatrix} \begin{bmatrix} -0.4115 \\ -0.7757 \\ -0.4785 \end{bmatrix} = \begin{bmatrix} -0.4109 \\ -0.7772 \\ -0.4765 \end{bmatrix}$$

and

$$V_{22}^3 r^3 = V_{22}^3 \bar{U}_1^3 = \begin{bmatrix} 0.3046 & 0.2180 & 0.4053 \\ 0.2180 & 0.9316 & -0.1269 \\ 0.4053 & -0.1269 & 0.7636 \end{bmatrix} \begin{bmatrix} -0.8339 \\ 0.2614 \\ 0.4861 \end{bmatrix} = \begin{bmatrix} -0.5074 \\ -0.7147 \\ -0.4813 \end{bmatrix}$$

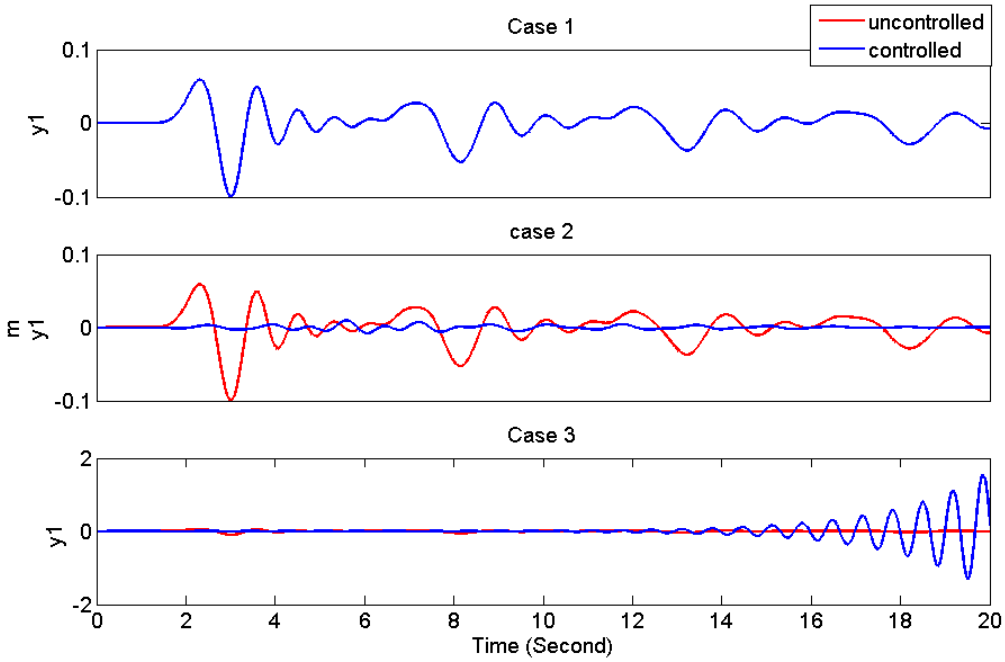

Figure 4.13. Displacement of m_1 with operating eigenvalues ($\lambda_1, \lambda_3,$ and λ_5) due to an impulse input on m_{10}. Case 1: $r^1 = \bar{U}_3^1$, $r^2 = \bar{U}_3^2$, and $r^3 = \bar{U}_3^3$, Case 2: $r^1 = \bar{U}_2^1$, $r^2 = \bar{U}_1^2$, and $r^3 = \bar{U}_1^3$, Case 3: $r^1 = \bar{U}_1^1$, $r^2 = \bar{U}_2^2$, and $r^3 = \bar{U}_1^3$

Therefore, W in Equation (3.51) is found by combining the previous results as

$$W = \begin{bmatrix} -0.6705 & -0.4109 & -0.5074 \\ -0.1216 & -0.7772 & -0.7147 \\ 0.7318 & -0.4765 & -0.4813 \end{bmatrix}$$

Also V in Equation (3.50) becomes

$$V = \begin{bmatrix}
-0.0105 + 0.0007i & -0.0005 + 0.0030i & 0.0042 + 0.0009i \\
0.0201 - 0.0013i & 0.0009 - 0.0050i & -0.0055 - 0.0012i \\
-0.0281 + 0.0019i & -0.0010 + 0.0054i & 0.0030 + 0.0007i \\
0.0339 - 0.0022i & 0.0008 - 0.0042i & 0.0016 + 0.0003i \\
-0.0368 + 0.0024i & -0.0003 + 0.0016i & -0.0050 - 0.0011i \\
0.0368 - 0.0024i & -0.0003 + 0.0016i & 0.0050 + 0.0011i \\
0.0330 - 0.0037i & 0.0417 - 0.0077i & 0.0491 - 0.0045i \\
-0.0880 + 0.0085i & 0.0076 + 0.0047i & 0.0020 - 0.0011i \\
0.0630 - 0.0061i & -0.0070 - 0.0043i & -0.0037 + 0.0020i \\
-0.0328 + 0.0032i & 0.0041 + 0.0026i & 0.0028 - 0.0015i \\
-0.0009 - 0.0930i & -0.0252 - 0.0060i & -0.0094 + 0.0336i \\
0.0018 + 0.1785i & 0.0425 + 0.0101i & 0.0123 - 0.0440i \\
-0.0025 - 0.2495i & -0.0462 - 0.0110i & -0.0067 + 0.0240i \\
0.0030 + 0.3003i & 0.0353 + 0.0084i & -0.0035 + 0.0125i \\
-0.0033 - 0.3268i & -0.0132 - 0.0031i & 0.0113 - 0.0405i \\
0.0033 + 0.3268i & -0.0132 - 0.0031i & -0.0113 + 0.0405i \\
0.0166 + 0.2935i & 0.0463 + 0.3612i & 0.0152 + 0.4006i \\
-0.0315 - 0.7824i & -0.0439 + 0.0628i & 0.0079 + 0.0168i \\
0.0226 + 0.5597i & 0.0403 - 0.0577i & -0.0144 - 0.0307i \\
-0.0118 - 0.2917i & -0.0240 + 0.0343i & 0.0110 + 0.0235i
\end{bmatrix}$$

And finally, according to Equation (3.52), gain matrix K is

$$K = W(CV)^{-1} = 1.0 \times 10^3 \begin{bmatrix}
-1.3205 + 0.8684i & -0.8670 - 0.1560i & -0.1337 + 0.3649i \\
1.5734 + 3.2494i & -1.5268 - 0.5539i & 0.1758 + 1.1900i \\
0.7264 - 0.5496i & -1.0190 - 0.0599i & -0.8965 - 0.3157i
\end{bmatrix}$$

The real part of the control gain matrix is considered

$$K = 1.0 \times 10^3 \begin{bmatrix}
-1.3205 & -0.8670 & -0.1337 \\
1.5734 & -1.5268 & 0.1758 \\
0.7264 & -1.0190 & -0.8965
\end{bmatrix}$$

Table 4.5 and 4.6 show the inner product of the closed-loop eigenvectors associated with the operating eigenvalues to themselves for all three cases. Elements of Table 4.5 are an index of the orthogonality of the eigenvectors. The maximum amounts of the inner products are written in red. When the inner product of two eigenvectors is close to zero, it means that the eigenvectors are almost orthogonal. An inner product close to unity means that the associated eigenvectors are almost parallel.

Table 4.5 shows that case 2, which is a desirable solution to the vibration isolation of the proposed system, have lesser parallel eigenvectors than that of case 4. It can be seen that for case 2, the most parallel eigenvectors are eigenvectors 5 and 3 with inner product of 0.4137, 7, and 13 with inner product of 0.7255, 9, and 11 with inner product of 0.6032, 11, and 13 with inner product of 0.7495, 15, and 13 with inner product of 0.4794, 17, and 13 with inner product of 0.6353, 19, and 13 with inner product of 0.5243. The same inner product for case 3 can be extracted from Table 4.6. For case 3, the most parallel eigenvectors are eigenvectors 5 and 3 with inner product 0.6441, 7, and 5 with inner product of 0.4357, 9 , and 7 with inner product of 0.6254, 11 , and 7 with inner product of 0.9542, 13, and 7 with inner product of 0.9695, 13, and 11 with inner product of 0.9328, 17 , and 11 with inner product of 0.7065, 19, and 7 with inner product of 0.9574, 19, and 11 with inner product of 0.9526, 19, and 13 with inner product of 0.9195. It is seen that there are some closed-loop eigenvectors that are almost parallel when their index is higher than 0.9.

Additionally, there is a relationship between the basis of the null space generated by each operating eigenvalue and their corresponding open-loop eigenvector. The inner product of the open-loop eigenvectors of the operating eigenvalues and their conjugates by the specific combination of the null space that results the zero gain matrix is a complex number which has an absolute value of one. This means that these two vectors are perfectly parallel in the sense of inner product. The closed-loop eigenvectors and the basis of the null space; however, do not show this relationship. In fact none of the closed-loop eigenvectors are orthogonal to the null space basis combination that leads to the zero gain matrix. The results are shown in Tables 4.7 - 4.9.

Table 4.5. Inner products of eigenvectors with themselves, case 2
Maximum amounts of the inner products are in red

		Case 2									
		Closed-loop eigenvectors									
		1	3	5	7	9	11	13	15	17	19
Closed-loop eigenvectors	1	1.0000	0.0739	0.0070	0.0878	0.0074	0.0764	0.0957	0.0544	0.0562	0.0764
	3	0.0739	1.0000	0.4137	0.1184	0.0186	0.1020	0.1087	0.0180	0.0436	0.0659
	5	0.0070	0.4137	1.0000	0.1413	0.0097	0.1245	0.1649	0.1313	0.1055	0.1487
	7	0.0878	0.1184	0.1413	1.0000	0.3486	0.4530	0.7255	0.4319	0.4969	0.5005
	9	0.0074	0.0186	0.0097	0.3486	1.0000	0.6032	0.2073	0.0502	0.0675	0.0915
	11	0.0764	0.1020	0.1245	0.4530	0.6032	1.0000	0.7495	0.3864	0.4587	0.4618
	13	0.0957	0.1087	0.1649	0.7255	0.2073	0.7495	1.0000	0.4794	0.6353	0.5243
	15	0.0544	0.0180	0.1313	0.4319	0.0502	0.3864	0.4794	1.0000	0.2691	0.4493
	17	0.0562	0.0436	0.1055	0.4969	0.0675	0.4587	0.6353	0.2691	1.0000	0.2796
	19	0.0764	0.0659	0.1487	0.5005	0.0915	0.4618	0.5243	0.4493	0.2796	1.0000
sum		1.5352	1.9628	2.2466	4.3039	2.404	4.4155	4.6906	3.27	3.4124	3.598
norm		1.0199	1.1044	1.1333	1.6058	1.2426	1.6539	1.7571	1.3649	1.4255	1.4350

Table 4.6. Inner products of eigenvectors with themselves, case 3
Maximum amounts of the inner products are in red

		Case 3									
		Closed-loop eigenvectors									
		1	3	5	7	9	11	13	15	17	19
Closed-loop eigenvectors	1	1.0000	0.1004	0.0100	0.1815	0.1184	0.1748	0.1726	0.0199	0.0930	0.1661
	3	0.1004	1.0000	0.6441	0.1519	0.2150	0.1800	0.1567	0.0193	0.1339	0.1811
	5	0.0100	0.6441	1.0000	0.4357	0.3865	0.4483	0.4251	0.0506	0.2579	0.4315
	7	0.1815	0.1519	0.4357	1.0000	0.6294	0.9542	0.9695	0.0505	0.6741	0.9574
	9	0.1184	0.2150	0.3865	0.6294	1.0000	0.6112	0.5925	0.0741	0.1916	0.5557
	11	0.1748	0.1800	0.4483	0.9542	0.6112	1.0000	0.9328	0.1624	0.7065	0.9526
	13	0.1726	0.1567	0.4251	0.9695	0.5925	0.9328	1.0000	0.1389	0.6764	0.9195
	15	0.0199	0.0193	0.0506	0.0505	0.0741	0.1624	0.1389	1.0000	0.0947	0.1555
	17	0.0930	0.1339	0.2579	0.6741	0.1916	0.7065	0.6764	0.0947	1.0000	0.7843
	19	0.1661	0.1811	0.4315	0.9574	0.5557	0.9526	0.9195	0.1555	0.7843	1.0000
sum		2.0367	2.7824	4.0897	6.0042	4.3744	6.1228	5.984	1.7659	4.6124	6.1037
norm		1.0743	1.2658	1.5463	2.2059	1.6374	2.2025	2.1721	1.0441	1.7790	2.2055

Table 4.7. Inner product of open-loop and closed-loop eigenvectors to $V_{12}^{1}\bar{U}_{3}^{1}$, corresponding to the first operating eigenvalue

Eigenvector number i	Open-loop eigenvector $\times V_{12}^{1}\bar{U}_{3}^{1}$	Absolute value	Closed-loop eigenvector $\times V_{12}^{1}\bar{U}_{3}^{1}$	Absolute value
1	-0.2649 + 0.9643i	1	-0.0622 + 0.2793i	0.2862
2	-0.2595 + 0.9397i	0.9749	0.0918 - 0.2837i	0.2981
3	0	0	-0.0260 + 0.0929i	0.0965
4	0	0	-0.0233 + 0.0848i	0.088
5	0	0	0.0050 - 0.0200i	0.0206
6	0	0	0.0057 - 0.0187i	0.0196
7	0	0	-0.0623 + 0.2212i	0.2298
8	0	0	-0.0573 + 0.2123i	0.2199
9	0	0	-0.0569 + 0.1816i	0.1903
10	0	0	-0.0426 + 0.1786i	0.1836
11	0	0	-0.0005 + 0.0372i	0.0372
12	0	0	-0.0181 + 0.0313i	0.0361
13	0	0	-0.1076 + 0.4637i	0.476
14	0	0	-0.1409 + 0.4410i	0.463
15	0	0	0.0190 + 0.0033i	0.0193
16	0	0	-0.0176 - 0.0067i	0.0188
17	0	0	-0.2190 - 0.4621i	0.5113
18	0	0	0.4137 - 0.2774i	0.4981
19	0	0	0.1351 - 0.0835i	0.1588
20	0	0	-0.0714 - 0.1373i	0.1548

Table 4.8. Inner product of open-loop and closed-loop eigenvectors to $V_{12}^2\bar{U}_3^2$, corresponding to the second operating eigenvalue

Eigenvector number i	Open-loop eigenvector $\times V_{12}^2\bar{U}_3^2$	Absolute value	Closed-loop eigenvector $\times V_{12}^2\bar{U}_3^2$	Absolute value
1	0	0	-0.0102 + 0.0156i	0.0187
2	0	0	-0.0094 + 0.0139i	0.0168
3	0.5500 - 0.8352i	1	-0.0274 + 0.0414i	0.0497
4	0.5365 - 0.8121i	0.9733	-0.0257 + 0.0391i	0.0468
5	0	0	-0.0111 + 0.0153i	0.0189
6	0	0	-0.0091 + 0.0154i	0.0179
7	0	0	0.1859 + 0.1203i	0.2214
8	0	0	-0.1792 - 0.1205i	0.2159
9	0	0	0.3636 - 0.7385i	0.8231
10	0	0	0.5216 - 0.6089i	0.8017
11	0	0	0.3385 - 0.6155i	0.7025
12	0	0	0.4210 - 0.5388i	0.6838
13	0	0	-0.1456 + 0.1265i	0.1929
14	0	0	-0.0572 + 0.1784i	0.1874
15	0	0	-0.0599 + 0.0800i	0.0999
16	0	0	-0.0481 + 0.0832i	0.0961
17	0	0	-0.0598 + 0.0260i	0.0652
18	0	0	-0.0003 + 0.0632i	0.0632
19	0	0	0.1077 - 0.1679i	0.1995
20	0	0	0.1082 - 0.1597i	0.1929

Table 4.9. Inner product of open-loop and closed-loop eigenvectors to $V_{12}^3 \bar{U}_3^3$, corresponding to the third operating eigenvalue.

Eigenvector number i	Open-loop eigenvector $\times V_{12}^3 \bar{U}_3^3$	Absolute value	Closed-loop eigenvector $\times V_{12}^3 \bar{U}_3^3$	Absolute value
1	0	0	-0.0041 + 0.0269i	0.0272
2	0	0	-0.0036 + 0.0240i	0.0243
3	0	0	0.0059 - 0.0275i	0.0281
4	0	0	0.0022 - 0.0263i	0.0264
5	0.1454 - 0.9894i	1	-0.0111 + 0.0735i	0.0744
6	0.1426 - 0.9598i	0.9703	-0.0101 + 0.0694i	0.0701
7	0	0	-0.2100 + 0.3877i	0.4409
8	0	0	0.0865 + 0.4205i	0.4293
9	0	0	-0.0902 + 0.4759i	0.4844
10	0	0	-0.0498 + 0.4685i	0.4711
11	0	0	-0.2261 - 0.1244i	0.2581
12	0	0	0.2453 - 0.0522i	0.2508
13	0	0	-0.0115 - 0.0011i	0.0116
14	0	0	0.0110 + 0.0022i	0.0112
15	0	0	-0.0317 + 0.1172i	0.1214
16	0	0	-0.0034 + 0.1165i	0.1165
17	0	0	-0.0297 + 0.3497i	0.351
18	0	0	-0.0703 + 0.3321i	0.3395
19	0	0	-0.0518 + 0.1120i	0.1234
20	0	0	0.0166 + 0.1179i	0.1191

4.3.1 Eigenvectors and eigenvalues specifications associated with stable and unstable closed-loop systems

Eigenvalues for the 3 cases are presented in Table 4.10. Eigenvalues 7 and 8 for case 3 have a positive real value which means the controlled system is unstable. The distributions of the poles for all the cases are illustrated in Figures 4.14 and 4.15. Also eigenvectors 11 and 13 for both cases 2 and 3 have been plotted in Figures 4.16 and 4.17. Inner product of these eigenvectors for case 2 is 0.7495 and for case 3 is 0.9328, which obviously means that they are far from being orthogonal, especially in case 3. It can be seen in Figure 4.16 that the elements of the eigenvectors that have larger values, have different signs for both real and imaginary parts. This reduces the value of the inner product of two eigenvectors since the product of the two large elements almost cancel each other out. On the other hand, it can be seen from Figure 4.17 that larger elements of eigenvectors 11 and 13 have the same sign both for real and imaginary parts. This increases the value of the inner product of the two eigenvectors. It is interesting to note that the largest elements of the eigenvectors are the elements corresponding to the location of the actuators.

Table 4.10. Eigenvalues of the systems in case 1, case 2 , and case 3

	Open-loop/ case 1	Case 2	Case 3
1	-0.4919 - 8.8396i	-0.1203 - 2.1557i	-0.1248 - 2.2409i
2	-0.4919 + 8.8396i	-0.1203 + 2.1557i	-0.1248 + 2.2409i
3	-0.4683 - 8.5692i	-0.1572 - 3.8638i	-0.1656 - 3.9605i
4	-0.4683 + 8.5692i	-0.1572 + 3.8638i	-0.1656 + 3.9605i
5	-0.4310 - 8.1246i	-0.1759 - 4.1781i	-0.1961 - 4.3655i
6	-0.4310 + 8.1246i	-0.1759 + 4.1781i	-0.1961 + 4.3655i
7	-0.3831 - 7.5146i	-0.6471 - 9.1125i	0.3819 - 9.3124i
8	-0.3831 + 7.5146i	-0.6471 + 9.1125i	0.3819 + 9.3124i
9	-0.3285 - 6.7516i	-0.4369 - 8.8223i	-0.2963 - 6.2233i
10	-0.3285 + 6.7516i	-0.4369 + 8.8223i	-0.2963 + 6.2233i
11	-0.2715 - 5.8510i	-0.4146 - 8.6097i	-1.1801 - 7.9088i
12	-0.2715 + 5.8510i	-0.4146 + 8.6097i	-1.1801 + 7.9088i
13	-0.2169 - 4.8308i	-0.2622 - 8.0067i	-0.4191 - 8.8335i
14	-0.2169 + 4.8308i	-0.2622 + 8.0067i	-0.4191 + 8.8335i
15	-0.1690 - 3.7117i	-0.2428 - 5.9611i	-0.4602 - 8.5760i
16	-0.1690 + 3.7117i	-0.2428 + 5.9611i	-0.4602 + 8.5760i
17	-0.1317 - 2.5164i	-0.3002 - 7.3360i	-0.2954 - 7.1851i
18	-0.1317 + 2.5164i	-0.3002 + 7.3360i	-0.2954 + 7.1851i
19	-0.1081 - 1.2683i	-0.2428 - 6.9540i	-0.2445 - 7.9317i
20	-0.1081 + 1.2683i	-0.2428 + 6.9540i	-0.2445 + 7.9317i

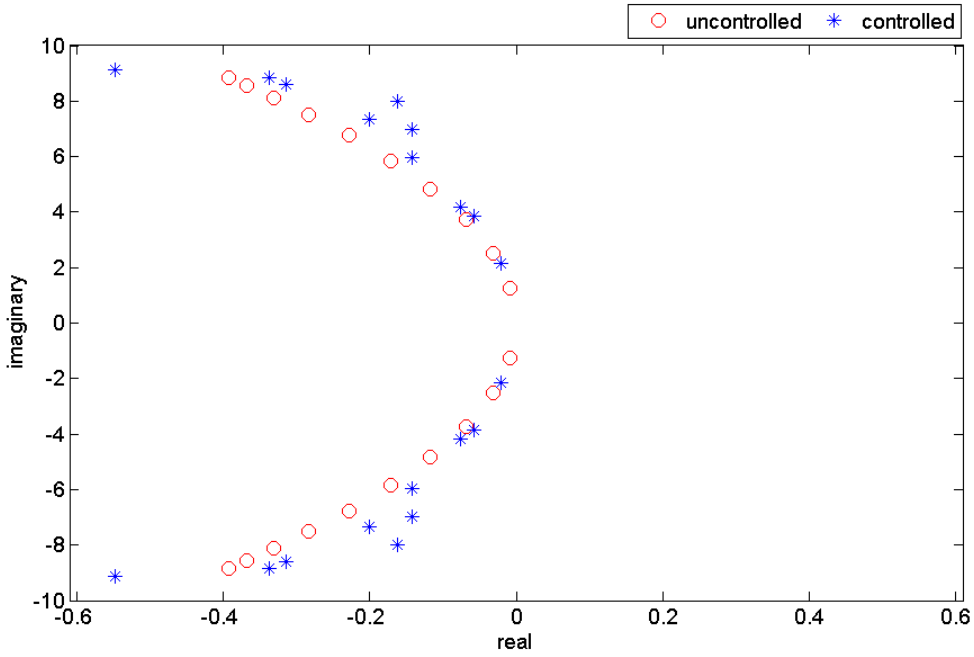

Figure 4.14. Closed-loop poles of case 2

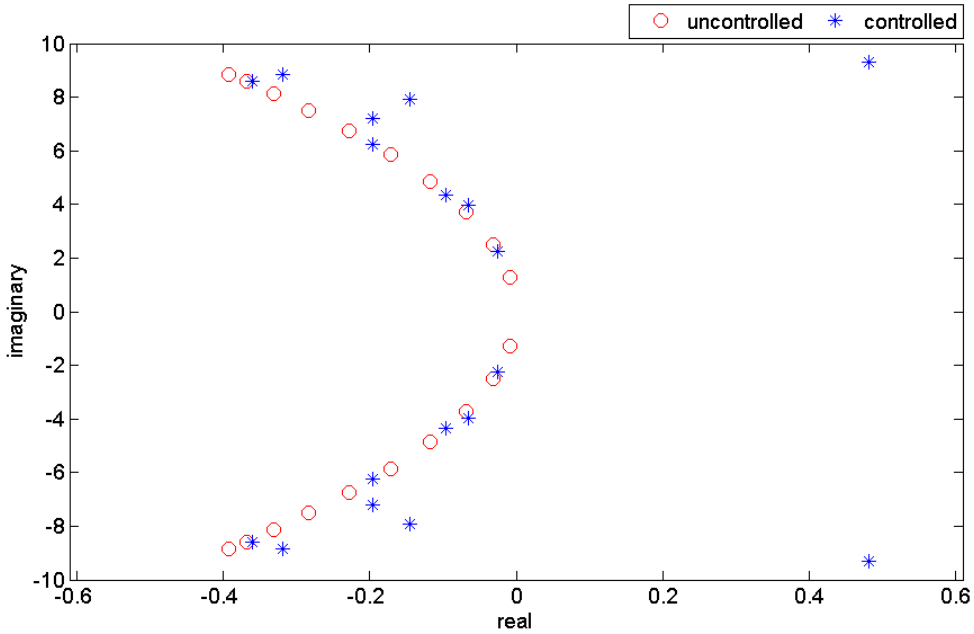

Figure 4.15. Closed-loop poles of case 3

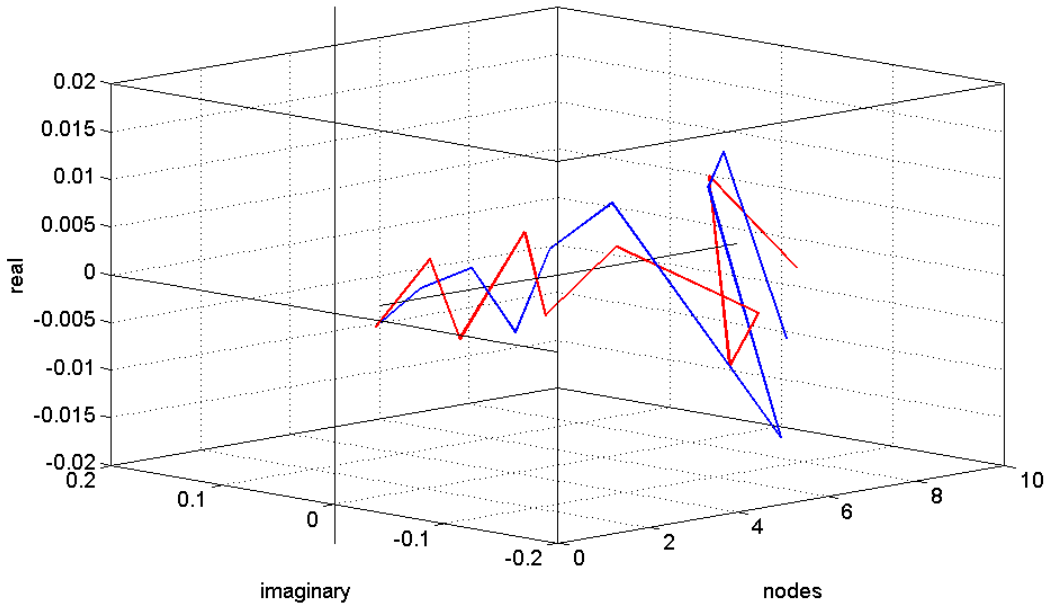

Figure 4.16. Closed-loop eigenvectors 11 and 13 for case 2

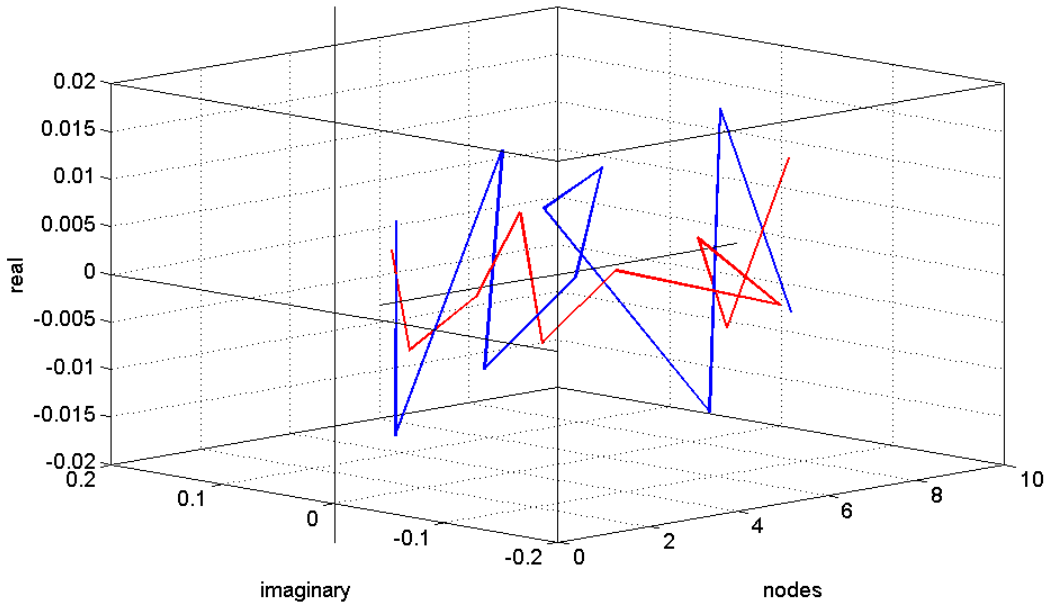

Figure 4.17. Closed-loop eigenvectors 11 and 13 for case 3

4.4. Notes on the number of the pairs of collocated actuators and sensors

The system shown in Figure 4.1 is considered in three different configurations. Case 1, has two actuators located on masses 6 and 7; case 2 has 3 actuators located on masses 6, 7 and 8 and finally case 3 has 4 actuators on masses 6, 7, 8 , and 9. The objective of this comparison is to determine the effect of the number of actuators on a system that its state matrix is tri-diagonal.

Considering an impulse input at mass 10, the results for the vibration displacements at mass 1 are shown on Figure 4.18. In case 1 the operating eigenvalues are 1 and 3, the operating eigenvalues in case 2 are 1, 3, and 5, and for case 3 the operating eigenvalues are 1, 3, 5, and 7. For case 1, U_2^1 and U_1^2 have generated the most desirable result. For case 2, the result is generated by U_2^1, U_1^2, and U_1^3. Also, for case 3, the result is generated by U_2^1, U_3^2, U_1^3, and U_3^4. It is seen that the amplitude of vibration for m_1 is reduced in case 1 by 67.16%. For cases 2 and 3 the reductions are 88.06% and 92.54%, respectively. Considering the fact that the state matrix of the model is tri-diagonal, it can be seen that if the number of actuators are more than 3, amplitude of vibration reduces drastically. The reduction of the amplitude for the case with 4 actuators might not worth the cost. Table 4.11 shows the amplitude reductions for all the states for the three cases. Commonly, the amplitude of vibrations in the isolated areas has been reduced, while in the confined area have been increased. Figure 4.19 presents the phase portraits of m_1 for open-loop and all three cases with different numbers of actuators. It can be seen that reduction in the amplitude of vibration from case 3 to case 4 is negligible, due to small changes in the value of their overshoots.

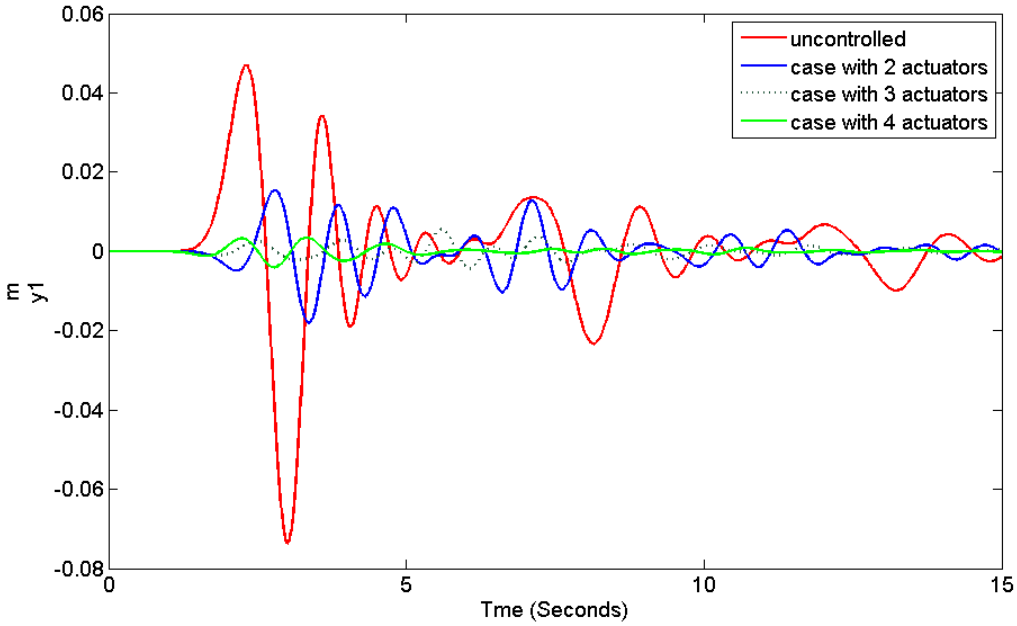

Figure 4.18. Comparison of displacements of m_1

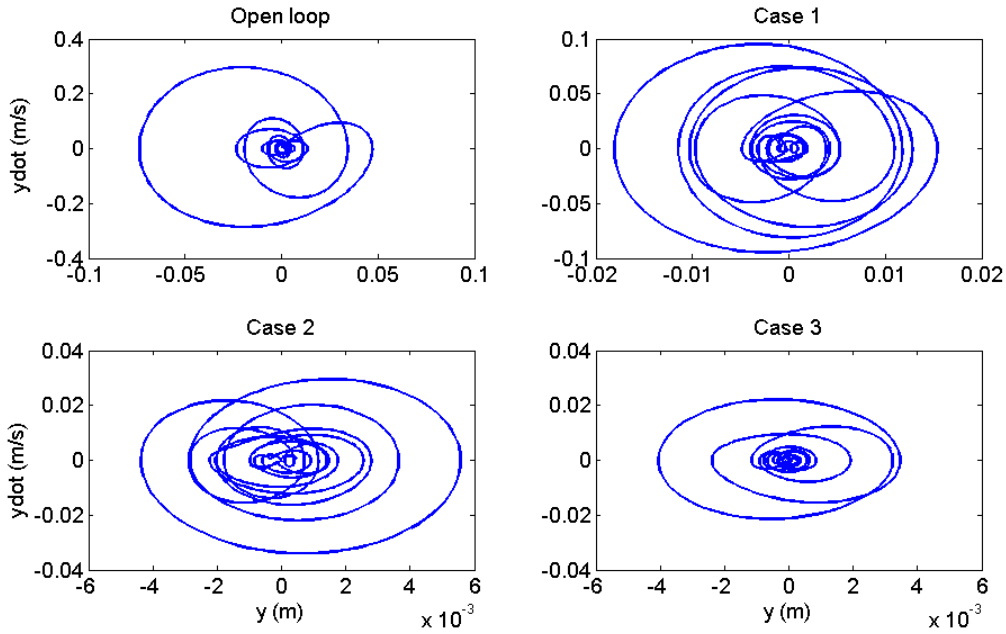

Figure 4.19. Phase plan associated with the vibration of m_1 for different number of inputs (Note: The scales are different)

Table 4.11. Maximum values of states in case 1, case 2 , and case 3 in comparison to open-loop values and their relative reduction percentages

state	open-loop	case 1	reduction percentage	case 2	reduction percentage	case 3	reduction percentage
1	0.0469	0.0154	67.16	0.0056	88.06	0.0035	92.54
2	0.0681	0.0162	76.21	0.0046	93.25	0.0031	95.45
3	0.0745	0.0147	80.27	0.0038	94.90	0.0029	96.11
4	0.0795	0.016	79.87	0.0058	92.70	0.0034	95.72
5	0.0851	0.0181	78.73	0.0065	92.36	0.004	95.30
6	0.0918	0.0208	77.34	0.0074	91.94	0.005	94.55
7	0.0998	0.0653	34.57	0.0738	26.05	0.0107	89.28
8	0.1101	0.1088	1.18	0.0673	38.87	0.0076	93.10
9	0.1244	0.1244	0.00	0.1234	0.80	0.0868	30.23
10	0.1504	0.1504	0.00	0.1504	0.00	0.1502	0.13
11	0.2966	0.0951	67.94	0.0295	90.05	0.0221	92.55
12	0.1433	0.0581	59.46	0.0314	78.09	0.0131	90.86
13	0.2147	0.0784	63.48	0.0303	85.89	0.0145	93.25
14	0.1653	0.0788	52.33	0.0396	76.04	0.0177	89.29
15	0.1869	0.0865	53.72	0.0544	70.89	0.0228	87.80
16	0.215	0.1019	52.60	0.0562	73.86	0.0316	85.30
17	0.2535	0.5107	-101.46	0.5487	-116.45	0.077	69.63
18	0.3116	0.3106	0.32	0.5269	-69.09	0.0509	83.66
19	0.4175	0.4175	0.00	0.417	0.12	0.5642	-35.14
20	1	1	0.00	1	0.00	1	0.00

Actuators' force of cases 1, 2, and 3 are presented in Figure 4.20. The results show that the two actuators which are closer to the disturbance apply more force in order to confine the vibration to the required area. Also it can be seen that between the two adjacent actuators to the disturbance, it is not necessary for the closer actuator to apply higher forces to the system. Table 4.12 presents the maximum force of the actuators for cases 1, 2, and 3.

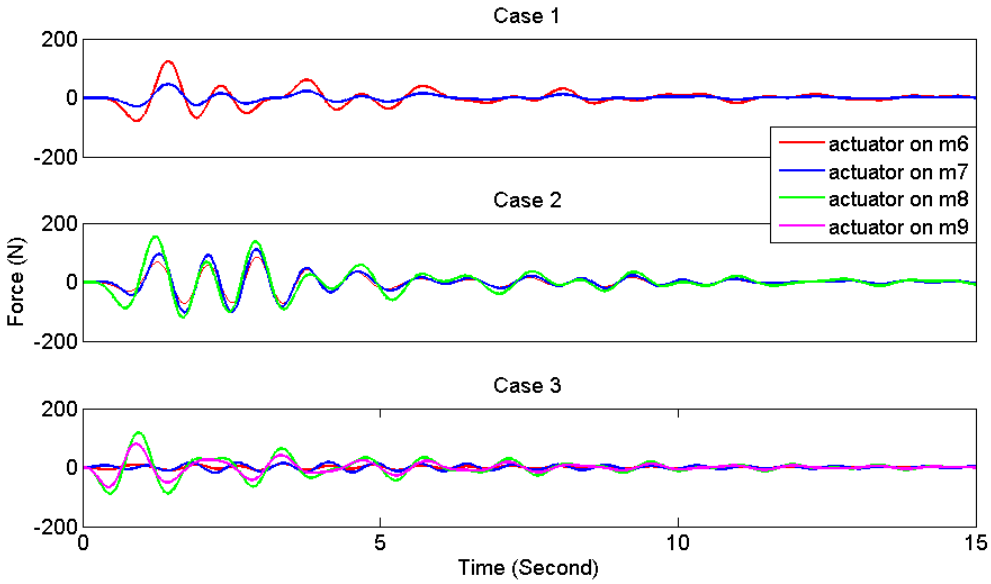

Figure 4.20. Actuator forces of the closed-loop systems with different numbers of inputs

Table 4.12. Maximum actuator forces (N) on different nodes for case 1, case 2 and case 3

node	case 1	case 2	case 3
6	123.02	84.86	12.44
7	45.86	111.16	17.64
8	-	154.06	118.11
9	-	-	80.25

Figure 4.21 shows the distribution of the closed-loop eigenvalues for the three cases. It is seen that the eigenvalues of the different cases are not related. Since in the case 2, U_2^1 is used as the coefficients of the null space associated with its first operative eigenvalue, its first two closed-loop eigenvalues remain intact.

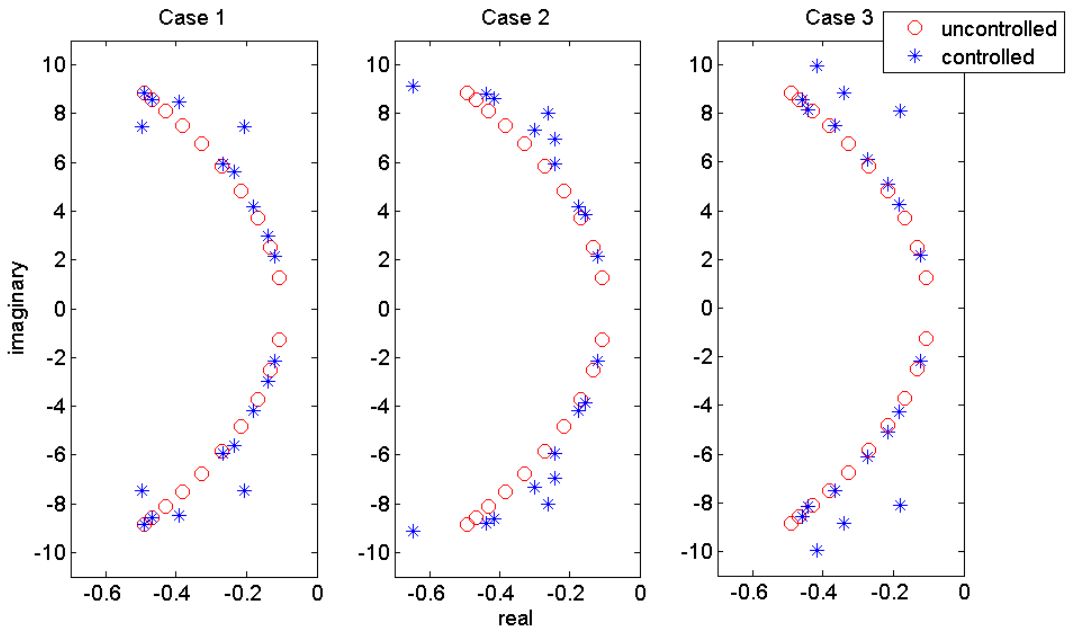

Figure 4.21. Eigenvalues of the closed-loop systems with different number of inputs

4.5. Progressive application of orthogonal eigenstructure control

Orthogonal eigenstructure control of systems result in $m^m - 1$ closed-loop systems and the designer should identify the most desirable one from this set. The advantage of the orthogonal eigenstructure control over other eigenstructure assignment techniques as well as classical pole placement is its independent of the designer. There is no need to define a desirable closed-loop eigenvector or the location for the dominant poles of the system. There are; however, some closed-loop systems as the result of the orthogonal eigenstructure control that are not stable. In this article, it is shown how orthogonal eigenstructure control can be applied progressively to a stable system expecting that the unstable result to converge to stable and desirable ones.

As an example, the system shown in Figure 4.1 is considered. It is assumed that there are three control actuators on m_6, m_7, and m_8. An impulse input is applied at m_{10}. Applying orthogonal eigenstructure control shows that $r^1 = \bar{U}_2^1$, $r^2 = \bar{U}_1^2$, and $r^3 = \bar{U}_1^3$, generates the most desirable vibration suppression, and $r^1 = \bar{U}_1^1$, $r^2 = \bar{U}_2^2$, and $r^3 = \bar{U}_1^3$ leads to an unstable closed-loop system. The latter case is considered for progressive

application of the orthogonal eigenstructure control, and the result is compared to the most desirable solution of control application at step 1 that is $r^1 = \bar{U}_2^1$, $r^2 = \bar{U}_1^2$, and $r^3 = \bar{U}_1^3$.

The control gain associate with the step 1 is

$$K_1 = 1.0 \times 10^3 \begin{bmatrix} -3.141 & -0.759 & 0.070 \\ -10.380 & -0.362 & -2.190 \\ -3.119 & -0.617 & -1.194 \end{bmatrix}$$

The state matrix of the closed-loop system is defined as $A_c = A + BK_1C$. If the orthogonal eigenstructure control is applied to the newly found system, it yields

$$A_c = A + BK_1C + BK_2C \tag{4.10}$$

where

$$K_2 = 1.0 \times 10^3 \begin{bmatrix} -0.2444 & 0.0352 & 0.0858 \\ 9.0677 & -1.6441 & 1.1465 \\ 5.7022 & -0.2108 & -0.0172 \end{bmatrix}$$

It implies that the appropriate control gain is the progressive summation of the gain matrices of the intermediate steps;

$$A_c = A + B(K_1 + K_2)C = A + BKC \tag{4.11}$$

Therefore,

$$K = K_1 + K_2 = 1.0 \times 10^3 \begin{bmatrix} -0.5585 & -0.0407 & 0.0928 \\ 8.0297 & -1.6803 & 0.9275 \\ 5.3903 & -0.2725 & -0.1366 \end{bmatrix}$$

Figure 4.22 depicts the eigenvalues of the open-loop system, closed-loop system resulted in step1, and the closed-loop after using the orthogonal eigenstructure control. If the gain matrix K that was determined earlier is used, then the open-loop system will directly be transferred to the final closed-loop system of step 2. A comparison between the vibration at m_1 for the unstable closed-loop system of step1, the stable closed-loop system of step 2, and the most desirable closed-loop of step 1 has been shown in Figure 4.23. The closed-loop system of step 2 suppresses the vibrations slightly better than the most desirable closed-loop system of step 1. If the open-loop eigenvalues that are close to the origin are used, more unstable closed-loop systems will be resulted in comparison to the cases when the operating eigenvalues are far from the origin. The progressive application of orthogonal eigenstructure control allows for a simpler application of the orthogonal eigenstructure control.

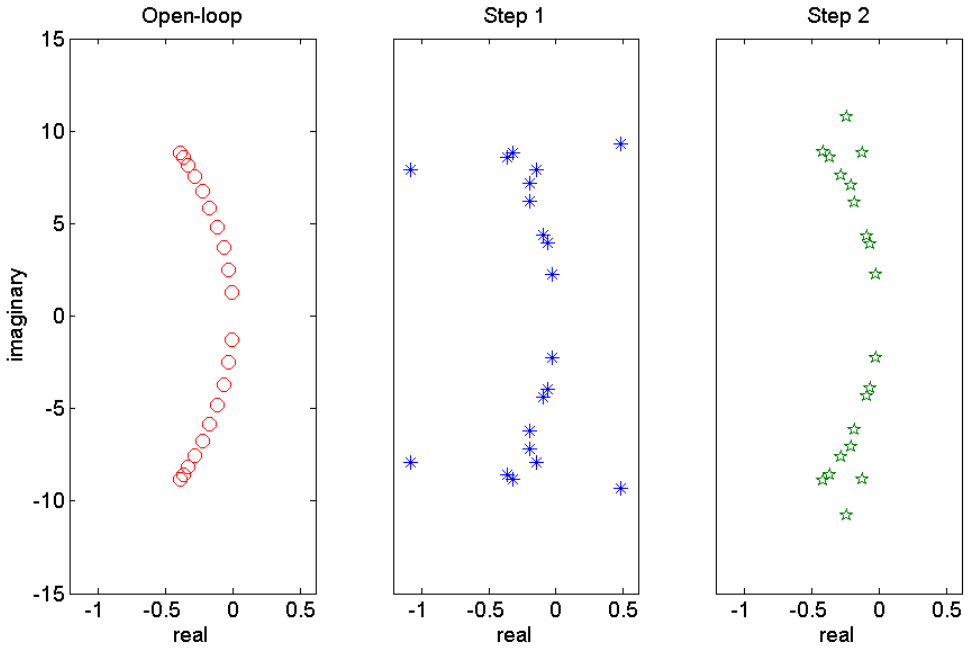

Figure 4.22. Eigenvalues of the open-loop system and closed-loop at steps 1 and 2 of the progressive application of the control

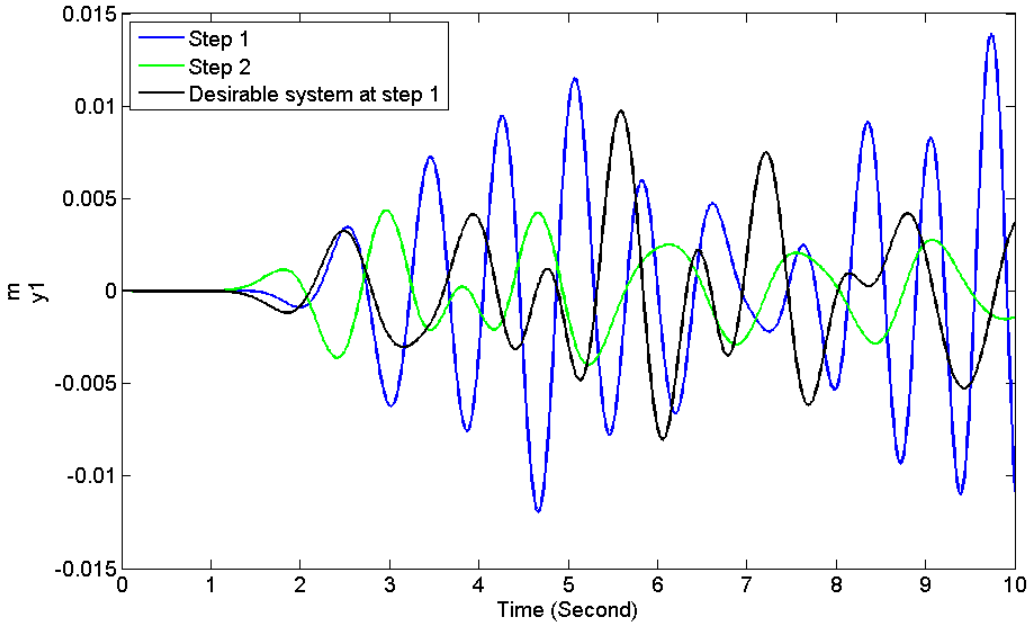

Figure 4.23. Time histories of the vibrations at m_1 comparing the an unstable closed-loop system at step 1,the most desirable closed-loop system at step1 and a desirable closed-loop system at step 2

Figure 4.24 illustrates the progressive application of orthogonal eigenstructure control. Figure 4.24a shows that each open-loop eigenvalue is the intersection of the open-loop eigenvector set and the achievable eigenvector set of the closed-loop system. Depending on the number of pairs of actuators and sensors m, orthogonal eigenstructure control finds $m-1$ orthogonal vectors within the achievable eigenvector set for each open-loop eigenvector. If the closed-loop systems do not include a desirable one, one of the closed-loop systems is chosen as shown in Figure 4.24b. This system is considered as a new system that needs to be controlled, and orthogonal eigenstructure control is applied for the second time as shown in Figure 4.24c. $m-1$ orthogonal vectors to the eigenvectors of the new system is found that are within the achievable eigenvector set. Finally, a desirable solution may be found as shown in Figure 4.24d. This procedure can be applied to the system several times; increasing the number of closed-loop systems unboundedly. As a result, the limitation on the number of the closed-loop systems is eliminated.

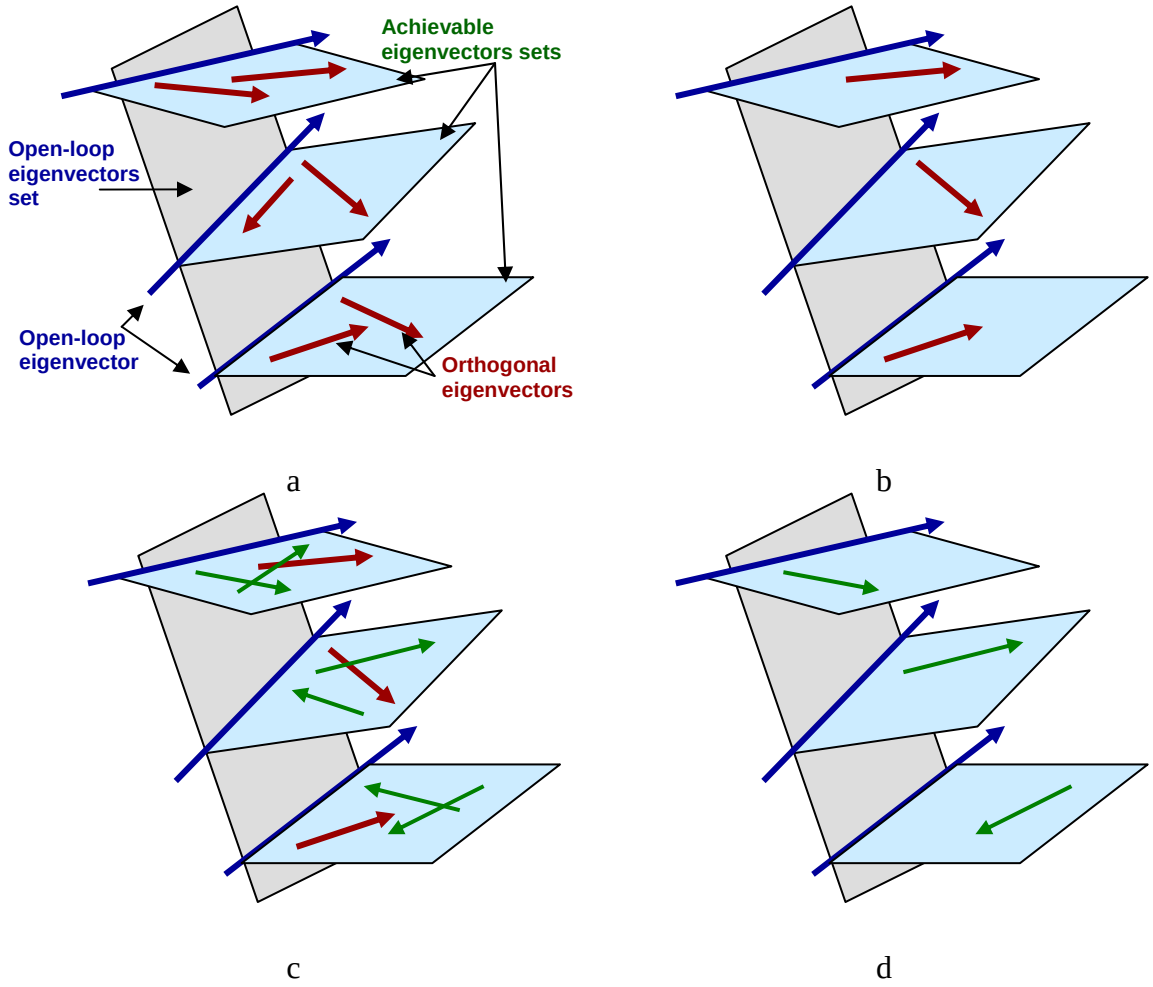

Figure 4.24. Schematics of progressive application of orthogonal eigenstructure control

The reason that some of the closed-loop systems are unstable is the effect of the control gain matrix. Even though the goal of orthogonal eigenstructure control is to orthogonalize some of the eigenvectors, it slightly changes the other eigenvectors of the system. If the eigenvectors of the system changes in such a way that two or more pairs of eigenvectors become parallel in the sense that their inner product becomes unity or close to unity, the state matrix becomes deficient [83].

Eigenvalues of the closed-loop and open-loop systems are presented in Table 4.13. The eigenvalue associated with mode 7 is the unstable eigenvalue and the eigenvalue associated with the mode 11 is the eigenvalue that is moved away from the cluster of the eigenvalues. The mid-point of these two extreme eigenvalues can be determined as -0.2988 + 8.6172i. It is interesting to observe that this value is very close to the open-loop

eigenvalue of mode 7, which is moved to the right half plane. The closed-loop system is deficient because the product of the eigenvectors associated with modes 7 and 11 is 0.9541 + 0.0147i. The magnitude of this product is 0.9542 indicating two parallel eigenvectors within the system.

Table 4.13. Eigenvalues of the open-loop and closed-loop systems

	Open-loop eigenvalues	Closed-loop eigenvalues
1	-0.3919 + 8.8446i	-0.0248 + 2.2443i
2	-0.3919 - 8.8446i	-0.0248 - 2.2443i
3	-0.3683 + 8.5741i	-0.0656 + 3.9637i
4	-0.3683 - 8.5741i	-0.0656 - 3.9637i
5	-0.3310 + 8.1293i	-0.0961 + 4.3690i
6	-0.3310 - 8.1293i	-0.0961 - 4.3690i
7	-0.2831 + 7.5191i	0.4817 + 9.3193i
8	-0.2831 - 7.5191i	0.4817 - 9.3193i
9	-0.2285 + 6.7558i	-0.1962 + 6.2273i
10	-0.2285 - 6.7558i	-0.1962 - 6.2273i
11	-0.1715 + 5.8547i	-1.0794 + 7.9150i
12	-0.1715 - 5.8547i	-1.0794 - 7.9150i
13	-0.1169 + 4.8342i	-0.3191 + 8.8388i
14	-0.1169 - 4.8342i	-0.3191 - 8.8388i
15	-0.0690 + 3.7149i	-0.3602 + 8.5809i
16	-0.0690 - 3.7149i	-0.3602 - 8.5809i
17	-0.0317 + 2.5197i	-0.1957 + 7.1891i
18	-0.0317 - 2.5197i	-0.1957 - 7.1891i
19	-0.0081 + 1.2729i	-0.1448 + 7.9367i
20	-0.0081 - 1.2729i	-0.1448 - 7.9367i

4.6. Summary

Orthogonal eigenstructure control is a feedback control that can be applied to the linear systems. Singular value decomposition is used to find the basis of the null space corresponding to each operating eigenvalue. The application of the control method to the systems with collocated actuators and sensors has been presented in this dissertation so far.

This method eliminates the need for defining the desired eigenvectors. Desired eigenvectors usually are not usually achievable that leads to some algorithmic error.

Moreover, defining of the desired eigenvectors is a difficult task that is based on trial and error with complicated considerations for observing the smoothness in their shaping. This new method provides control gain matrix to shape the eigenvectors of the system into achievable ones. This way the task of defining desired eigenvectors which is called “the design freedom” is eliminated and the smallest phase plane for some nodes in the isolated area can be used as criteria for the desirable result.

Possibility of smaller actuator forces is another common outcome of this new method, since this method neither require the closed-loop eigenvalues to be the same as open-loop ones nor specifies their locations. As a result, the eigenvalues and corresponding eigenvectors are consistent. Since the actuators and sensors are collocated, the closed-loop and open-loop state matrices have equal traces. As a result this method keeps the average of the closed-loop eigenvalues the same as open-loop ones. The closed loop eigenvalues are moved by the algorithm in order to meet the eigenvectors considerations.

Progressive application of orthogonal eigenstructure control, broaden the set of the closed-loop systems unboundedly. This technique, transfers the unstable closed-loop systems to desirable systems. Because of the linearity, the final control gain matrix is the summation of the control gain matrices of the intermediate steps.

Chapter 5

Discrete Systems: Non-collocated Actuators and Sensors

A reality of practical application of control systems is the failure of sensors and actuators. The ability of the closed-loop system to continue to perform satisfactorily in the event of a failure is critical to the practical value of the controller. Another important practical aspect of the control method is the robustness of the controller in the case of actuator or sensor failure. In this task, the knowledge about the overlap between achievable eigenvector sets associated with different number of actuators needs to be developed. Therefore, to design a fail-safe control law, we need to be able to design the control for non-collocated actuators and sensors, or control systems with different number of actuators and sensors. This part of the proposed study addresses the need for a method that is independent of the placement or numbers of actuators and sensors and continues to perform robustly in the presence of sensor or actuator failure.

An orthogonal eigenstructure control method with collocated actuators and sensors was explained in chapter 4. To address the issue of components failure that happens in practical applications, the application of the method is extended to non-collocated actuators and sensors, including cases that have different number of actuators and sensors. To design a fail-safe control law, designing a controller for the cases that the actuators and sensors are not collocated is helpful. Also, for application of orthogonal eigenstructure control as a general control methodology, it is necessary to consider the systems that may not have equal number of actuators and sensors. The proposed method is based on adding virtual actuators and sensors to the closed-loop system in order to extend the application of the orthogonal eigenstructure control to systems with non-collocated actuators and sensors as well as the systems with different numbers of actuators and sensors.

Using the discrete system shown in Figure (4.1), the cases that will be discussed next include: 1) equal numbers of non-collocated actuators and sensors, 2) fewer actuators than sensors, and 3) fewer sensors than actuators. The disturbance source is maintained as a unit impulse on m_{10}. A procedure for applying the orthogonal eigenstructure control to the systems with no restrictions on the location and number of the actuators and sensors is presented.

5.1. Equal number of actuators and sensors

Replacing the gain matrix K in Equation (3.51) from Equation (3.50) yields

$$A_c = A + \Delta = A + BW(CV)^{-1}C \tag{5.1}$$

where

$$\Delta = BKC = BW(CV)^{-1}C \tag{5.2}$$

If the closed-loop system is a full state feedback, then C and V are square matrices. Therefore,

$$\Delta = BW(CV)^{-1}C = BWV^{-1}C^{-1}C = BWV^{-1}\ , \tag{5.3}$$

which shows the full-state feedback system is independent of C.

The necessary condition for a square CV matrix is having equal number of sensors and actuators. If the number of actuators and sensors are different, CV is a non-square matrix and Equation (3.50) cannot be used for finding the gain matrix. In Equation (5.1), $(CV)^{-1}$ exists if CV is a square and nonsingular matrix, which requires C to be a full-rank matrix since V is generally a full-rank matrix. This implies that it is not necessary that actuators and sensors be collocated, as long as $(CV)^{-1}$ exist.

Now, as an example, let's consider the system of Figure 4.1 when the actuators are located on m_{5-7} and the sensors are placed on m_{4-6}, implying that two of the actuators and sensors are collocated and one is not. The procedure for finding the gain matrix is similar to the earlier example of collocated actuators and sensors. The orthogonal eigenstructure control results in $r^1 = \bar{U}_1^1$, $r^2 = \bar{U}_1^2$, and $r^3 = \bar{U}_2^3$ as the coefficient vectors that are needed to find the gain matrix. For this case, the non-zero elements of B and C matrices are

$$B(15,1) = B(16,2) = B(17,3) = -1/50$$

$$C(1,4) = C(2,5) = C(3,6) = 1$$

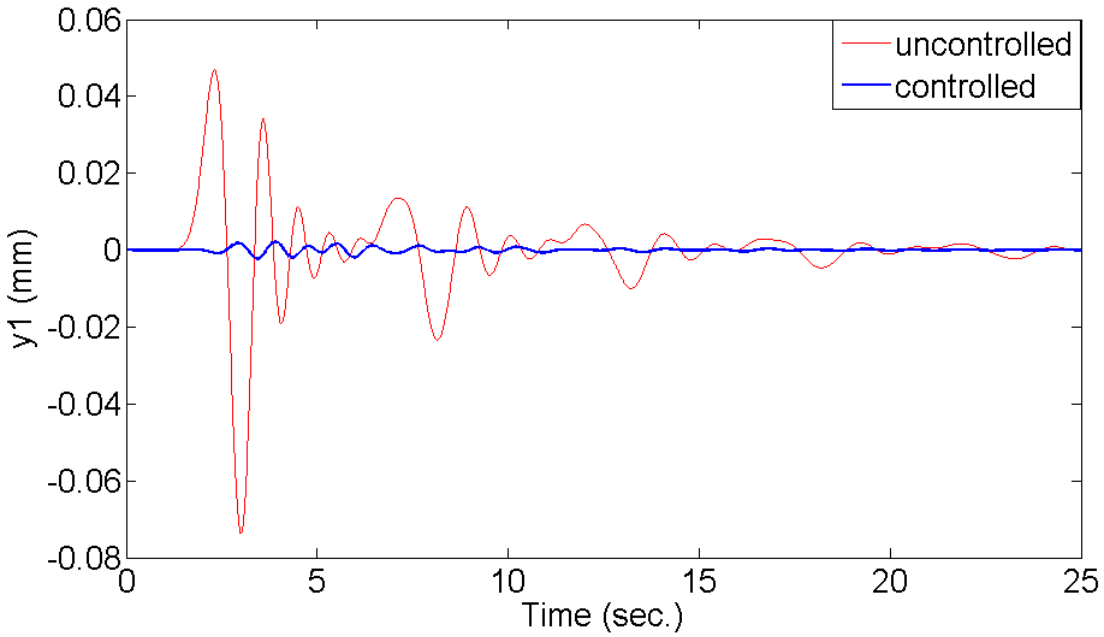

Figure 5.1. Displacement of mass 1 (m_1) due to a unit impulse at m_{10} , non-collocated actuators and sensors

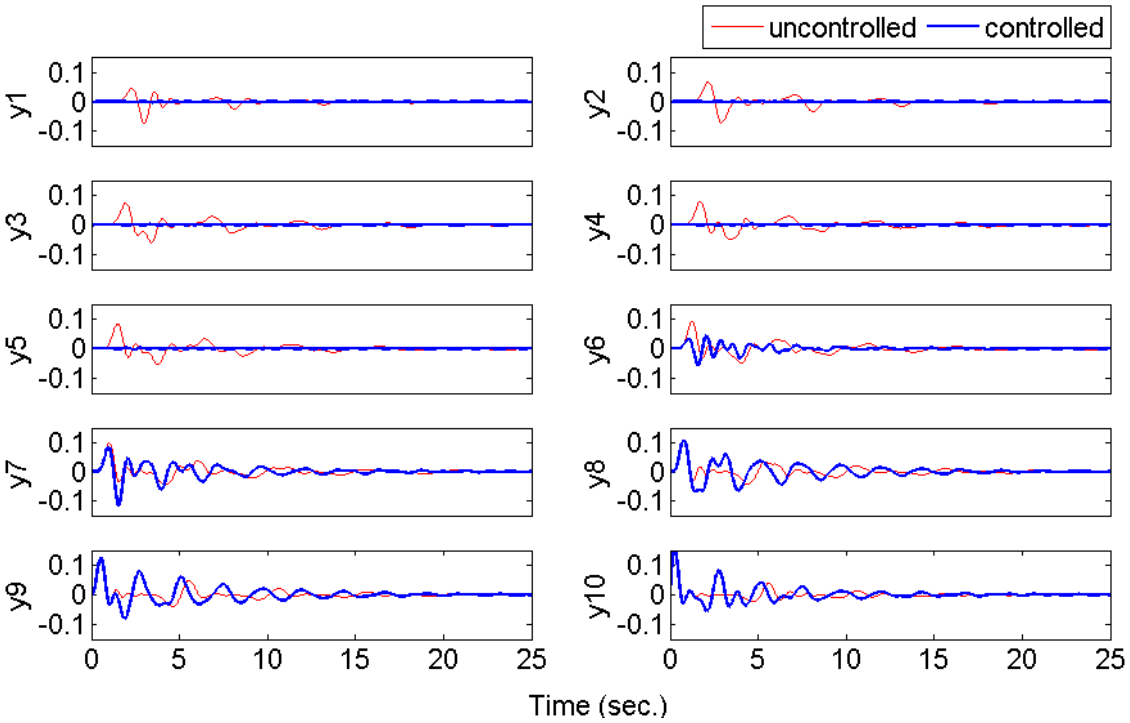

Figure 5.2. Displacement of masses due to a unit impulse at m_{10}, with non-collocated actuators and sensors

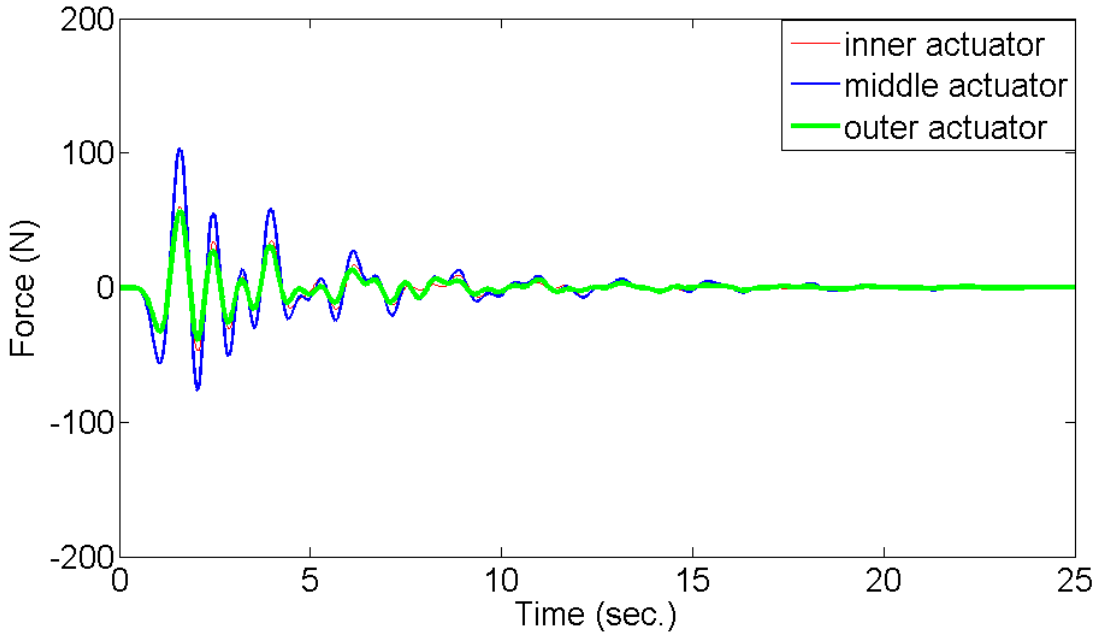

Figure 5.3. Actuation forces for the system with non-collocated actuators and sensors

The displacement of m_1 and all the masses of the system are presented in Figures 5.1 and 5.2 , respectively. Significant isolation can be seen at the isolated region that includes m_{1-4}. m_{5-7} are located in transient region and show both isolated and confined behavior, similar to the problem with collocated actuators and sensors. m_{8-10} are in confined region and show that their amplitude of vibrations have not changed significantly. Figure 5.3 shows the control forces. The maximum control force at the inner, middle, and outer actuators are 60.3, 103.1, and 56.8 N, respectively. It can be seen that the actuation force of the inner and outer actuators are very close to each other. The significant reduction in the displacements at the isolated region indicates the applicability of the method does regardless of the locations of the actuators and sensors.

5.2. More sensors than actuators

When the number of sensors is more than the number of actuators, the orthogonal eigenstructure control is still able to suppress the vibrations at the intended isolation region. In this case, the number of rows of C becomes more than the number of columns of B. Since the number of columns of V is equal to the number of columns of B, CV is non-square and Equation (3.50) cannot be used directly.

To overcome this issue, the idea of virtual elements is proposed. In this case, virtual actuators are added to the system model in order to have equal number of actuators and sensors. The elements of B associated with the virtual actuators are non-zero numbers, with the simplest choice being unity, which is what is used for this example. As shown in the previous example, regardless of the collocation of the actuators and sensors, Equation (3.50) can be used to find the gain matrix when the numbers of actuators and sensors are equal. It can be shown that if the rows of the gain matrix associated with the virtual actuators are set to zero, the closed-loop eigenvectors are within the achievable eigenvector set.

To show that the closed-loop eigenvectors belong to the achievable eigenvector set, an example of a system with equal number of actuators and sensors is considered for

instance, and the result of eliminating one of the actuators is discussed. A system of 10 masses similar to system of Figure 4.1 with actuators located on m_{6-7} and sensors placed on m_{6-8} is considered. A virtual actuator is added to m_8. The elements of the added column of B are zero, except for the element corresponding to the virtual actuator that is assigned to be unity. Therefore, the non-zero elements of B and C are

$$B(16,1) = B(17,2) = B(18,3) = -1/50$$

$$C(1,6) = C(2,7) = C(3,8) = 1$$

The vibration of masses and the force at different actuators due to unit impulse disturbance to m_{10} are presented in Figures 5.2 and 5.3, respectively.

Following the same procedure as the earlier example, we have

$$V_{22}^{1\,*} V_{22}^{1} = \bar{U}^{1} \bar{\Lambda}^{1} \bar{U}^{1*}$$

$$= \begin{bmatrix} 0.5872 & 0.3785 & -0.3135 \\ 0.3793 & 0.6521 & 0.2881 \\ -0.3151 & 0.2890 & 0.7606 \end{bmatrix} \begin{bmatrix} 0.5872 & 0.3793 & -0.3151 \\ 0.3785 & 0.6521 & 0.2890 \\ -0.3135 & 0.2881 & 0.7606 \end{bmatrix} = \begin{bmatrix} 0.5872 & 0.3793 & -0.3151 \\ 0.3785 & 0.6521 & 0.2890 \\ -0.3135 & 0.2881 & 0.7606 \end{bmatrix}$$

$$= \begin{bmatrix} 0.6431 & -0.6692 & 0.3723 \\ -0.5898 & -0.1228 & 0.7982 \\ 0.4884 & 0.7329 & 0.4737 \end{bmatrix} \begin{bmatrix} 0 & 0 & 0 \\ 0 & 1 & 0 \\ 0 & 0 & 1 \end{bmatrix} \begin{bmatrix} 0.6431 & -0.5898 & 0.4884 \\ -0.6692 & -0.1228 & 0.7329 \\ 0.3723 & 0.7982 & 0.4737 \end{bmatrix}$$

The open loop system can be regenerated using the eigenvectors associated with zero eigenvalues of $V_{12}^{i\,*} V_{12}^{i}$. Therefore,

$$V_{22}^{1} \bar{U}^{1} = \bar{\lambda}^{1} \bar{U}^{1}$$

$$= \begin{bmatrix} 0.5872 & 0.3793 & -0.3151 \\ 0.3785 & 0.6521 & 0.2890 \\ -0.3135 & 0.2881 & 0.7606 \end{bmatrix} \begin{bmatrix} 0.6431 \\ -0.5898 \\ 0.4884 \end{bmatrix} = (0) \begin{bmatrix} 0.6431 \\ -0.5898 \\ 0.4884 \end{bmatrix} = \begin{bmatrix} 0 \\ 0 \\ 0 \end{bmatrix}$$

The third row of the V_{22}^1 is set to zero and the new matrix is called $\widehat{V}_{22}^1$.

$$\widehat{V}_{22}^{1\,*}\widehat{V}_{22}^1 = \widehat{U}^1\widehat{\Lambda}^1\widehat{U}^{1*}$$

$$= \begin{bmatrix} 0.5872 & 0.3785 & 0 \\ 0.3793 & 0.6521 & 0 \\ -0.3151 & 0.2890 & 0 \end{bmatrix}\begin{bmatrix} 0.5872 & 0.3793 & -0.3151 \\ 0.3785 & 0.6521 & 0.2890 \\ 0 & 0 & 0 \end{bmatrix} = \begin{bmatrix} 0.4881 & 0.4696 & -0.0756 \\ 0.4696 & 0.5691 & 0.0690 \\ -0.0756 & 0.0690 & 0.1828 \end{bmatrix}$$

$$= \begin{bmatrix} -0.6431 & -0.3597 & -0.6761 \\ 0.5898 & 0.3305 & -0.7369 \\ -0.4884 & 0.8726 & 0.0004 \end{bmatrix}\begin{bmatrix} 0 & 0 & 0 \\ 0 & 0.2401 & 0 \\ 0 & 0 & 1 \end{bmatrix}\begin{bmatrix} -0.6431 & 0.5898 & -0.4884 \\ -0.3597 & 0.3305 & 0.8726 \\ -0.6761 & -0.7369 & 0.0004 \end{bmatrix}$$

The open-loop system can be regenerated again, since the eigenvectors associated with zero eigenvalue of $V_{22}^{i\,*}V_{22}^i$ and $\widehat{V}_{22}^{i\,*}\widehat{V}_{22}^i$ are identical.

$$\widehat{V}_{22}^1\widehat{U}^1 = \widehat{\lambda}^1\widehat{U}^1$$

$$= \begin{bmatrix} 0.5872 & 0.3793 & -0.3151 \\ 0.3785 & 0.6521 & 0.2890 \\ 0 & 0 & 0 \end{bmatrix}\begin{bmatrix} 0.6431 \\ -0.5898 \\ 0.4884 \end{bmatrix} = (0)\begin{bmatrix} 0.6431 \\ -0.5898 \\ 0.4884 \end{bmatrix} = \begin{bmatrix} 0 \\ 0 \\ 0 \end{bmatrix}$$

and

$$V_{22}^1\widehat{U}^1 = \begin{bmatrix} 0.5872 & 0.3793 & -0.3151 \\ 0.3785 & 0.6521 & 0.2890 \\ -0.3135 & 0.2881 & 0.7606 \end{bmatrix}\begin{bmatrix} 0.6431 \\ -0.5898 \\ 0.4884 \end{bmatrix} = \begin{bmatrix} 0 \\ 0 \\ 0 \end{bmatrix}$$

This implies that both V_{22}^1 and $\widehat{V}_{22}^1$ can regenerate the open-loop eigenvector using the eigenvector associated with zero eigenvalue of $V_{22}^{i\,*}V_{22}^i$ and $\widehat{V}_{22}^{i\,*}\widehat{V}_{22}^i$, respectively. Therefore, using $\widehat{V}_{22}^1$ with any other eigenvectors of $\widehat{V}_{22}^{i\,*}\widehat{V}_{22}^i$, leads to a closed-loop eigenvector orthogonal to the open-loop one [84].

To establish a procedure for this case, we start adding virtual actuators equal to the difference between the number of actuators and sensors. The virtual actuators are not

necessary to be collocated with the sensors. The rows of the final gain matrix associated with the virtual actuators are set to zero. Furthermore, the elements associated with the virtual actuators in B matrix are arbitrary and can be set to unity for simplicity. Since arbitrary elements are added to B and B is used for defining the achievable eigenvectors set, the basis of the null spaces of possible closed-loop systems are not necessarily identical, even though they are orthogonal to their corresponding open-loop eigenvectors.

The results that have been shown are associated with the first operating eigenvalue with negative real parts farthest from the origin. Similar results for the second and the third operating eigenvalues can be achieved. Therefore, the third row of W in Equation (3.49) is zero. Using Equation (3.50), the gain matrix K has a third row of zeros. This implies that the gains associated with the third actuator (i.e. the virtual actuator) are zero, while the gains associated with the control actuators are non-zero.

Using $r^1 = \bar{U}_2^1$, $r^2 = \bar{U}_1^2$, and $r^3 = \bar{U}_1^3$, the gain matrix before setting the third row to zero is

$$K = 1.0 \times 10^3 \begin{bmatrix} -1.3211 & -0.8670 & -0.1340 \\ 1.5735 & -1.5267 & 0.1759 \\ 0.7271 & -1.0190 & -0.8962 \end{bmatrix}$$

After setting the third row to zero, the reduced gain matrix becomes

$$K = 1.0 \times 10^3 \begin{bmatrix} -1.3211 & -0.8670 & -0.1340 \\ 1.5735 & -1.5267 & 0.1759 \\ 0 & 0 & 0 \end{bmatrix}$$

Figure 5.4 compares the displacements of m_1 due to a unit impulse to m_{10} when non-reduced and reduced gain matrices have been used. It can be seen that the maximum displacement when the reduced gain matrix has been used is 4.2 mm while for the other case it is 5.8 mm. The vibration of the case when the reduced gain matrix has been used decays slightly slower. Figure 5.5 shows displacement for masses m_{1-10} due to a unit

impulse input at m_{10}. Good isolation is achieved at m_{1-6}. When the reduced gain matrix has been used, m_6 is part of the isolated region and its displacement is reduced significantly, while using a non-reduced gain matrix, as can be seen on Figure 5.2, the vibration at m_6 has not been isolated. m_{7-8} and m_{9-10} belong to the transition and confined regions respectively, similar to Figure 5.2 of the earlier problem that a non-reduced gain matrix has been used. Figure 5.6 shows the actuation forces of two control actuators. Maximum actuation forces of the inner and middle actuators are 97.1 N and 77.8 N, respectively. The actuation force of the inner actuator is 21 times higher than the actuation force at the inner actuator when non-reduced gain matrix is used. The middle actuator shows 31% reduction at the maximum actuation force in comparison to the case with non-reduced gain matrix.

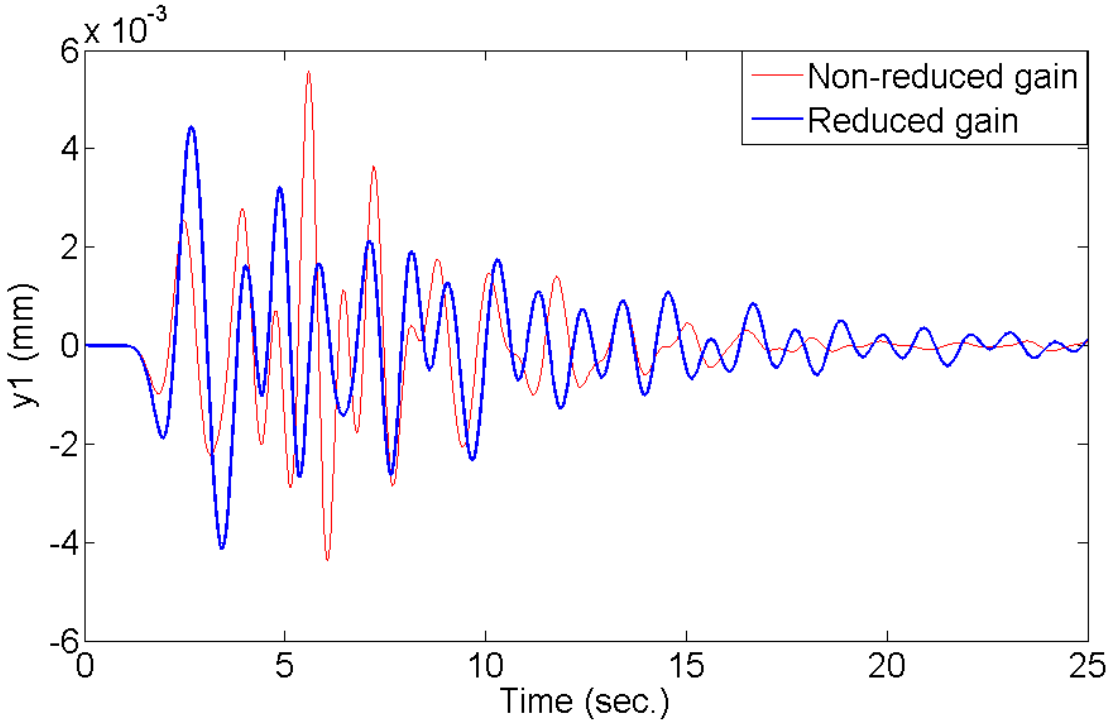

Figure5.4. Comparison of displacement of m_1 due to a unit impulse at m_{10}, before and after reducing the gain matrix

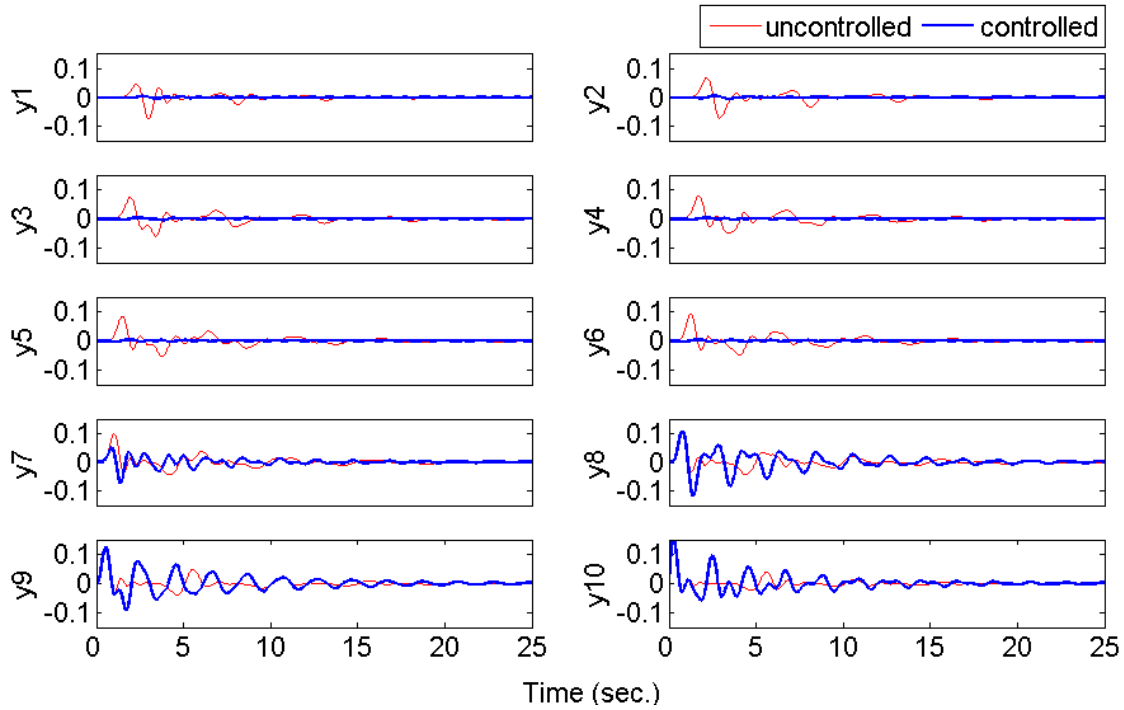

Figure 5.5. Comparison of displacement of masses due to a unit impulse at m_{10}, using reduced gain matrix for the case with 3 sensors and 2 actuators

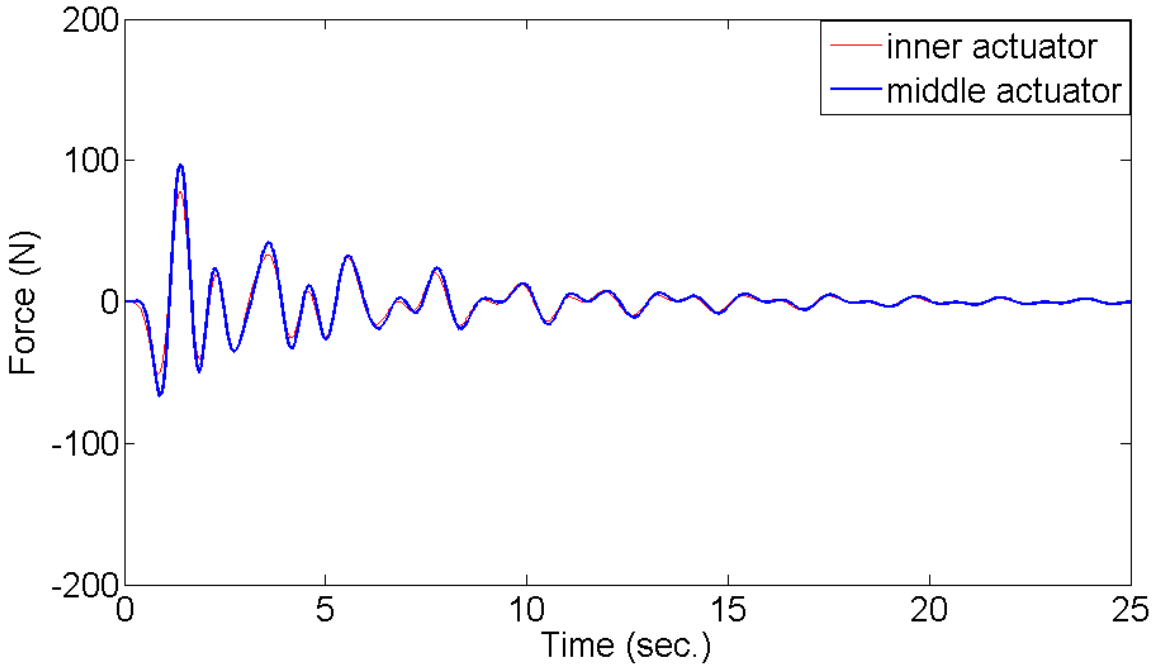

Figure 5.6. Actuation forces for a system with 3 sensors, 2 actuators using reduced gain matrix

5.3. Fewer sensors than actuators

When there are fewer sensors than the actuators, virtual sensors are added to the system in order to have an equal number of sensors and actuators; much in the same manner as the earlier case where we added virtual actuators. Therefore, a number of rows equal to the difference between the number of actuators and sensors are added to output matrix C. Recalling the gain matrix in Equation (3.50), one can determine that in order to have columns of zero associated with the virtual sensors, either W or $(CV)^{-1}$ must have zero elements at the corresponding columns. If the associated columns of W is set to zero, the Equations (3.38) and (3.39) will not hold, and the closed-loop eigenvectors will not belong to the achievable eigenvector set that is defined by the basis of the null space of the closed-loop systems. Alternatively, to set the required columns of $(CV)^{-1}$ equal to zero, we can add equal number of rows with large elements to C while keeping C full-rank. Since the gain matrix is determined using Equation (3.50), $(CV)^{-1}$ will have columns of zeros that are associated with the virtual sensors. Because the output matrix C has no role in defining the achievable eigenvectors, the closed-loop eigenvectors are within the achievable eigenvectors set.

To better illustrate this method, the system of Figure 4.1 with two sensors on m_{6-7} and three actuators on m_{6-8} is considered. A virtual sensor is added to m_8. Following the same procedure as the previous examples, we get

$$V_{22}^{1\,*}V_{22}^{1} = \bar{U}^{1}\bar{\Lambda}^{1}\bar{U}^{1*}$$

$$= \begin{bmatrix} 0.5872 & 0.3785 & -0.3135 \\ 0.3793 & 0.6521 & 0.2881 \\ -0.3151 & 0.2890 & 0.7606 \end{bmatrix}\begin{bmatrix} 0.5872 & 0.3793 & -0.3151 \\ 0.3785 & 0.6521 & 0.2890 \\ -0.3135 & 0.2881 & 0.7606 \end{bmatrix} = \begin{bmatrix} 0.5872 & 0.3793 & -0.3151 \\ 0.3785 & 0.6521 & 0.2890 \\ -0.3135 & 0.2881 & 0.7606 \end{bmatrix}$$

$$= \begin{bmatrix} 0.6431 & -0.6692 & 0.3723 \\ -0.5898 & -0.1228 & 0.7982 \\ 0.4884 & 0.7329 & 0.4737 \end{bmatrix}\begin{bmatrix} 0 & 0 & 0 \\ 0 & 1 & 0 \\ 0 & 0 & 1 \end{bmatrix}\begin{bmatrix} 0.6431 & -0.5898 & 0.4884 \\ -0.6692 & -0.1228 & 0.7329 \\ 0.3723 & 0.7982 & 0.4737 \end{bmatrix}$$

The third column of V_{22}^{1} is set to zero and the new matrix is called $\widehat{V}_{22}^{1}$

$$\hat{V}_{22}^{1*}\hat{V}_{22}^{1} = \hat{U}^{1}\hat{\Lambda}^{1}\hat{U}^{1*}$$

$$= \begin{bmatrix} 0.5872 & 0.3785 & -0.3135 \\ 0.3793 & 0.6521 & 0.2881 \\ 0 & 0 & 0 \end{bmatrix} \begin{bmatrix} 0.5872 & 0.3793 & 0 \\ 0.3785 & 0.6521 & 0 \\ -0.3135 & 0.2881 & 0 \end{bmatrix} = \begin{bmatrix} 0.5872 & 0.3793 & 0 \\ 0.3785 & 0.6521 & 0 \\ 0 & 0 & 0 \end{bmatrix}$$

$$= \begin{bmatrix} 0 & -0.7370 & 0.6759 \\ 0 & 0.6759 & 0.7370 \\ 1 & 0 & 0 \end{bmatrix} \begin{bmatrix} 0 & 0 & 0 \\ 0 & 0.2385 & 0 \\ 0 & 0 & 1 \end{bmatrix} \begin{bmatrix} 0 & 0 & 1 \\ -0.7370 & 0.6759 & 0 \\ 0.6759 & 0.7370 & 0 \end{bmatrix}$$

Multiplying $\hat{V}_{22}^{1}$ and V_{22}^{1} by $\hat{U}^{1}$ gives

$$\hat{V}_{22}^{1}\hat{U}^{1} = \hat{\Lambda}^{1}\hat{U}^{1}$$

$$= \begin{bmatrix} 0.5872 & 0.3793 & 0 \\ 0.3785 & 0.6521 & 0 \\ -0.3135 & 0.2881 & 0 \end{bmatrix} \begin{bmatrix} 0 & -0.7370 & 0.6759 \\ 0 & 0.6759 & 0.7370 \\ 1 & 0 & 0 \end{bmatrix} = \underbrace{\begin{bmatrix} 0 & -0.1764 & 0.6764 \\ 0 & 0.1618 & 0.7365 \\ 0 & 0.4257 & 0.0005 \end{bmatrix}}_{\begin{matrix} 1 & 2 & 3 \end{matrix}}$$

$$V_{22}^{1}\hat{U}^{1} = \hat{\Lambda}^{1}\hat{U}^{1}$$

$$= \begin{bmatrix} 0.5872 & 0.3793 & -0.3151 \\ 0.3785 & 0.6521 & 0.2890 \\ -0.3135 & 0.2881 & 0.7606 \end{bmatrix} \begin{bmatrix} 0 & -0.7370 & 0.6759 \\ 0 & 0.6759 & 0.7370 \\ 1 & 0 & 0 \end{bmatrix} = \underbrace{\begin{bmatrix} -0.3151 & -0.1764 & 0.6764 \\ 0.2890 & 0.1618 & 0.7365 \\ 0.7606 & 0.4257 & 0.0005 \end{bmatrix}}_{\begin{matrix} 1 & 2 & 3 \end{matrix}}$$

Columns 2 and 3 of the product matrices are identical. Column 1 indicates that the closed-loop system cannot be regenerated when the eigenvector associated with the zero eigenvalue of the modified matrix is used. If $\hat{U}_{1}^{1}$ could create the open loop system, then the first column of $V_{22}^{1}\hat{U}_{1}^{1}$ would be zero.

To address this issue, the proposed method of virtual elements needs to be implemented by finding a way to have appropriate zero columns in $(CV)^{-1}$. Since C does not contribute in defining the achievable set of closed-loop eigenvectors, the final closed-loop system possesses eigenvectors that belong to the achievable eigenvectors of the system.

In this example, C is a $2 \times n$ matrix. If another row is added to C, with elements that are several orders of magnitude larger than the norm of C, it leads to a gain matrix K with a third column of zero elements. Adding a row to C changes CV to a square matrix that has an inverse, and as a result the gain matrix K can be determined. Note that the elements of C associated with the control actuators have zero elements on the columns that corresponds to the location of the virtual actuator and vice versa. The non-zero elements of B and C matrices are

$$B(16,1) = B(17,2) = B(18,3) = -1/50$$
$$C(1,6) = C(2,7) = 1 \qquad C(3,7) = 1 \times 10^{10}$$

Using $r^1 = \bar{U}_2^1$, $r^2 = \bar{U}_1^2$, and $r^3 = \bar{U}_1^3$, the gain matrix becomes;

$$K = 1.0 \times 10^3 \begin{bmatrix} -0.5087 & -0.9922 & 0 \\ -1.2498 & -1.6758 & 0 \\ 1.3654 & -0.9892 & 0 \end{bmatrix}$$

Figure 5.7 compares the displacement of m_1 when non-reduced and reduced gain matrices are used. The disturbance is a unit impulse at m_{10}. The maximum displacements when non-reduced and reduced gain matrices are used are 5.6 and 5.8 mm, respectively. The result show that the response of the system with reduced gain matrix decays slightly faster.

Figure 5.8 shows the displacements of masses m_{1-10} due to a unit impulse at m_{10}. Significant isolation can bee seen at m_{1-6}. A comparison of the results with those in Figure 5.2 for the non-reduced gain matrix indicates that the displacement of m_6 is reduced significantly, while the case with non-reduced gain does not isolate the vibration at m_6. Masses m_{7-8} and m_{9-10} belong to the transition and confined regions respectively, the same as the case with a non-reduced gain matrix.

The force of the control actuators are shown on Figure 5.9. The maximum force at the inner, middle, and outer actuators are 75.8, 77.0, and 111.2 N respectively. Comparing theses results with the results of the case with non-reduced gain matrix reveals that the actuation force of the inner actuator is increased 16 times, the middle actuators is decreased 2.8%, and the outer actuator is increased 4.7 times.

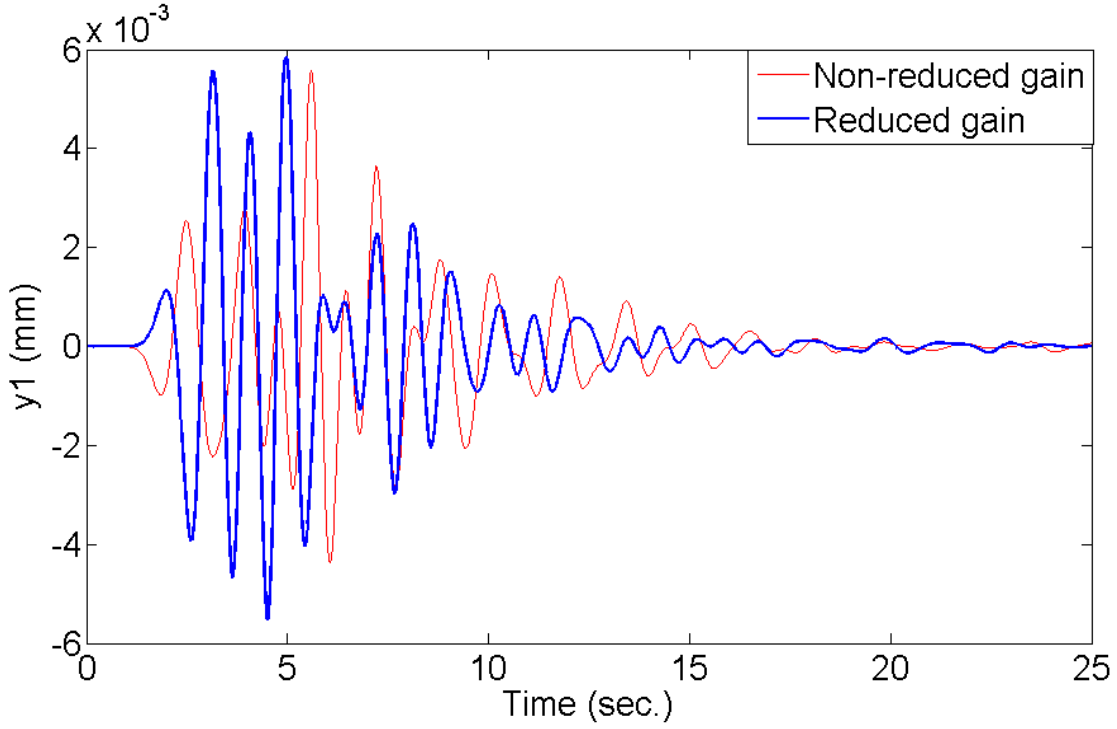

Figure 5.7. Comparison of displacement of m_1 due to a unit impulse at m_{10}, before and after reducing the gain matrix

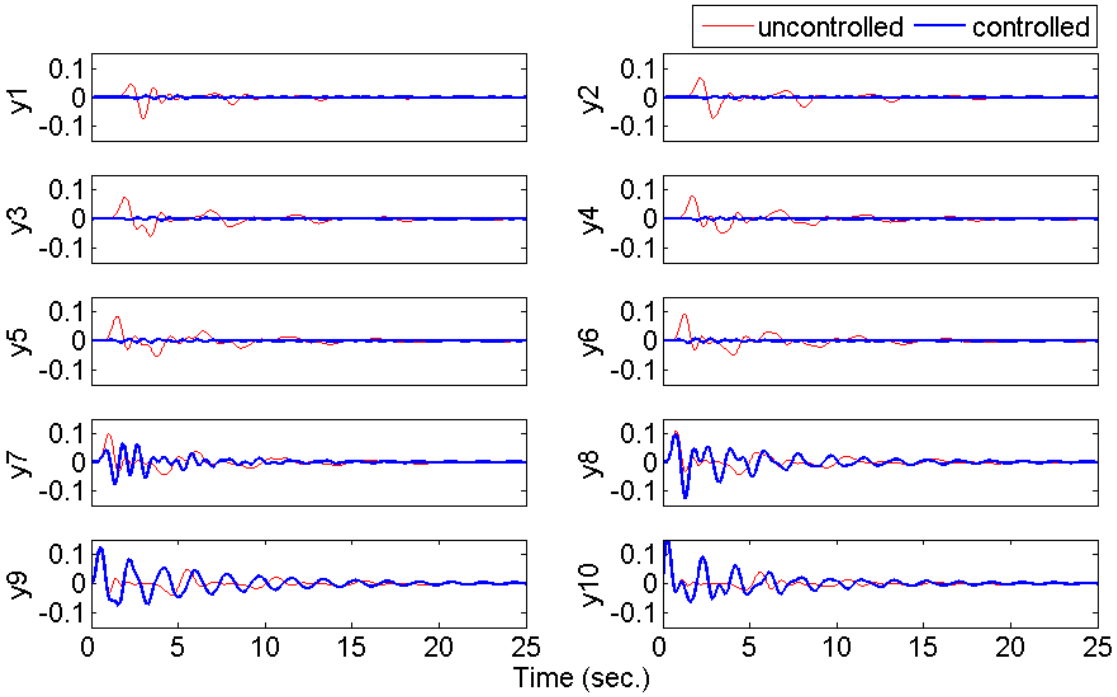

Figure 5.8. Comparison of displacement of masses due to a unit impulse at m_{10}, using reduced gain matrix for the case with 2 sensors and 3 actuators

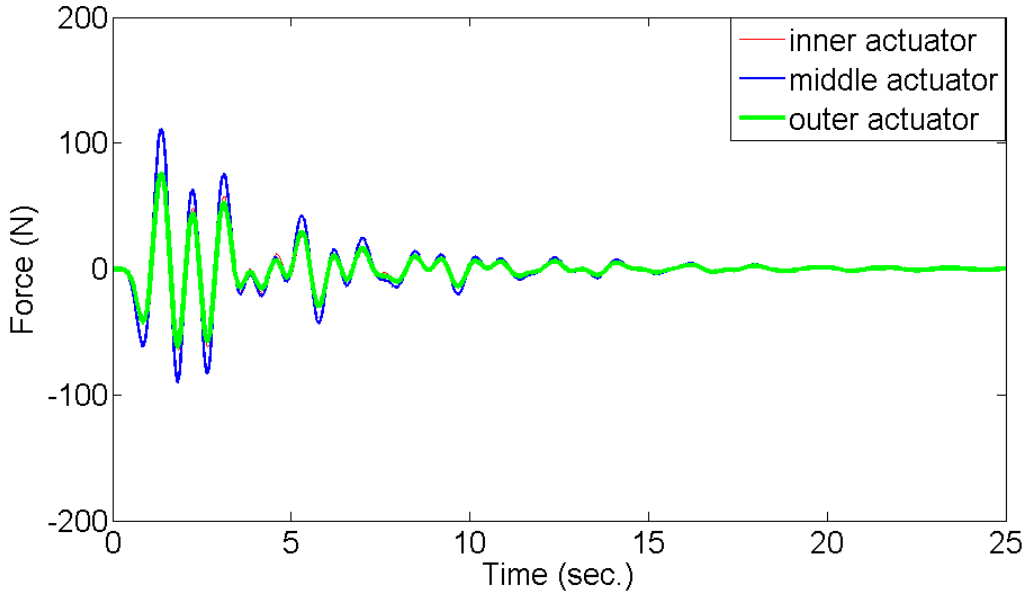

Figure 5.9. Actuation forces for a system with 2 sensors, 3 actuators using reduced gain matrix

5.4. Procedure for orthogonal eigenstructure control with non-collocated actuators and sensors

The following step-by-step procedure is developed for the application of the orthogonal eigenstructure control as a feedback control scheme regardless of the number of actuators and sensors:

1. Define state space realization of the system similar to Equations (3.2-3.7)

2. Determine m eigenvalues of the open-loop system with negative real parts farthest from the origin, where m is the number of the actuators or sensors, whichever is greater

3. Using the virtual elements, add associated rows to C with very large elements or columns to B with arbitrary elements

4. Define state space realization of the system similar to Equation (3.2)

5. Using λ_i determined in step 2, define the non-square matrix $S_{\lambda i}$ as Equation (3.14)

6. Apply SVD to $S_{\lambda i}$ generated from step (3)

7. Partition the right unitary matrix V_i and define V_{12}^i and V_{22}^i according to Equation (3.17)

8. Calculate $V_{12}^{i*}V_{12}^i$

9. Find the eigenvalue matrix $\bar{\Lambda}^i$ and eigenvector matrix $\bar{U}^i$ for the Hermitian matrix $V_{12}^{i*}V_{12}^i$, using Equation (3.14)

10. Choose the j th eigenvector $\bar{U}_j^i$ associated with the j th eigenvalue λ_j^i and define $r^i = \bar{U}_j^i$

11. Calculate $v^i = V_{12}^i r^i$ and $w^i = V_{22}^i r^i$

12. Repeat steps (3) to (9) m times and find v_i and w_i for all the operating eigenvalues

13. Define the matrices V and W by appending v^i and w^i resulting from steps (9) and (10) according to Equations (3.48) and (3.49)

14. Find the gain matrix K using Equation (3.50)

15. Set the columns or rows of the gain matrix K associated with the virtual actuators or sensors to zero

16. Go to step 8, change the index j and repeat the algorithm m^m times. Note that the regenerated open-loop is included in the results

17. Choose the gain matrix K from $m^m - 1$ closed-loop systems that provides the fastest possible convergence to zero and the smallest overshoot for the isolated states. The closed-loop system with the smallest phase plane for the isolated states shows those characteristics.

5.5. Summary

The application of the orthogonal eigenstructure control is extended beyond the systems with collocated sensors and actuators. Orthogonal eigenstructure control is a feedback control that has been recently developed by the authors for vibration isolation purpose. This method regenerates the open-loop eigenvectors and at the same time determines all of the eigenvectors that are orthogonal to the open-loop eigenvectors. Since there are many systems that have limitations on the number or location of actuators and sensors, the application of this method has been extended to include systems with non-collocated actuators and sensors. The proposed method is based on adding virtual actuators and sensors to the system for the cases that the number of the actuators and sensors are not equal. Four examples used to show how the orthogonal eigenstructure control can be applied to the systems with non-collocated actuators and sensors and to the systems with

different number of actuators and sensors. The results show that using virtual actuators and sensors, leads to isolation of the states at the isolated region. The reduction of the maximum displacement using reduced gain matrices are very close to the ones of a closed-loop system with non-reduced gain matrix. The actuation forces at the control actuators increase when the gain matrix of the closed-loop system is replaced with its reduced form. Finally, an algorithm for the vibration isolation of the systems using orthogonal eigenstructure control is proposed that considers the possible situations regarding the actuators and sensors of the systems.

Chapter 6

Applications to High Order Systems

As an example of a system with large degrees of freedom, a plate that is simply supported along its four edges is considered, and the orthogonal eigenstructure control is used to suppress vibrations induced by a point source of disturbance. The plate is assumed to be a square steel plate with length and width of 40 cm, and a thickness of 1 mm. The Young's modulus of the material is 2.09×10^9 N/m^2 and the Poisson's ratio is 0.31. Finite element method is used for modeling the plate. Matlab is used for simulating the response of the plate. Figure 6.1 shows the plate, the assigned nodes, and the elements on the plate.

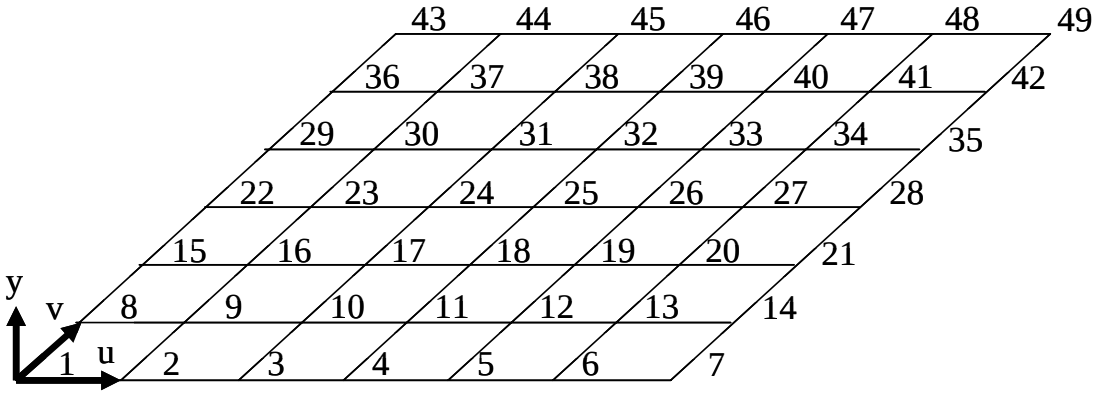

Figure 6.1. Elements and nodes of the square plate that is simply supported at all edges

Mindlin plate theory that includes transverse shear deformation is used to define the displacement field of the plate [85]. The procedures for determining the local mass and stiffness matrices are reported in [85]. Linear quadrilateral elements are used to model the plate. Each node has three degrees of freedom, including two in-plane displacements in u and v directions and a transverse displacement along y axis. Since the model consists of 49 nodes, global mass and stiffness matrices, M and K_s in Equation (3.1), are 149×149.

For damping matrix D_d, a linear damping $D_d = 0.2M + 0.002K_s$ after scaling the mass and stiffness matrices, is assumed. When the second order system of Equation (3.1) is transferred to a first order realization of Equation (3.2), the dimension of the state matrix A is 298×298. The boundary conditions are applied, and the eigenvalues of the open-loop system is calculated and shown in Figure 6.2.

6.1. Effect of the operating eigenvalues

Four areas have been considered to choose the operating eigenvalues. The operating eigenvalues must be substituted in Equation (3.14) to find the appropriate control gain matrix. Since using complex conjugates of the operating eigenvalues results in similar closed-loop systems, we use only the operating eigenvalues with positive imaginary parts. The disturbance force applied to the plate is a sine wave with a frequency of 300 Hz and amplitude of 10 N. The disturbance force is normal to the plate and causes bending of the plate. Three control actuators are considered to be on nodes 18, 25, and 32 in order to have the vibration cancellation while they are not surrounding the disturbance source. The displacements of the same nodes are used for feedback which indicates collocation of actuators and sensors. As stated in chapter 3, there are 26 resulting closed-loop systems as the outcomes of the orthogonal eigenstructure control, and the most desirable closed-loop system has to be identified from them.

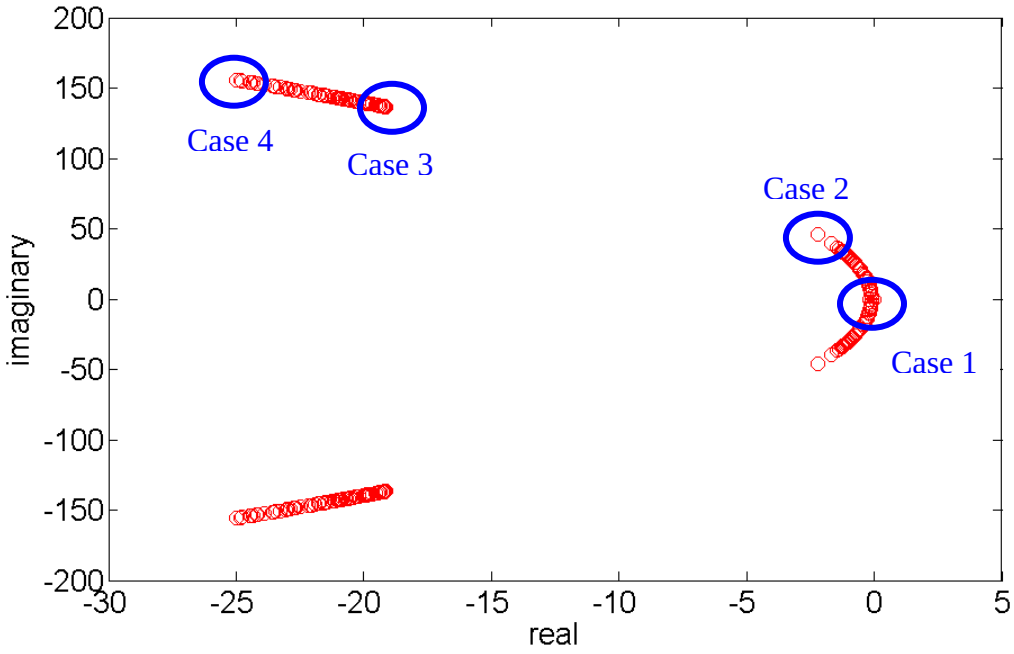

Figure 6.2. Open-loop eigenvalues of the first order realization of the plate, and four different areas for the operating eigenvalues

6.1.1. Case 1: operating eigenvalues at the right eigenvalue cluster and close to origin

For the case 1, the operating eigenvalues are -0.2349 + 11.6115i, -0.1555 + 7.4495i, and -0.1301 + 5.4826i. The possible closed-loop systems include 6 unstable, and 21 stable systems. The only acceptable closed-loop system can be achieved when $r^1 = \bar{U}_1^1$, $r^2 = \bar{U}_2^2$, and $r^3 = \bar{U}_1^3$. $r^i = \bar{U}_j^i$ implies that the coefficient vector r^i associated with the ith operating eigenvalue is the jth eigenvector in the eigenvector matrix $\bar{U}^i$ calculated using equation (3.42). For the rest of the stable systems, the control effort does not attenuate vibrations. The control gain matrix that yields the only desirable closed-loop system is

$$K = \begin{bmatrix} -540.8461 & -374.6068 & 211.4074 \\ -700.4144 & 196.5303 & -168.8743 \\ -560.3060 & -382.0424 & 242.0038 \end{bmatrix}$$

Figure 6.3, which shows the displacement at the nodes of the open-loop and closed-loop systems, indicates that vibrations attenuation is not significant. Figure 6.4 shows the eigenvalues of the open-loop and closed-loop system. It is noted that the closed-loop poles are not displaced outside of the open-loop poles loci; they remain in the vicinity of the open-loop poles. Actuation forces are shown on Figure 6.5. The maximum actuation forces are 11.2 N on nodes 18, 15.8 N on node 25, and 11.6 on node 32. The actuation forces are larger than the disturbance force magnitude.

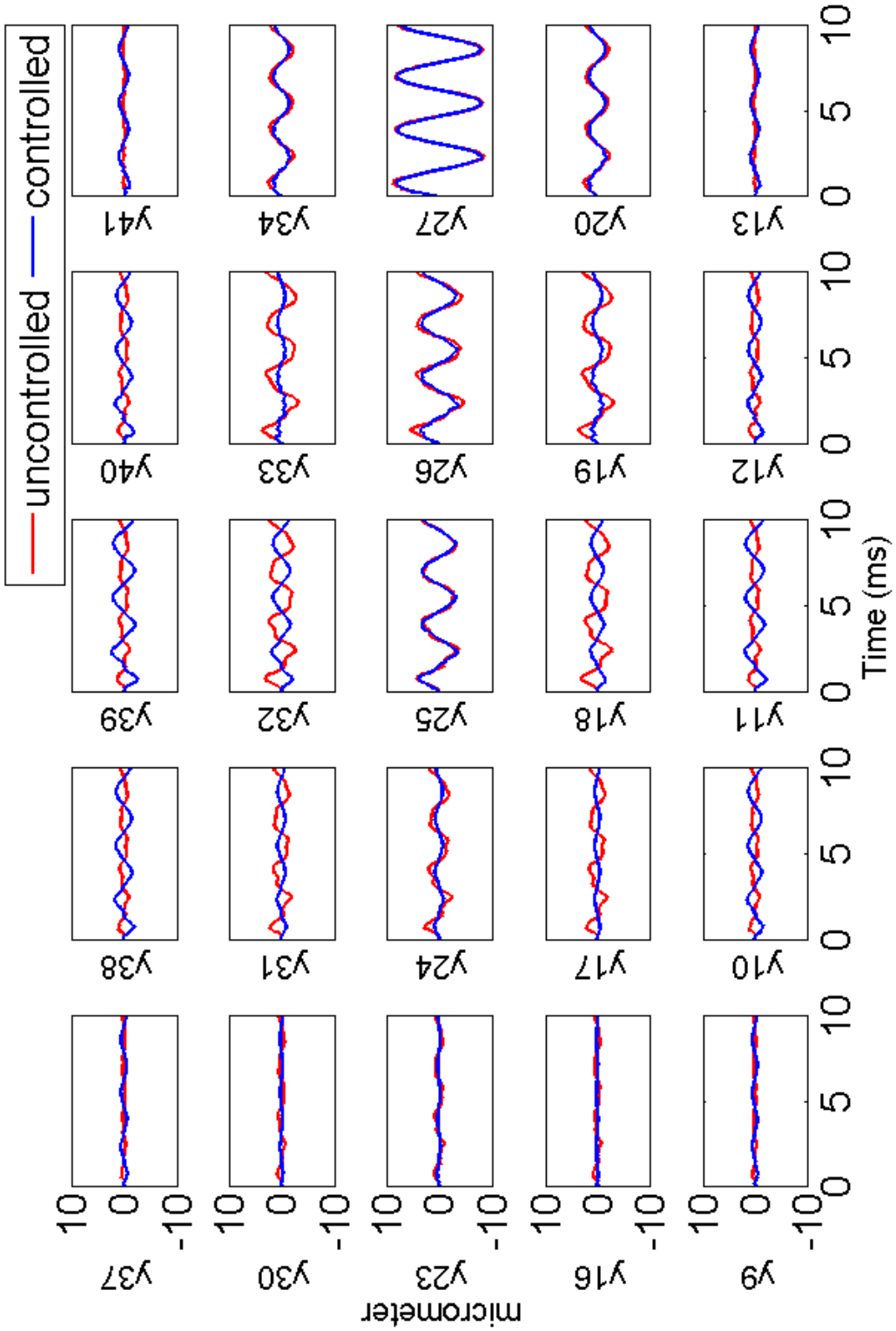

Figure 6.3. Transverse displacement at nodes of the plate for case 1,with operating eigenvalues at the right eigenvalue cluster and close to origin

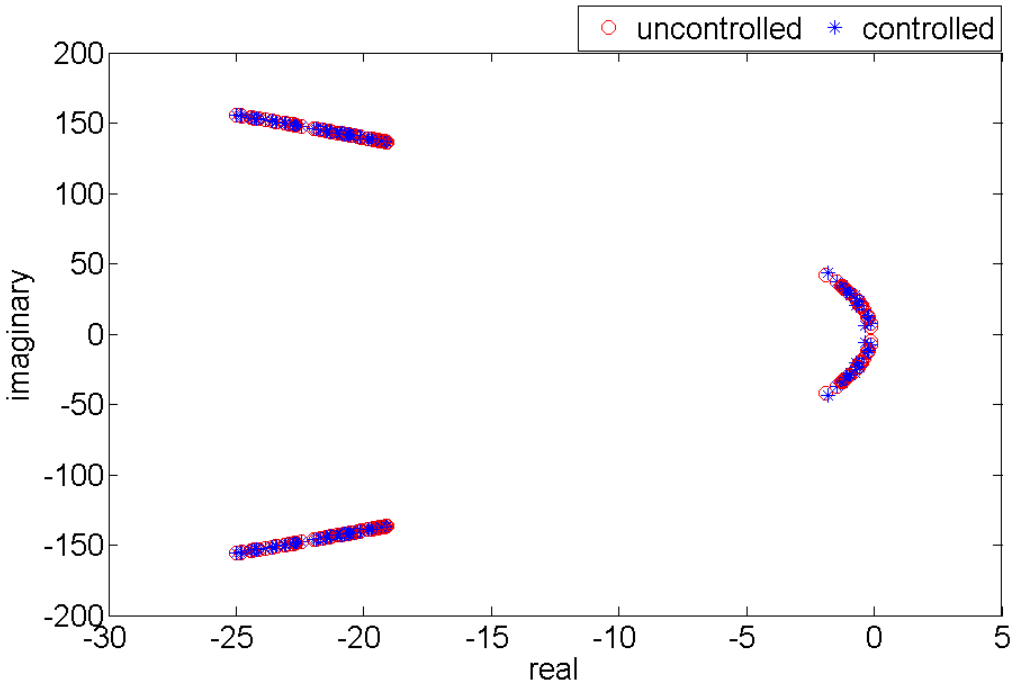

Figure 6.4. Eigenvalues of the open-loop and close-loop system for case 1, with operating eigenvalues at the right eigenvalue cluster and close to origin

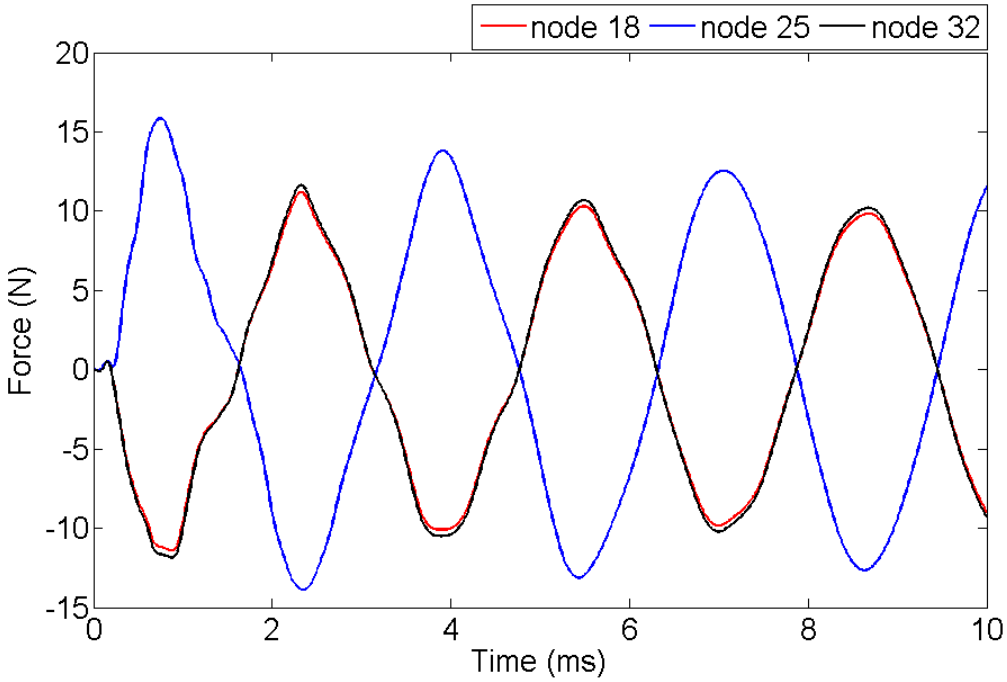

Figure 6.5. Actuation forces for case 1, with operating eigenvalues at the right eigenvalue cluster and close to origin

6.1.2. Case 2: operating eigenvalues at the right eigenvalue cluster and far from origin

For case 2, the operating eigenvalues are -1.8767 + 42.1091i, -1.4634 + 36.8949i, and -1.2746 + 34.2488i. The possible closed-loop systems include 12 unstable, and 15 stable systems. Only three of the stable systems are unacceptable since they do not suppress the vibration. The most desirable closed-loop system, which has the acceptable vibration suppression and low actuation forces, can be reached when $r^1 = \bar{U}_1^1$, $r^2 = \bar{U}_2^2$, and $r^3 = \bar{U}_1^3$. The control gain matrix is

$$K = 1.0 \times 10^3 \begin{bmatrix} -0.9266 & -0.9672 & -1.7274 \\ -0.0556 & -0.5020 & 0.6328 \\ -0.7657 & -0.9279 & -1.7156 \end{bmatrix}$$

Figure 6.6 shows the displacement at the nodes. Good vibration cancellation is achieved especially at the nodes that are not between the source of disturbance and the control actuators. The distributions of the poles of the closed-loop and open-loop system are depicted in Figure 6.7. It is seen that two pairs of the closed-loop poles are moved away from the locus of the open-loop poles. Figure 6.8 shows the actuation force at different nodes. The maximum actuation forces are 1.86 N at node 18, 2.41 N at node 25, and 1.84 at node 32. The actuation forces are smaller than the disturbance force and considerably smaller than those of case 1. Better vibration suppression occurs, as compared to case 1

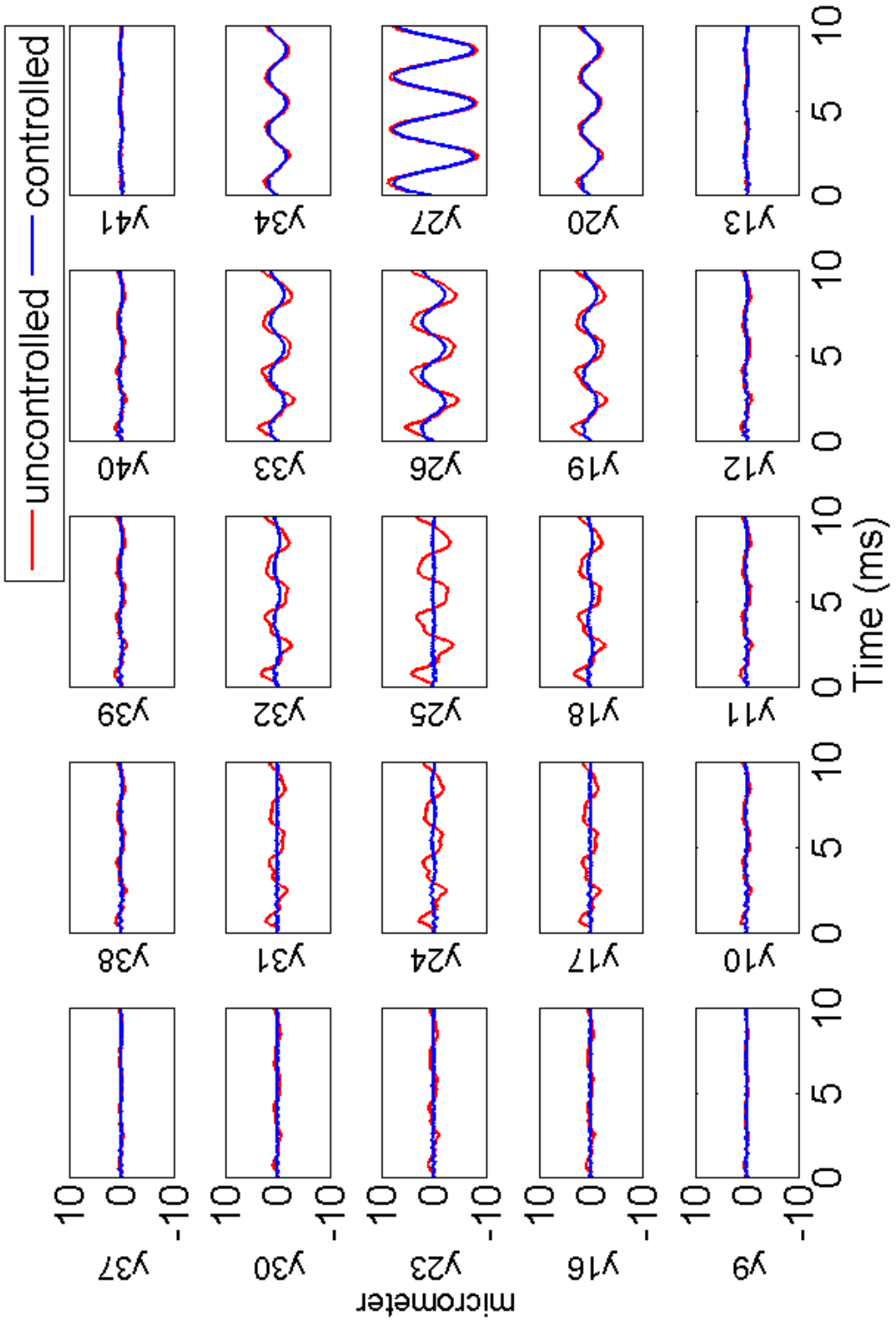

Figure 6.6. Transverse displacement at nodes of the plate for case 2, with operating eigenvalues at the right eigenvalue cluster and far from origin

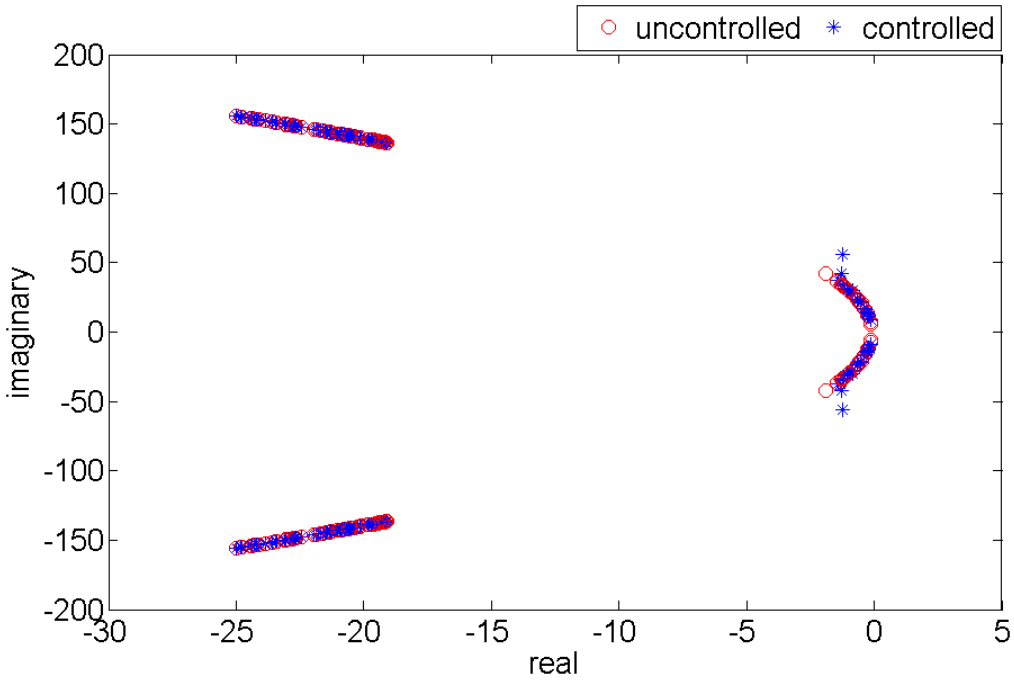

Figure 6.7. Eigenvalues of the open-loop and close-loop system for case 2, with operating eigenvalues at the right eigenvalue cluster and far from origin

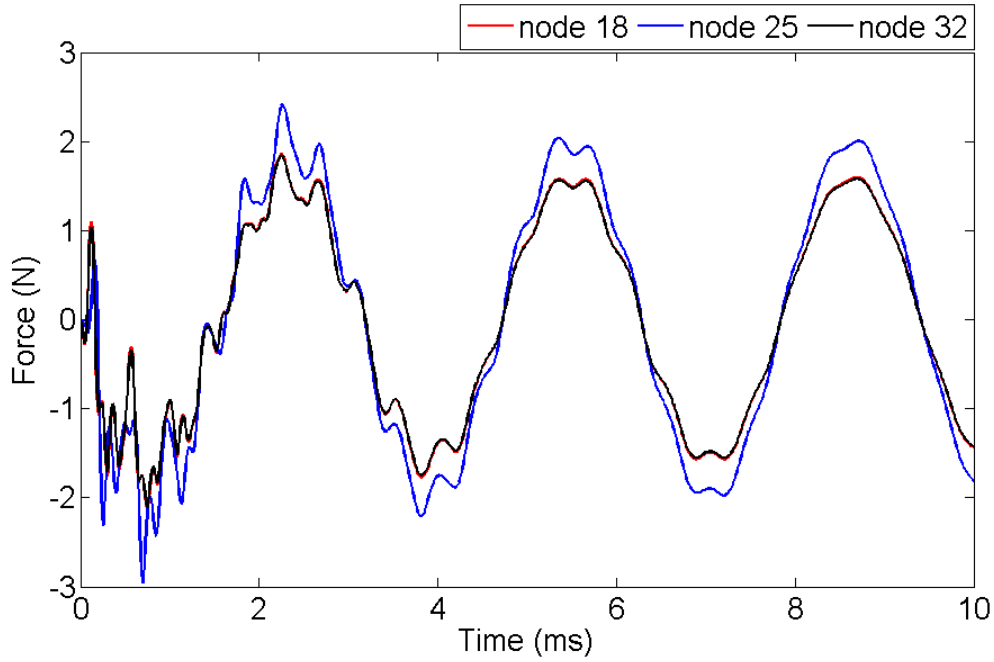

Figure 6.8. Actuation forces for case 2, with operating eigenvalues at the right eigenvalue cluster and far from origin

6.1.3. Case 3: operating eigenvalues at the left eigenvalue cluster and close to origin

For case 3, the operating eigenvalues are -19.1368 + 136.6404i, -19.1094 + 136.5437i, and -19.1094 + 136.5437i. Figure 6.9 shows the displacement at different nodes of the plate and the suppression of vibration. The control efforts significantly reduce the vibration in the plate. The 26 control gain matrices of the resulting closed-loop systems converge to

$$K = 1.0 \times 10^4 \begin{bmatrix} -1.8568 & -0.0263 & 0.0465 \\ -0.0532 & -1.8832 & -0.0536 \\ 0.0444 & -0.0271 & -1.8600 \end{bmatrix}$$

It is interesting to see that the off-diagonal elements of the gain matrix are 2 orders of magnitude smaller than the diagonal elements indicating minimal coupling among the actuators. This shows that the control is decoupled. In this case, three pairs of the closed-loop poles are moved away from the open-loop poles cluster as shown in Figure 6.10. The distance between the displaced poles in case 3 is larger than the distance of the displaced poles of case 2. Figure 6.11 shows the actuation forces. The maximum actuation forces are 0.85 N on node 18, 3.92 N on node 25, and 0.85 on node 32. A comparison between the actuation forces of case 3 and 2 shows that in case 3, the fluctuation of the amplitudes of the control forces is slower than in case 2.

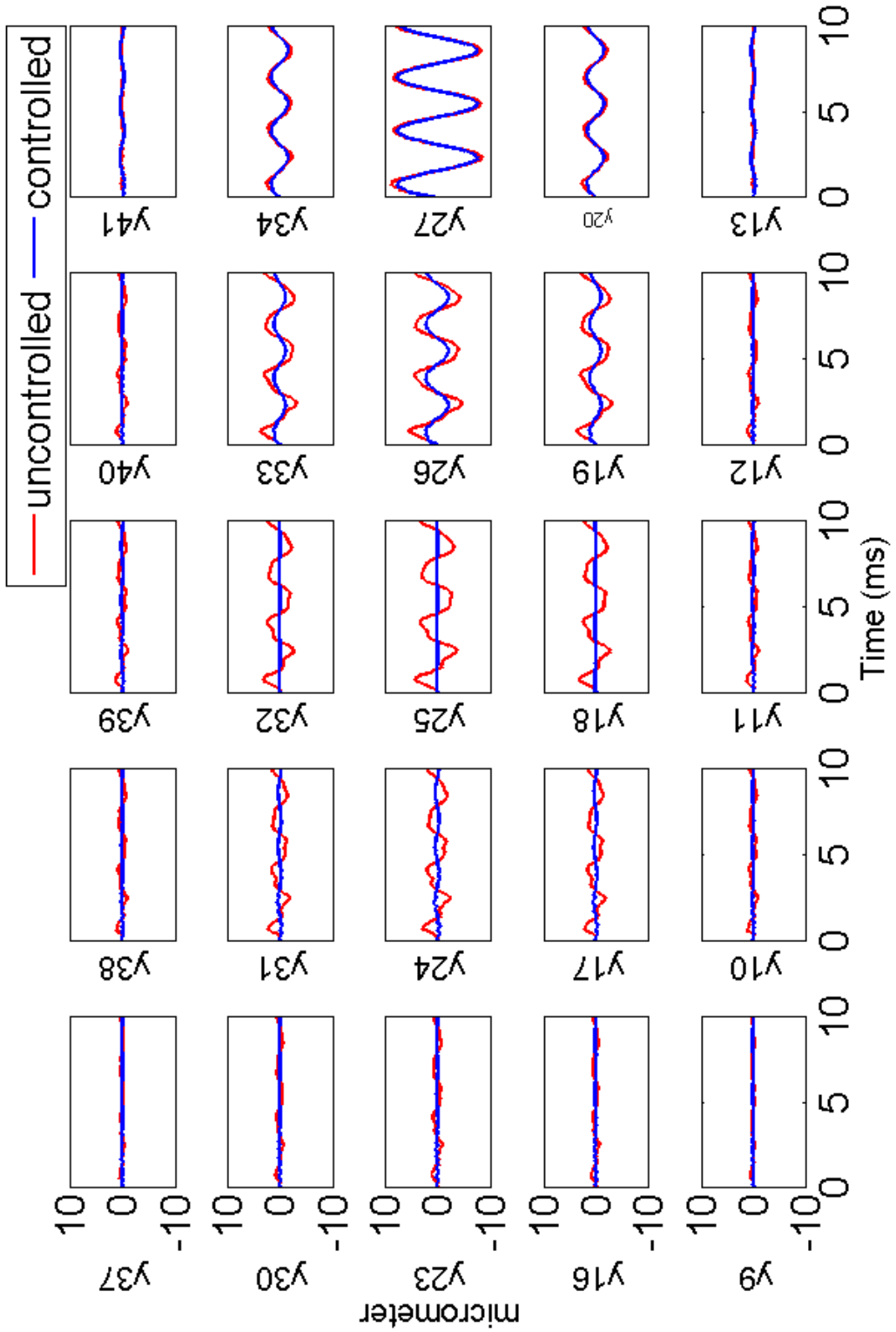

Figure 6.9. Transverse displacement at nodes of the plate for case 3, with operating eigenvalues at the left eigenvalue cluster and close to origin

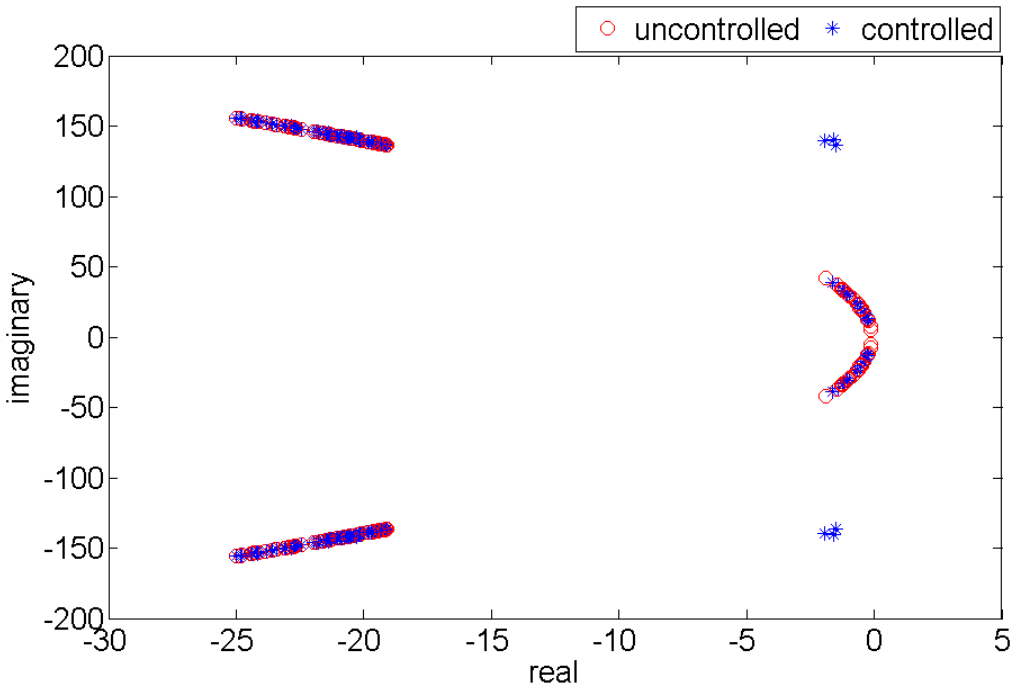

Figure 6.10. Eigenvalues of the open-loop and close-loop system for case 3, with operating eigenvalues at the left eigenvalue cluster and close to origin

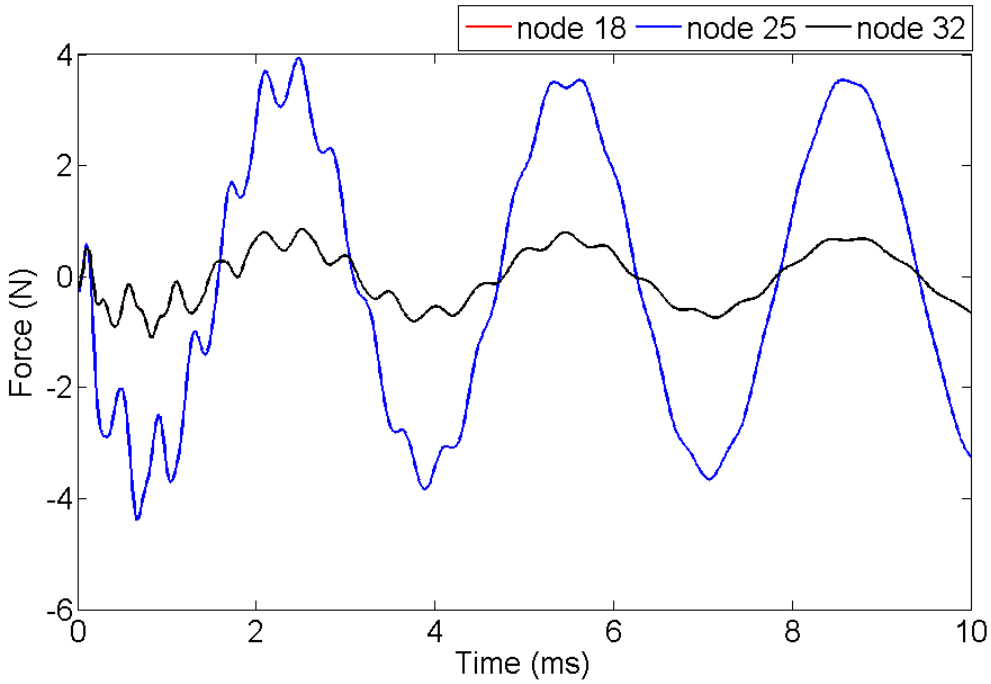

Figure 6.11. Actuation forces for case 3, with operating eigenvalues at the left eigenvalue cluster and close to origin

6.1.4. Case 4: operating eigenvalues at the left eigenvalue cluster and far from origin

For case 4, the operating eigenvalues are -24.9799 + 155.743i, -24.9799 + 155.743i, and -24.8108 + 155.2264i. The closed-loop systems are identical, and the control gain matrices converge to

$$K = 1.0 \times 10^4 \begin{bmatrix} -2.1998 & 0.0196 & 0.0156 \\ 0.0127 & -2.1497 & 0.0379 \\ -0.0137 & -0.0719 & -2.2532 \end{bmatrix}$$

The control gain matrix in this case, similar to case 3, has small off-diagonal elements in comparison to the diagonal elements. Suppression of vibration in the nodes of the plate can be seen in Figure 6.12. Figure 6.13 shows the distribution of the open-loop and closed-loop poles. It shows three pairs of the closed-loop poles moved away from the locus of the open-loop poles. They moved slightly further from the poles in case 3. Actuation forces can be seen in Figure 6.14. The maximum actuation forces are 0.85 N at node 18, 3.94 N at node 25, and 0.85 at node 32. Interestingly, the actuation forces for this case are almost identical to those for case 3.

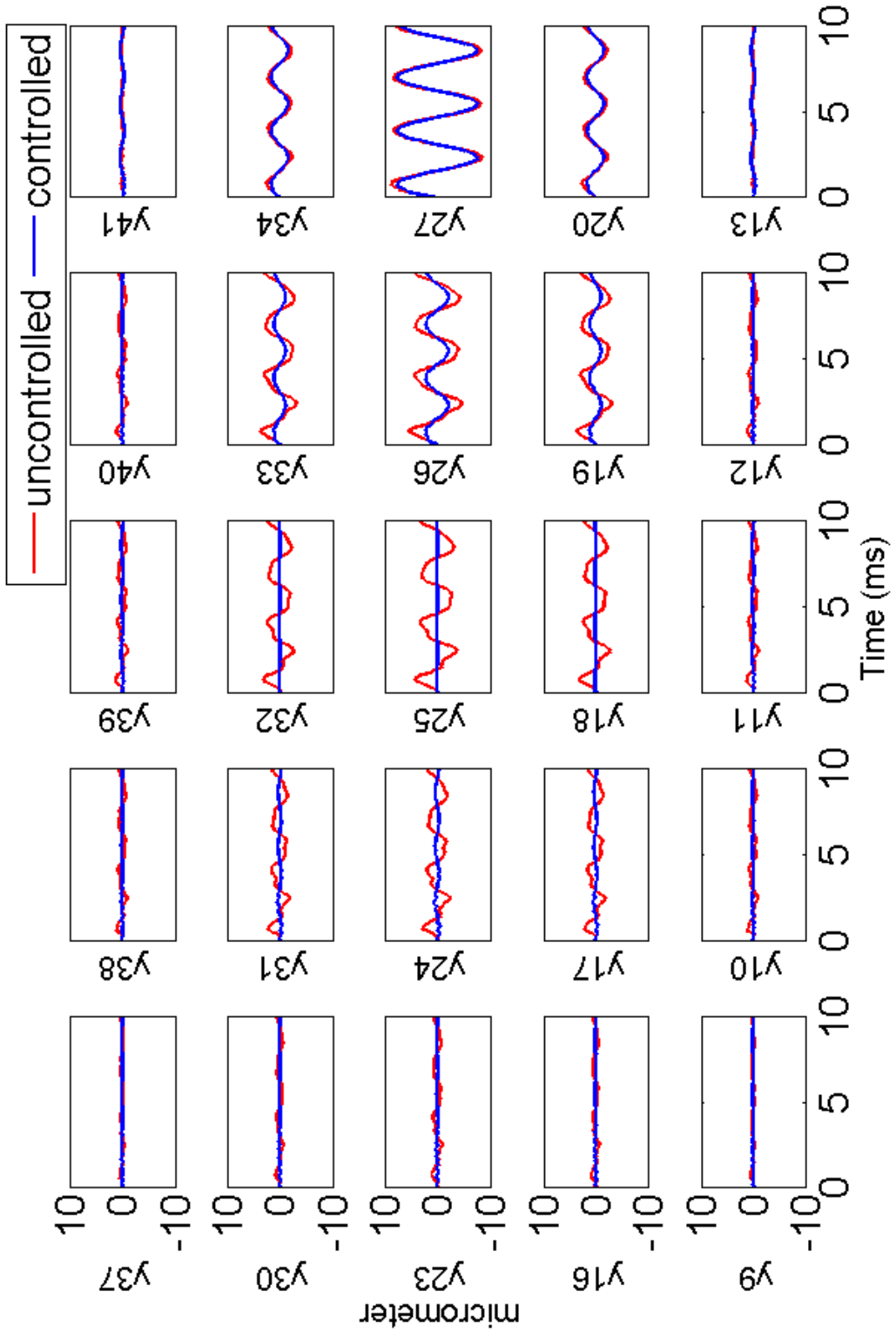

Figure 6.12. Transverse displacement at nodes of the plate for case 4, with operating eigenvalues at the left eigenvalue cluster and far from origin

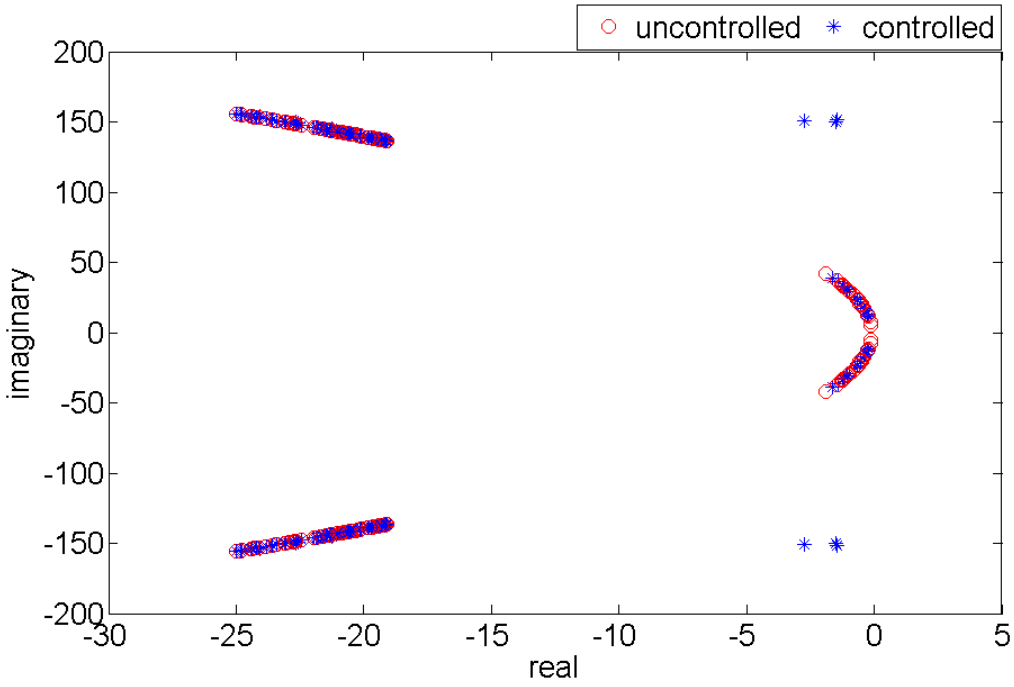

Figure 6.13. Eigenvalues of the open-loop and close-loop system for case 4, with operating eigenvalues at the left eigenvalue cluster and far from origin

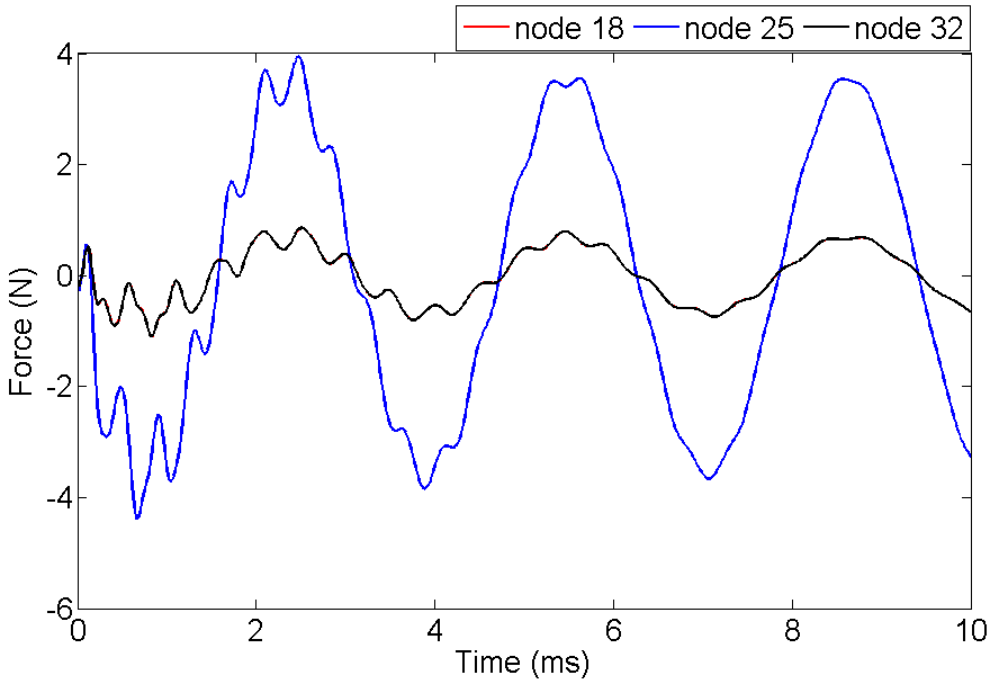

Figure 6.14. Actuation forces for case 4, with operating eigenvalues at the left eigenvalue cluster and far from origin

To examine the effect of larger diagonal elements in comparison to small off-diagonal elements of the control gain matrix in cases 3 and 4, we set the off-diagonal elements equal to zero to simulate the closed-loop system again. The displacement plots are not altered noticeably. The same can be seen for the actuation forces when the off-diagonal elements are set to zero and the results are compared to the original results. This indicates that the feedback signals for each actuator can be decoupled from the other feedback signals, if the operating eigenvalues are chosen appropriately.

A closer look at the closed-loop poles in case 4 shows that almost all the eigenvalues have slightly moved. Figure 6.15 shows the right cluster poles with positive imaginary parts. It is not possible to relate any of the closed-loop poles to the open-loop ones. Except for three of the eigenvalues, the rest have moved within the open-loop poles loci. Figure 6.16 depicts the left cluster poles with positive imaginary parts. Eight of the poles have moved slightly away from the open-loop poles loci and the rest of them have moved within the loci. Therefore, low actuation forces are needed to move the poles away from the open-loop locations, as stated by Slater et al. [46].

To further investigate the effect of the operating eigenvalues a region is considered within the s-plane. The complex numbers with real parts within [-30 -2] range and imaginary parts within [0 200] range are used as operating eigenvalues. The increment for the imaginary parts is 5, and it is 2 for the real parts. Since three operating eigenvalues are needed, if the middle one is chosen to be -20+175i, for example, the other two operating eigenvalues are -20+174i and -20+176i. Figure 6.17 shows the operating eigenvalues that result in desirable closed-loop systems that attenuate plate vibrations significantly. If they are chosen from the left part, the control gain matrices for all the possible closed-loop systems are converged to one matrix, in which the diagonal elements are larger than the off-diagonal ones. Also, less fluctuation in their actuation forces can be seen. Further investigations are needed to find possible relationship between the model parameters and the distribution of the operating eigenvalues that may result in a robust control, for various systems.

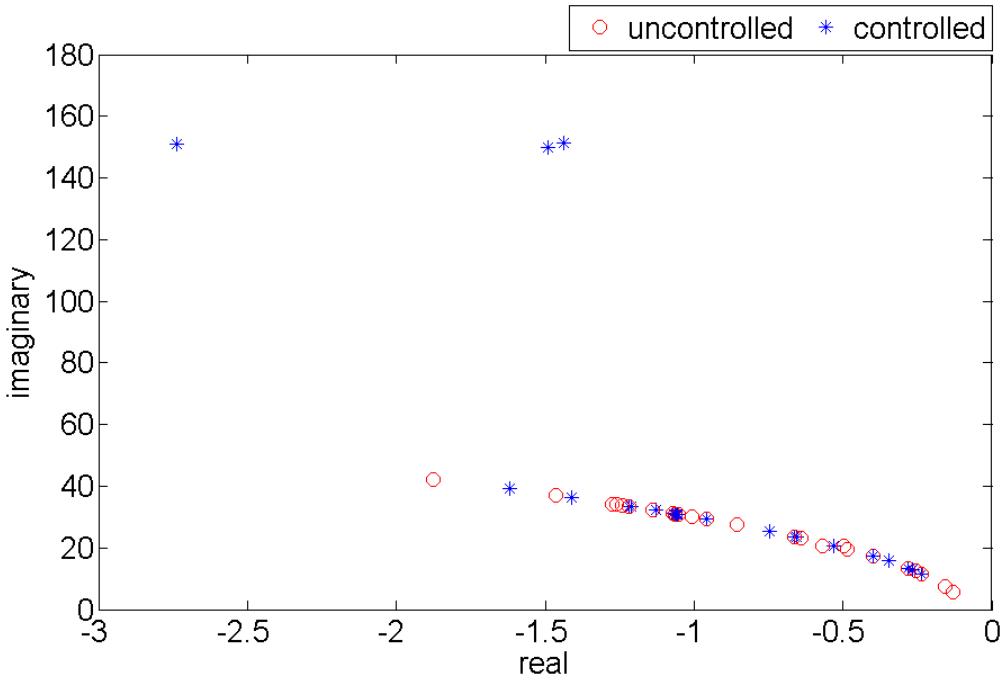

Figure 6.15. Distribution of eigenvalues in cluster close to origin at case 4

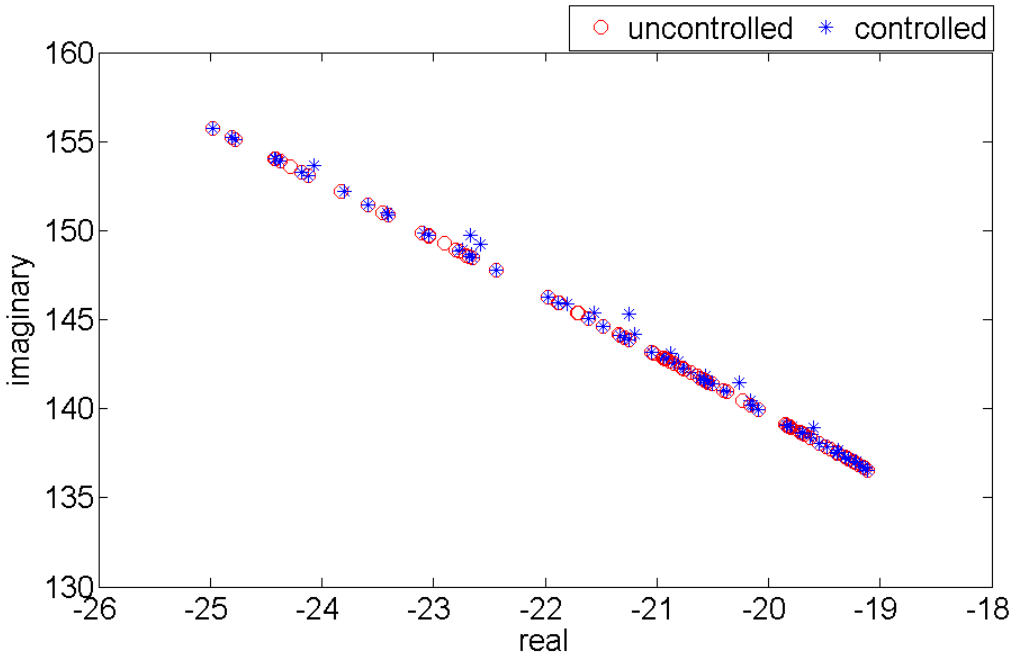

Figure 6.16. Distribution of eigenvalues in cluster far from origin at case 4

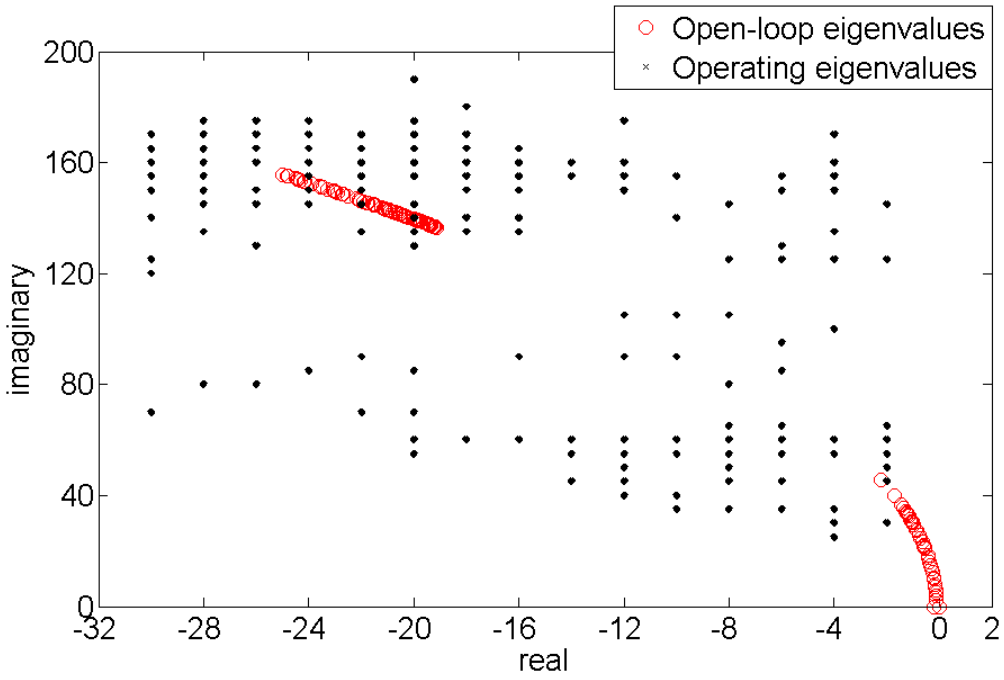

Figure 6.17. Distribution of operating eigenvalues for case 4 that generate acceptable closed-loop systems

6.2. Isolation of vibrations in a plate using non-collocated actuators and sensors

The plate problem is revisited. We consider five cases with different scenarios for the actuators:

Case 1: plate with 3 working actuators, (section 6.2.1)

Case 2: plate similar to case 1 with failed middle actuator, (section 6.2.2)

Case 3: plate similar to case 1 with failed outer actuator, (section 6.2.3)

Case 4: plate with two control actuators at the location of working actuators of case 2, (section 6.2.4)

Case 5: plate with two actuators at the location of working actuators of case 3, (section 6.2.5)

Since the operating eigenvalues have negative real parts farthest from the origin, for all the cases the operating eigenvalues are -24.9799 + 155.743i, -24.9799 + 155.743i, and

-24.8108 + 155.2264i. Since using complex conjugates of the operating eigenvalues results in similar closed-loop systems, only the operating eigenvalues with positive imaginary parts have been used.

We assume that the sensors are collocated with the actuators and the signals from the sensors are used for feedback. There are 26 possible closed-loop systems for the system with 3 actuators, and there are 3 possible closed-loop systems when there are 2 actuators on the system.

6.2.1. Case 1: plate with 3 working actuators

As shown in section 6.1, when the greatest open-loop eigenvalues are chosen as the operating eigenvalues, all of the closed-loop systems are identical, the off-diagonal elements are small in comparison to diagonal elements, and the control is decoupled. In this case the control gain matrices converge to the following matrix.

$$K = 1.0 \times 10^4 \begin{bmatrix} -2.1656 & 0.0420 & 0.0267 \\ 0.0034 & -2.1985 & 0.0030 \\ -0.0319 & -0.0444 & -2.2220 \end{bmatrix}$$

In fact, setting the off-diagonal elements to zero does not change the results noticeably. Figure 6.18 shows that the suppression of vibrations on different nodes of the plate. Actuator forces are shown in Figure 6.19. The maximum actuation forces are 0.86 N at nodes 19, 6.60 N at node 26, and 0.86 N at node 33. Because of the symmetry, the actuation forces of the actuators at nodes 19 and 33 are identical. Figure 6.20 illustrates the distributions of the open-loop and closed-loop poles. It shows that three pairs of the closed-loop poles are moved away from the locus of the open-loop poles.

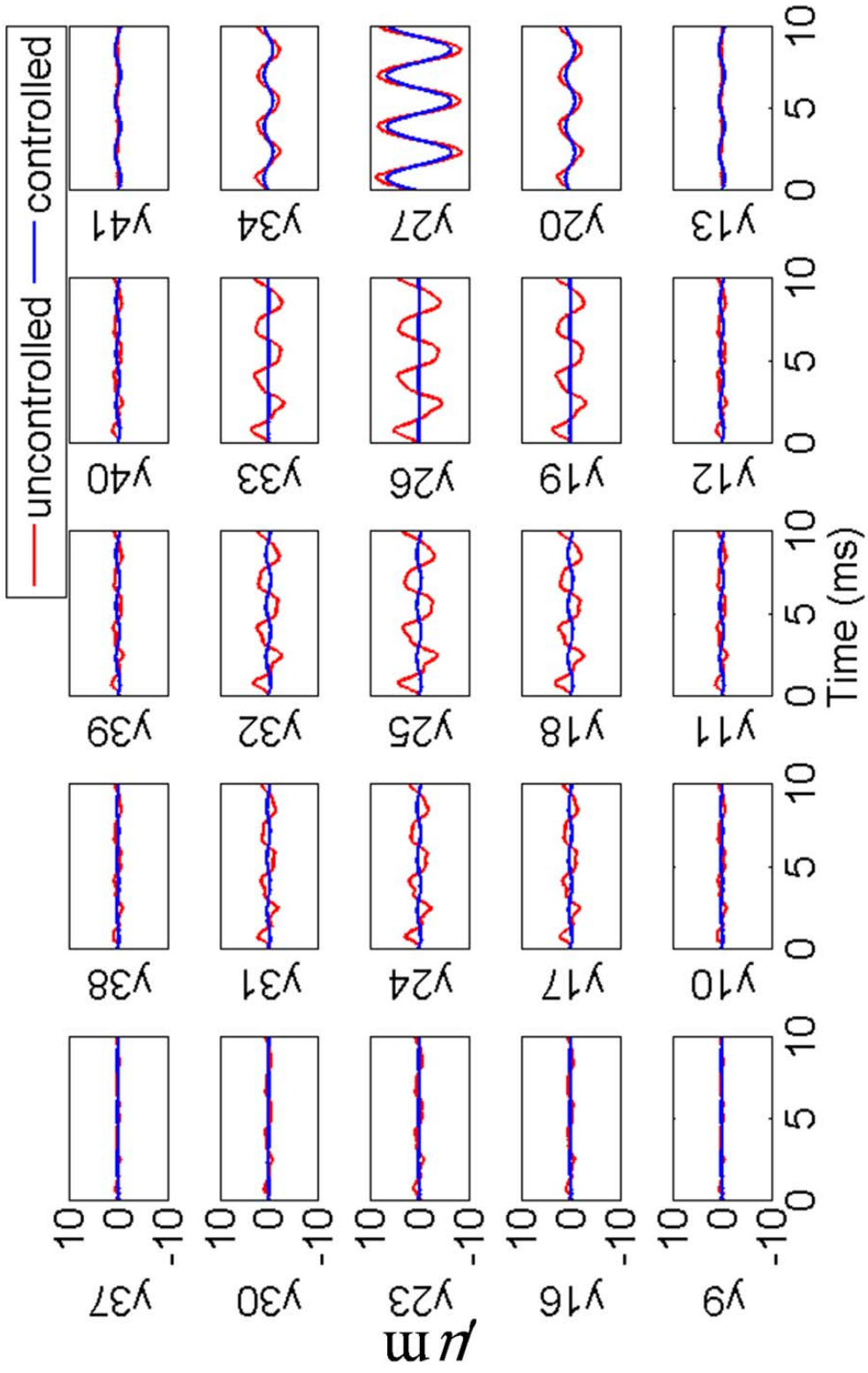

Figure 6.18. Case 1. Displacements of the nodes of plate due to a 300 Hz sine wave disturbance at node 27, actuators are at nodes 19, 26, and 33

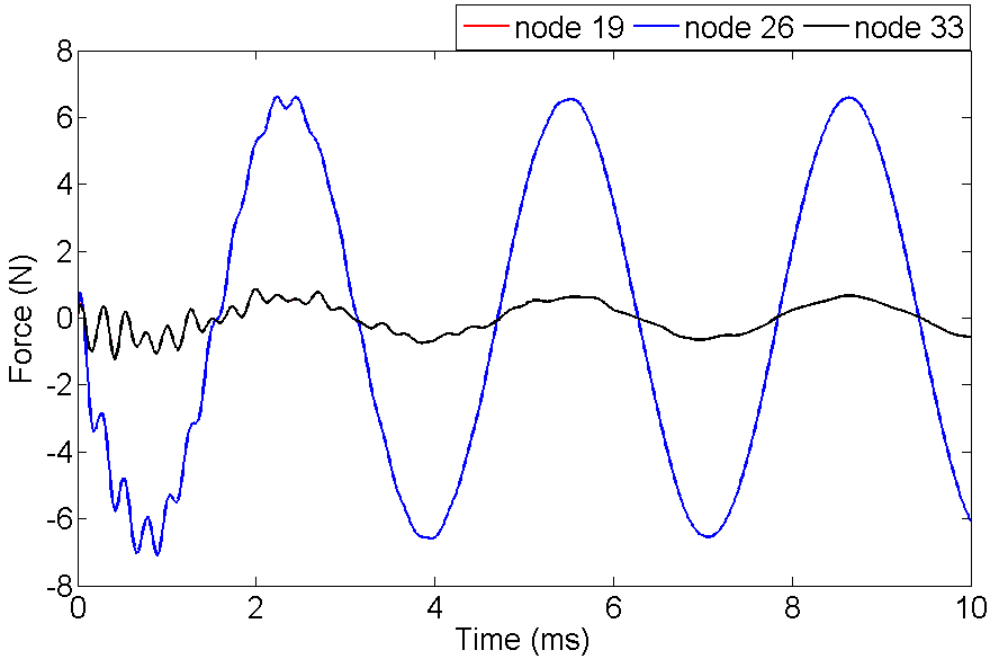

Figure 6.19. Case 1. Actuator forces for disturbance amplitude equals to 10 N. Actuators at nodes 19 and 33 have identical forces due to symmetry

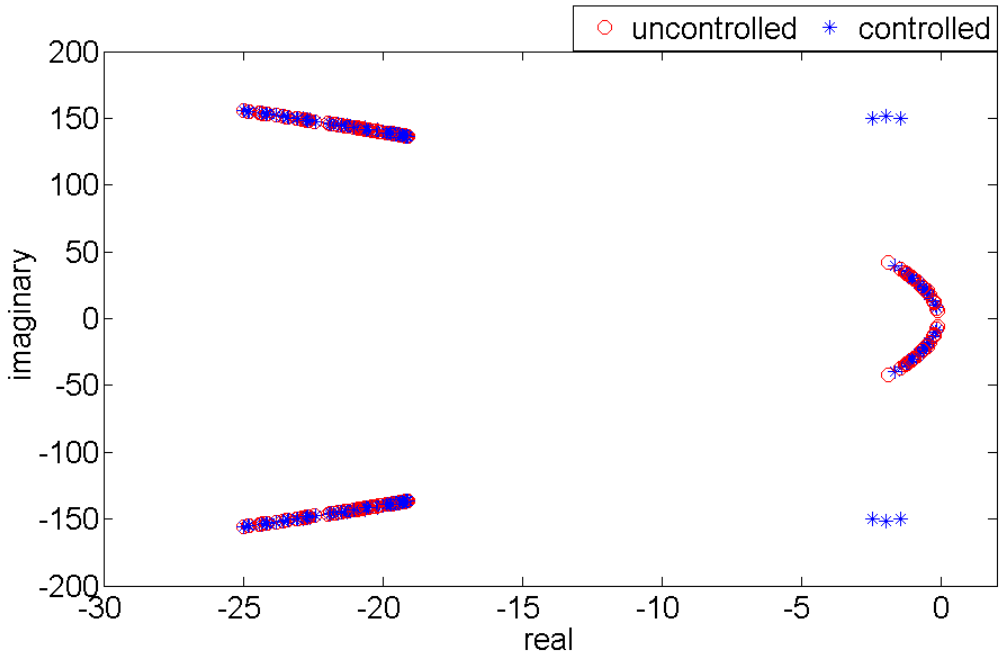

Figure 6.20. Case 1. Eigenvalues of the open-loop and closed-loop system

6.2.2. Case 2: plate with 2 working actuators and failed middle actuator

We assume that the middle actuator located on node 33 is failed. This results in setting the middle row of the control gain matrix to zero. Figure 6.21 shows the displacement of the nodes of the plate. The noticeable difference is the displacement of node 26, which has a failed actuator. Maximum actuation forces are shown on Figure 6.22. The middle actuator has not applied any force to the system. The maximum actuation force on the actuator on node 19 is 3.94 N, and on the node 33 is 4.12 N. Actuation forces have increased in comparison to case 1. The slight difference is because the control gain matrix is not symmetric. The control gain matrix is

$$K = 1.0 \times 10^4 \begin{bmatrix} -2.1656 & 0.0420 & 0.0267 \\ 0 & 0 & 0 \\ -0.0319 & -0.0444 & -2.2220 \end{bmatrix}$$

Figure 6.23 shows the closed-loop and open-loop poles of the system. It is seen that two closed-loop poles have moved away from the open-loop poles cluster, as is expected since there are two working actuators. Comparing Figures 6.23 and 6.20, one finds that the moved closed-loop poles are placed in similar region.

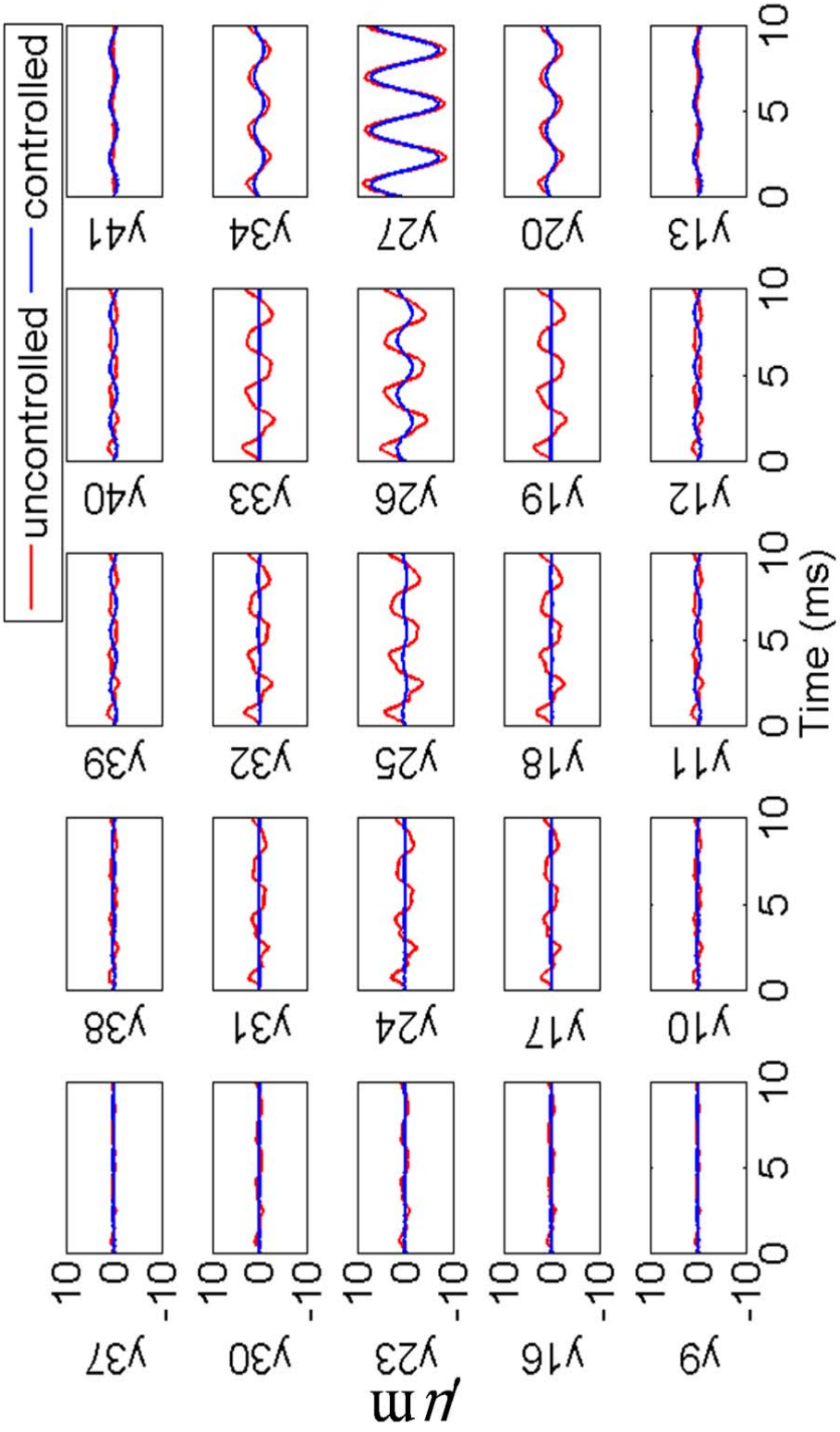

Figure 6.21. Case 2. displacements of the nodes of plate due to a 300 Hz sine wave disturbance on node 27, actuators are on nodes 19, 26, and actuator on node 33 is failed

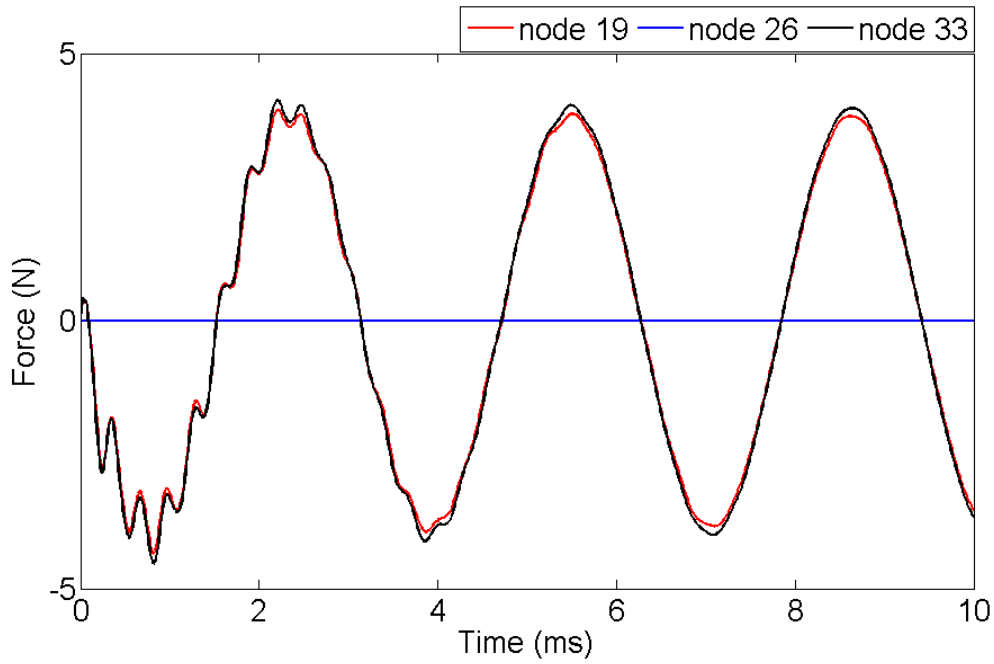

Figure 6.22. Case 2. Actuator forces for disturbance amplitude equals to 10 N. Actuators at nodes 19 and 33 have identical forces due to symmetry. Actuator on node 26 has zero force because of the failure

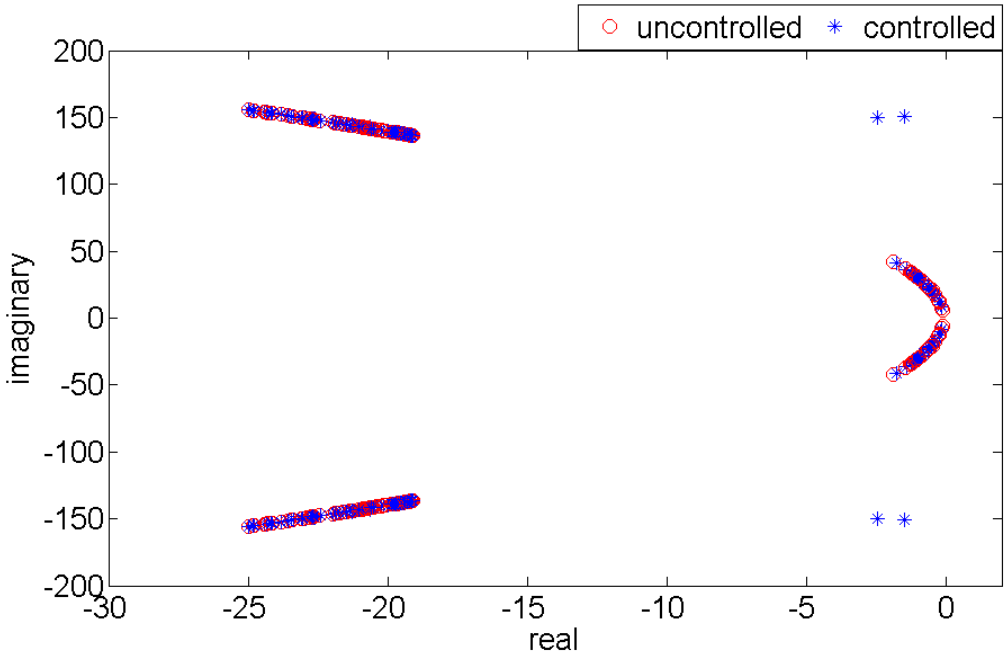

Figure 6.23. Case 2. Eigenvalues of the open-loop and closed-loop system

6.2.3. Case 3: plate with 2 working actuators and failed outer actuator

In this case, we assume that the faulty actuator is located at node 33. Therefore the control gain matrix is

$$K = 1.0 \times 10^4 \begin{bmatrix} -2.1656 & 0.0420 & 0.0267 \\ 0.0034 & -2.1985 & 0.0030 \\ 0 & 0 & 0 \end{bmatrix}$$

The displacement shown on Figure 6.24 shows a good isolation on different nodes of the plate. The displacement at node 25, however, is different form case 1, because of the failed actuator. Time history of the actuation forces are shown in Figure 6.25. The maximum actuator force at node 19 is 0.72 N, at node 26 is 7.2 N, which are very close to force in case 1.

Figure 6.26 shows the displacement of the middle node of the plate for cases 1, 2, and 3. The amplitude of vibrations for all the cases are very close. Nodal displacements for case 3 are in phase with those observed for case 1. In case 2, however, there is 90 degrees phase shift with respect to case 1.

The results for cases 3 and 4 indicate that orthogonal eigenstructure control continues to perform in a robust manner in the presence of the actuator failure. Failure of each of the actuators only has a local effect on vibration suppression, but the overall vibration suppression in plate remains intact.

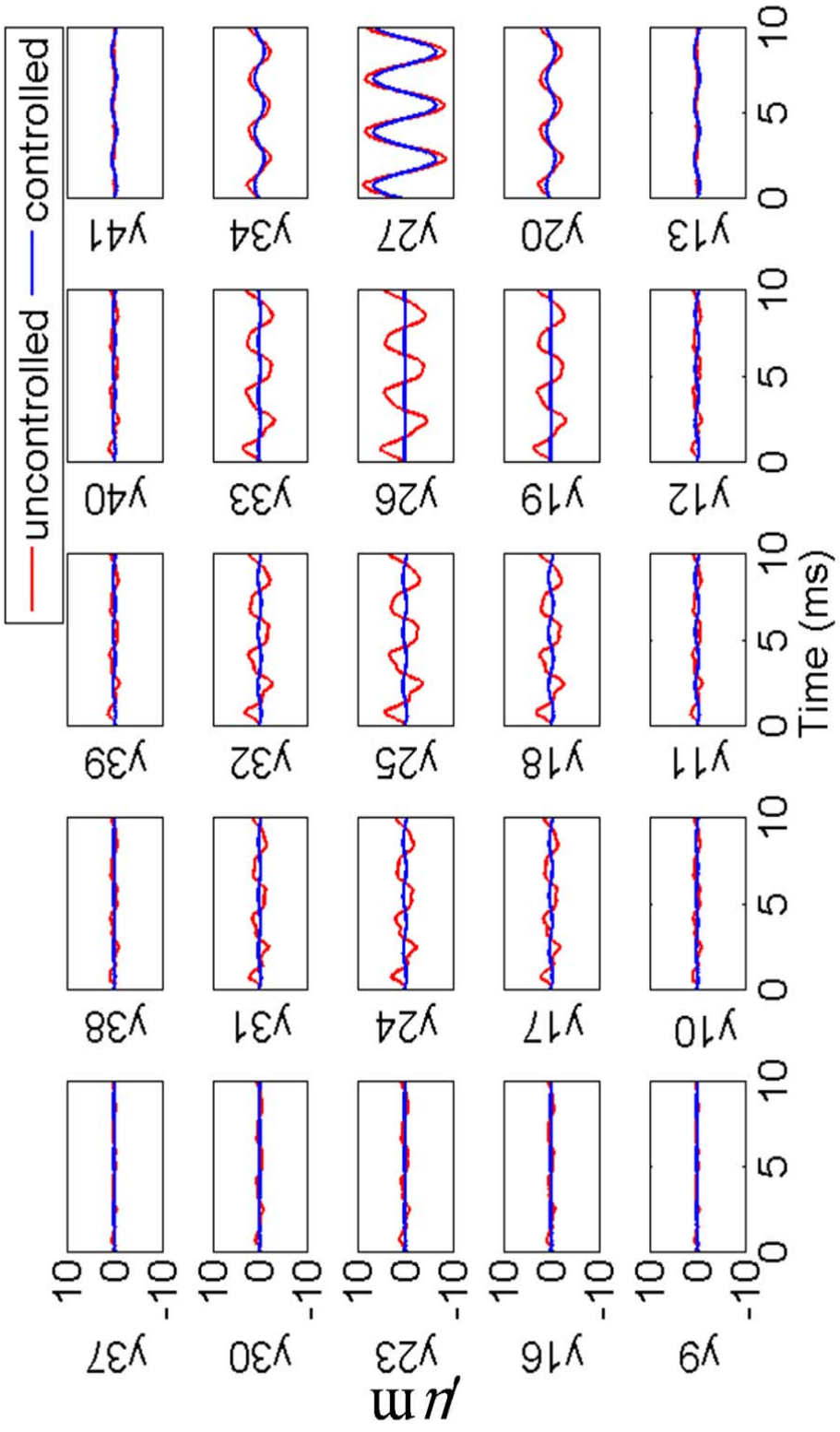

Figure 6.24. Case 3. Displacements of the nodes of plate due to a 300 Hz sine wave disturbance on node 27, actuators are on nodes 19, 33, and actuator on node 26 is failed

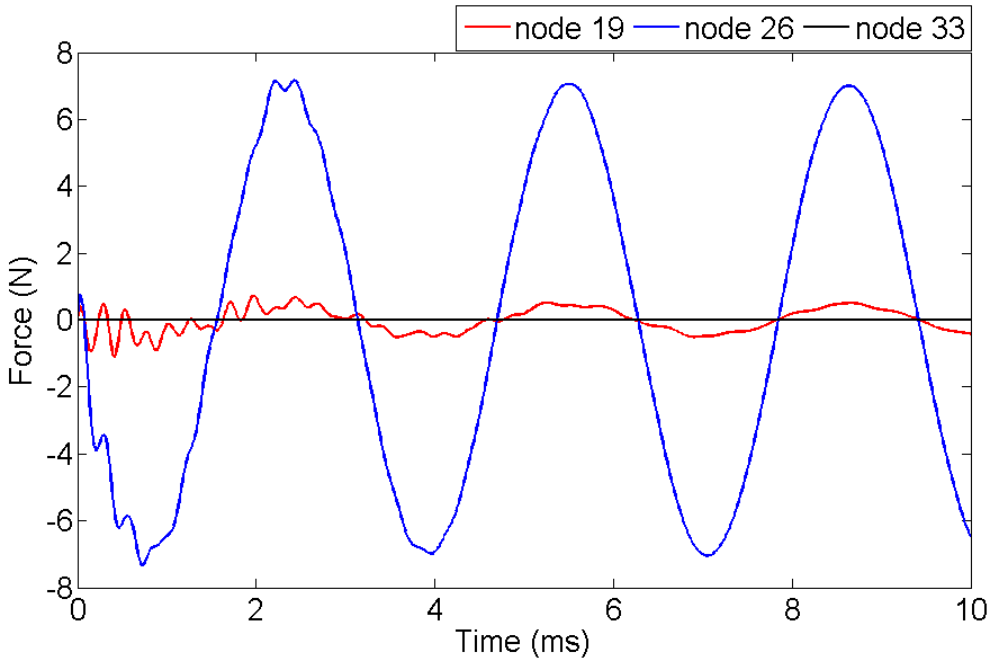

Figure 6.25. Case 3. Actuator forces for disturbance amplitude equals to 10 N. Actuator on node 33 has zero force because of the failure

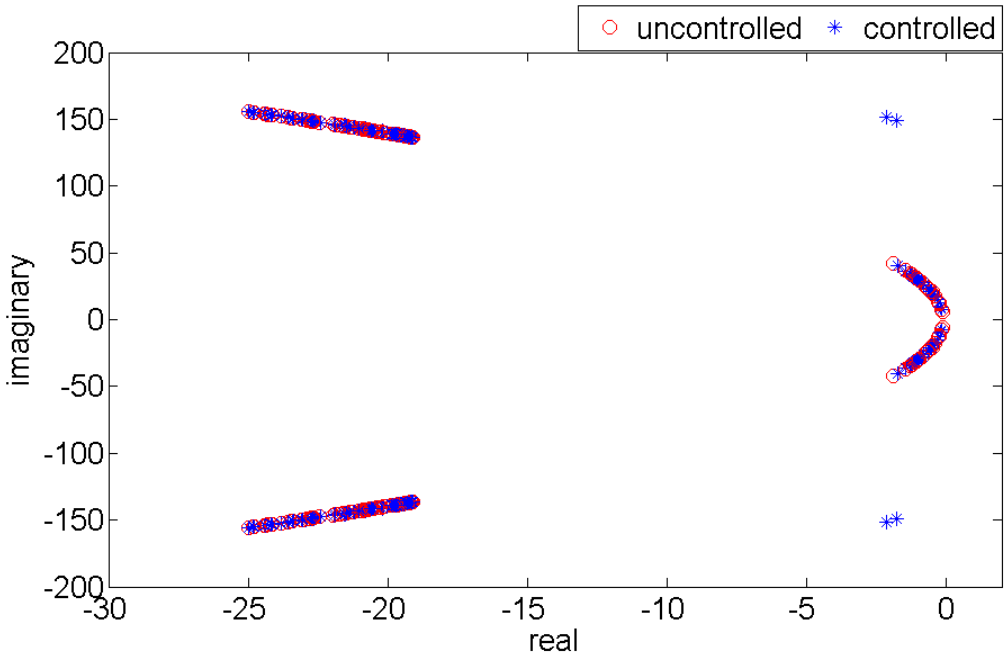

Figure 6.26. Case 3. Eigenvalues of the open-loop and closed-loop system

6.2.4. Case 4: plate with 2 working actuators similar to case 2

Case 4 includes the control of vibrations with 2 working actuators at nodes 19 and 33. It is similar to case 2 except that there are no failed actuators. The control gain matrix is

$$K = 1.0 \times 10^4 \begin{bmatrix} -2.2027 & 0.0028 \\ 0.0028 & -2.2027 \end{bmatrix}$$

which is symmetric due to the geometrical symmetry of plate and the location of the actuators and disturbance. The gain matrix has the same properties as case 1. The off diagonal elements are three orders of magnitudes smaller than the diagonal elements. Therefore, the gain matrix is nearly diagonal. Figure 6.28 shows displacements at different nodes on the plate. Similar to the earlier cases, a good isolation can be seen throughout the plate. A comparison between displacements at node 25, the middle point in plate, is shown in Figure 6.29. This shows that the displacements for the two cases are identical. The time history of the actuator forces are shown in Figure 6.30. The maximum force at nodes 19 and 33 are identically 4.03 N, which is close to the actuation forces in case 2. The distribution of the eigenvalues of the open-loop and closed-loop systems is shown in Figure 6.31. Two of the closed-loop system's eigenvalues are moved away from the cluster of the open-loop eigenvalues, similar to the ones in case 2.

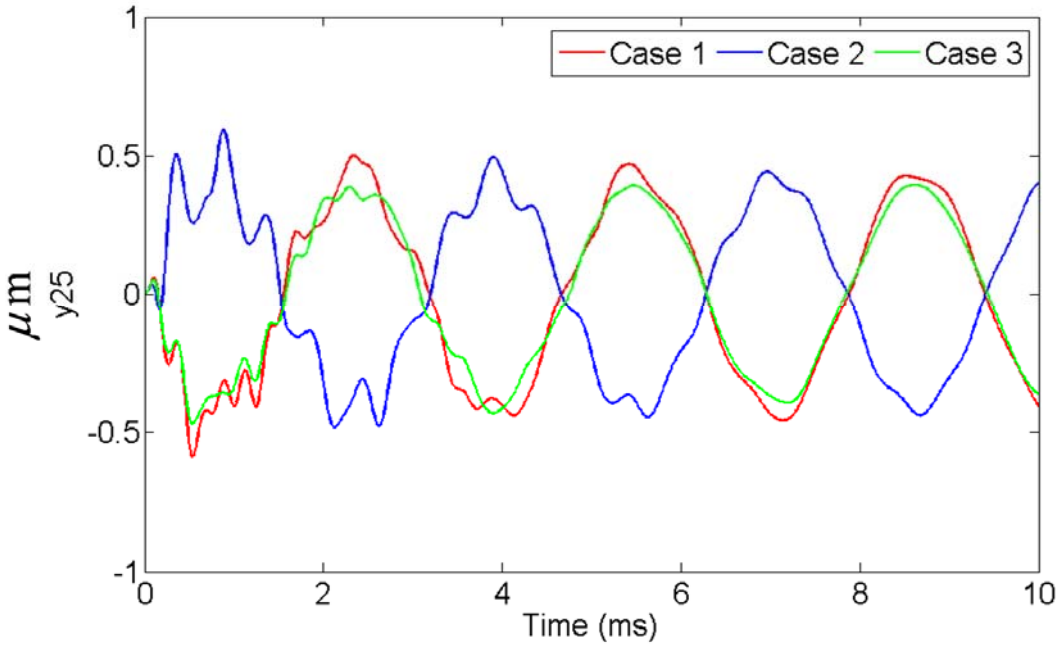

Figure 6.27. Displacement of middle point of plate for cases 1, 2, and 3

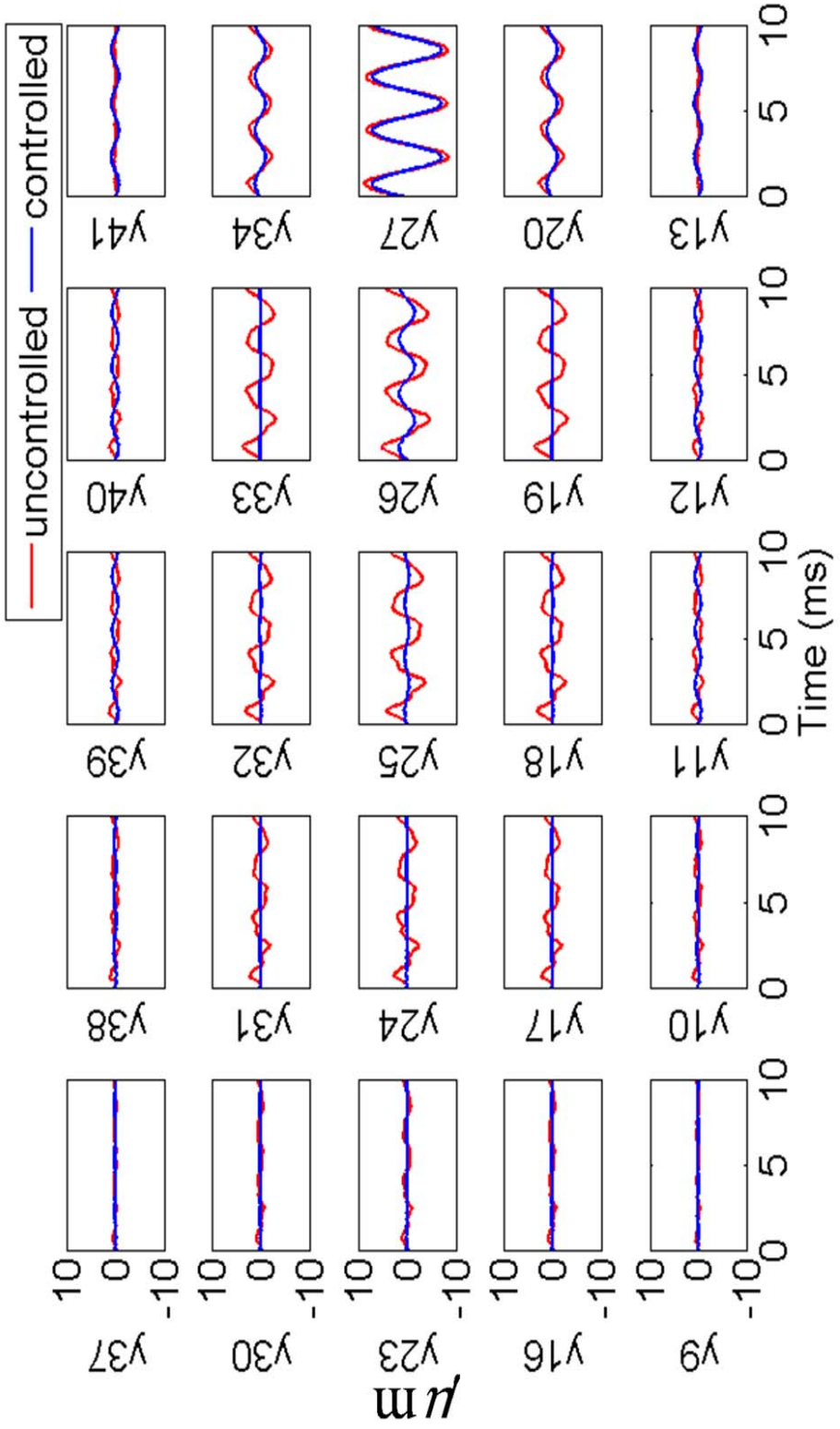

Figure 6.28. Case 4. Displacements of the nodes of plate due to a 300 Hz sine wave disturbance on node 27, actuators are on nodes 19, 26

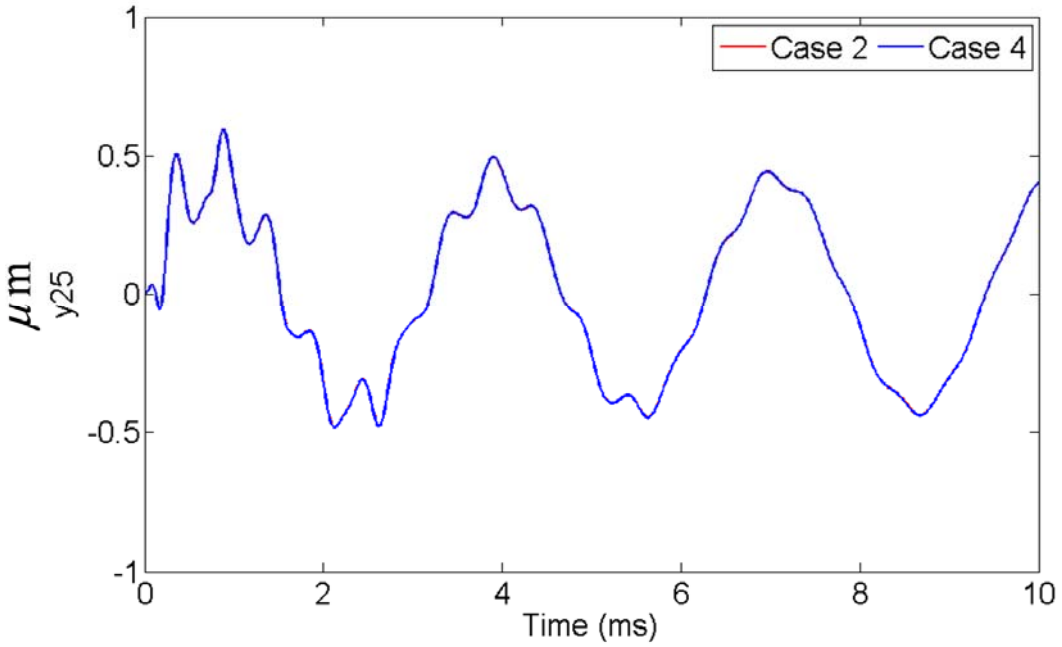

Figure 6.29. Identical displacement at middle point of plate for cases 2 and 4

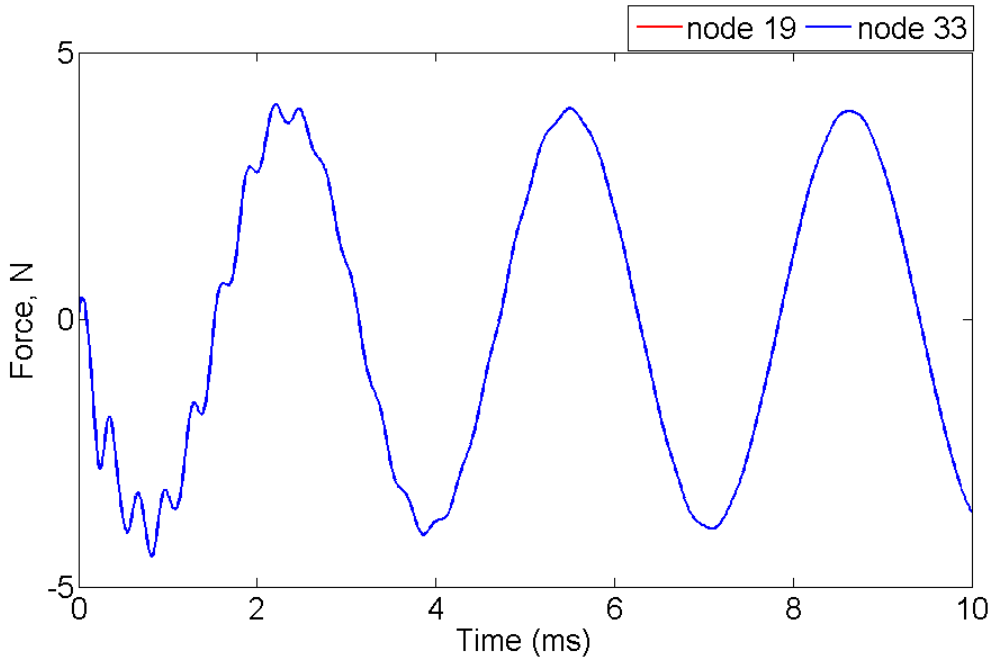

Figure 6.30. Case 4. Identical actuator forces for disturbance amplitude equals to 10 N.

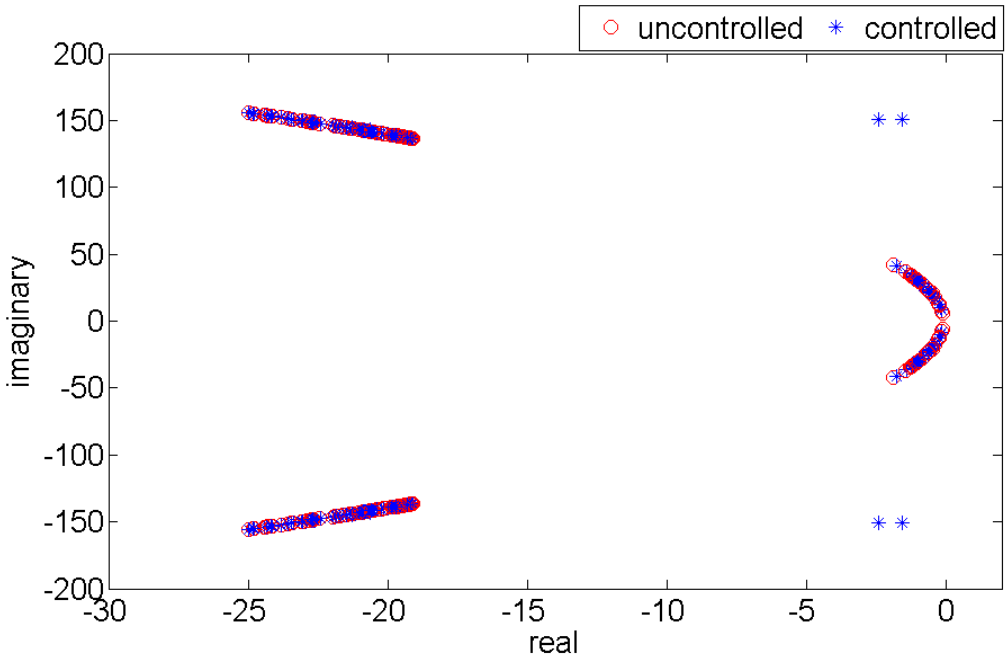

Figure 6.31. Case 4. Eigenvalues of the open-loop and closed-loop system

6.2.5. Case 5: plate with 2 working actuators similar to case 3

Case 5 discusses the vibration isolation of the plate using two actuators that are placed at nodes 19 and 26, the same locations as the working actuators for case 3. The control gain matrix is

$$K = 1.0 \times 10^4 \begin{bmatrix} -2.2027 & -0.0032 \\ -0.0026 & -2.2064 \end{bmatrix}$$

which is very similar to case 4. Figure 6.32 shows vibration pattern that are similar to the earlier cases. The identical displacements of the middle point of the plate for case 3 and 5 are depicted in Figure 6.33. Also, the time histories of the actuation forces are shown in Figure 6.34. The Maximum actuation forces of the actuators at nodes 19 and 26 are 0.73 N, and 7.16 N respectively, which is very close to case 3. Similar to earlier cases, two of the closed-loop eigenvalues have moved away from the open-loop cluster, as seen in Figure 6.35.

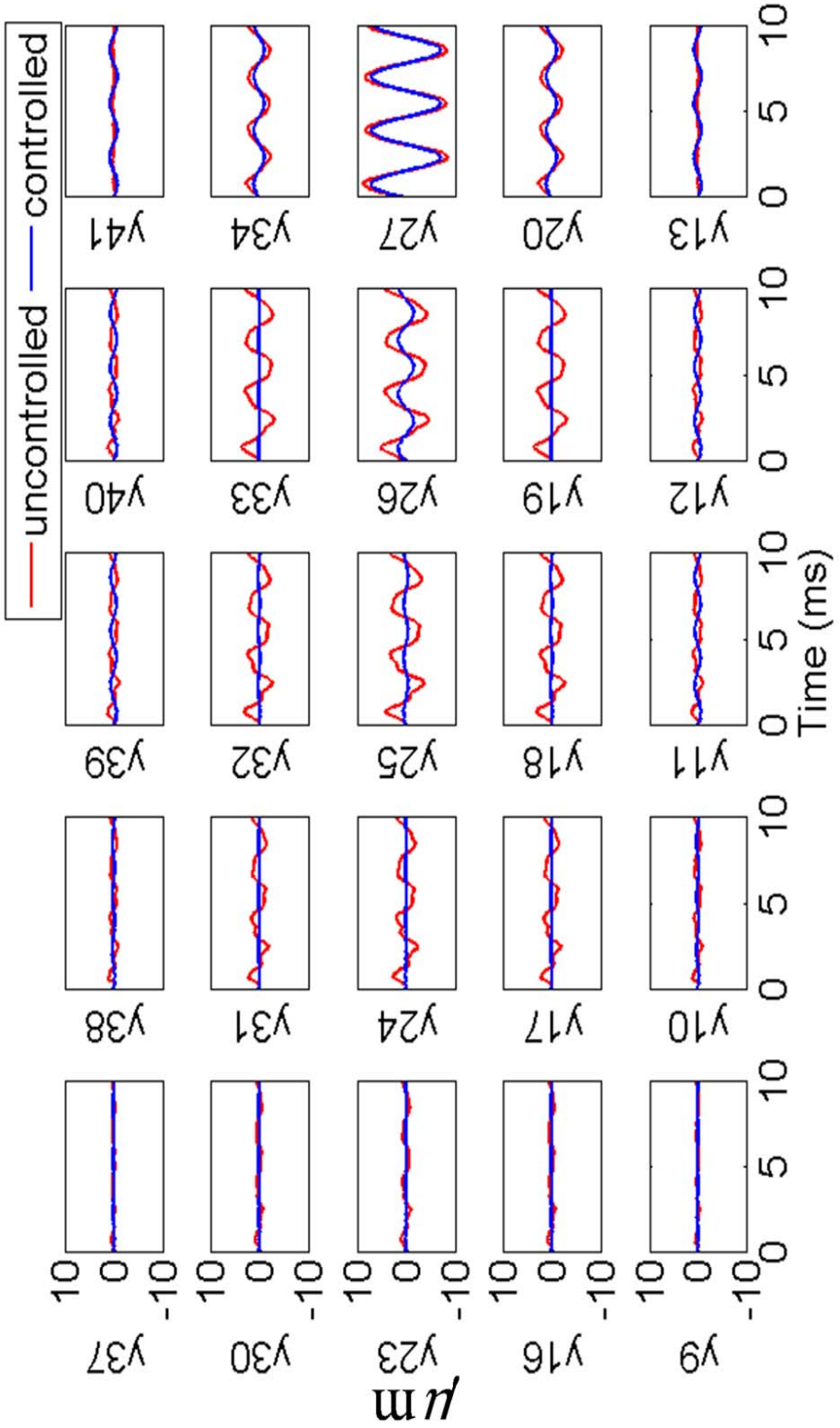

Figure 6.32. Case 5. Displacements of the nodes of plate due to a 300 Hz sine wave disturbance on node 27, actuators are on nodes 19, 26

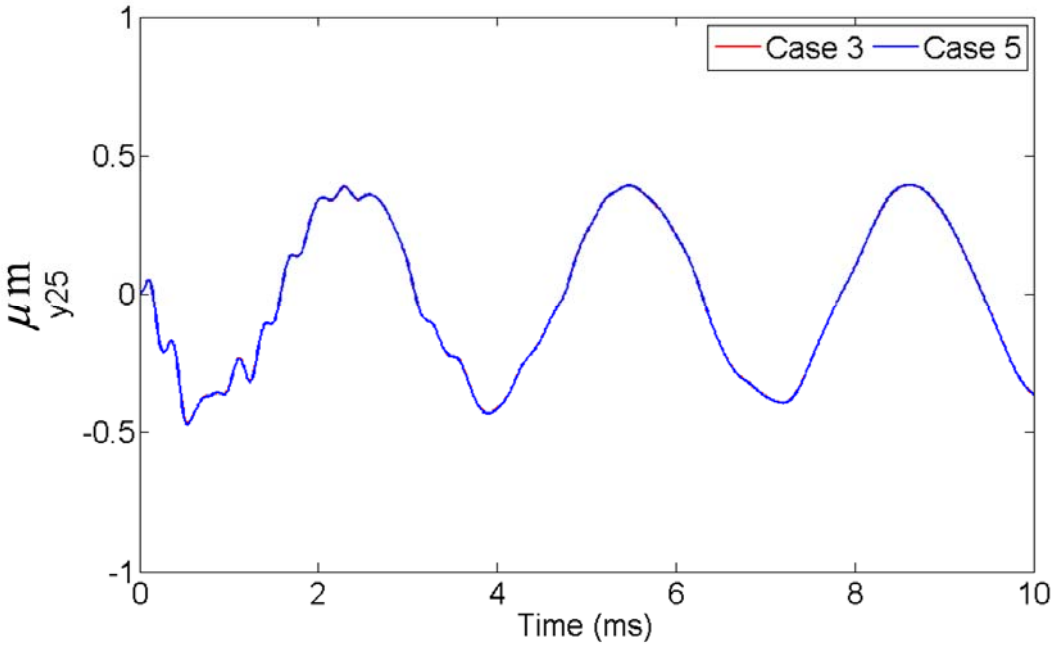

Figure 6.33. Identical displacement of middle point of plate for cases 2, and 4

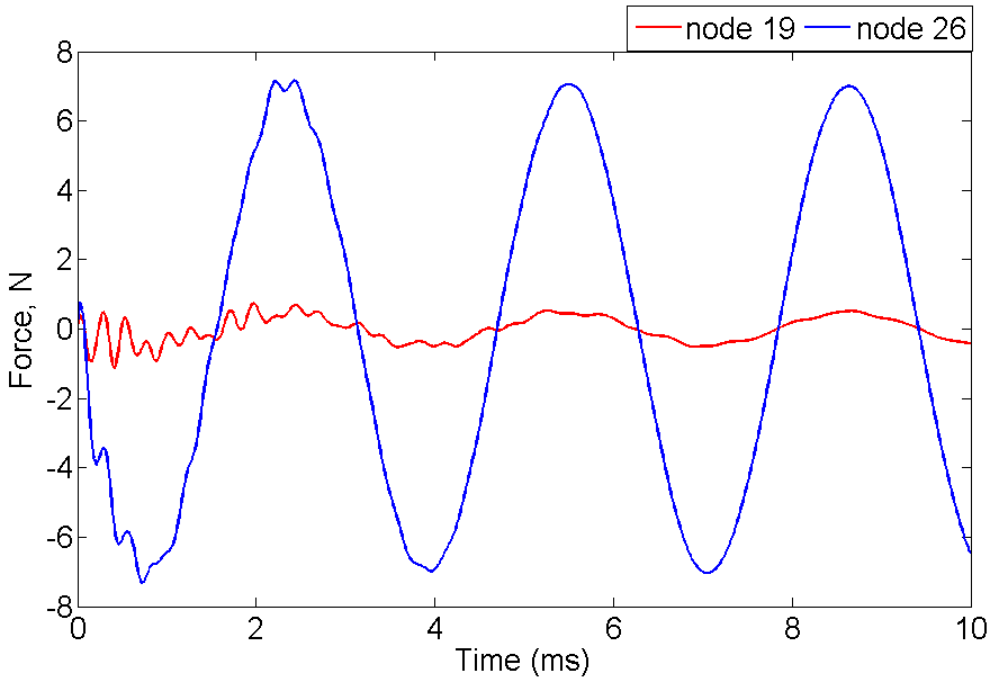

Figure 6.34. Case 5. Actuator forces for disturbance amplitude equals to 10 N.

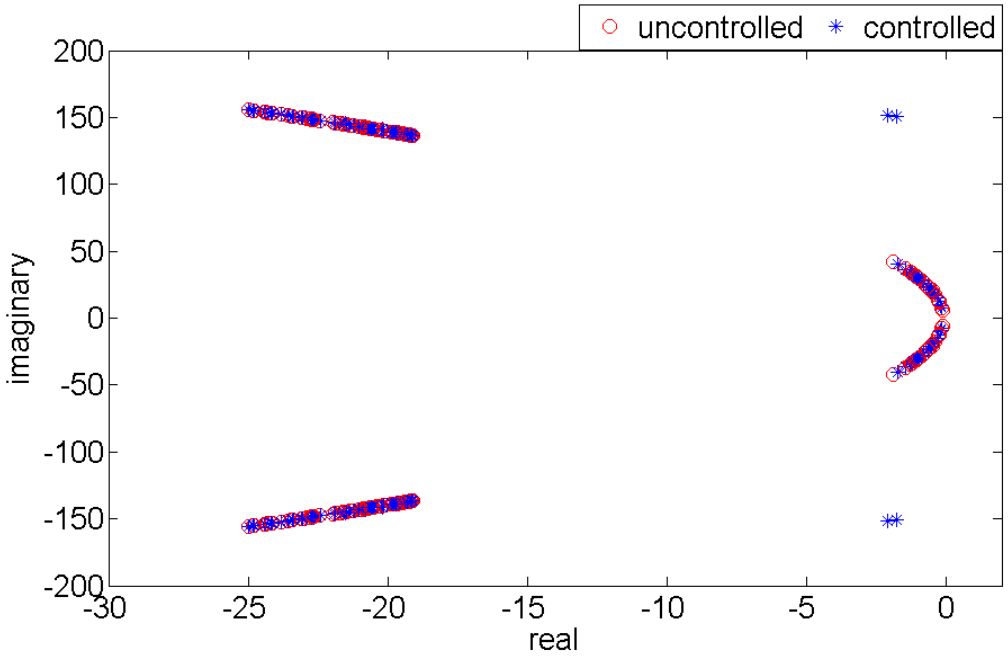

Figure 6.35. Case 5. Eigenvalues of the open-loop and closed-loop system

Comparing the results for cases 2 and 3 to case 1, one can see a reliable control design when orthogonal eigenstructure control is used. The actuator forces for working actuators in cases 2 and 3 are very close to the forces for cases in which all three actuators work. Similar displacement time history can be seen throughout the plate except at nodes with failed actuators. Moreover, comparing cases 4 to 2 and cases 5 to 3, shows that there is a slight difference between the system with one failed actuator and the system that are designed with two actuators. Orthogonal eigenstructure control with three actuators is robust in the presence of actuator failure

Table 6.1 shows the closed-loop eigenvalues that are moved away from the locus of the open-loop eigenvalues. It is seen that for all cases, the poles are placed in a small region. The rest of the closed-loop eigenvalues are moved slightly on the locus of the open-loop poles, without noticeable deviation away from the cluster.

Table 6.1. Moved closed-loop poles in cases 1to 5

	Pair 1	Pair 2	Pair 3
Case1	-1.99 ± 151.35i	-1.43 ± 15.17i	-2.47 ± 150.08i
Case 2	-1.50 ± 150.79i	-2.46 ± 150.13i	
Case 3	-1.78 ± 148.91i	-2.11 ± 151.25i	
Case 4	-1.56 ± 150.95i	-2.40 ± 150.60i	
Case 5	-1.78 ± 150.54i	-2.11 ± 151.19i	

6.3. Effect of scaling the control gain matrix

It is usual in control practice that the overall control gain matrix is scaled up or down in order to compensate the effect of uncounted parameters. Since orthogonal eigenstructure control is a model-based control method, the major source of uncertainty is inaccurate model of the system. In practice, system identification algorithms are used to estimate a model for the structures such as plates. In order to assess the effect and limits of scaling the control gain matrix determined by orthogonal eigenstructure control, we consider the finite element model of the plate depicted in Figure 6.1. The disturbance is a 300 Hz sinusoidal input to the node 27. The control actuators are considered to be located on nodes 25, and 26. The same open-loop eigenvalues that were chosen in sections 6.2.4, and 6.2.5 are the operating eigenvalues. The control gain is

$$K = 1.0 \times 10^4 \begin{bmatrix} \text{-2.2125} & \text{-0.0429} \\ \text{-0.0431} & \text{-2.2072} \end{bmatrix}$$

The control gain is multiplied by 1/10, 1/3, 1/2, 2, and 3 and the change in the locations for the closed-loop poles, actuation forces and the maximum amount of displacement at different nodes are compared. Figure 6.36 shows the change in the peak amplitude of the nodes at different overall control gain. It shows that scaling up the control gain with overall control gains 2 and 3, slightly improve the suppression of vibrations. The vibration suppression decreases when the control gain is scaled down by 1/0, 13, and 1/2. Figure 6.37 shows the pole plots of the controlled plate with different overall gain scales. It is seen that by scaling down the control gain, the two closed-loop poles that moved

away from the loci becomes closer to loci. On the other hand, those poles become farther from the open-loop poles loci when the control gain is scaled up. When the overall gain is multiplied by 2, and 3, the locations of new poles imply less amount of damping. When the overall control gain is multiplied by 3.6, the vibrations become very large. Figure 6.38 shows the control actuation forces. It shows that scaling up the control gains does not change the actuation force significantly.

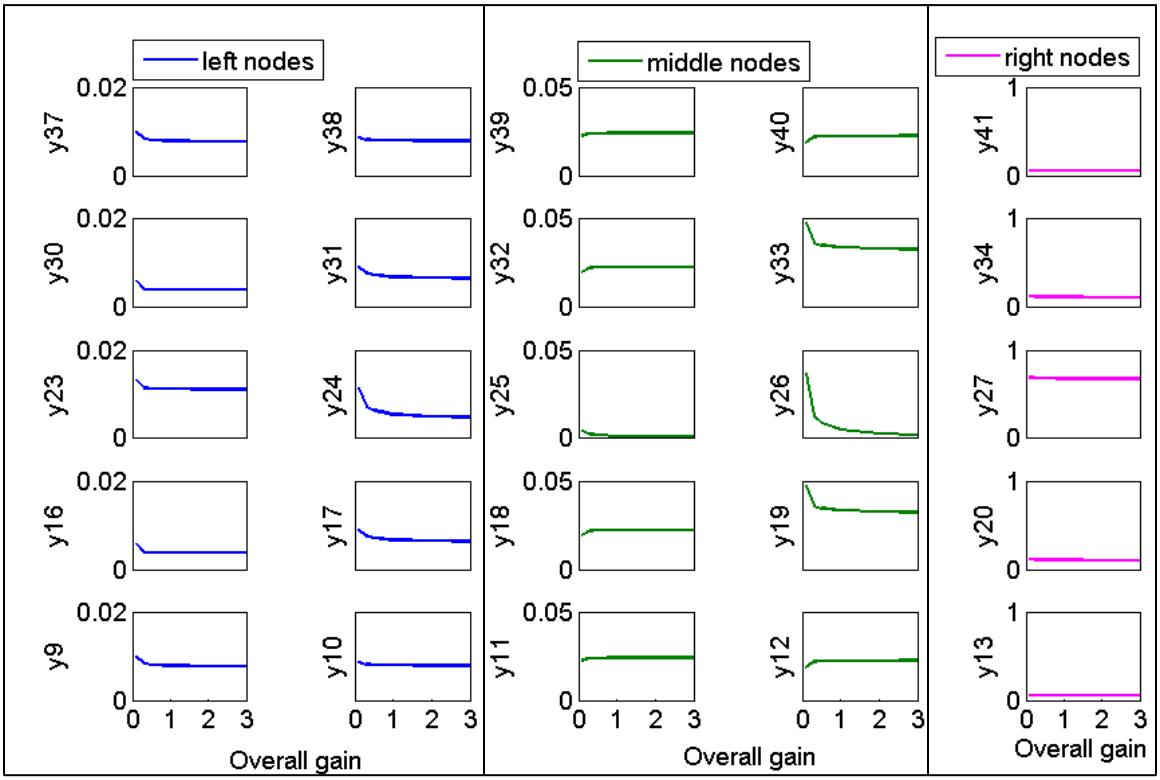

Figure 6.36. Maximum displacements (in μm) at plate nodes with different overall gain scale; a) left nodes, b) middle nodes, c) right nodes. Subplots a, b, and c have different y axis scale

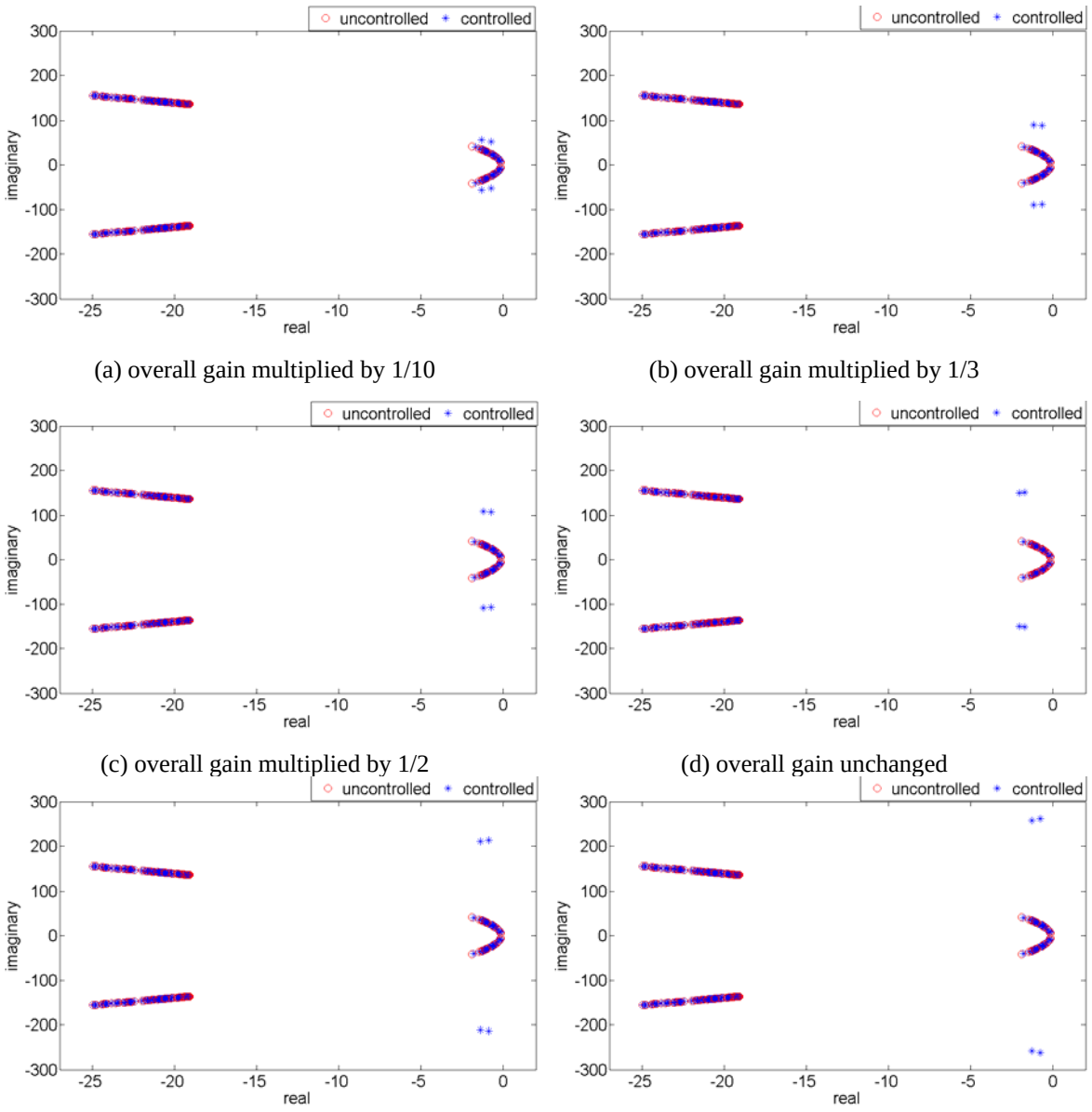

(a) overall gain multiplied by 1/10

(b) overall gain multiplied by 1/3

(c) overall gain multiplied by 1/2

(d) overall gain unchanged

(e) overall gain multiplied by 2

(f) overall gain multiplied by 3

Figure 6.37. Pole plots of controlled plate with different scaled overall gain

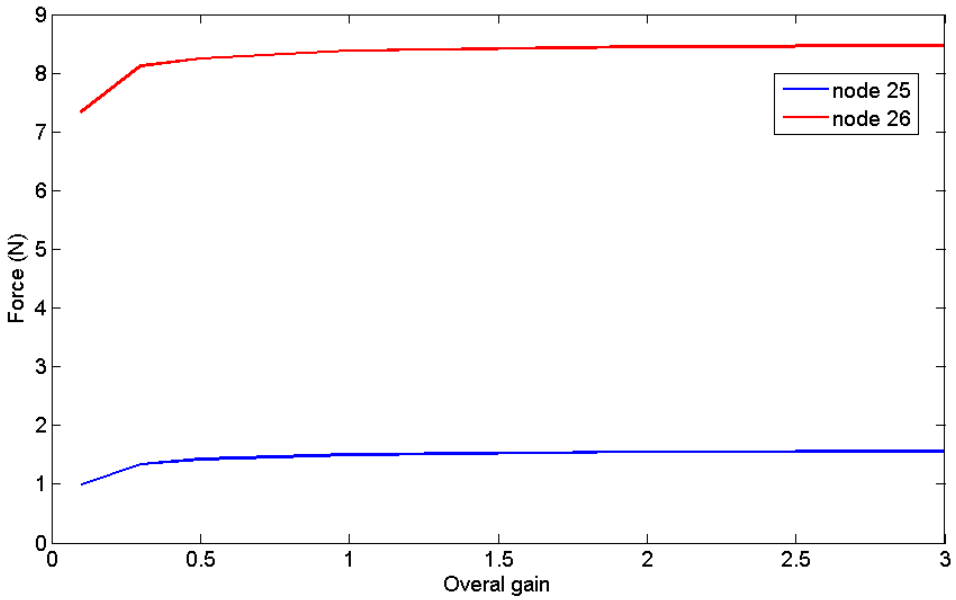

Figure 6.38. Maximum actuation forces due to different overall gain scale

6.4. Summary

Finite element model of a steel plate has been used to show the application of the orthogonal eigenstructure control for vibration cancellation. A sinusoidal disturbance has been applied to the plate and three actuators have been used to reduce the vibration in the plate. The effect of the operating eigenvalues has been shown by choosing them from different areas of the locus of the open-loop eigenvalues. When the closest open-loop eigenvalues to origin are chosen as operating eigenvalues, the resulting set of closed-loop systems contains only one stable closed-loop system. By choosing the open-loop eigenvalues farther from the origin, we showed that the resulting closed-loop systems converge, due to convergence of their respective control gain matrices. The control scheme has decoupled channels, since gain matrices have diagonal elements several orders of magnitude larger than the off-diagonal elements. Also, the actuation forces become significantly smaller than the disturbance. To further investigate the operating eigenvalues and find the map of appropriate operating eigenvalues, a range of complex numbers are used as operating eigenvalues. It is shown that the open-loop eigenvalues are

confident candidates for the operating eigenvalues; however, the operating eigenvalues are not limited to them.

To investigate the robustness of orthogonal eigenstructure control, finite element model of a plate, as an example of a system with high degrees of freedom has been considered. Five cases have been considered for different scenarios with the actuators of the plate and the results have been compared. It is seen that when the operating eigenvalues are the farthest open-loop eigenvalues from the origin, a very reliable and almost decoupled control can be achieved. Behaviors of the systems with failed actuators are very close to the behavior of the system with healthy actuators. Moreover, the cancellations of vibration in the systems with failed actuators are almost identical to the systems that are primarily designed for two actuators. While there is no need to define the required locations for the closed-loop poles, few pairs of the closed-loop eigenvalues are moved away from the locus of the open-loop eigenvalues. The number of pairs of the moved eigenvalues is equal to the number of the actuators in each case. Since in all the cases the closed-loop eigenvalues are moved to one specific area, the behaviors of all the systems are similar and the control is robust to the actuator failure.

Chapter 7

Experiments

In this chapter, the experimental setup is described. This setup is used for investigating the application of orthogonal eigenstructure control for suppressing the vibrations in a steel plate. The hardware that are used and the process for defining the range of frequency for vibrations cancellation are described. Also, Active vibration cancellation of test plate due to tonal and wide-band disturbances is tested. Orthogonal eigenstructure control has been used for finding the control gains

7.1. Test plate and the frame

A standard 20-gauge galvanized steel test plate, shown in Figure 7.1, has been used for evaluating the applicability of orthogonal eigenstructure control. This plate is clamped to the frame using 14 bolts that are tightened to a torque of 25 Nm. The size of the plate is 600mm by 500mm; however, since the clamping area is 50 mm from each edge, the size of plate that it's dynamic is taken into the account for the test is 500mm by 400mm. A detail description of the clamp frame and the bottom box structure can be found in Jeric's thesis [86].

A bridge is mounted on top of the bottom box, to hold the electromagnetic actuator. It also is used for routing the cables from the high voltage amplifier to the piezoelectric actuators. The bridge can slide along the length of the plate. The height of the electromagnetic actuator from the plate is also adjustable. The electromagnetic actuator is secured by a double mesh retainer. The cage that holds the electromagnetic actuator can slide along the length of the bridge. Therefore, the electromagnetic actuator can be placed directly over any point of the plate.

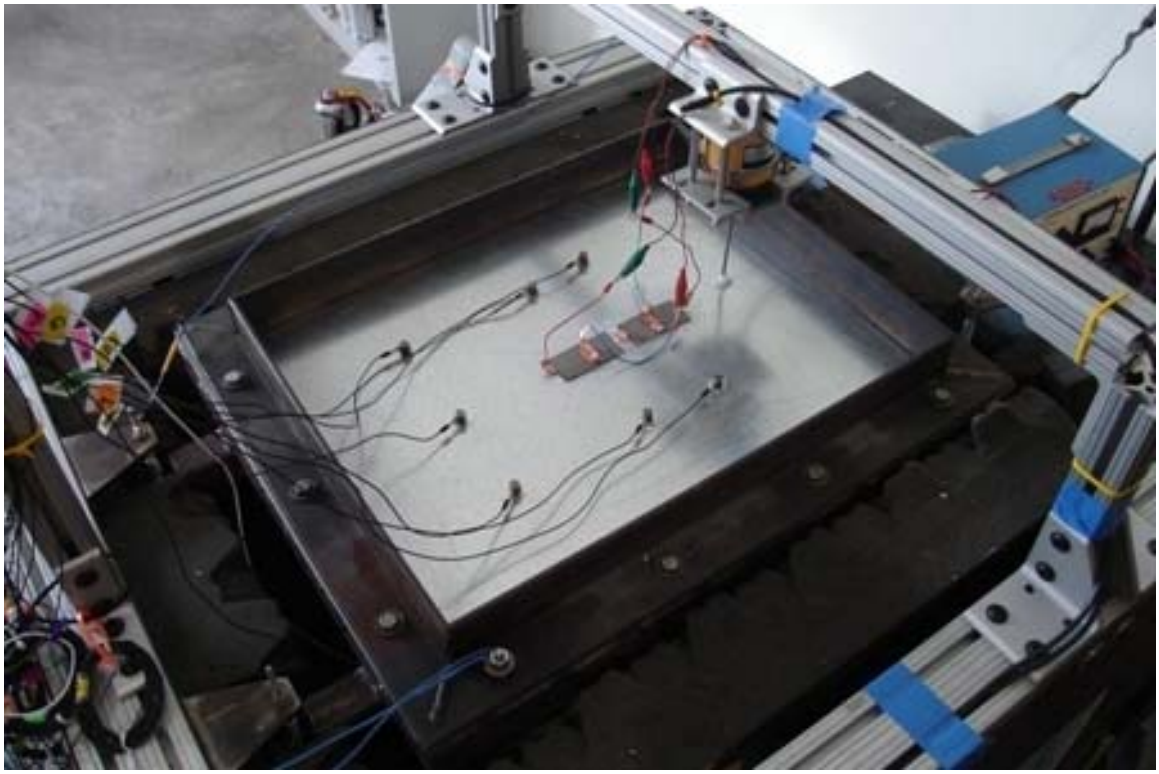

Photo by Mohammad Rastgaar, July 2008
Figure 7.1. Test plate mounted on the frame structure

7.1.1. Electromagnetic actuator

The electromagnetic actuator is part of the P1906 Linear Vibration Apparatus manufactured by Cussons Technology. Figure 7.2 shows the electromagnetic actuator secured in its cage. This electromagnetic actuator is used for applying the disturbance input to the plate. A stinger made of a threaded rod M4-0.7 is used to transfer the force and displacement from the actuator to the plate. At the tip of the stinger a Nylon Spacer made by Hillman, UPC 008236708202, with outer diameter of 1/4 in, inner diameter of 0.140 in, and length of 1/2 in is placed to provide a smooth area that is glued to the plate. Duro Super Glue, UPC 079340018013, has been used for attaching the spacer to the plate. The stinger is glued 85 mm from the right edge on the axis of symmetry of the short side of the plate.

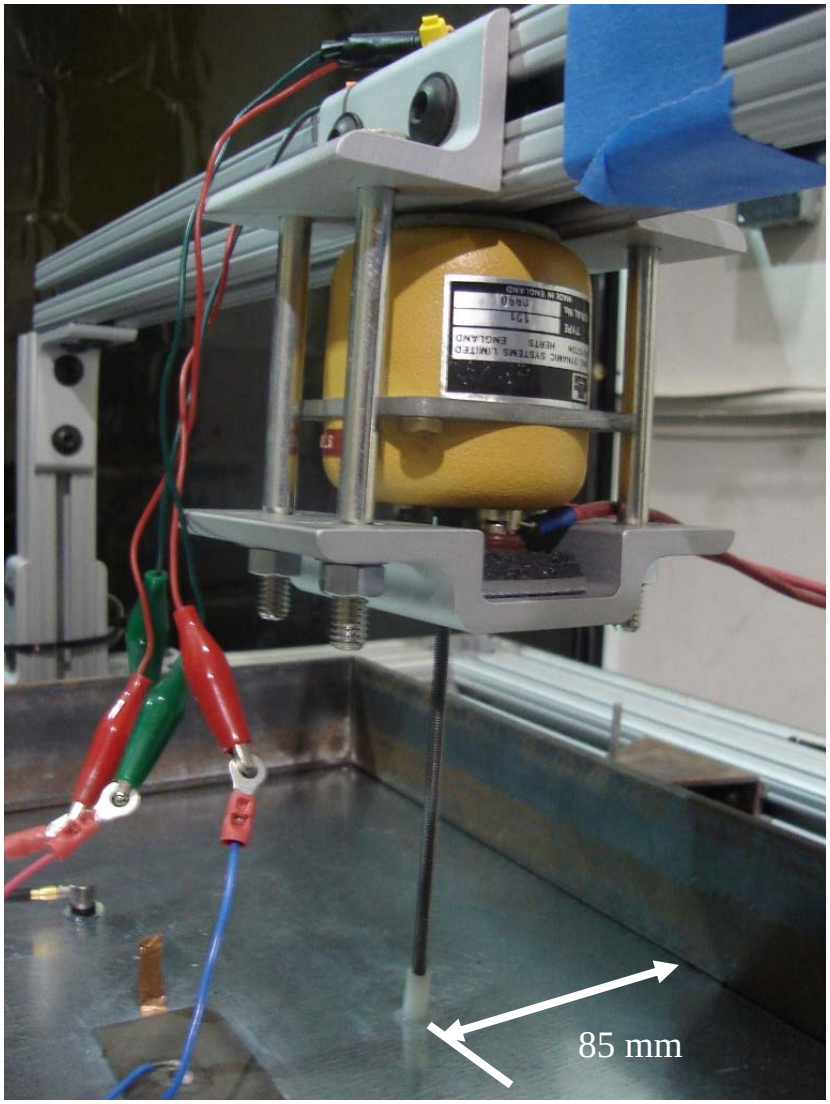

Photo by Mohammad Rastgaar, January 2008
Figure 7.2. Electromagnetic actuator and the stinger

7.1.2. Amplifier for electromagnetic actuator

The amplifier shown in Figure 7.3 is the drive unit of the P1906 Linear Vibration Apparatus manufactured by Cussons Technology. It is driven by an external oscillator and may be regarded as an operational amplifier with a voltage gain of unity from DC to 10 kHz.

Photo by Mohammad Rastgaar, January 2008
Figure 7.3. Amplifier for the Electromagnetic actuator

7.1.3. Piezoelectric actuators

Two high performance piezoelectric actuators T234-A4CL-503X from Piezo systems, Inc. are used as control actuators. The 2.5 in by 1.25 in piezo elements are composite reinforced bending bimorphs made of PSI-5A4E and have thickness of 0.034 in. It is X poled for series bending operation, so it needs two wires for upper and lower surfaces. The piezo ceramic weight 9.7 g and its rated voltage is ±250 V. The mounted piezo actuators are shown in Figure 7.4.

A 1/4 in wide copper foil tape with conductive adhesive has been attached to the lower surface of the piezoelectric ceramic, before gluing it to the test plate. The tape has a peel-off liner. The copper tape is 0.0035 in thick and consists of a 0.0014 in thick foil with 0.0021 in of acrylic adhesive.

Before applying the glue, the area of test plate that the piezoelectric actuators will be placed must be prepared. First, fine abrasive cloth was used to prepare the test plate, and then a denatured alcohol used to clean the surface of test plate.

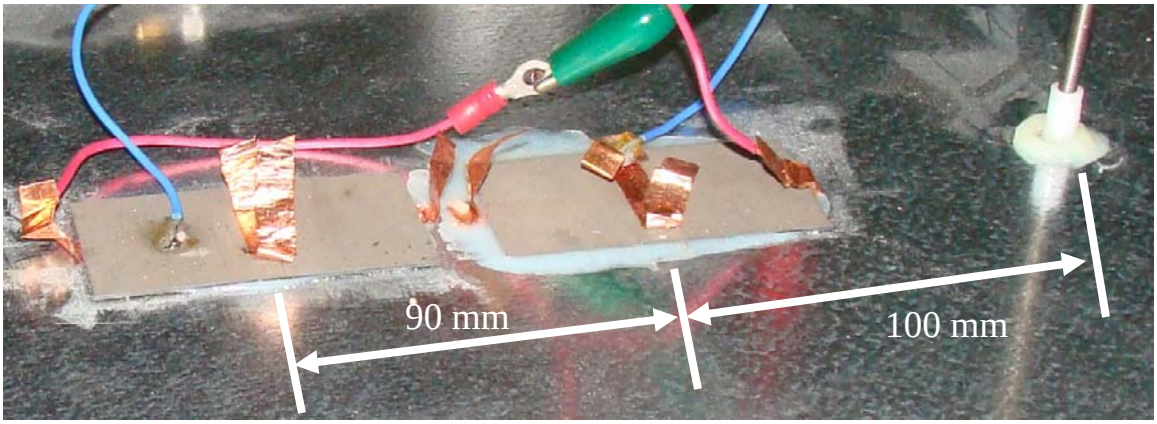

Photo by Mohammad Rastgaar, July 2008
Figure 7.4. Piezoelectric actuators mounted on the test plate

High strength epoxy gel S-210/21045 from Devcon, UPC 078143210457, was used to attach the piezoelectric actuator to the test plate. Upon applying the glue, 30 lb of weight was placed on top of the piezoelectric ceramics to provide enough pressure for better bonding. The pressure was removed after 1 hour. Figure 7.4 shows that one piezoelectric actuator is placed in the middle of the plate and the second one at a distance of 100 mm away from the first one along the large dimension of the plate. The distance between the second piezoelectric actuator and the electromagnetic actuator is 85 mm.

7.1.4. High voltage amplifier for piezoelectric actuators

A two channel non-inverting high voltage piezo-driver (amplifier) PZD700 manufactured by Trek is used to provide control signals to the piezoelectric actuators. The output voltage of the piezo-driver is within 0 to ±700 V with a current range of 0 to ±100 mA. The amplifier, shown in Figure 7.5, have an adjustable output gain 0 to 300 V/V, and has a signal bandwidth of greater than 50 kHz for all voltage ranges.

Photo by Mohammad Rastgaar, January 2008
Figure 7.5. High voltage PZD 700 piezo-drivers from Trek

7.1.5. PCB accelerometers

PCB accelerometers, model U352L65 ICP with nominal sensitivity of 100 mV/g, are used to measure the acceleration of different points of plate. Seven accelerometers are placed on the top surface of the test plate and three of the accelerometers that are collocated with the actuators are mounted on the lower surface of the test plate. Hot glue has been used to mount the accelerometers to the test plate. Each accelerometer has a sensitivity that may slightly deviates from 100 mV/g , which must be implemented during data acquisition process. The accelerometer arrangement on the plate is shown in Figure 7.6. The accelerometers are equally spaced in the transversal direction which is 100 mm. Sensors 1, 2, and 3 are collocated with actuators and are placed at the bottom side of the plate. Table 7.1 presents the specification of each sensor.

Table 7.1. Specifications of sensors

sensor	Serial number	Sensitivity (mV/g)	Sensitivity (mV/ms $^{-2}$)
1	77903	99.1	10.10
2	77904	101.7	10.37
3	77905	99.1	10.10
4	78089	99.6	10.15
5	78088	103.3	10.53
6	78090	100	10.27
7	77968	99.8	10.18
8	77970	100.2	10.21
9	77967	98.9	10.09
10	77969	100.5	10.25

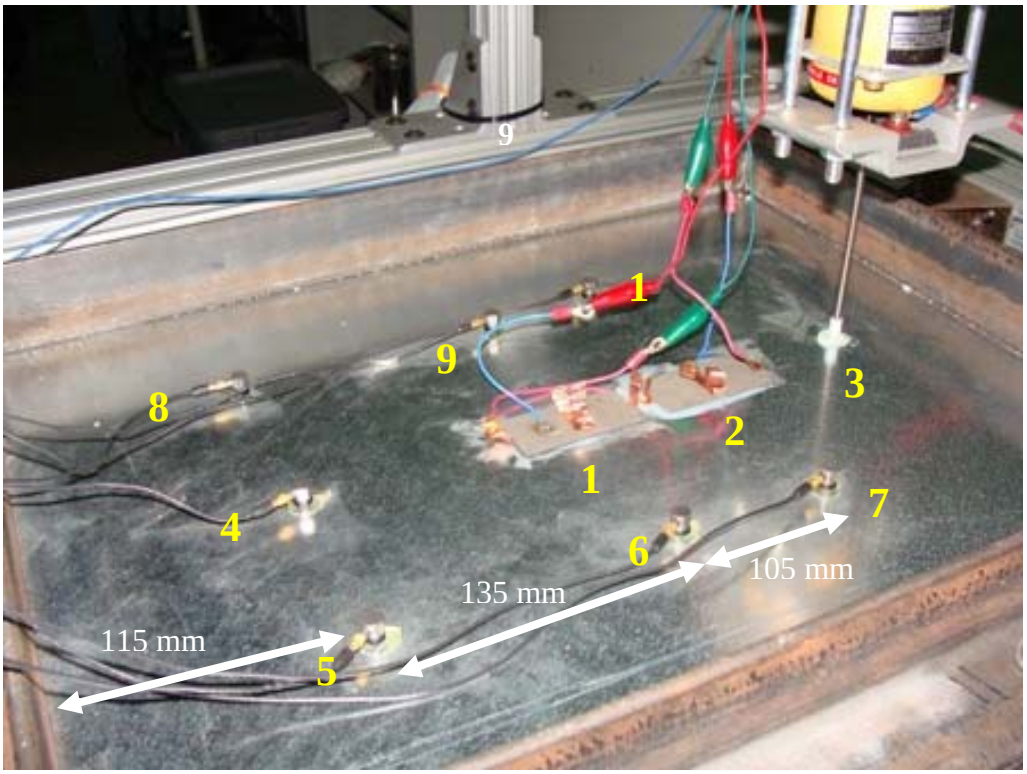

Photo by Mohammad Rastgaar, July 2008
Figure 7.6. Accelerometer locations on test plate

7.1.6. Signal conditioner

A 20 channel ICP 584 series signal conditioner from PCB Piezotronics, Inc., shown in Figure 7.7 was used. The amplification gain of this signal conditioner can be set to 1, 10, and 100. The signal conditioner gain was set to 100.

Photo by Mohammad Rastgaar, January 2008

Figure 7.7. PCB ICP series 584 signal conditioner

7.1.7. Patch panel

A 16 channel patch panel 070C29 from PCB Piezotronics, Inc. was used for transferring accelerometer measurements to a signal conditioner. The measurements were routed to the patch panel, shown in Figure 7.8, through BNC jacks and transferred to the signal conditioner through a DB50 pin cable.

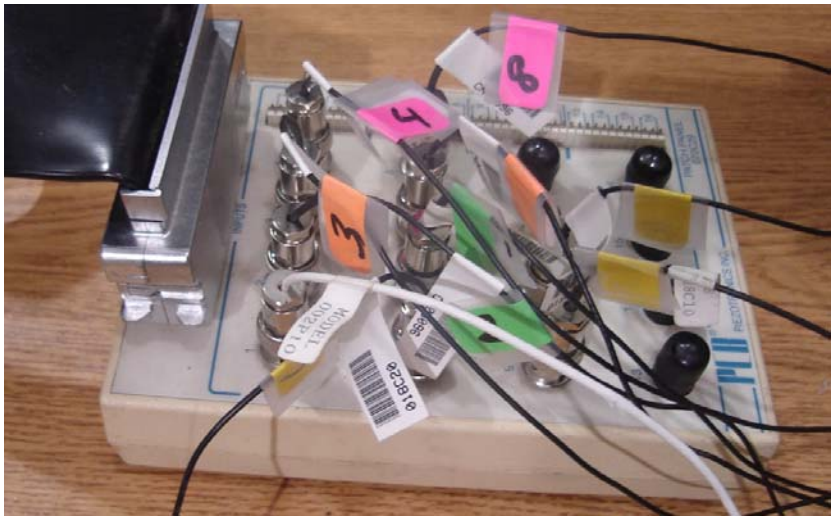

Photo by Mohammad Rastgaar, January 2008

Figure 7.8. Patch panel 070C29from PCB Piezotronics

7.1.8. Junction box

Figure 7.9 shows a custom made junction box. The junction box is connected to the dSPACE AutoBox through a 48 pin cable. All of the signals from signal conditioner come to the junction box and then transfer to the AutoBox. Also, the control commands from AutoBox were routed to this junction box, and then sent to the high voltage PZD700 piezo-driver.

Photo by Mohammad Rastgaar, July 2008
Figure 7.9. Junction box

7.1.9. dSPACE and AutoBox

The AutoBox, shown in Figure 7.10, contains a DS 100e processor and is one of the main components for controlling the plate. The AutoBox includes an analog to digital converter DS2201ADC, a digital to analog converter DS2201DAC, and an I/O card with twenty inputs and eight outputs that are used for collecting data and output control signals. The AutoBox CPU is accessible by ControlDesk software that is installed on a laptop through an Ethernet connection.

Photo by Mohammad Rastgaar, January 2008
Figure 7.10. dSpace Autobox

7.2. Modeling and Software

The test software includes Matlab 6.1 with Simulink, and dSPACE Control Desk Developer version 2.1.1. The test setup is generated in Simulink that are shown on Figure 7.11-7.14. The model for closed-loop control of the plate is uploaded through the Control Desk to the AutoBox processor. The Control Desk is a real time interface that provides the accessibility to the AutoBox processor for monitoring the signals, collecting the data, or changing the control parameters. The Control Desk interface is shown on Figure 7.15.

Figure 7.11 shows the block diagram used for data acquisition and closed-loop control. Accelerometer signals, after passing through the signal conditioner, come into the AutoBox through the analog-to-digital converter DS2201ADC. The real time control commands are routed to the piezoelectric actuators through the digital-to-analog converter DS2201DAC. The random disturbance signals for the electromagnetic shaker also passes through digital-to-analog converter.

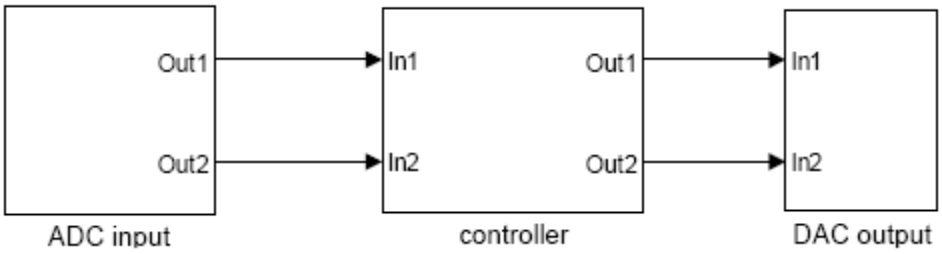

Figure 7.11. Simulink models of the closed-loop system using two sensors and actuators

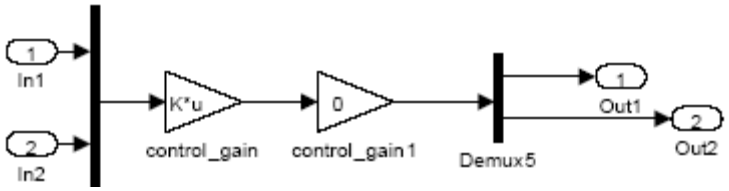

Figure 7.12. Controller blocks of the closed-loop system using two sensors and actuators

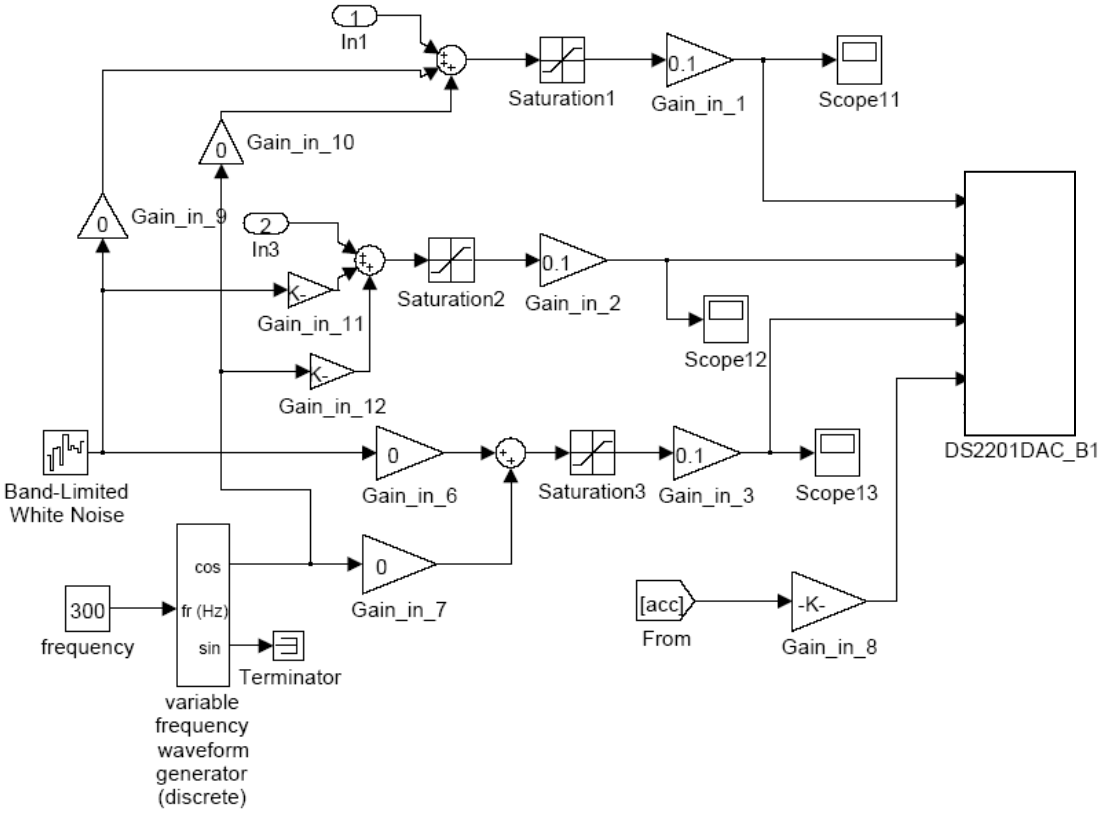

Figure 7.13. DAC block

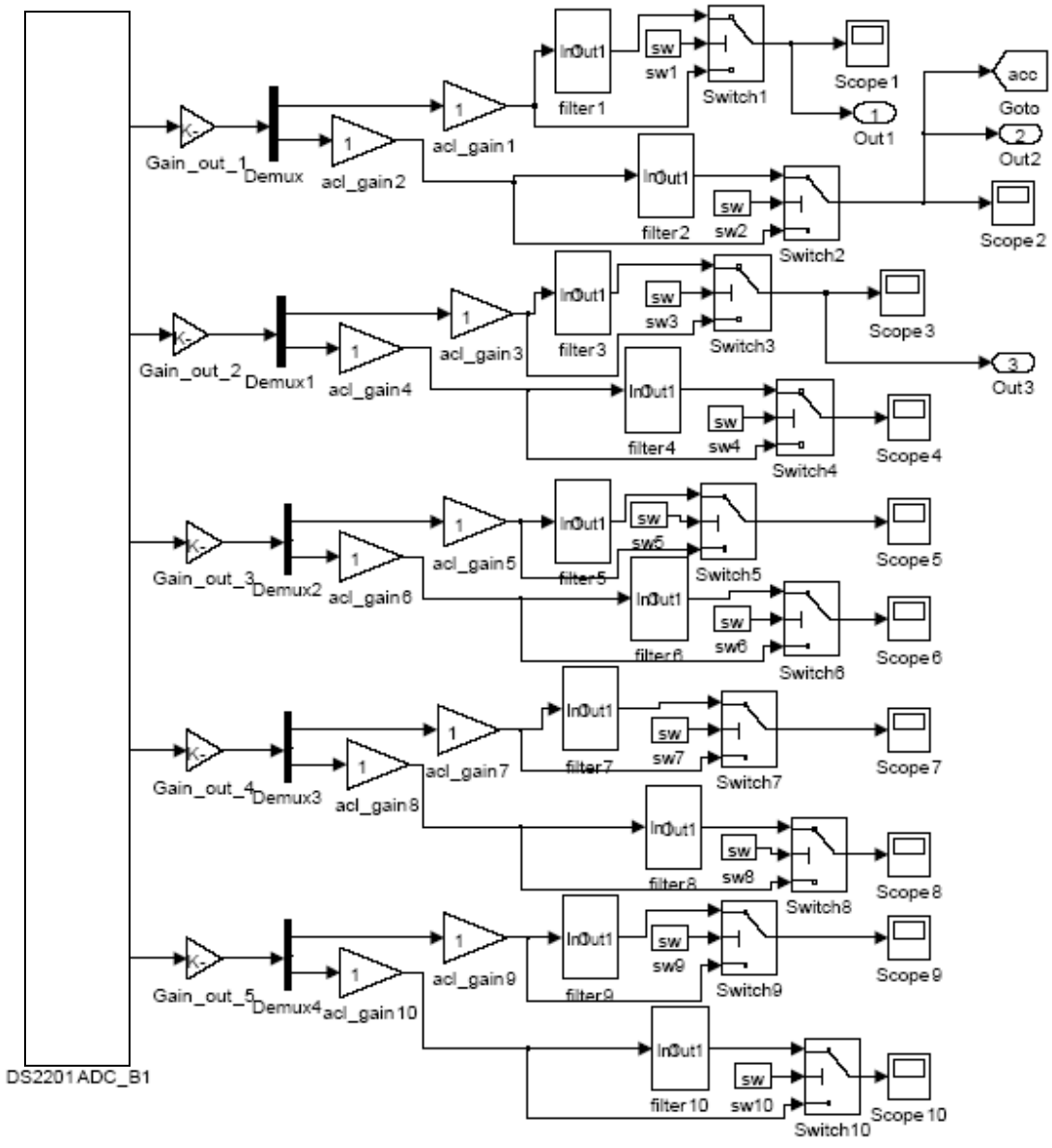

Figure 7. 14. ADC block

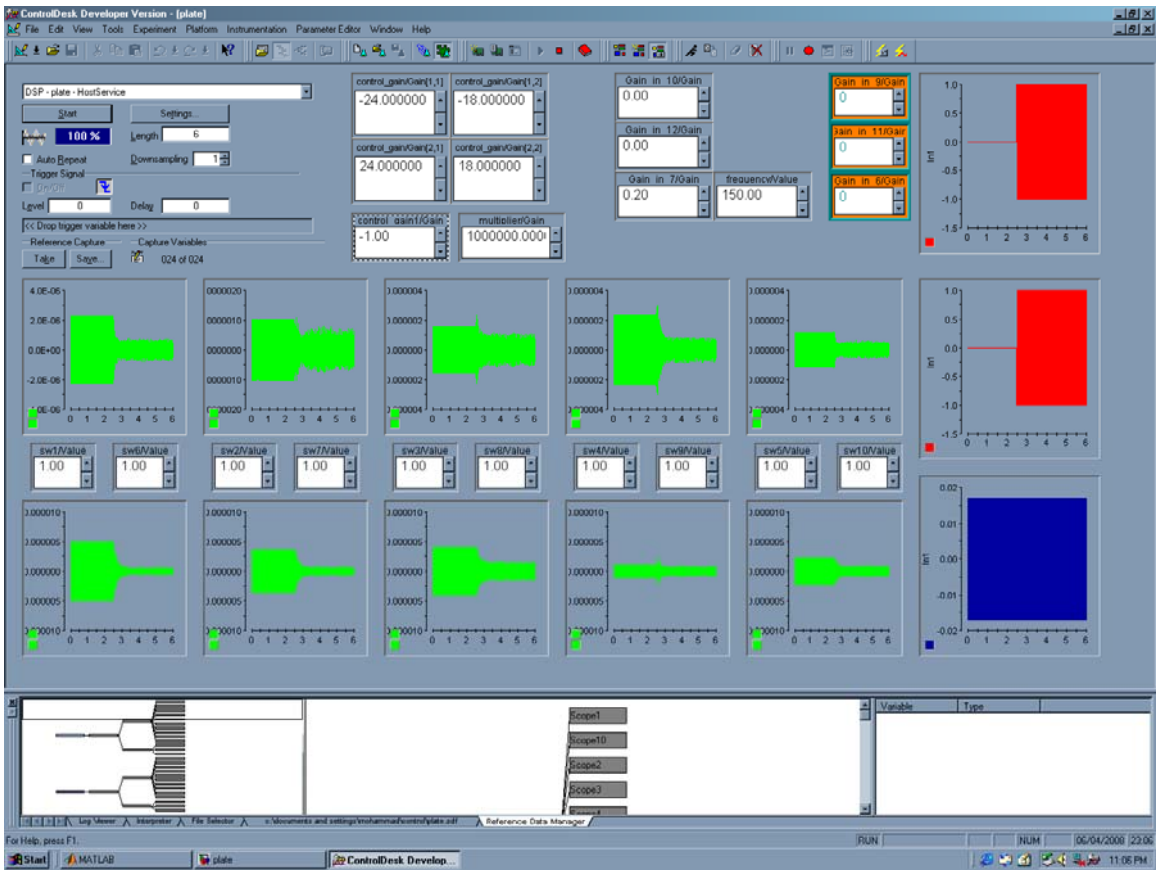

Figure 7. 15. Control Desktop interface

7.3. System Identification

Prediction-Error Method has been used for system identification, in order to find the state space model of the test plate. Matlab command “pem”, from System Identification Toolbox, provides the prediction-error minimization algorithm for users[87]. It finds separate models from data between each actuator and sensor, and combines these SISO models to generate a MIMO system. For our experiment, the plate model is identified using the test data when the piezoelectric actuators are used as the source of input to the plate. The data collected from the sensors collocated with the piezoelectric actuators are used for system identification. This method, finds a transfer functions between the command signal to each piezoelectric actuator and the displacement at the collocated accelerometer. The transfer functions do not incorporate the effect of non-collocated actuators. Two transfer functions are transferred to state space model, without feedthrough matrix.

7.4. Characteristics of plate dynamics and the location of the actuators

Two types of actuators have been used in the experiments: 1) an electromagnetic shaker that is the source of disturbance, and 2) piezoelectric actuators for controlling the plate. To better understand the dynamics of these actuators, the frequency response between the command signals to each actuator and their mechanical responses are plotted using a HP Analyzer. The accelerometer measurements are used as the metric for the magnitude of the force applied to the plate. The excitation is a periodic chirp input with the frequency range of 0 to 400 Hz, and peak amplitude of 1 V. Figures 7.16-18 show the frequency response and the associated coherence of the three actuators mentioned above.

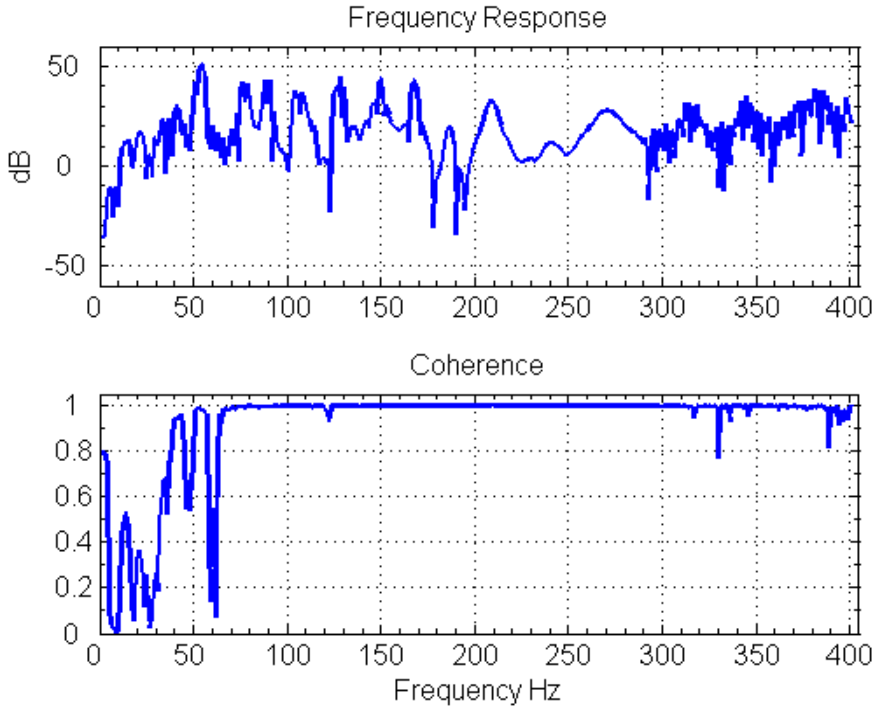

Figure 7. 16. Frequency response and coherence of the electromagnetic actuator and its collocate sensor

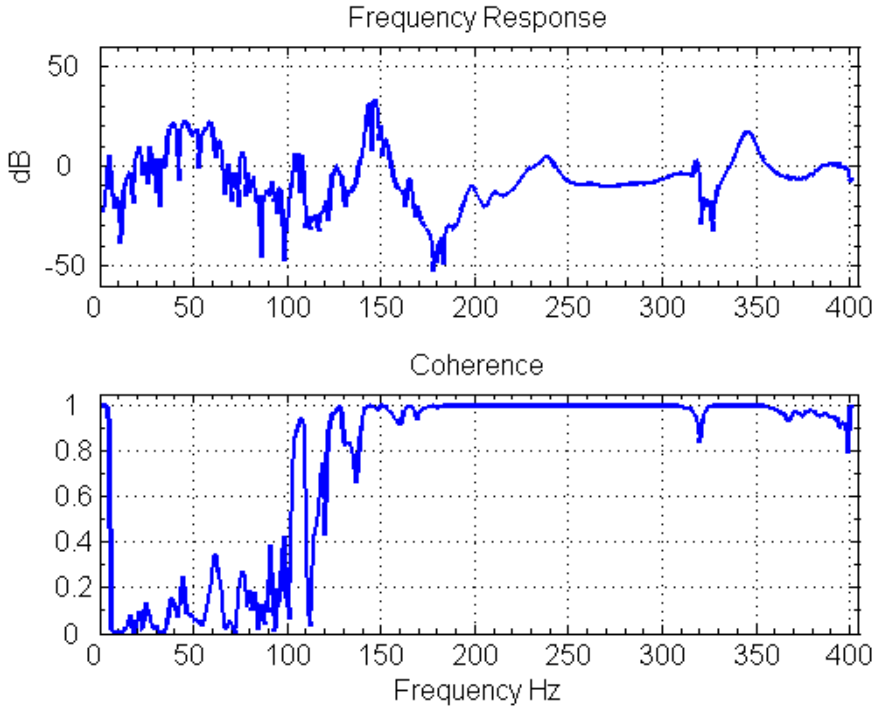

Figure 7. 17. Frequency response and coherence of the piezoelectric actuator located at the center of plate and its collocated sensor

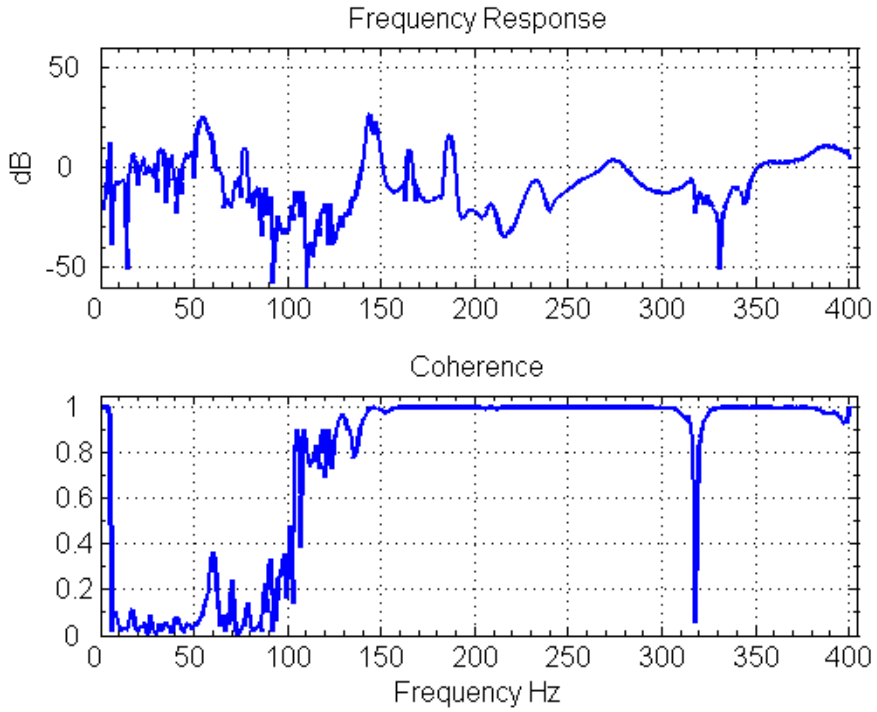

Figure 7. 18. Frequency response and coherence of the piezoelectric actuator located off-center of plate and its collocated sensor

Figure 7.16 shows the frequency response and coherence due to the input from electromagnetic shaker and the response at the collocated sensor. It is observed that the coherence is acceptable from 70Hz to 400 Hz. Also, this figure shows that the magnitude of the frequency response plot does not change rapidly over the range of 200 Hz to 300 Hz relative to the rest of the frequency range. Therefore, to validate the applicability of the orthogonal eigenstructure control, the frequency range of 200-300 Hz is considered as the first candidate to investigate the applicability of the orthogonal eigenstructure control for vibration cancellation. Similar behavior is observed for the two piezoelectric actuators. The frequency range of 200-300 Hz has 4 distinct natural frequencies that increase the chance of having a better performance for system identification.

Now that a target range of frequency for the excitation has been chosen, it is important to find the appropriate locations for the control actuators. To do so, the results of the finite element modeling of the test setup documented in [86] is considered. Also, it is important to realize that since the electromagnetic actuator is mounted on the plate using a stinger, a boundary condition is added to the plate. This extra boundary condition acts as a hard point constraint against the plate and slightly shifts the mode shapes to the side opposite of the location of the stinger. Additionally, the piezoelectric actuators add to the local stiffness of the plate, causing an additional shift to the natural frequencies of the mode shapes reported in [86]. The center of the plate is an appropriate location for the first piezoelectric actuators that can cover odd mode numbers, especially modes (3, 1), (1, 4), (3, 2), and (3, 3). As was shown in the last chapter, when the control actuators are close to the disturbance source the vibrations in a larger area of the plate can be controlled. To keep the number of control actuators to a minimum and also maintain the symmetry of the plate, the location for the other piezoelectric actuator is chosen to be between the first piezoelectric actuator at the middle of the plate, and the disturbance actuator.

Next, we need to determine if the piezoelectric actuators can have sufficient authority (i.e. provide sufficient force) for controlling the plate. Figures 7.17 and 7.18 show the frequency response and associated coherence plots of the piezoelectric actuators at their collocated sensors. The coherence between the electrical voltage to the piezoelectric

actuators and their mechanical effects on plate (acceleration), do not have high coherence between 0 to 140 Hz. A frequency response similar to the frequency response to the electromagnetic actuator at its collocated sensor is seen for the piezoelectric actuators and their collocated sensors in the frequency range of 200-300 Hz. All the three actuators have four natural frequencies in this range and also the magnitudes of the frequency responses are lower than what is at the rest of the frequency range. This confirms that the control actuators would have sufficient control authority in the selected frequency range of 200-300 Hz.

Figure 7.19 shows the frequency response for the accelerometer collocated with the electromagnetic shaker and the rest of the accelerometers placed on the test plate utilizing the HP Analyze. The excitation is a chirp input to the electromagnetic shaker with the frequency range of 0 to 400 Hz and peak amplitude of 1 V. This frequency response plots show the transmissibility of mechanical force input, which is proportional to the acceleration at the location of applying the disturbance, to the resulting accelerations at different location on the plate. The FR plots are accompanied by coherence plot. The coherence plots show that the sensors close to the plate edges have low coherence, except for the frequency range of 200-300 Hz. A high coherence is important in controlling the plate.

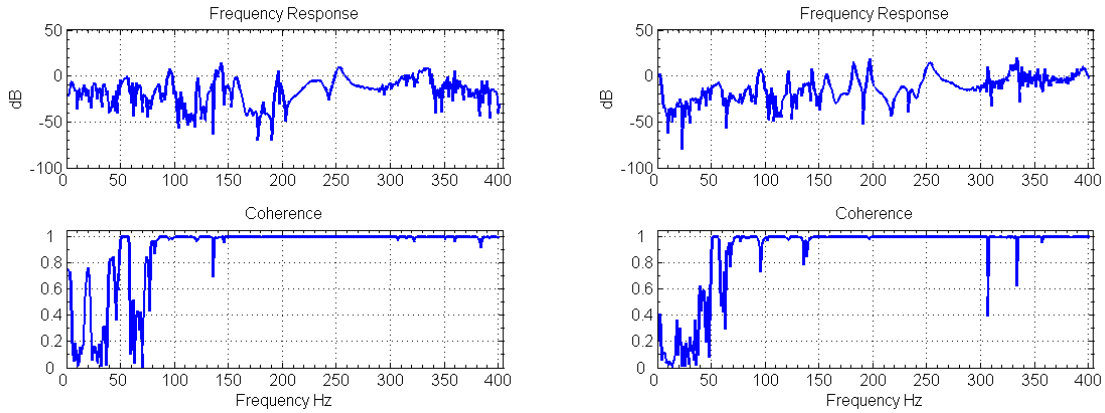

(a) FR between sensors 3 and 1

(b) FR between sensors 3 and 2

Figure 7. 19. continued

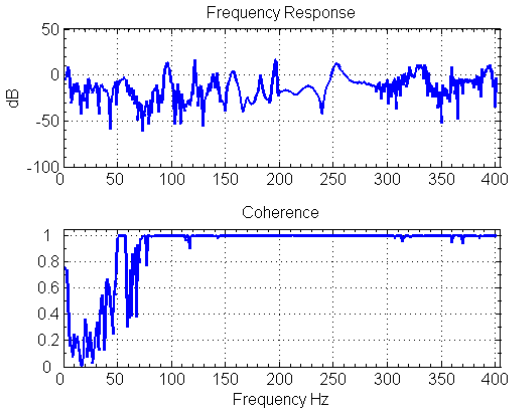

(c)
FR between sensors 3 and 4

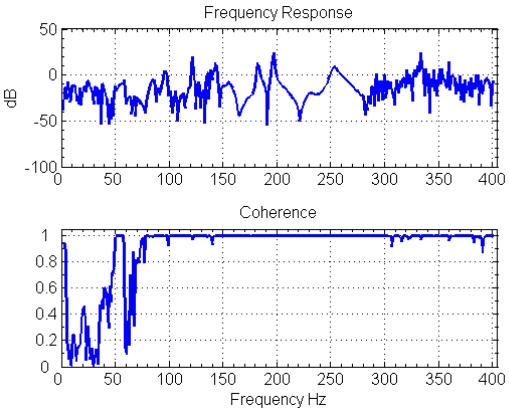

(d)
FR between sensors 3 and 5

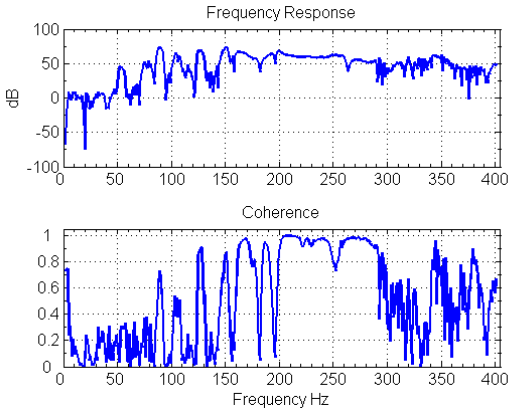

(e)
FR between sensors 3 and 6

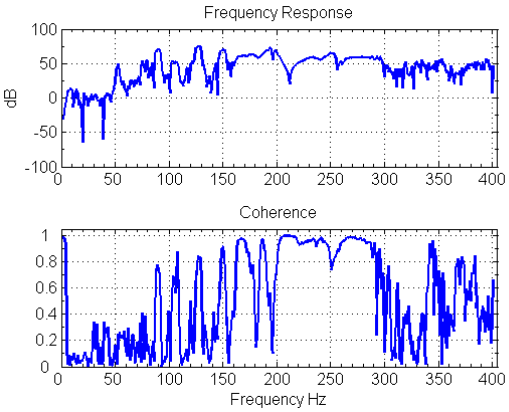

(f)
FR between sensors 3 and 7

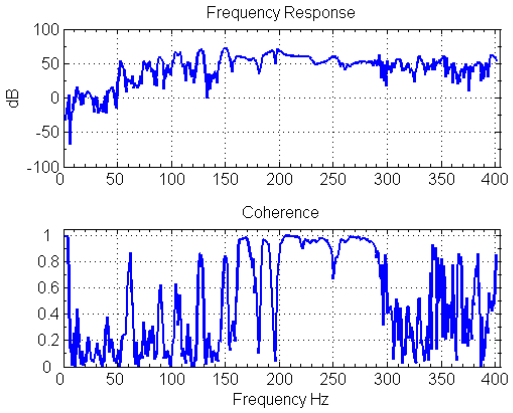

(g)
FR between sensors 3 and 8

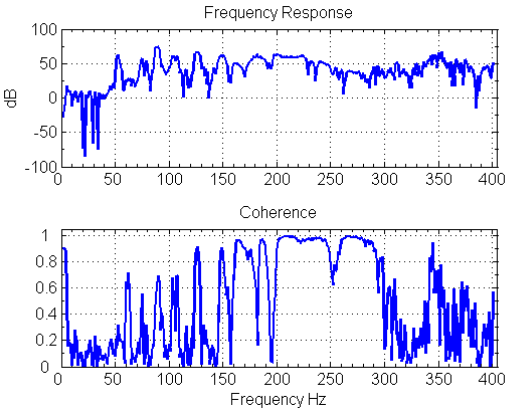

(h)
FR between sensors 3 and 9

Figure 7. 19. continued

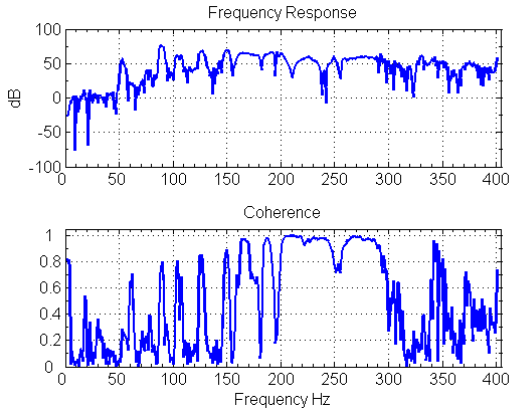

(i)
FR between sensors 3 and 10

Figure 7. 19. Frequency response and coherence between the acceleration of sensor collocated with electromagnetic actuator and the other accelerometers on test plate

An HP Analyzer has been used for a chirp signal excitation to the piezoelectric actuator at the center of the test plate with the range of frequency between 0 Hz to 400 Hz, and the amplitude of 1 V. Figure 7.20 shows the frequency response between the signals collected from the sensor collocated with the piezoelectric actuator mounted at the center of the plate, and the rest of the accelerometers placed on the test plate as well as the associated coherence plots. The frequency response plots show a similar dynamics at the frequency range of 200-300 Hz. Also, it shows that the coherence of the responses at all the sensors are close to 1 in this frequency range.

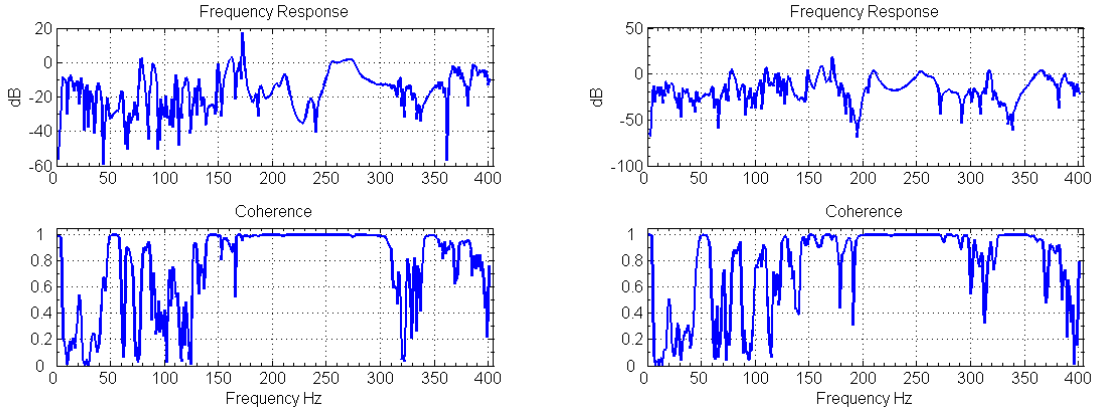

(a)
FR between sensors 1 and 2

(b)
FR between sensors 1 and 3

Figure 7. 20. Continued

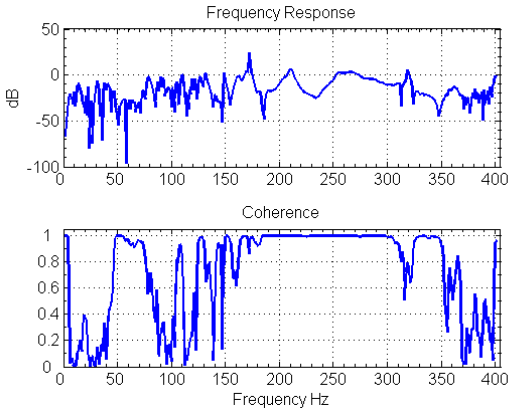

(c)
FR between sensors 1 and 4

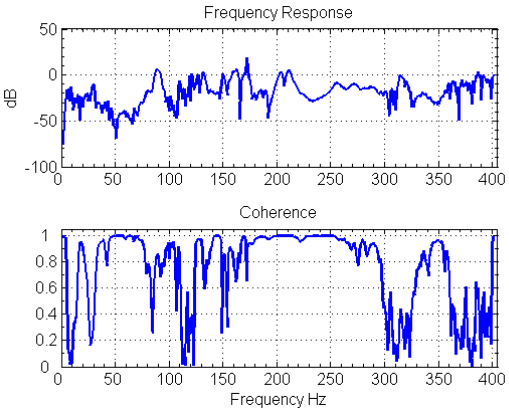

(d)
FR between sensors 1 and 5

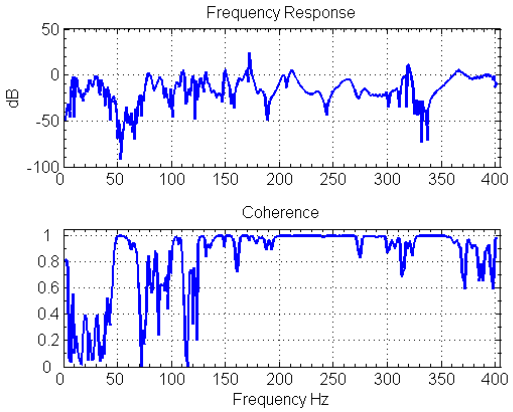

(e)
FR between sensors 1 and 6

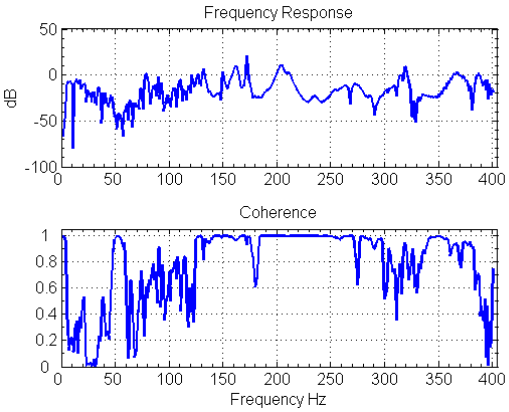

(f)
FR between sensors 1 and 7

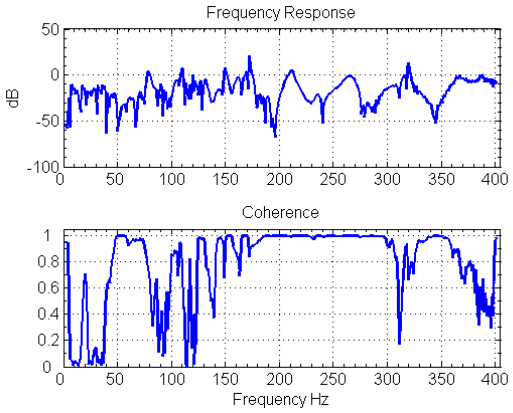

(g)
FR between sensors 1 and 8

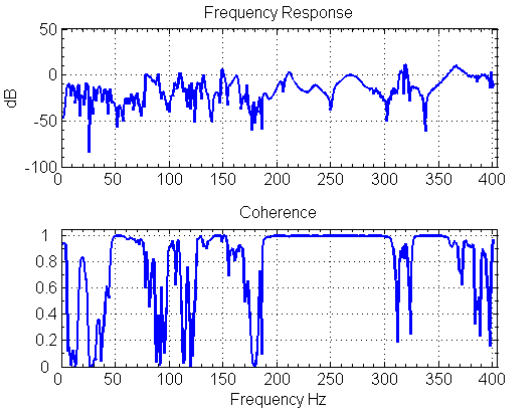

(h)
FR between sensors 1 and 9

Figure 7. 20. Continued

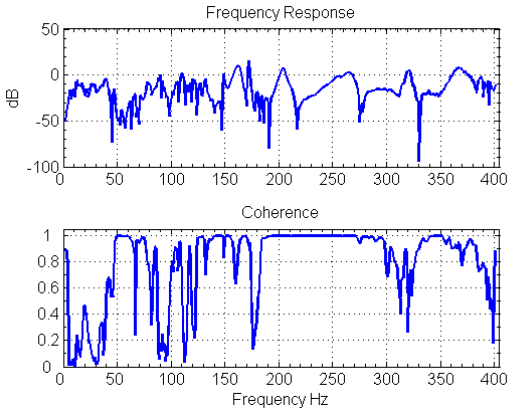

(i)
FR between sensors 1 and 10

Figure 7. 20. Frequency response and coherence between the acceleration of sensor collocated with piezoelectric actuator at the center of the plate and the other accelerometers

Similarly, An HP Analyzer has been used to excite the piezoelectric actuator mounted off-center of the test plate with a chirp signal in the range of frequency between 0 Hz to 400 Hz, and the amplitude of 1 V. Figure 7.21 depicts the frequency response between the signals collected from the sensor collocated with the piezoelectric actuator mounted off-center of the plate, and the rest of the accelerometers and the associated coherence plots. A similar behavior to Figure 7.20 can be observed.

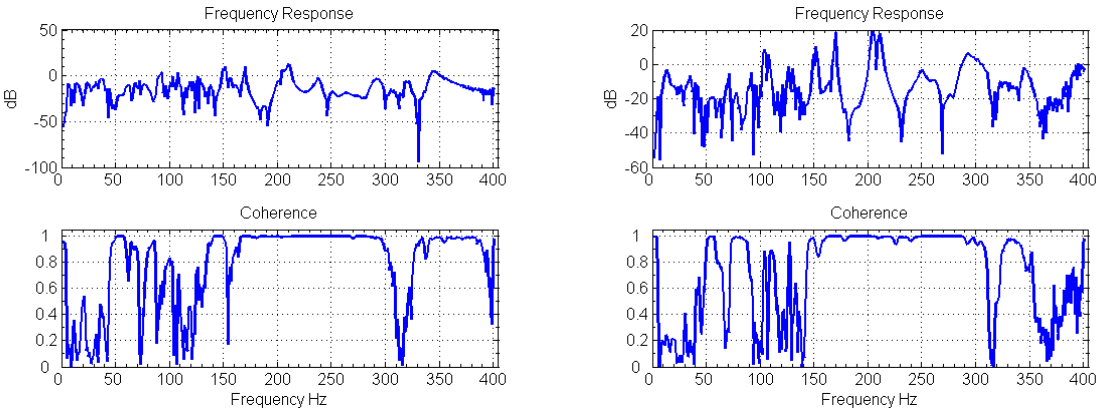

(a)
FR between sensors 2 and 1

(b)
FR between sensors 2 and 3

Figure 7. 21. Continued

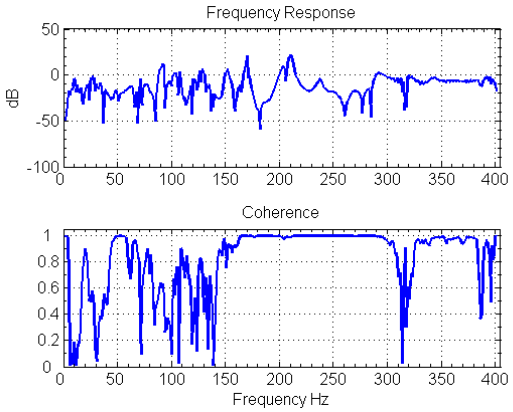

(c)
FR between sensors 2 and 4

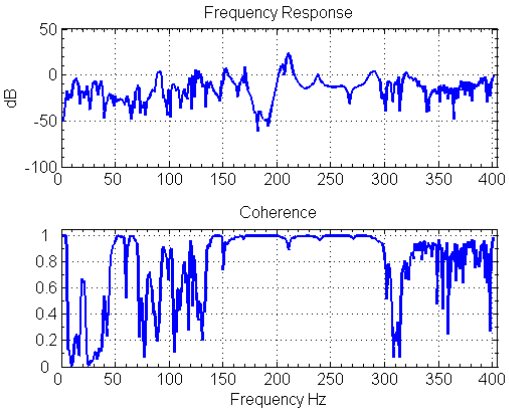

(d)
FR between sensors 2 and 5

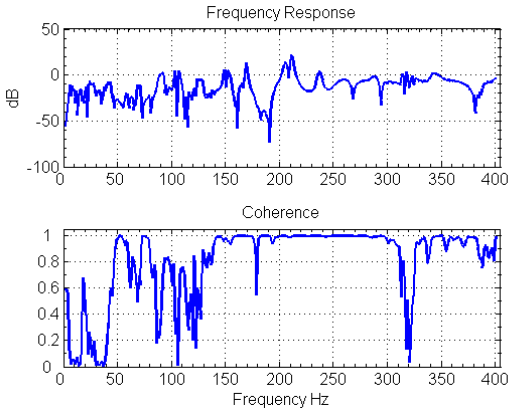

(e)
FR between sensors 2 and 6

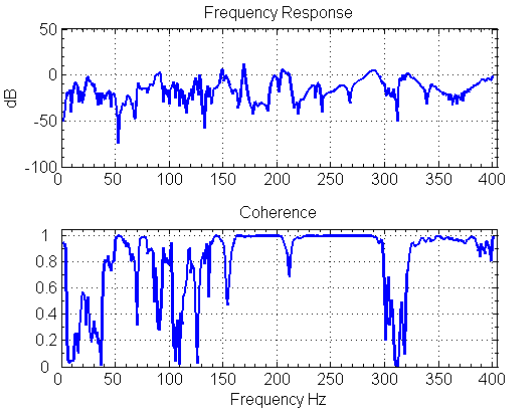

(f)
FR between sensors 2 and 7

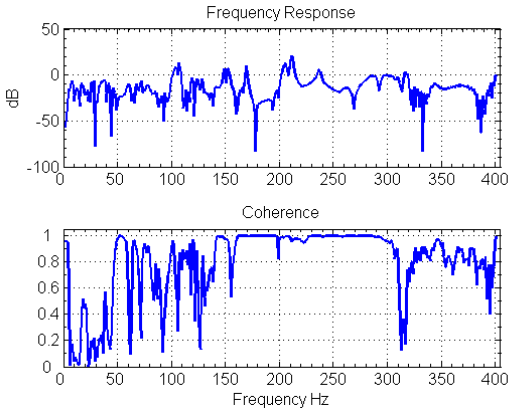

(g)
FR between sensors 2 and 8

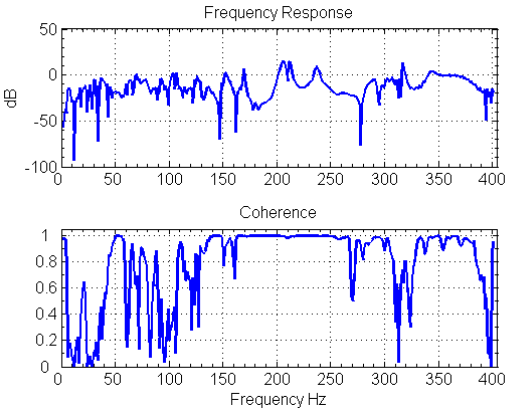

(h)
FR between sensors 2 and 9

Figure 7. 21. Continued

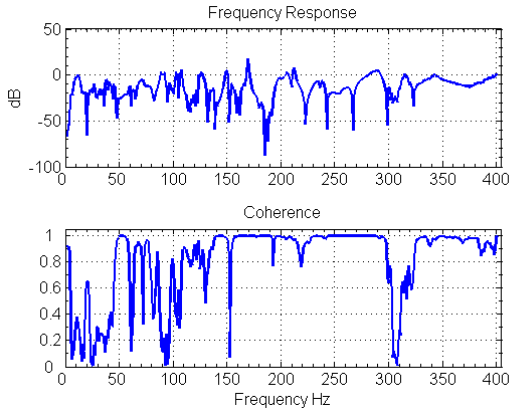

(i)
FR between sensors 2 and 10

Figure 7. 21. Frequency response and coherence between the acceleration of sensor collocated with the second piezoelectric actuator and the other accelerometers

7.5. Tonal Vibration Control

As shown in Figures 7.20 and 7.21, the frequency response plots show large peaks at 250 Hz and 207 Hz within 200-300 Hz frequency indicating those frequencies are the natural frequencies of the plate. Therefore, in this section, we study the cancellation of vibrations due to sinusoidal disturbances at 250 Hz and 207 Hz. The gain between the signal voltage that is set for electromagnetic actuator in Control Desktop and the actual voltage applied to the electromagnetic actuator is one. This gain for piezoelectric actuators is 20.

7.5.1.1 System identification experiment for tonal disturbance at 250 Hz

Two piezoelectric actuators are excited using a 250 Hz tonal signal with amplitude of 0.01 V. After two times integration and filtering of the data from sensors 1 and 2, the data is collected for 6 seconds with 3000 Hz sampling rate. Using the identification method described earlier, we estimate the state space model of the system with a dimension of 10. Figure 7.22 shows the filtered data read from the sensors. It is observed that the signals are not symmetric throughout the plate due to asymmetry of boundary conditions, place of piezoelectric actuators, electromagnetic actuators, and sensors. Figure 7.23 shows that the results for the estimated system are to 99% compatibility with the collected data.

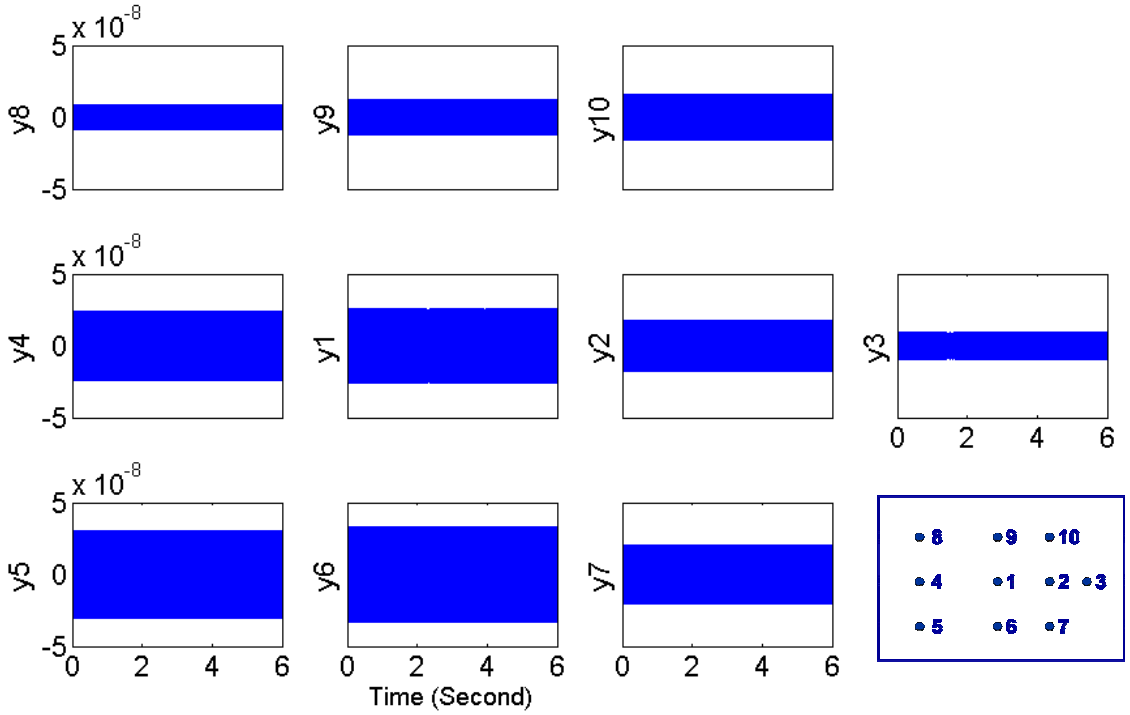

Figure 7.22. Displacement (Volts) at accelerometer locations for the 250 Hz tonal excitations with amplitude of 0.01 V.

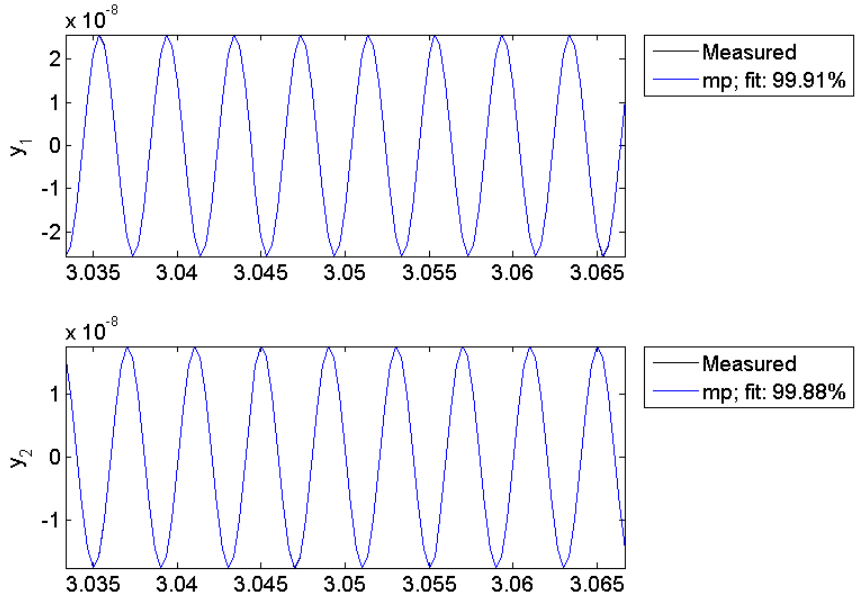

Figure 7.23. Comparison of results from estimated model and collected data at accelerometer locations for 250 Hz tonal excitation; y1: accelerometer 1; y2: accelerometer 2

7.5.1.2 Control of tonal disturbance at 250 Hz with 0.001 V amplitude

Applying the orthogonal eigenstructure control to the estimated model of the system resulted in previous experiment; one can find the control gain matrix. The amplitude of the disturbance signal is 0.001 V and the control gain matrix is

$K = \begin{bmatrix} -37 & -9.5 \\ 37 & 9.5 \end{bmatrix} \times 10^6$, As mentioned in section 7.3, the system identification method finds two transfer functions between each piezoelectric actuator and its collocated accelerometer displacement without considering the effect of non-collocated piezoelectric actuators. The result is a state space model with decoupled states. To compensate for this simplification, one of the elements of the control gain matrix needs to be tuned. The tuned gain would be

$$K = \begin{bmatrix} -37 & -2 \\ 37 & 9.5 \end{bmatrix} \times 10^6$$

During the test the controller turned on at $t \cong 2$ seconds, as shown in Figure 24, for the signals to the actuators. The control voltages to the piezoelectric actuators are the feedback signals from the accelerometers. The oscillation in the control voltages means that the transient vibrations of plate do not decay fast. It implies that the dissipation of energy, which can be interpreted as the effect of damping, is not a fast process. This effect can also be seen on Figure 7.25 that shows the displacements. The vibration at the accelerometers collocated with the control actuators and the accelerometers installed on the opposite side of the plate; that is, sensors 4, 5, and 8, have been suppressed.

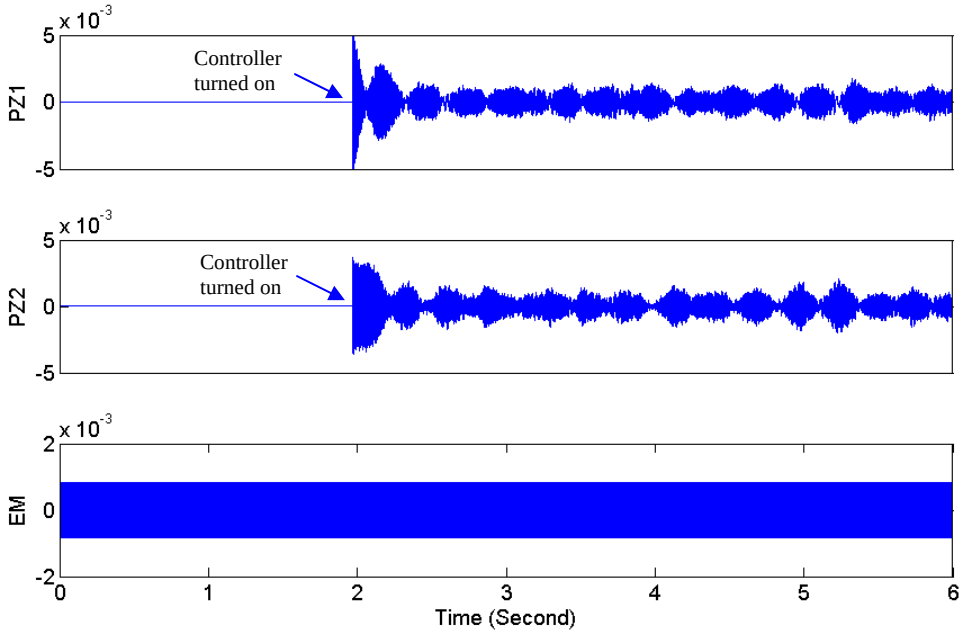

Figure 7.24. Signals to the actuators (Volts) for control of 250 Hz disturbance with amplitude of 0.001 V.; PZ1: piezoelectric actuator at center of plate; PZ2: piezoelectric actuator at off-center of plate; EM: electromagnetic shaker

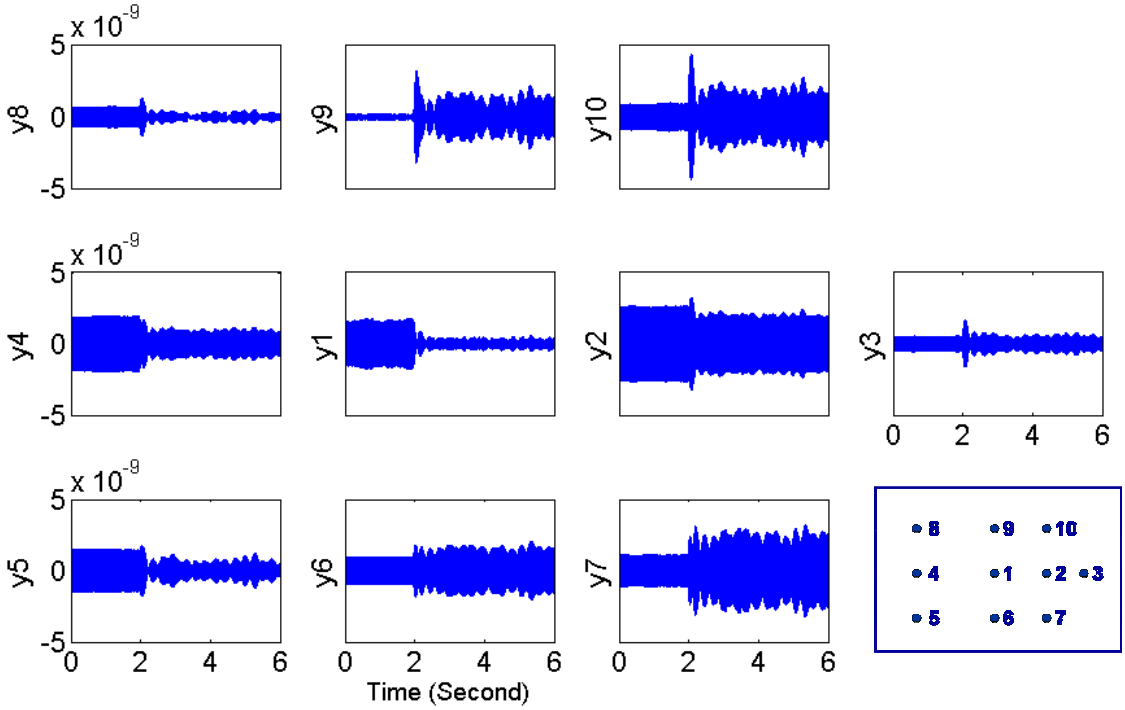

Figure 7.25. Displacement (Volts) at accelerometer locations for control of 250 Hz disturbance with amplitude of 0.001 V.

Table 7.2 shows the displacements at the accelerometers before and after controller turns on, and also the reduction percentage of their maximum amplitude. The maximum reduction of vibrations happens at the location of accelerometer 1, and the minimum amount happens at the location of accelerometer 2.

Table 7.2. Comparison of the maximum displacements at accelerometers before and after control of 250 Hz disturbance with amplitude of 0.001 V., maximum and minimum reductions are highlighted in red

Accelerometer	Maximum OL measurement (V)	Maximum CL measurement (V)	Percentage reduction
1	1.62e-09	4.95e-10	-69.52
2	2.64e-09	2.05e-09	-22.51
3	5.41e-10	6.49e-10	19.88
4	1.89e-09	1.03e-09	-45.51
5	1.53e-09	8.36e-10	-45.44
6	9.80e-10	1.67e-09	69.75
7	1.16e-09	2.73e-09	135.03
8	6.94e-10	3.57e-10	-48.56
9	2.57e-10	1.62e-09	529.94
10	9.12e-10	2.12e-09	132.19

7.5.1.3 Control of tonal disturbance at 250 Hz with 0.01 V amplitude

In this experiment, the amplitude of the disturbance signal is changed to 0.01 V. The controller turned on at $t \cong 1$ second, as shown in Figure 7.26, for the signals to the actuators. Figure 7.27 shows the displacements at the accelerometer locations, indicating that the transient vibrations decay faster than the earlier experiments. The pattern of suppression throughout the plate is similar to the previous experiment, and the suppression of vibration can be seen at sensors 1, 2, 4, 5, and 8. Table 7.3 shows the maximum amplitude of displacement measured at sensor locations before and after control. Similar to experiment 250-2, the maximum and minimum amounts of reduction of vibration are at sensors 1 and 2, respectively.

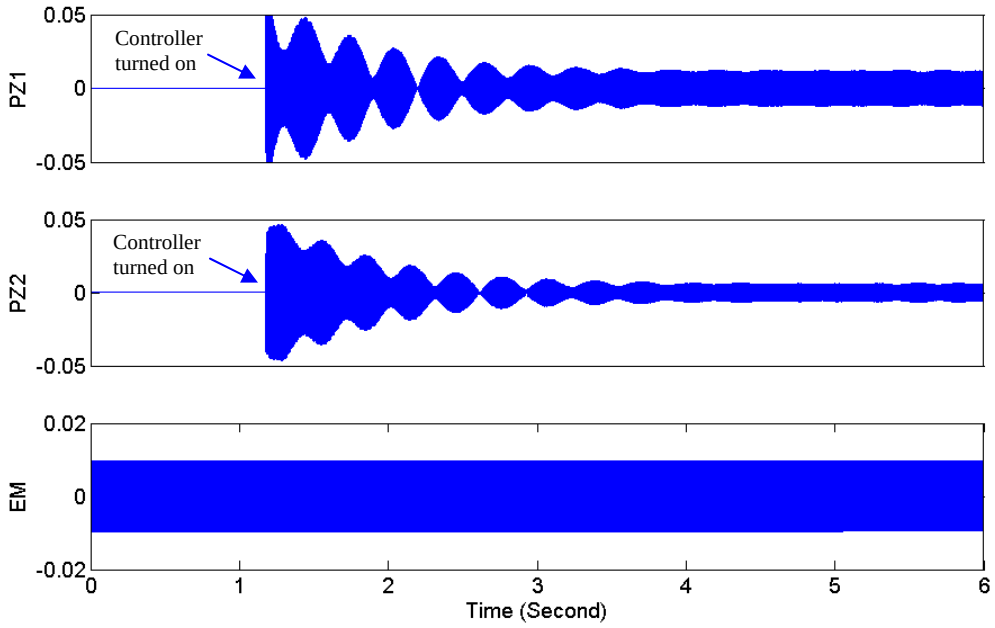

Figure 7.26. Signals to the actuators (Volts) for control of 250 Hz disturbance with amplitude of 0.01 V.; PZ1: piezoelectric actuator at center of plate; PZ2: piezoelectric actuator at off-center of plate; EM: electromagnetic shaker

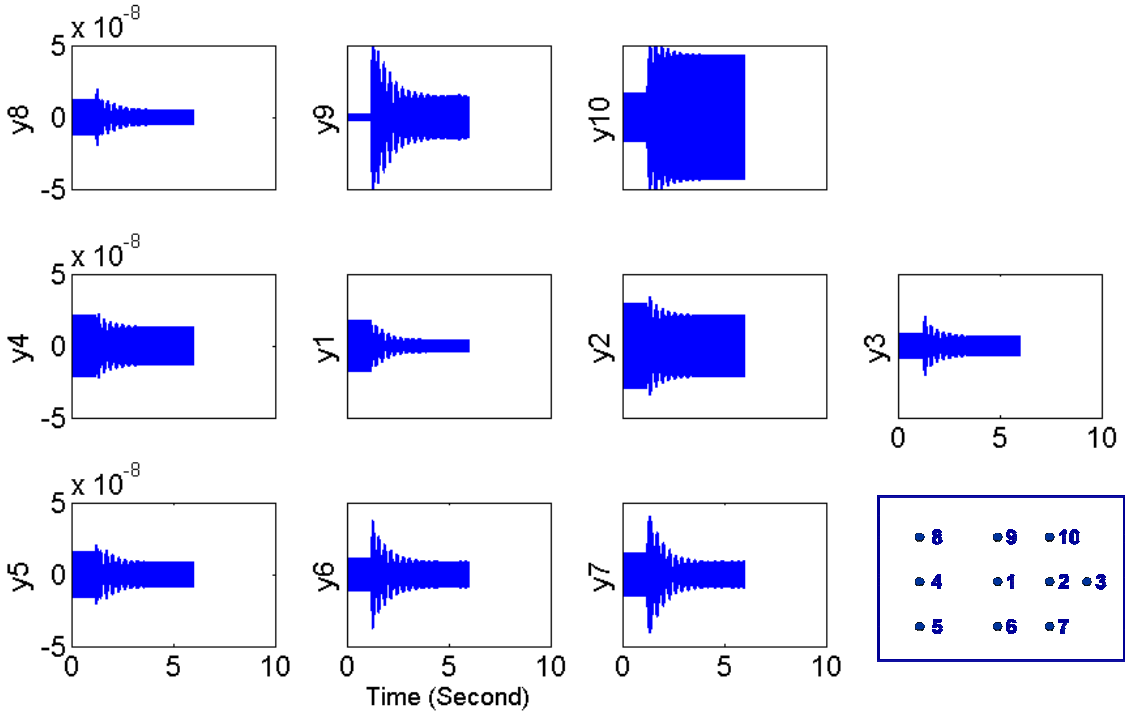

Figure 7.27. Displacement (Volts) at accelerometer locations for control of 250 Hz disturbance with amplitude of 0.001 V.

Table 7.3. Comparison of the maximum displacements at accelerometers before and after control of 250 Hz disturbance with amplitude of 0.001 V., maximum and minimum reductions are highlighted in red

Accelerometer	Maximum OL measurement (V)	Maximum CL measurement (V)	Percentage reduction
1	1.79e-08	4.47e-09	-74.98
2	2.92e-08	2.15e-08	-26.40
3	8.38e-09	6.86e-09	-18.09
4	2.13e-08	1.32e-08	-37.78
5	1.61e-08	8.88e-09	-44.95
6	1.1e-08	9.15e-09	-16.51
7	1.48e-08	9.37e-09	-36.46
8	1.19e-08	5.34e-09	-55.25
9	2.7e-09	1.53e-08	466.85
10	1.71e-08	4.34e-08	153.38

7.5.1.4. Control of tonal disturbance at 250 Hz with 0.02 V amplitude

In this experiment, the amplitude of the disturbance signal is 0.02 V. The control was turned on at $t \cong 1$ second, using the control gain matrix found earlier as shown in Figure 7.28. Figure 7.29 shows the displacements at the accelerometer locations, indicating that the transient vibrations decay faster than the earlier experiments. The pattern of suppression throughout the plate is improved in comparison to the previous experiments, as seen in suppression of vibration at all the sensors except for sensors 9 and 10. Table 7.4 shows the maximum amplitude of displacements on the plate at sensor locations before and after control. The maximum and minimum amounts of reduction of vibration are at sensors 1 and 7, respectively.

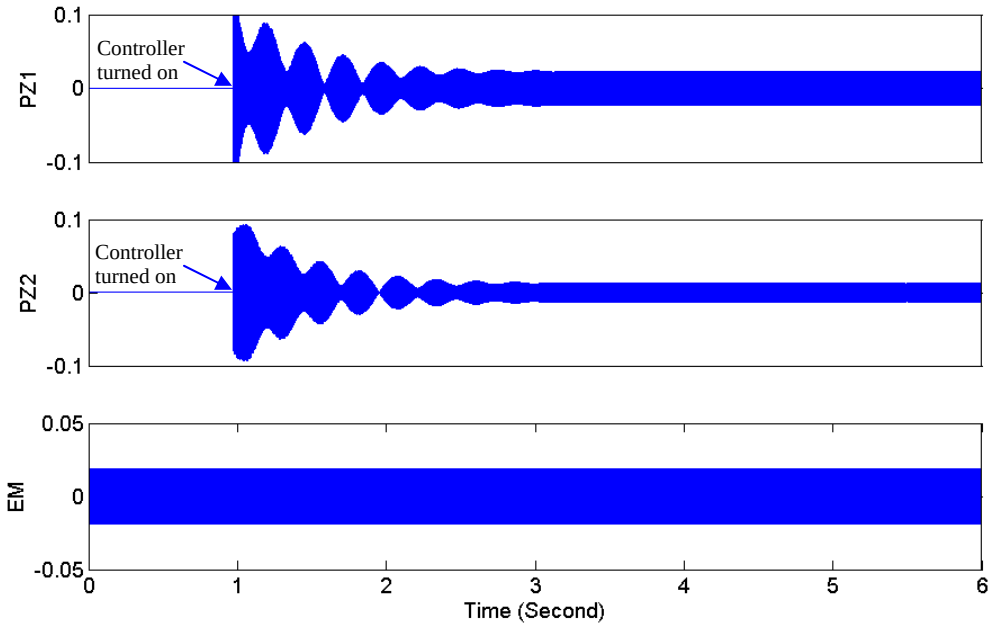

Figure 7.28. Signals to the actuators (Volts) for control of 250 Hz disturbance with amplitude of 0.02 V.; PZ1: piezoelectric actuator at center of plate; PZ2: piezoelectric actuator at off-center of plate; EM: electromagnetic shaker

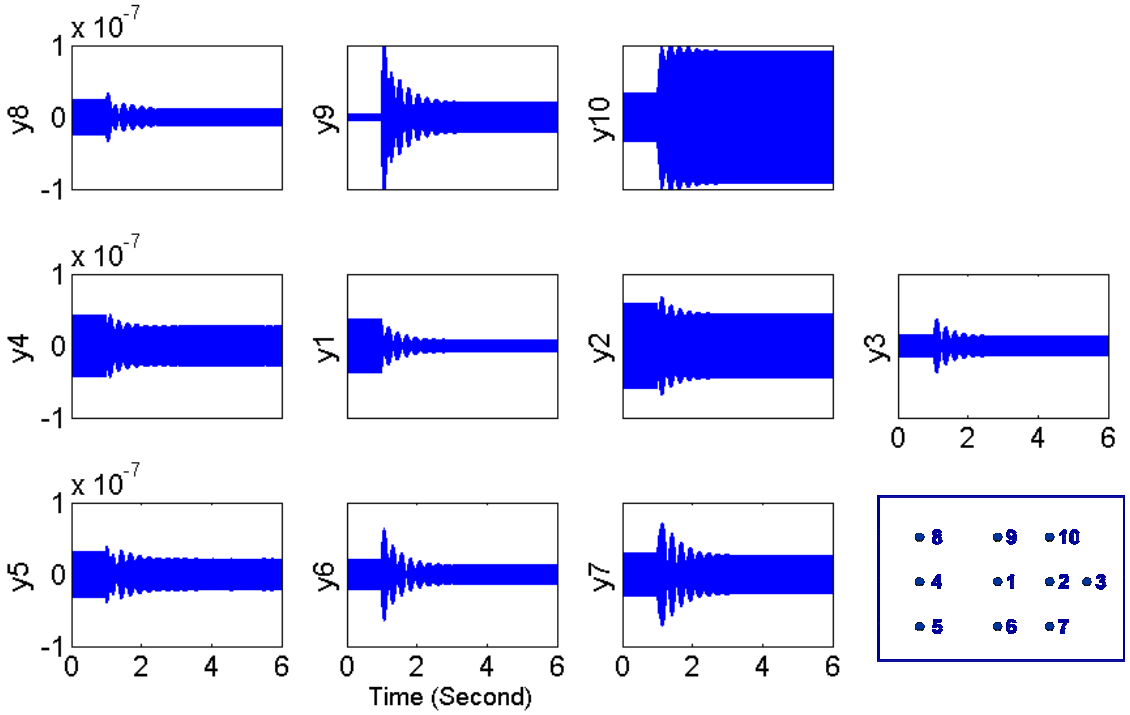

Figure 7.29. Displacement (Volts) at accelerometer locations for control of 250 Hz disturbance with amplitude of 0.02 V.

Table 7.4. Comparison of the maximum displacements at accelerometers before and after control of 250 Hz disturbance with amplitude of 0.02 V., maximum and minimum reductions are highlighted in red

Accelerometer	Maximum OL measurement (V)	Maximum CL measurement (V)	Percentage reduction
1	3.67e-08	8.72e-09	-76.22
2	5.95e-08	4.49e-08	-24.59
3	1.59e-08	1.38e-08	-13.18
4	4.32e-08	2.74e-08	-36.60
5	3.24e-08	2.19e-08	-32.49
6	2.18e-08	1.32e-08	-39.16
7	2.99e-08	2.71e-08	-9.361
8	2.41e-08	1.17e-08	-51.55
9	5.25e-09	2.15e-08	309.05
10	3.41e-08	9.2e-08	170.02

7.5.1.5. Control of tonal disturbance at 250 Hz with 0.03 V amplitude

The amplitude of the disturbance signal is 0.03 V in this experiment. The control was turned on at $t \cong 1$ second, using the control gain matrix found earlier, as shown in Figure 7.30. Figure 7.31 shows the displacements at the accelerometer locations, indicating that the transient vibrations decay faster than the earlier experiments. The pattern of suppression throughout the plate is similar to experiment 250-4, and the suppression of vibration occurs at accelerometer locations except to accelerometers 9 and 10. Table 7.5 shows the maximum amplitude of displacements on the plate at sensor locations before and after control. The maximum and minimum amounts of reduction of vibration are at sensors 1 and 7, respectively.

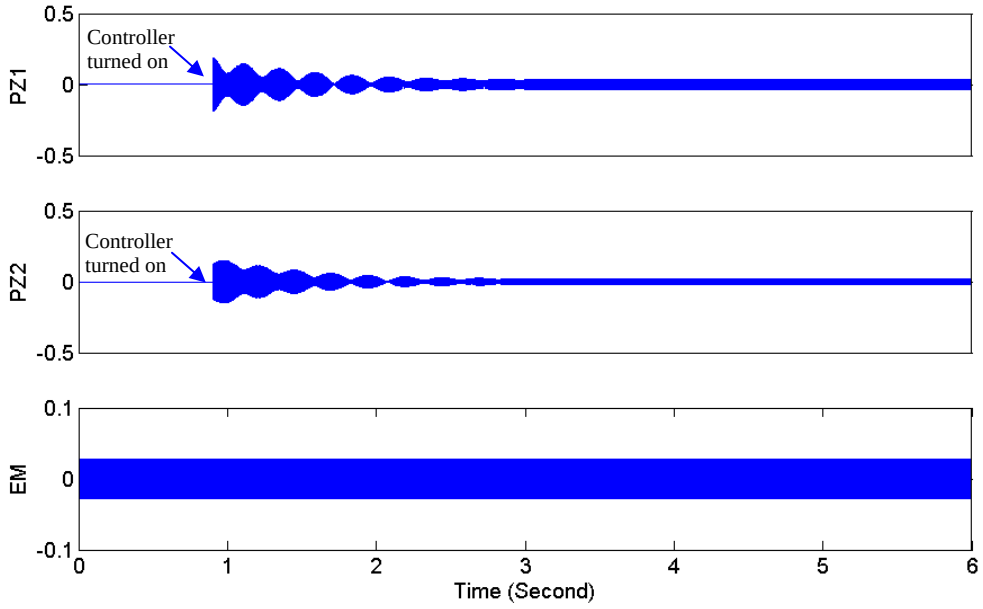

Figure 7.30. Signals to the actuators (Volts) for control of 250 Hz disturbance with amplitude of 0.03 V.; PZ1: piezoelectric actuator at center of plate; PZ2: piezoelectric actuator at off-center of plate; EM: electromagnetic shaker

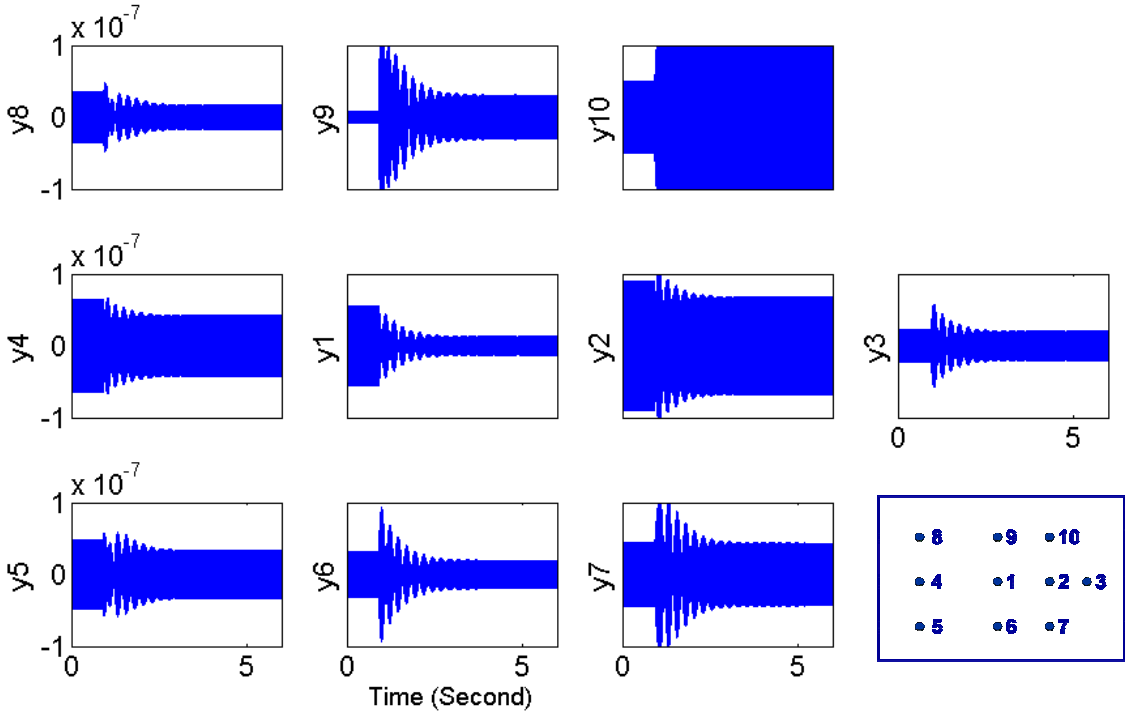

Figure 7.31. Displacement (Volts) at accelerometer locations for control of 250 Hz disturbance with amplitude of 0.03 V.

Table 7.5. Comparison of the maximum displacements at accelerometers before and after control of 250 Hz disturbance with amplitude of 0.03 V., maximum and minimum reductions are highlighted in red

Accelerometer	Maximum OL measurement (V)	Maximum CL measurement (V)	Percentage reduction
1	5.56e-08	1.3e-08	-76.69
2	8.95e-08	6.77e-08	-24.44
3	2.29e-08	2.02e-08	-11.74
4	6.51e-08	4.22e-08	-35.15
5	4.85e-08	3.33e-08	-31.34
6	3.23e-08	1.96e-08	-39.29
7	4.46e-08	4.34e-08	-2.81
8	3.53e-08	1.66e-08	-52.91
9	7.59e-09	3e-08	295.35
10	5e-08	1.39e-07	177.76

7.5.1.6. Control of tonal disturbance at 250 Hz with 0.05 V amplitude

In this experiment, the amplitude of the disturbance signal is 0.05 V. The control was turned on at $t \cong 1.5$ second, using the control gain matrix found earlier, as shown in Figure 7.32. Figure 7.33 shows the displacements at the accelerometer locations, indicating that the transient vibrations decay faster than the earlier experiments. The pattern of suppression throughout the plate is slightly different from the experiment 250-5, where the displacement at accelerometer 6 shows an increase in vibration. The suppression of vibration occur accelerometer location except accelerometers 6, 9, and 10. Table 7.6 shows the maximum amplitude of displacements on the plate at sensor locations before and after control. The maximum and minimum amounts of reduction of vibration are at sensors 1 and 3, respectively.

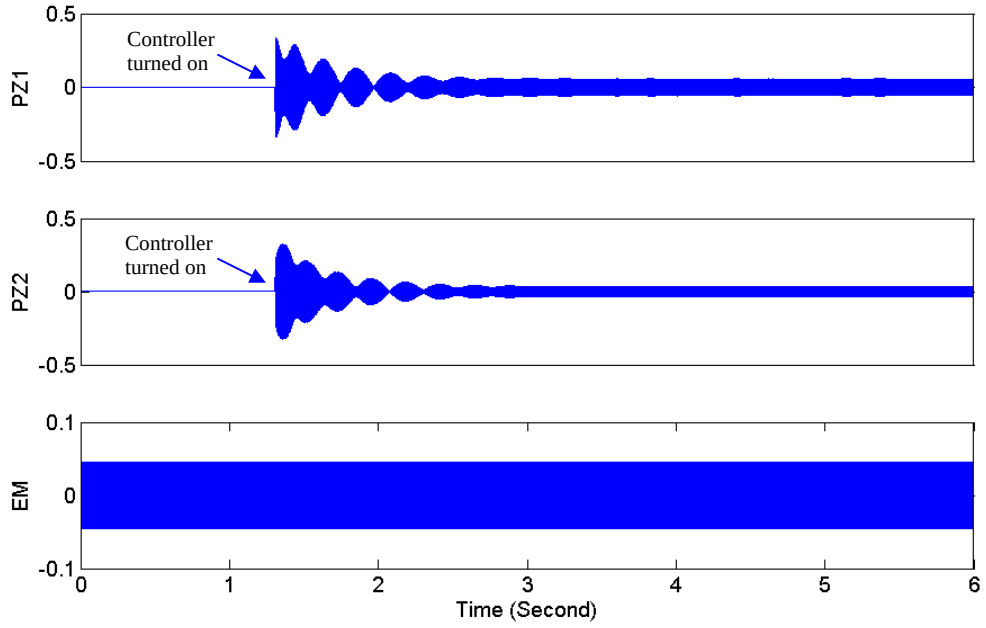

Figure 7.32. Signals to the actuators (Volts) for control of 250 Hz disturbance with amplitude of 0.05 V.; PZ1: piezoelectric actuator at center of plate; PZ2: piezoelectric actuator at off-center of plate; EM: electromagnetic shaker

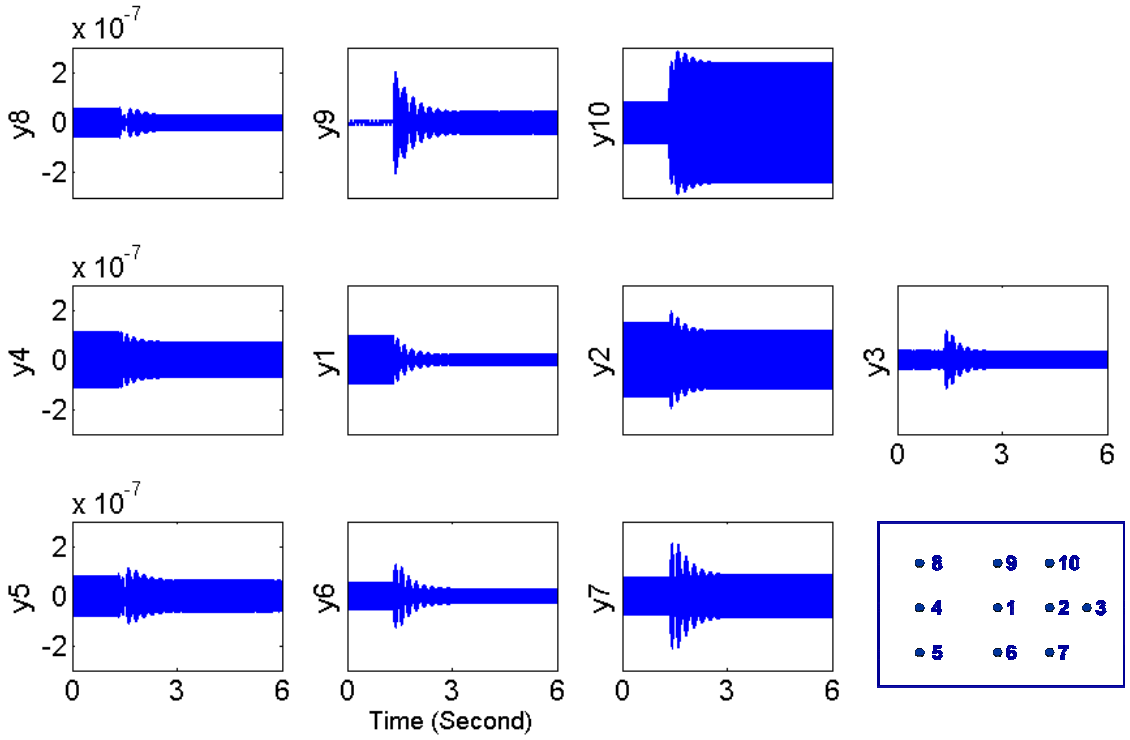

Figure 7.33. Displacement (Volts) at accelerometer locations for control of 250 Hz disturbance with amplitude of 0.05 V.

Table 7.6. Comparison of the maximum displacements at accelerometers before and after control of 250 Hz disturbance with amplitude of 0.05 V., maximum and minimum reductions are highlighted in red

Accelerometer	Maximum OL measurement (V)	Maximum CL measurement (V)	Percentage reduction
1	9.50e-08	2.18e-08	-77.07
2	1.52e-07	1.17e-07	-23.14
3	3.68e-08	3.45e-08	-6.54
4	1.10e-07	7.18e-08	-35.20
5	8.10e-08	6.33e-08	-21.96
6	5.34e-08	3.01e-08	-43.67
7	7.45e-08	8.67e-08	16.27
8	5.81e-08	3.03e-08	-47.95
9	1.17e-08	4.52e-08	286.29
10	8.21e-08	2.38e-07	190.08

7.5.1.7. Effect of disturbance power on control performance at 250 Hz

Figure 7.34 compares the percentage change of signals at each accelerometer when the amplitude of the disturbance changes. It is shown that the control gain has the most effect in reducing vibrations when the input to the electromagnetic shaker is 0.01 V. For 0.001 V, sensors 2, 3, 6, and 7 show increased vibrations. By changing the input to the electromagnetic shaker from 0.01 V to 0.05 V, the percentage of change in the amplitude of vibration change linearly, indicating the linearity of test setup.

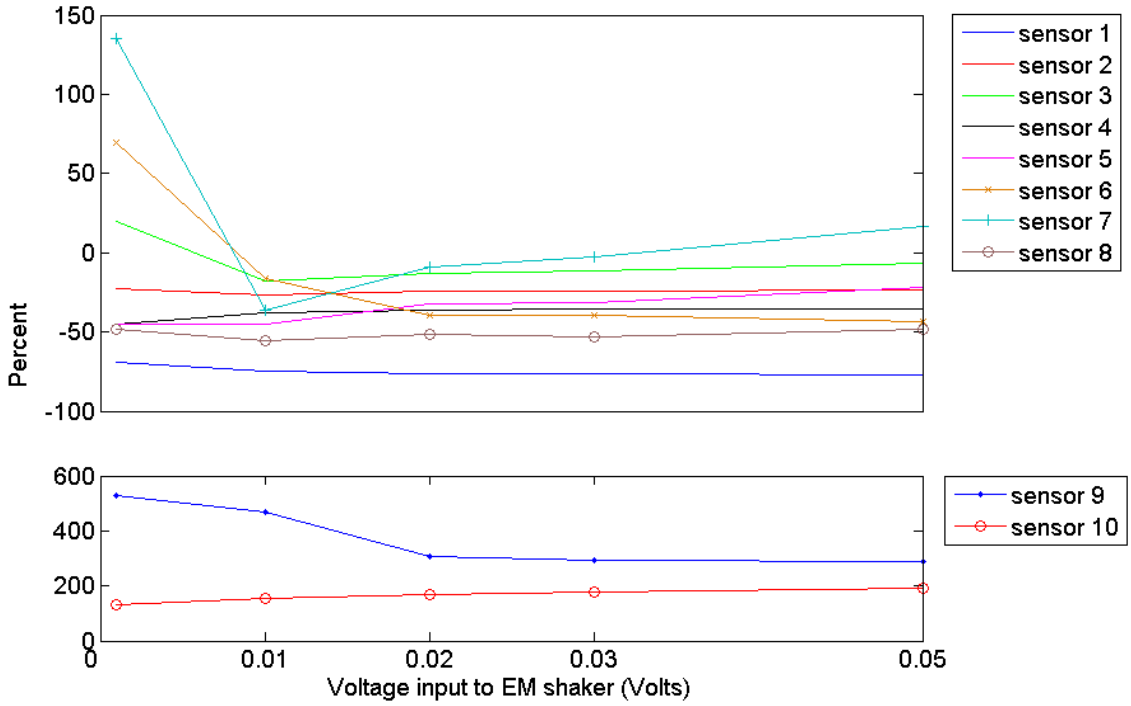

Figure 7.34. Percentage change of accelerometer measurements at various sensors for different voltages to electromagnetic shaker

7.5.2. Tonal Disturbance at 207 Hz

The other tonal frequency that is studied is 207 Hz because it is a natural frequency of plate within the 200-300 Hz frequency range and has a large peak as shown in Figures 7.20 and 7.21. We used two different control gains. One control gain matrix is determined by using orthogonal eigenstructure control applied to a new estimated state space model utilizing tonal command signals to the piezoelectric actuators with frequency of 207 Hz. The second control gain matrix is the same as the one that was used for the tests with the 250 Hz tonal disturbance. The latter is an attempt to find a gain matrix that can be used over a range of frequencies, rather than one specific frequency.

7.5.2.1. System identification experiment for tonal disturbance at 207 Hz

Two piezoelectric actuators are excited using a 207 Hz tonal signal with amplitude of 0.01 V. After two times integration and filtering of the data from sensors 1 and 2, the data is collected for 6 seconds with 3000 Hz sampling rate. Using the identification method described earlier, we estimate the state space model of the system with a dimension of 10. Figure 7.35 shows the filtered data read from the sensors. It is observed that the signals are not symmetric throughout the plate due to asymmetry of boundary conditions, place of piezoelectric actuators, electromagnetic actuators, and sensors. Figure 7.36 shows that the results for the estimated system are to 99% compatibility with the collected data.

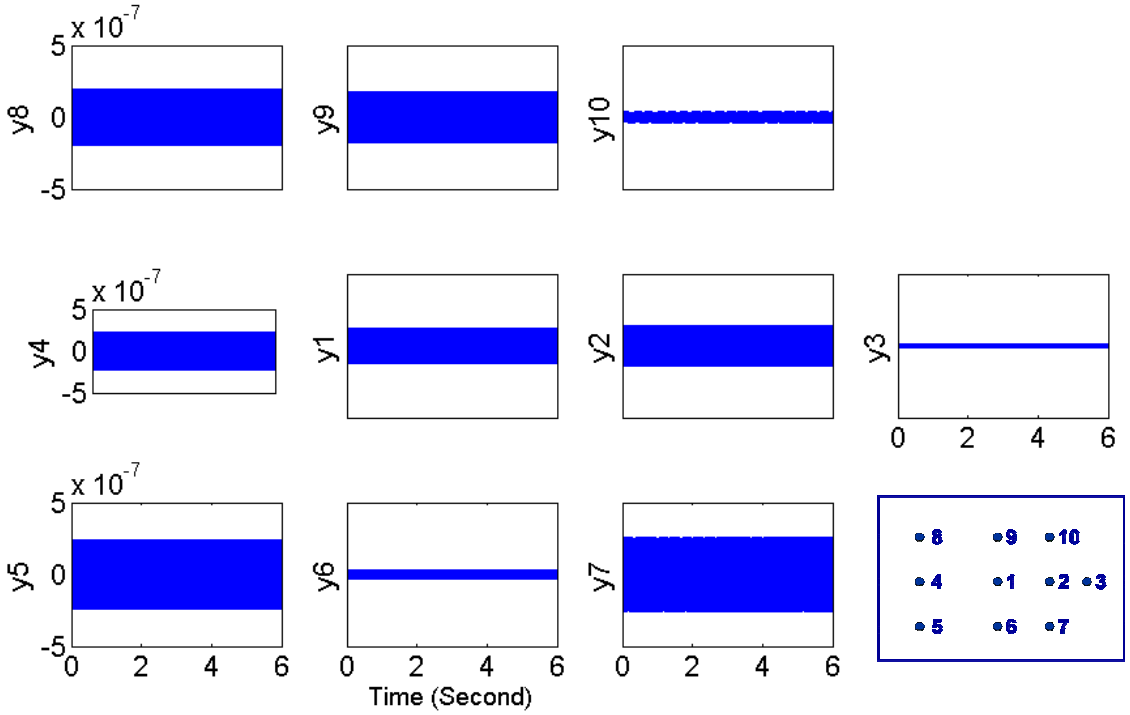

Figure 7.35. Filtered signals from sensors (Volts) for the 207 Hz tonal excitations with amplitude of 0.01 V.

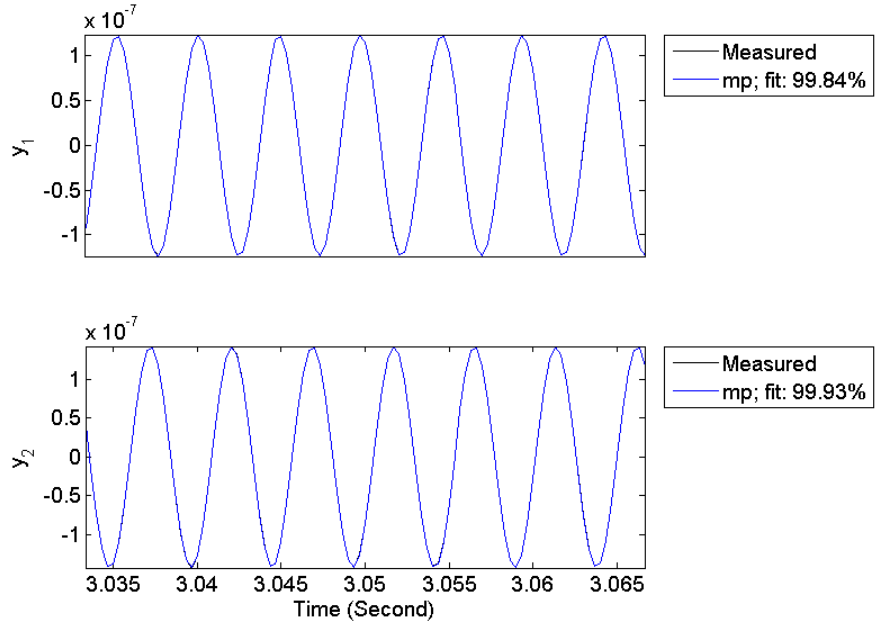

Figure 7.36. Comparison of results from estimated model and collected data at accelerometer locations for 207 Hz tonal excitation; y1: accelerometer 1; y2: accelerometer 2

7.5.2.2. Control of tonal disturbance at 207 Hz with 0.001 V amplitude

Applying the orthogonal eigenstructure control to the estimated model of the system resulted in previous experiment; one can find the control gain matrix. The amplitude of the disturbance signal is 0.001 V and the control gain matrix is

$$K = \begin{bmatrix} 9 & 12 \\ -9 & -12 \end{bmatrix} \times 10^6$$

As mentioned in section 7.3, the system identification method finds two transfer functions between each piezoelectric actuator and its collocated accelerometer displacement without considering the effect of non-collocated piezoelectric actuators. The result is a state space model with decoupled states. To compensate for this simplification, one of the elements of the control gain matrix needs to be tuned. The tuned gain would be

$$K = \begin{bmatrix} 9 & 12 \\ -9 & -21 \end{bmatrix} \times 10^6$$

During the test the controller turned on at $t \cong 3$ seconds, as shown in Figure 7.37, for the signals to the actuators. Figure 7.38 shows the displacements at the accelerometer locations. Suppression of vibrations occurs at all the accelerometer locations except to the accelerometers 4 and 7. Table 7.7 shows the maximum amplitude of displacement measured at sensor locations before and after control. The maximum and minimum amounts of reduction of vibrations are at accelerometers 2 and 8, respectively.

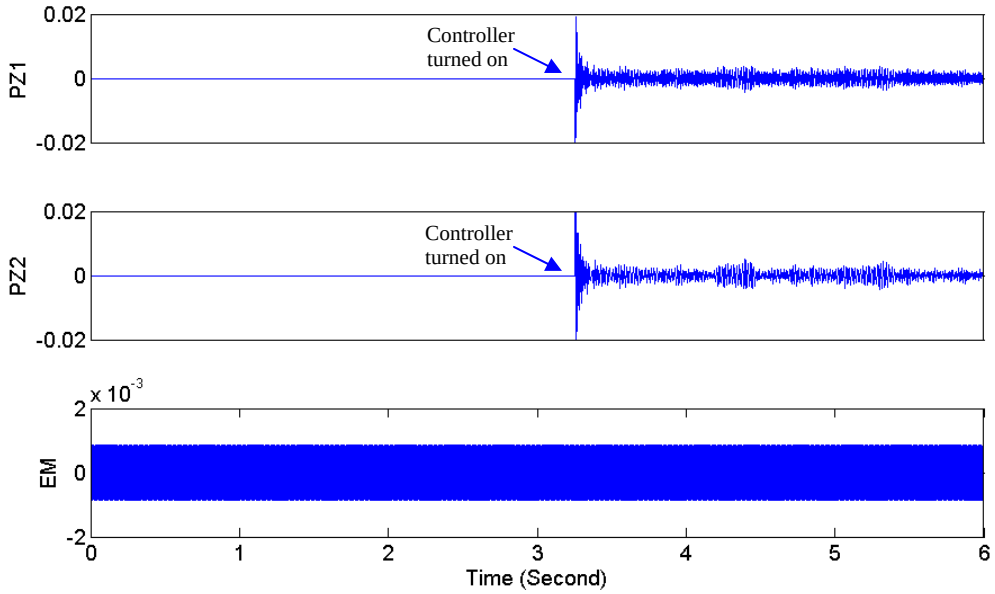

Figure 7.37. Signals to the actuators (Volts) for control of 207 Hz disturbance with amplitude of 0.001 V.; PZ1: piezoelectric actuator at center of plate; PZ2: piezoelectric actuator at off-center of plate; EM: electromagnetic shaker

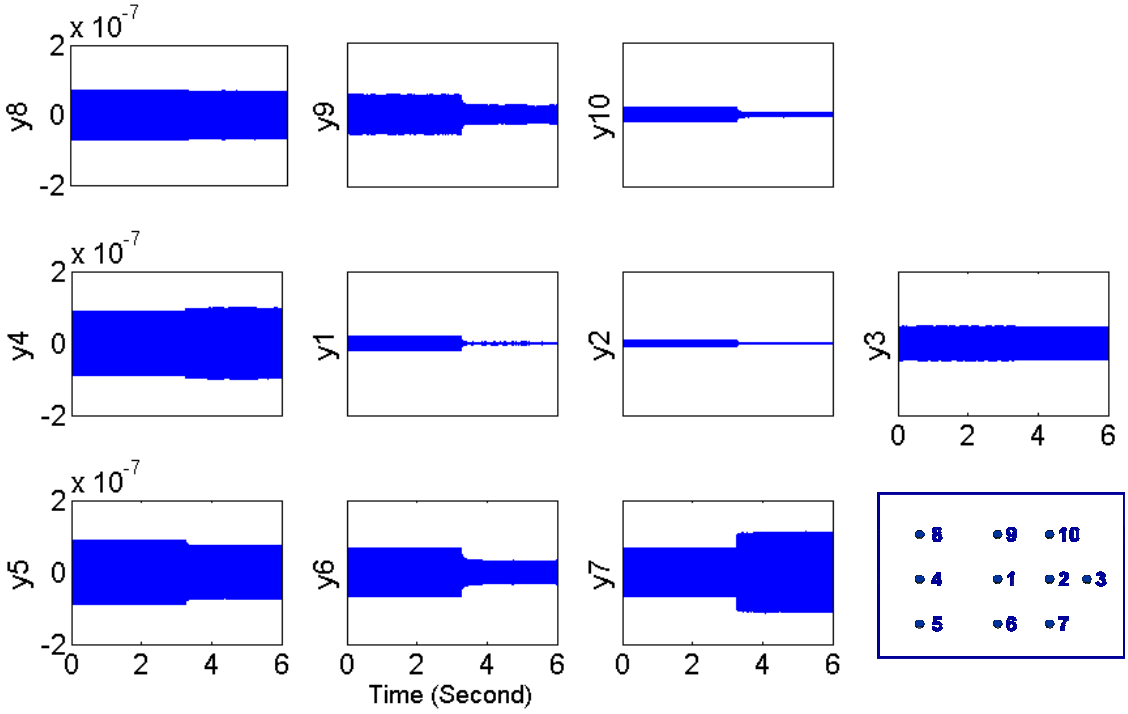

Figure 7.38. Displacement (Volts) at accelerometer locations for control of 207 Hz disturbance with amplitude of 0.001 V.

Table 7.7. Comparison of the maximum displacements at accelerometers before and after control of 207 Hz disturbance with amplitude of 0.001 V., maximum and minimum reductions are highlighted in red

Accelerometer	Maximum OL measurement (V)	Maximum CL measurement (V)	Percentage reduction
1	1.89e-08	3.33e-09	-82.41
2	9.9e-09	1.67e-09	-83.12
3	4.73e-08	4.47e-08	-5.52
4	8.9e-08	9.83e-08	10.51
5	8.94e-08	7.46e-08	-16.55
6	6.62e-08	3.36e-08	-49.23
7	6.83e-08	1.11e-07	62.23
8	7.11e-08	6.85e-08	-3.59
9	5.51e-08	2.72e-08	-50.68
10	2.1e-09	5.16e-10	-75.45

7.5.2.3. Control of tonal disturbance at 207 Hz with 0.01 V amplitude

The amplitude of the disturbance signal is changed to 0.01 V. The controller was turned on at $t \cong 1.5$ second, as shown in Figure 7.39, for the signals to the actuators. Figure 7.40 shows the displacements at the accelerometer locations. The pattern of suppression throughout the plate is different from the earlier experiment with 0.001 V amplitude of disturbance, where additional accelerometers 8 and 10 showed increased vibrations. Table 7.8 shows the maximum amplitude of displacement measured at sensor locations before and after control. The maximum and minimum amounts of reduction of vibration are at sensors 2 and 3, respectively.

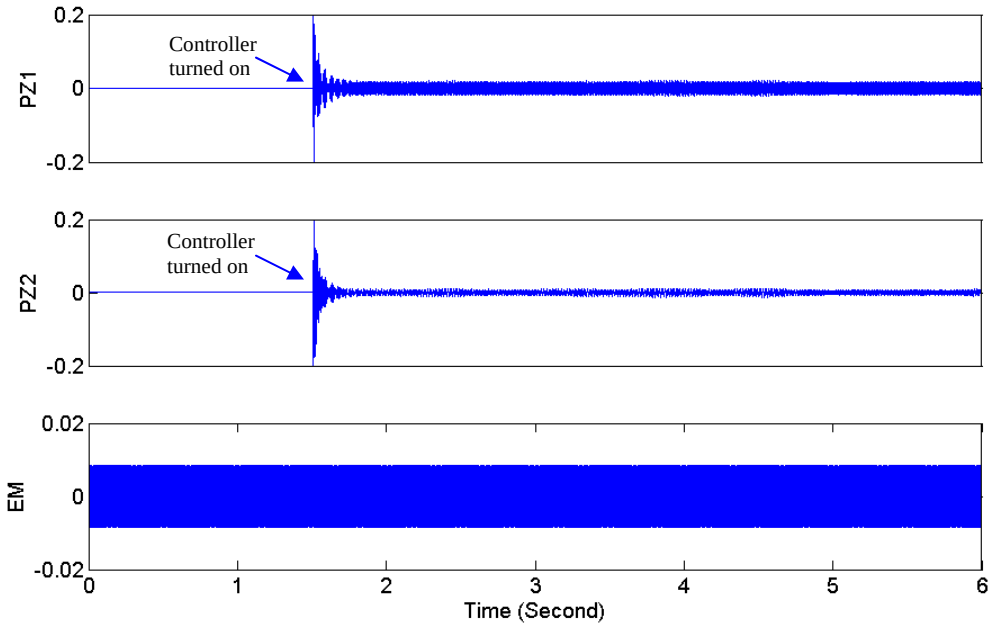

Figure 7.39. Signals to the actuators (Volts) for control of 207 Hz disturbance with amplitude of 0.01 V.; PZ1: piezoelectric actuator at center of plate; PZ2: piezoelectric actuator at off-center of plate; EM: electromagnetic shaker

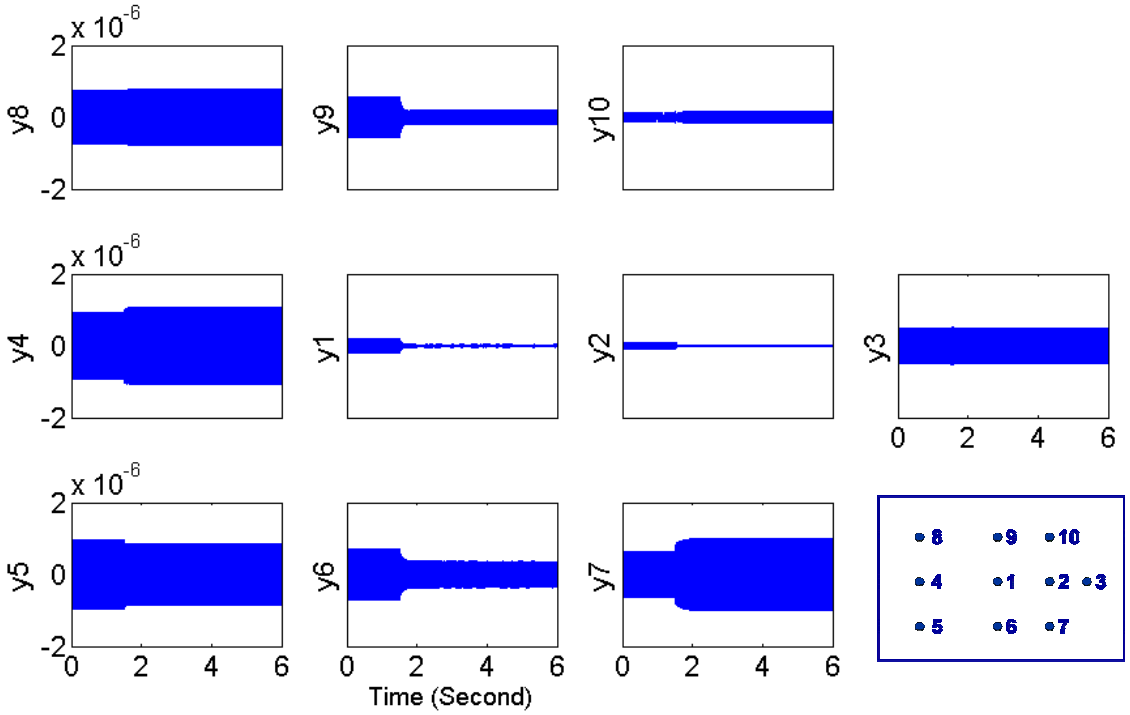

Figure 7.40. Displacement (Volts) at accelerometer locations for control of 207 Hz disturbance with amplitude of 0.01 V.

Table 7.8. Comparison of the maximum displacements at accelerometers before and after control of 207 Hz disturbance with amplitude of 0.01 V., maximum and minimum reductions are highlighted in red

Accelerometer	Maximum OL measurement (V)	Maximum CL measurement (V)	Percentage reduction
1	1.9e-07	3.66e-08	-80.74
2	8.24e-08	1.52e-08	-81.52
3	5.08e-07	4.85e-07	-4.59
4	9.29e-07	1.07e-06	14.92
5	9.6e-07	8.68e-07	-9.59
6	7.09e-07	3.63e-07	-48.72
7	6.34e-07	1.01e-06	59.66
8	7.56e-07	7.74e-07	2.32
9	5.67e-07	2.15e-07	-62.10
10	1.43e-08	1.52e-08	6.40

7.5.2.4. Control of tonal disturbance at 207 Hz with 0.01 V amplitude and control gain found for 250 Hz tonal disturbance

The increase in disturbance voltage decreased the overall vibration suppression in the plate. When the power of vibration increased, the effect of the natural frequency of 250 Hz signified. Therefore, in this experiment, the control gains determined in earlier experiments for controlling the tonal disturbance of 250 Hz is used to investigate the vibration cancellation in the test plate. The amplitude of the disturbance signal is changed to 0.01 V. The controller was turned on at $t \cong 2$ second, as shown in Figure 7.41, for the signals to the actuators. Figure 7.42 shows the displacements at the accelerometer locations. The pattern of suppression throughout the plate is different from the earlier experiment with previous test with, but is similar to the results of the control of the tonal disturbance at 250 Hz with 0.01 V amplitude, where the suppression of vibrations occur at all the accelerometers except to the accelerometers 4, 7, and 10. Table 7.9 shows the maximum amplitude of displacement measured at sensor locations before and after control. The maximum and minimum amounts of reduction of vibration are at sensors 2 and 3, respectively.

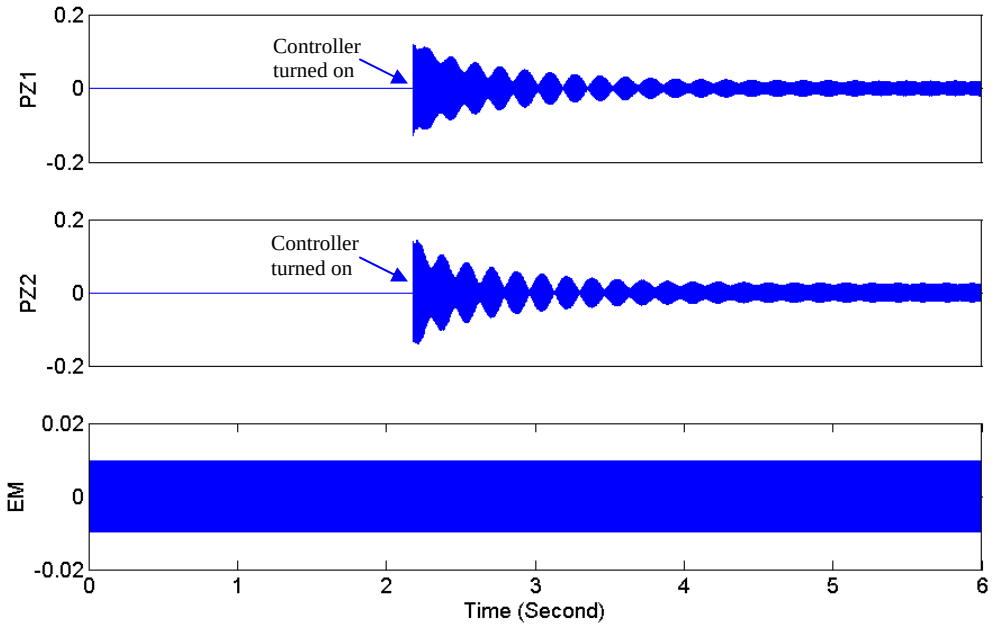

Figure 7.41. Signals to the actuators (Volts) for control of 207 Hz disturbance with amplitude of 0.01 V. and control gains associated with 250 Hz tonal disturbance; PZ1: piezoelectric actuator at center of plate; PZ2: piezoelectric actuator at off-center of plate; EM: electromagnetic shaker

The control gains determined from the system identification using tonal disturbance at 250 Hz suppresses the vibration throughout the plate in the areas behind the control actuators. This control gain matrix will be used for cancelling the vibration of a sine sweep disturbance with a frequency range of 200-300 Hz.

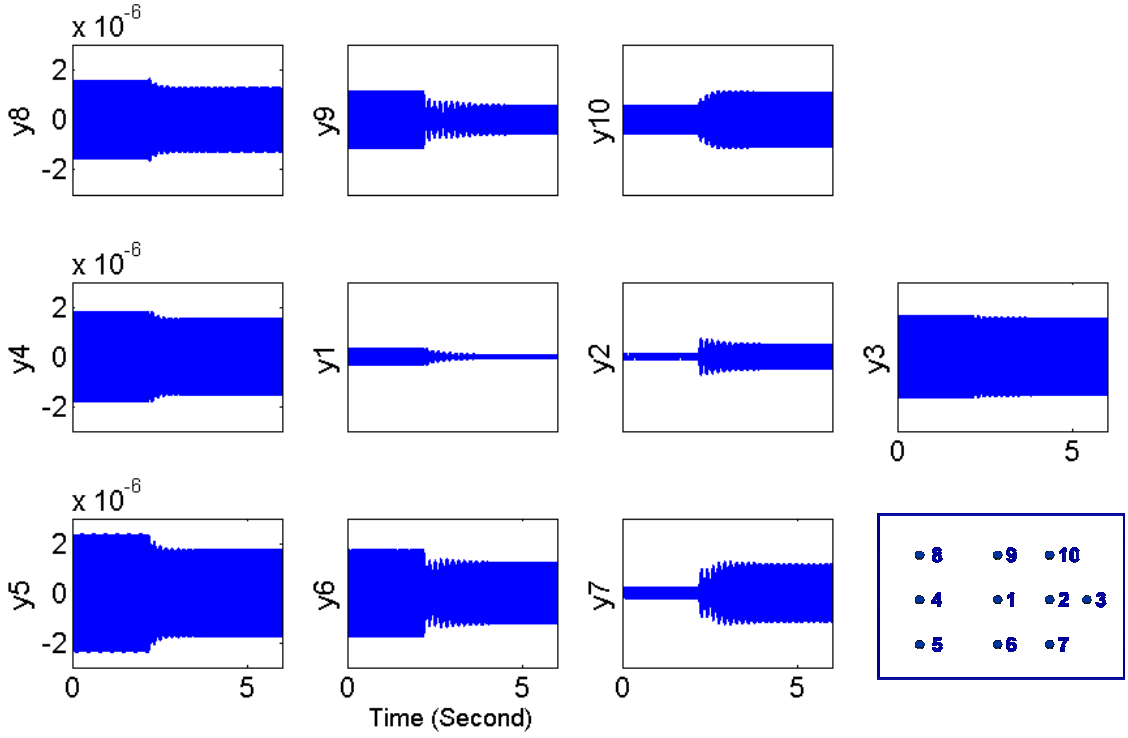

Figure 7.42. Displacement (Volts) at accelerometer locations for control of 207 Hz disturbance with amplitude of 0.01 V. and control gains associated with 250 Hz tonal disturbance

Table 7.9. Comparison of the maximum displacements at accelerometers before and after control of 207 Hz tonal disturbance with control gains associated with 250 Hz tonal disturbance, maximum and minimum reductions are highlighted in red

Accelerometer	Maximum OL measurement (V)	Maximum CL measurement (V)	Percentage reduction
1	3.42517e-07	7.93e-08	-76.84
2	1.52692e-07	5.11e-07	234.36
3	1.65561e-06	1.57e-06	-5.11
4	1.83485e-06	1.55e-06	-15.33
5	2.36915e-06	1.76e-06	-25.51
6	1.74714e-06	1.25e-06	-28.66
7	2.13183e-07	1.17e-06	448.18
8	1.58284e-06	1.29e-06	-18.74
9	1.16722e-06	5.87e-07	-49.74
10	5.75931e-07	1.1e-06	90.75

7.5.3. Tonal Disturbance at 150 Hz

As an example of a tonal disturbance with frequency outside the range of 200-300 Hz, a disturbance with a frequency of 150 Hz, which is one of the natural frequencies of the plate, was used. The piezoelectric actuators were excited using a 150 Hz tonal signal with amplitude of 0.02 V. The integrated and filtered data from accelerometers 1 and 2 were collected for 6 seconds with 3000 Hz sampling rate. A state space model of the system with a dimension of 10 is estimated. Figure 7.43 depicts how close the results are to the simulations of the estimated model of the plate with the collected data. They match each other with 99% compatibility.

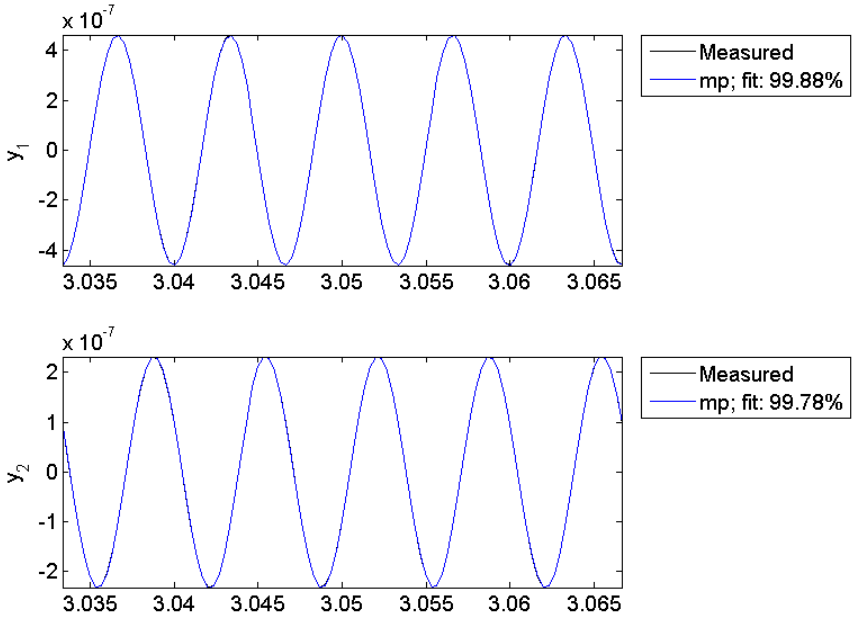

Figure 7.43. Comparison of results from estimated model
and collected data at accelerometer locations for the 207 Hz tonal excitations;
y1: accelerometer 1; y2: accelerometer 2

Orthogonal eigenstructure control has been used to find the control gain matrix for the estimated model of the plate is

$$K = \begin{bmatrix} -24 & -18 \\ 24 & 18 \end{bmatrix} \times 10^6$$

The disturbance voltage was 0.02 V. Figure 7.44 shows the command signals to the actuators indicating saturation of the piezoelectric actuators. Figure 7.45 shows the filtered signal from the accelerometers. The suppression of vibration occurs at all the locations. Table 7.10 shows the maximum amplitude of signals read at sensors with and without control. The maximum and minimum amounts of reduction of vibrations are at locations 7 and 9, respectively.

Figures 7.19a and 7.19b can be used to explain the saturation of the piezoelectric actuators. The magnitude of the frequency responses of the plots are small, indicating that they are located on nodes, when the source of the disturbance is the electromagnetic actuator. As a result, the calculated gain matrix is large, so that the low authority of the piezoelectric actuators.

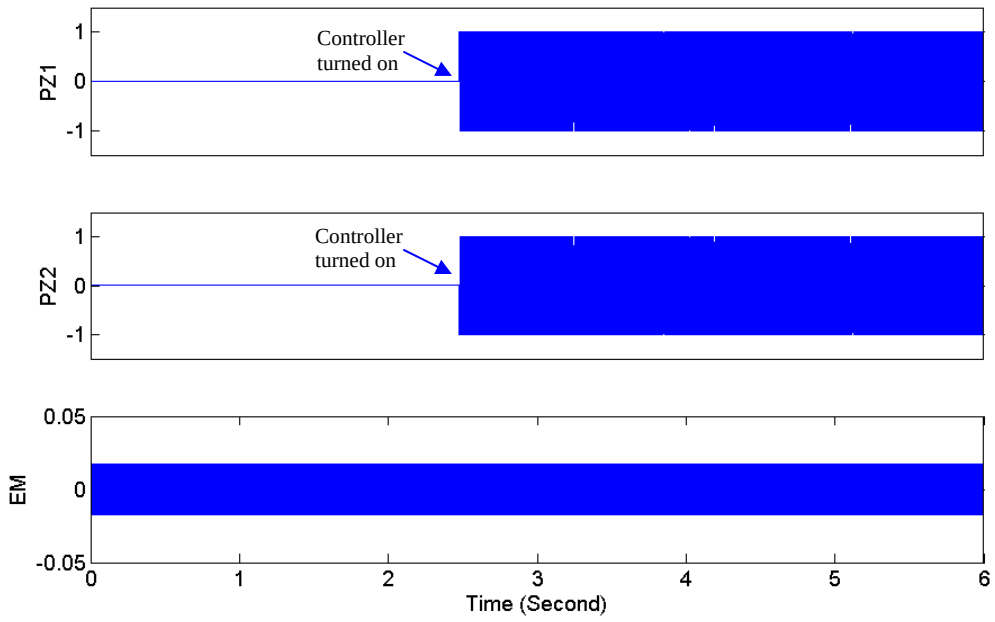

Figure 7.44. Signals to the actuators (Volts) for control of 150 Hz disturbance with amplitude of 0.02 V.; PZ1: piezoelectric actuator at center of plate; PZ2: piezoelectric actuator at off-center of plate; EM: electromagnetic shaker

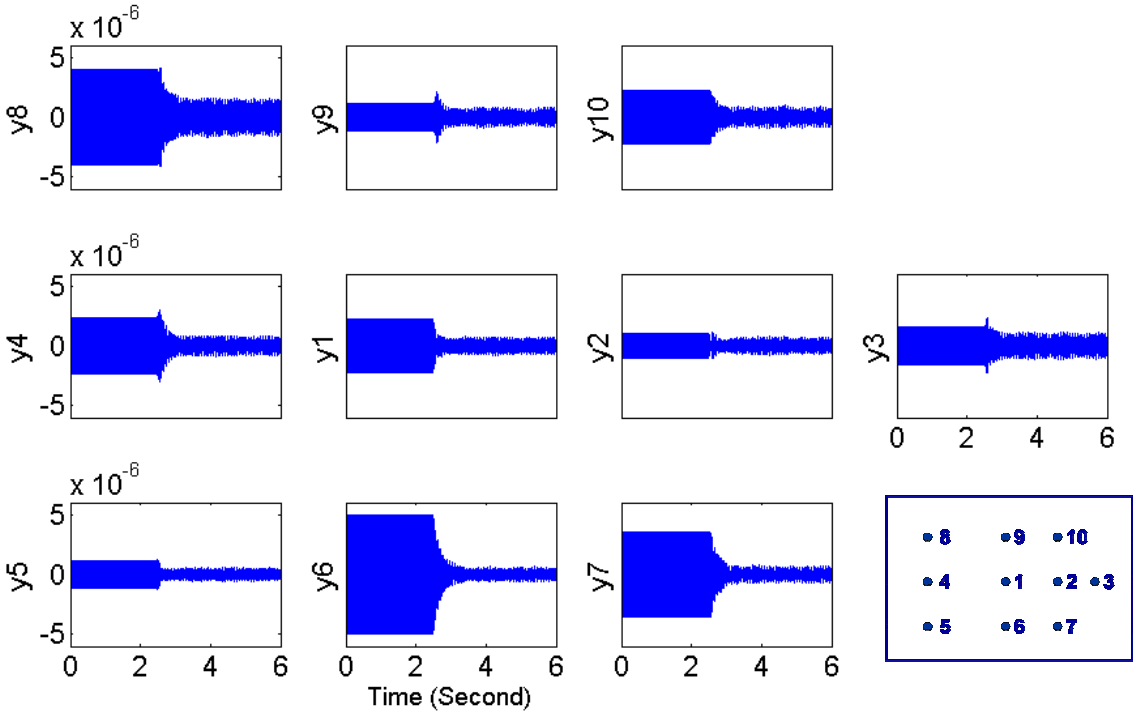

Figure 7.45. Displacement (Volts) for control of 150 Hz disturbance with amplitude of 0.02 V. at accelerometer locations

Table 7.10. Comparison of the maximum displacements at accelerometers before and after control of 150 Hz disturbance with amplitude of 0.02 V., maximum and minimum reductions are highlighted in red

Accelerometer	Maximum OL measurement	Maximum CL measurement	Percentage reduction
1	2.27e-06	7e-07	-69.10
2	1.01e-06	7.29e-07	-28.20
3	1.56e-06	1.1e-06	-29.75
4	2.33e-06	7.88e-07	-66.23
5	1.19e-06	5.59e-07	-52.85
6	5e-06	5.75e-07	-88.49
7	3.59e-06	7.51e-07	-79.09
8	3.98e-06	1.53e-06	-61.58
9	1.12e-06	8.1e-07	-27.80
10	2.23e-06	8.27e-07	-62.89

7.6. Wideband Control of Sine Sweep Disturbance with Frequency Range of 200-300 Hz

This section describes the various tests that were conducted with a wideband disturbance in the frequency range of 200-300 Hz. The results complement those presented in the earlier section by showing the capability of the controller for reducing wideband vibrations. Two experiments were performed. In the first experiment the control gain that was determined for the control of tonal disturbance at 250 Hz was used. In the second experiment, the same control gain by an overall tuning factor 2 was used.

7.6.1. Vibration control of Sine sweep disturbance

In this section the results of the control of a wideband disturbance is presented. A sine sweep was used to simulate a wideband disturbance in the range of 200-300 Hz with constant amplitude of 0.01 V. The sweep duration was 30 seconds and it was repeated until the test was stopped. The control gain was kept the same as the pure tone experiments with 250 Hz disturbance. The control gain matrix is

$$K = \begin{bmatrix} -37 & -9.5 \\ 37 & 9.5 \end{bmatrix} \times 10^6$$

Figure 7.46 shows the change in the amplitude of vibration at different accelerometers in time domain, where as Figure 7.47 depicts the control signals to the piezoelectric actuators. Figure 7.48 presents the ratio between the frequency responses of the controlled system. Amplitudes below 0 dB are presenting a reduction in the magnitude of the response in frequency domain. The largest reductions are observed in the range of 200-260 Hz. This is partly because of the natural frequency that is at 277 Hz. The control gain associated with the control of tonal disturbance at 250 Hz cannot suppress the vibration when the disturbance is a tonal input at 277 Hz. Therefore, the same effect can be seen at frequency range close to 277 Hz when the disturbance is a wideband signal.

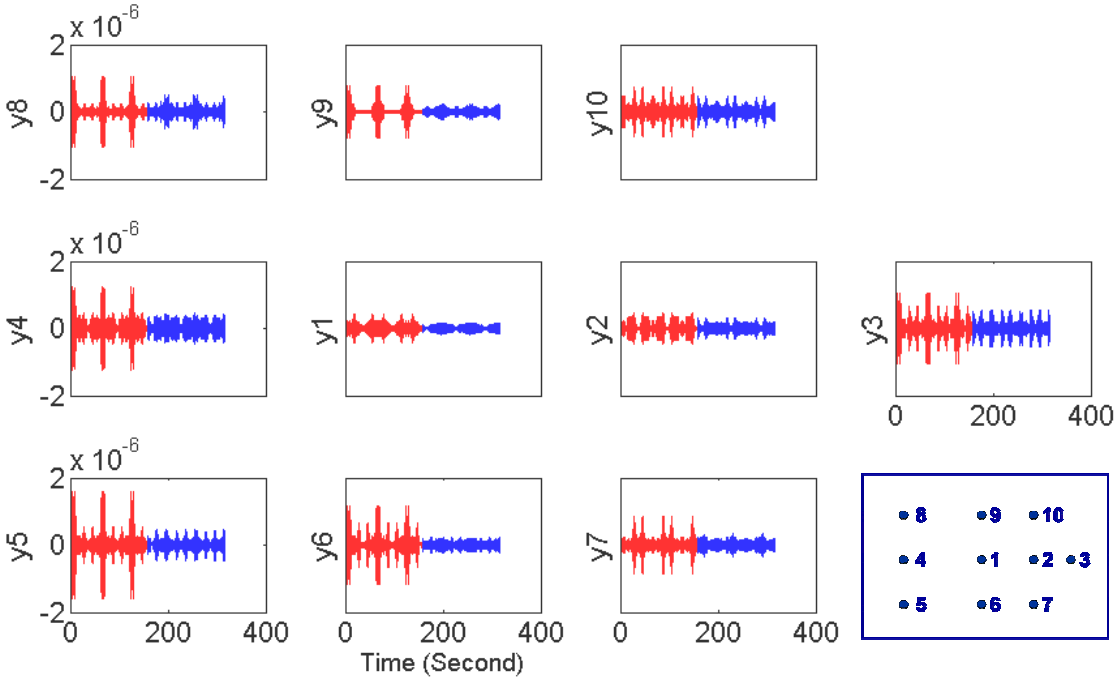

Figure 7.46. Displacement (Volts) at accelerometer locations;
before control (red) and after control (blue)

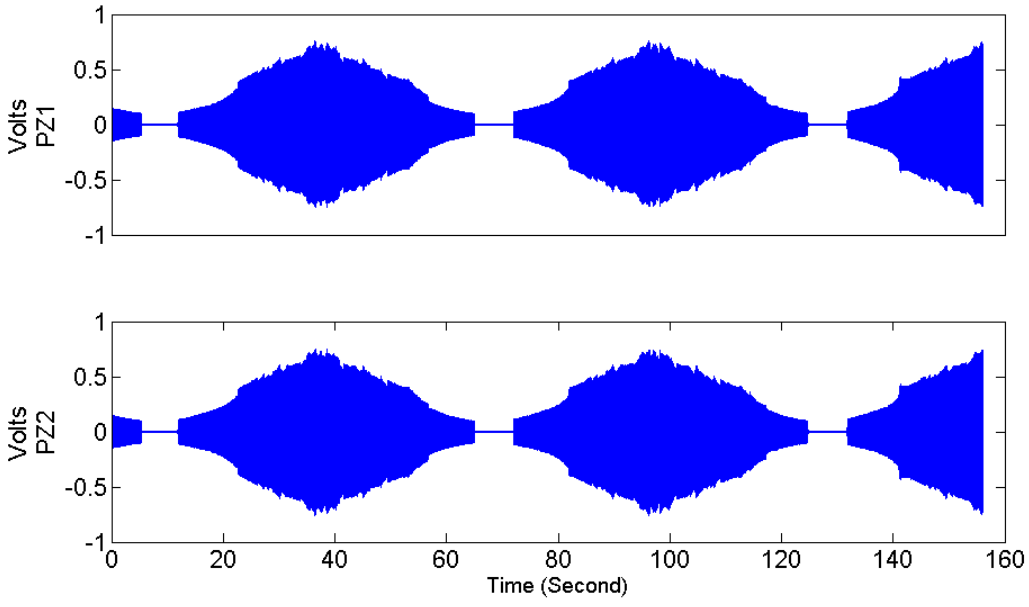

Figure 7.47. Signals to the actuators (Volts); PZ1: piezoelectric actuator at center of plate;
PZ2: piezoelectric actuator at off-center of plate

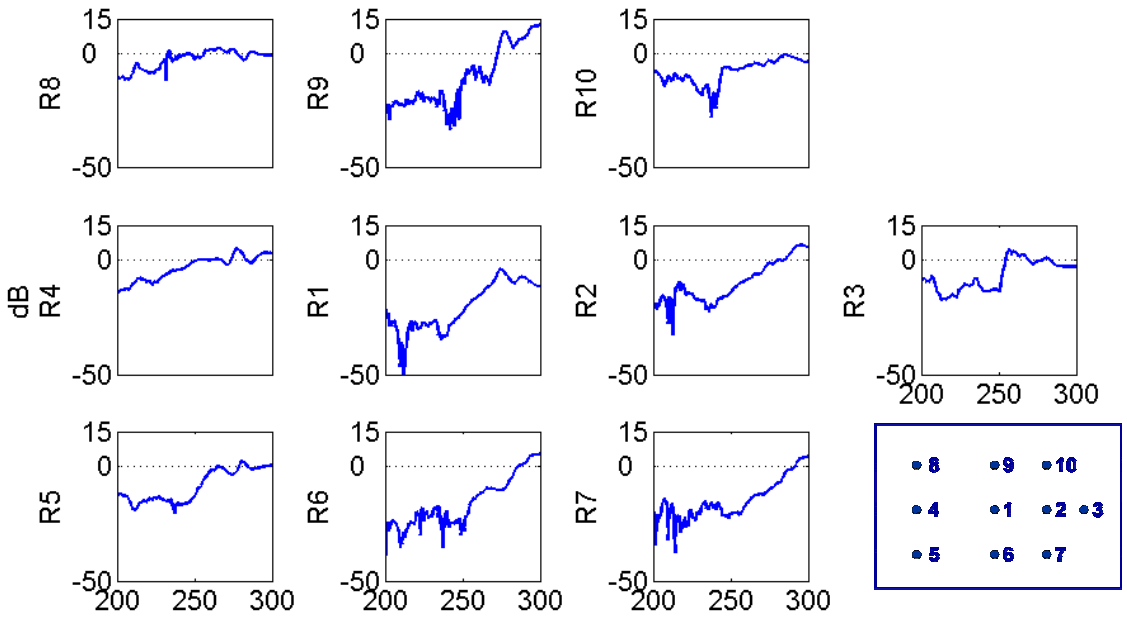

Figure 7.48. Ratio of frequency response to the sine sweep disturbance of controlled system to un-controlled system at various accelerometers

Figures 7.49-7.58 present the comparison between the frequency responses at each accelerometer to the disturbance signals. Figure 7.49 shows vibration reduction at the location of accelerometer 1 for the 200-300 Hz frequency range. The plate has a natural frequency at 273 Hz. Because of the effect of this natural frequency lower reduction of vibrations at frequency range of 270 Hz and beyond occur comparing to the frequency range of 200-270 Hz. The effect of this natural frequency is more significant in Figures 7.50-7.57. Amplitude of vibrations at the locations of accelerometers 2 to 9 are increased when the control is applied. Accelerometer 10 has similar frequency response plot as accelerometer 1, as can be seen in Figure 7.58. It shows that there is no increase in the amplitude of vibrations at frequencies 270 Hz and higher.

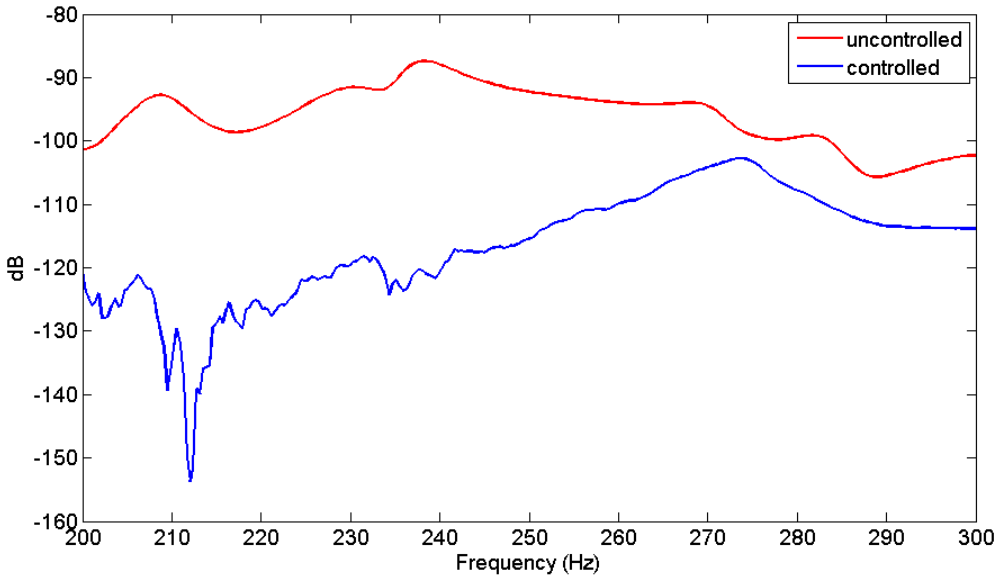

Figure 7.49. Frequency responses to the sine sweep disturbance at accelerometer 1

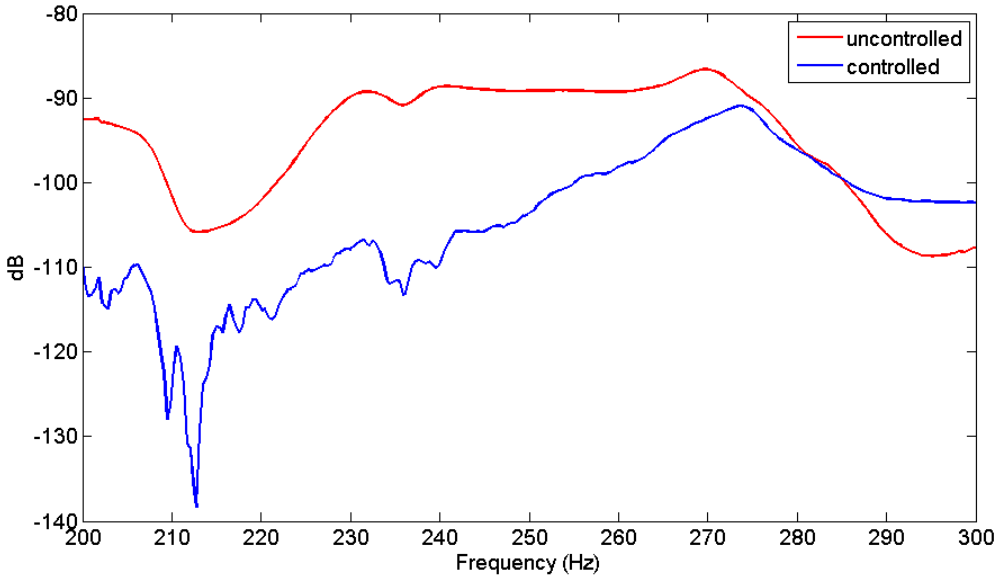

Figure 7.50. Frequency responses to the sine sweep disturbance at accelerometer 2

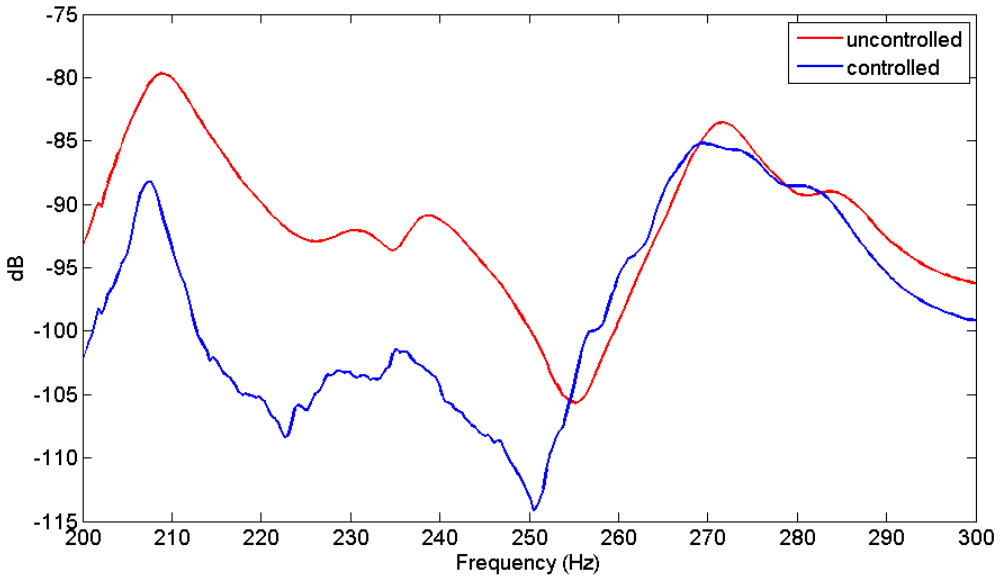

Figure 7.51. Frequency responses to the sine sweep disturbance at accelerometer 3

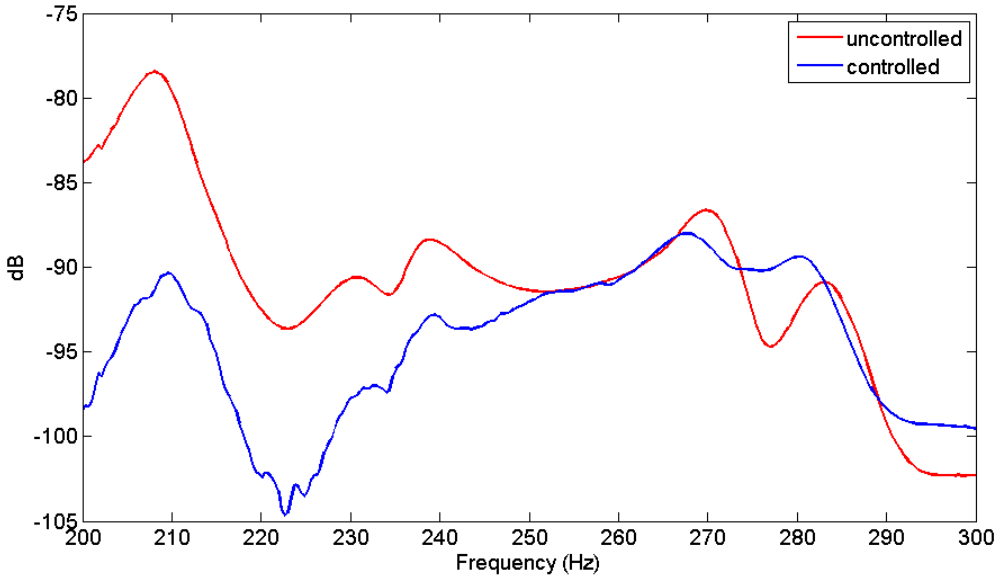

Figure 7.52. Frequency responses to the sine sweep disturbance at accelerometer 4

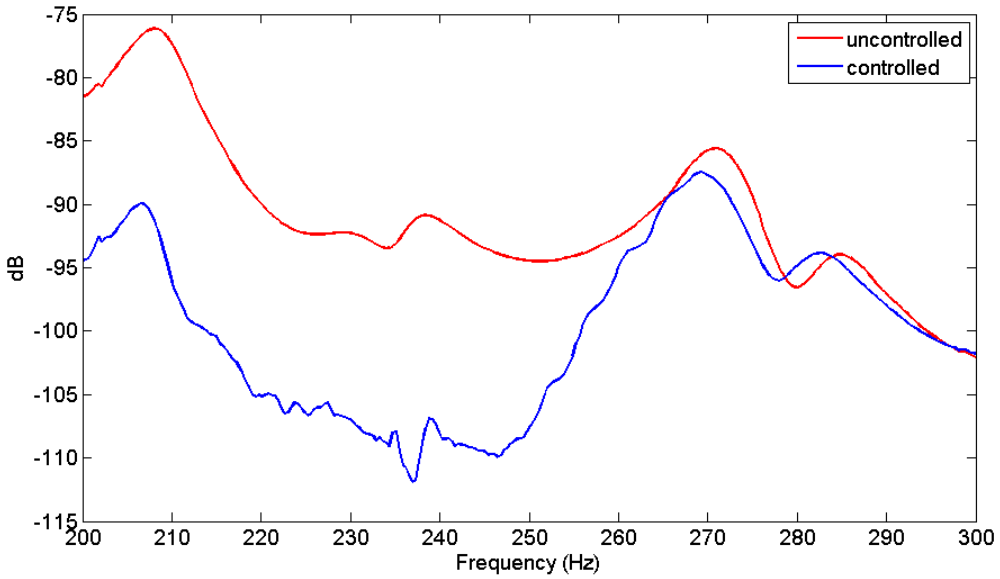

Figure 7.53. Frequency responses to the sine sweep disturbance at accelerometer 5

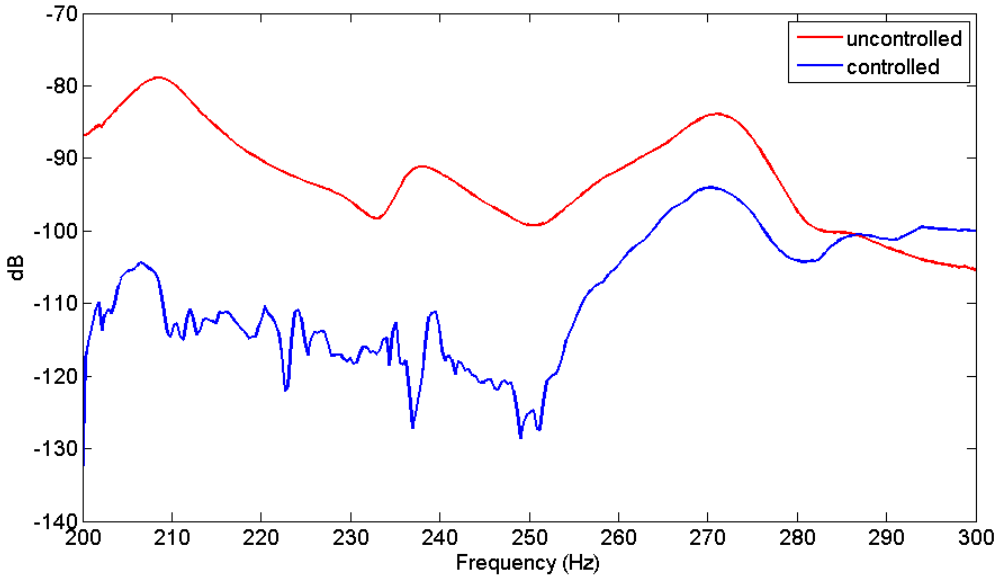

Figure 7.54. Frequency responses to the sine sweep disturbance at accelerometer 6

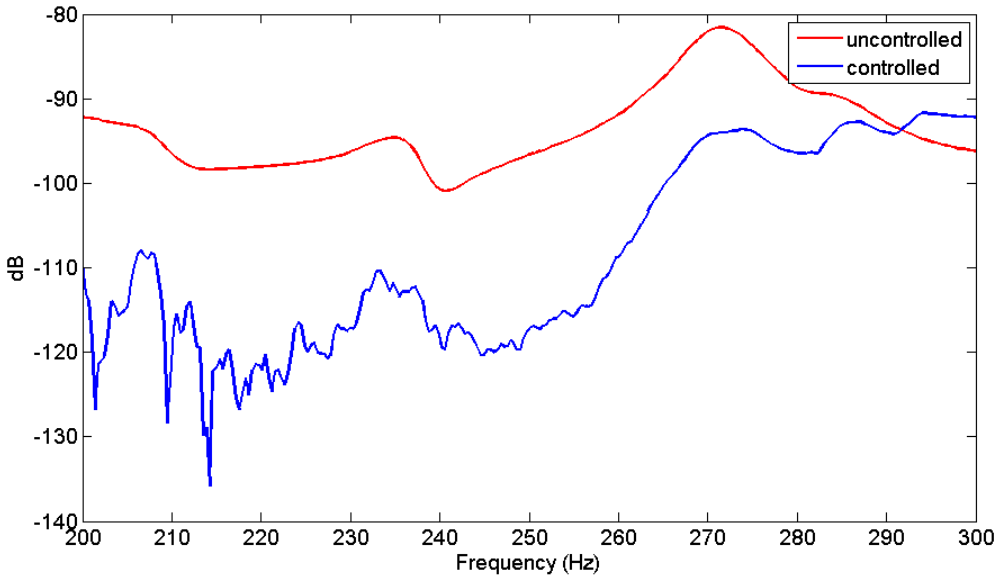

Figure 7.55. Frequency responses to the sine sweep disturbance at accelerometer 7

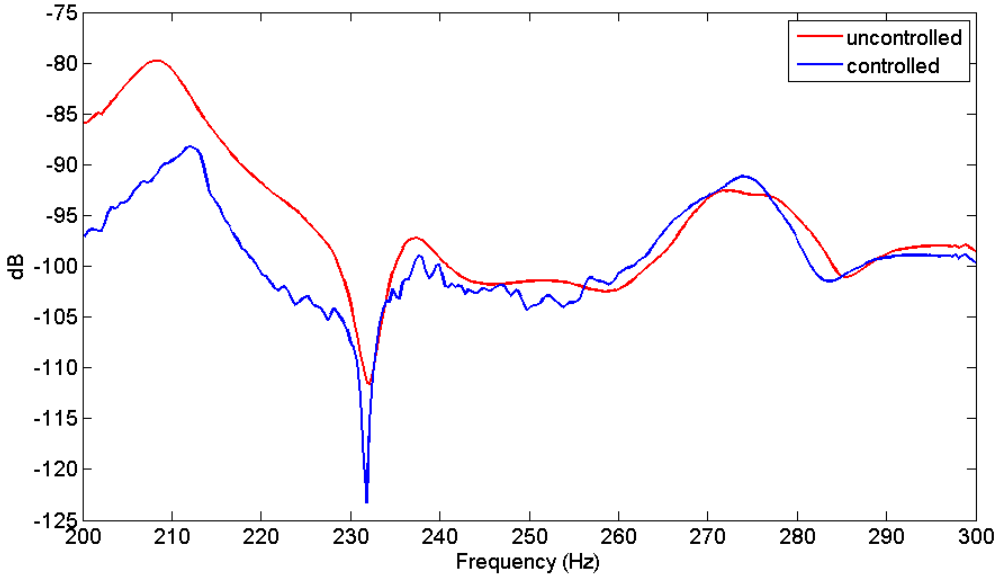

Figure 7.56. Frequency responses to the sine sweep disturbance at accelerometer 8

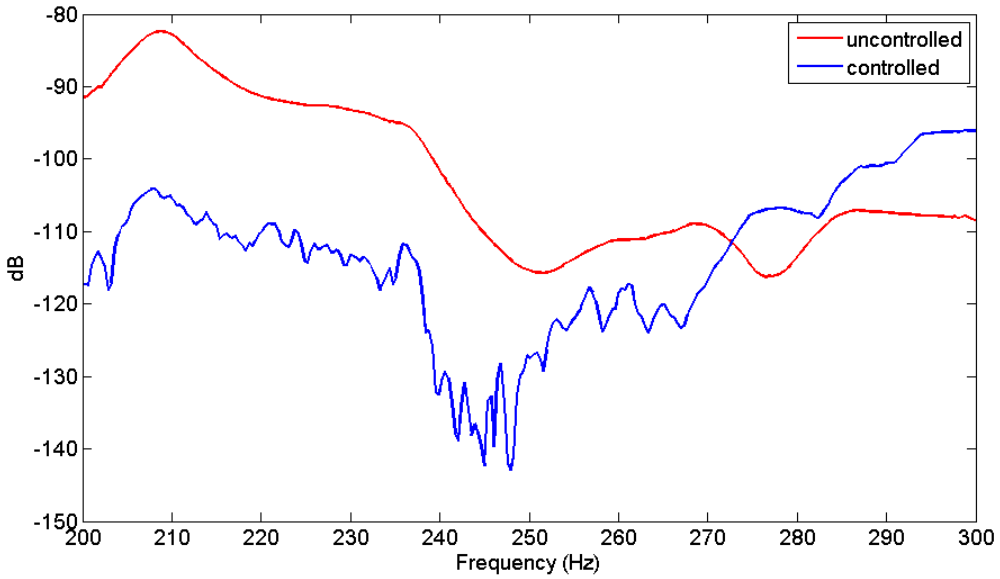

Figure 7.57. Frequency responses to the sine sweep disturbance at accelerometer 9

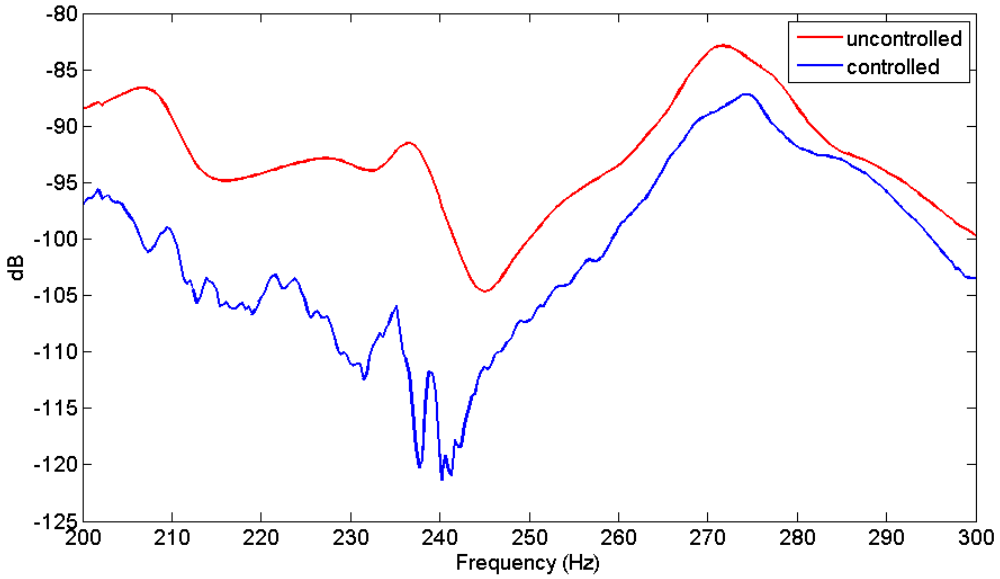

Figure 7.58. Frequency responses to the sine sweep disturbance at accelerometer 10

7.6.2. Vibration control of Sine sweep disturbance with tuned control gain

The results in this section are for the exact same setup as the previous section, except that the overall control gain was doubled to compensate for the simplifications of the system identification method that was used. The change was made in order to determine if high gains can result in more vibration isolation; or, isolation across a broader frequency band. The effect of scaling the overall gain in simulation of a system with high degrees o freedom has been discussed earlier in section 6.3.

Figure 7.59 shows the change in vibrations amplitude at different accelerometers in time domain. Figure 7.60 depicts the control signals to the piezoelectric actuators that are increased relative to the previous wideband experiment. Figure 7.61 presents the ratio between the frequency responses of the controlled system, to the uncontrolled system to the disturbance signal applied to the electromagnetic actuator. Values below 0 dB present a reduction in the frequency response magnitude. A great reduction in the frequency responses is seen in almost the entire frequency range of 200-300 Hz, except at the location of accelerometers 4, and 8. Figure 7.62 shows a comparison of these ratios between the current experiment and previous one. Larger gains result in better control and larger reductions of vibrations.

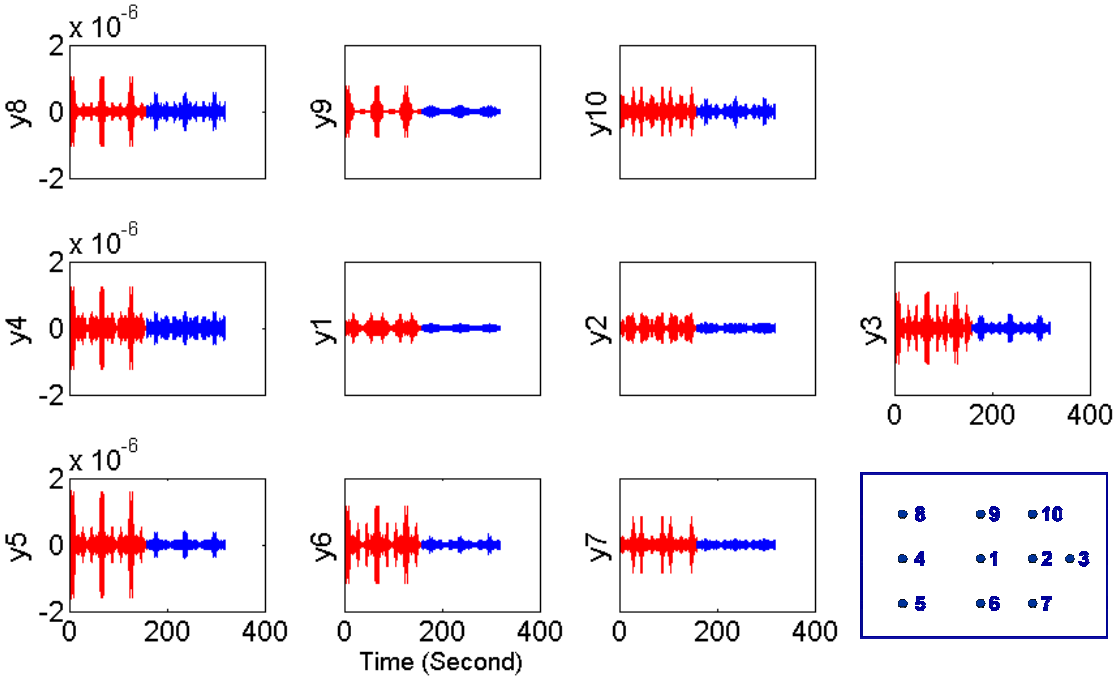

Figure 7.59. Displacement (Volts) at accelerometer locations;
before control (red) and after control (blue)

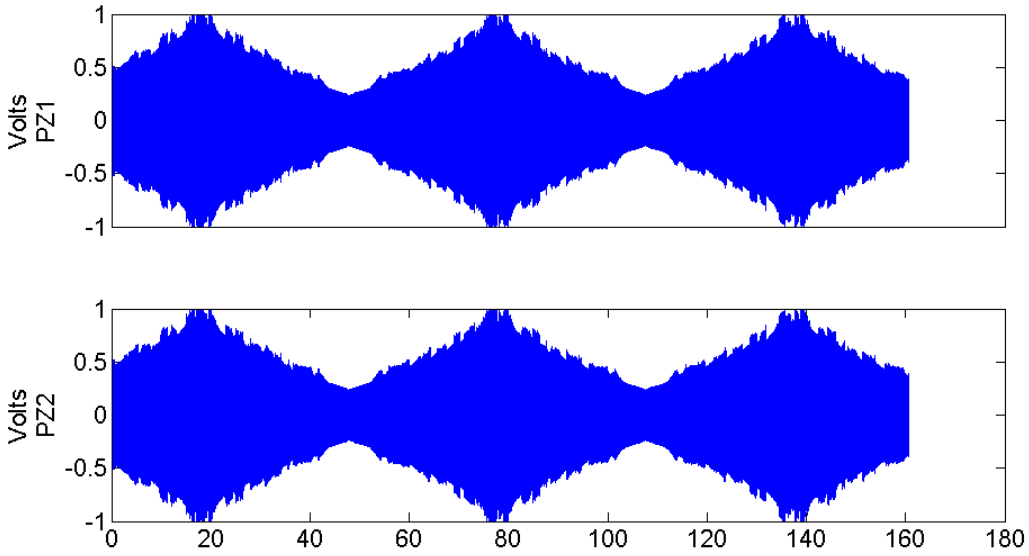

Figure 7.60. Signals to the actuators (Volts); PZ1: piezoelectric actuator at center of plate;
PZ2: piezoelectric actuator at off-center of plate

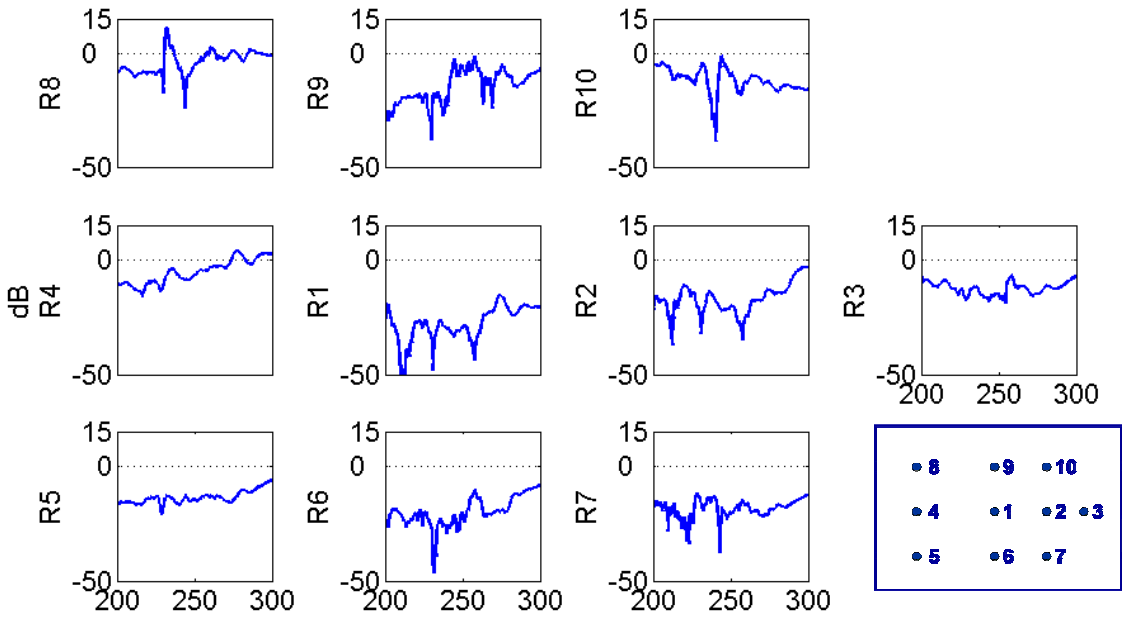

Figure 7.61. Ratio of frequency response to the sine sweep disturbance of controlled system to un-controlled system at various accelerometers

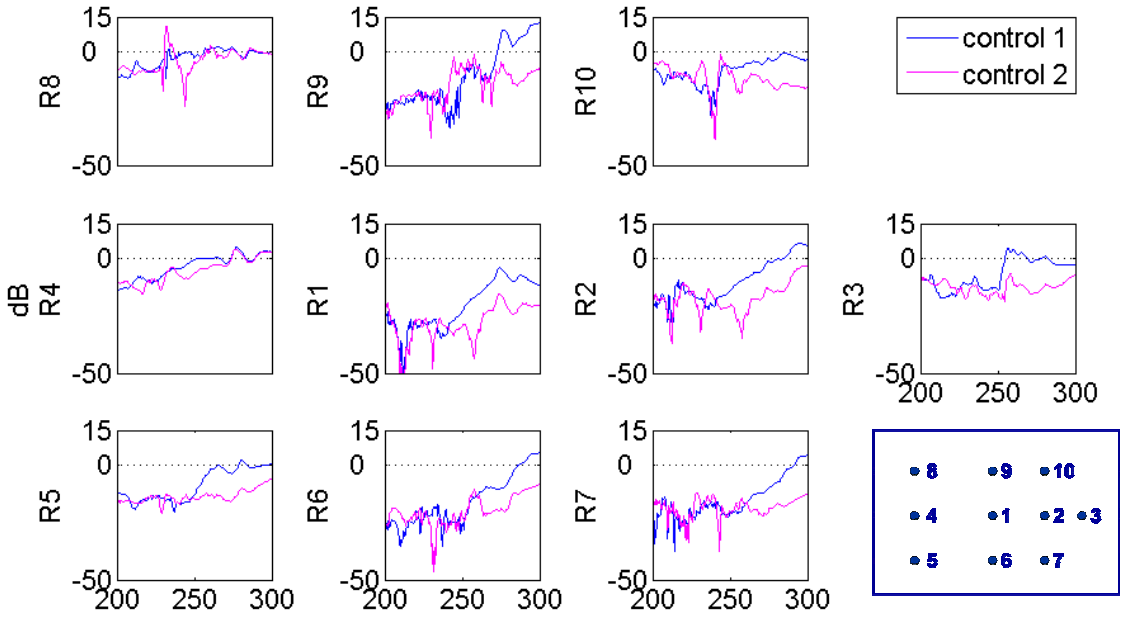

Figure 7.62. Ratio of frequency response to the sine sweep disturbance of controlled system to un-controlled system at various accelerometers with two different control gains (comparison of Figure 7.48 and 7.61)

Figures 7.63-7.72 presents the comparison between the frequency responses to the disturbance at accelerometers 1 to 10 respectively. Doubling the overall control gain reduces the effect of the natural frequency of plate at 273 Hz on the frequency response plots. Vibration cancellation occurs in entire frequency range of 200-300 Hz at all the accelerometers except to the accelerometers 4 and 8, as can be seen in Figures 7.66, and 7.70.

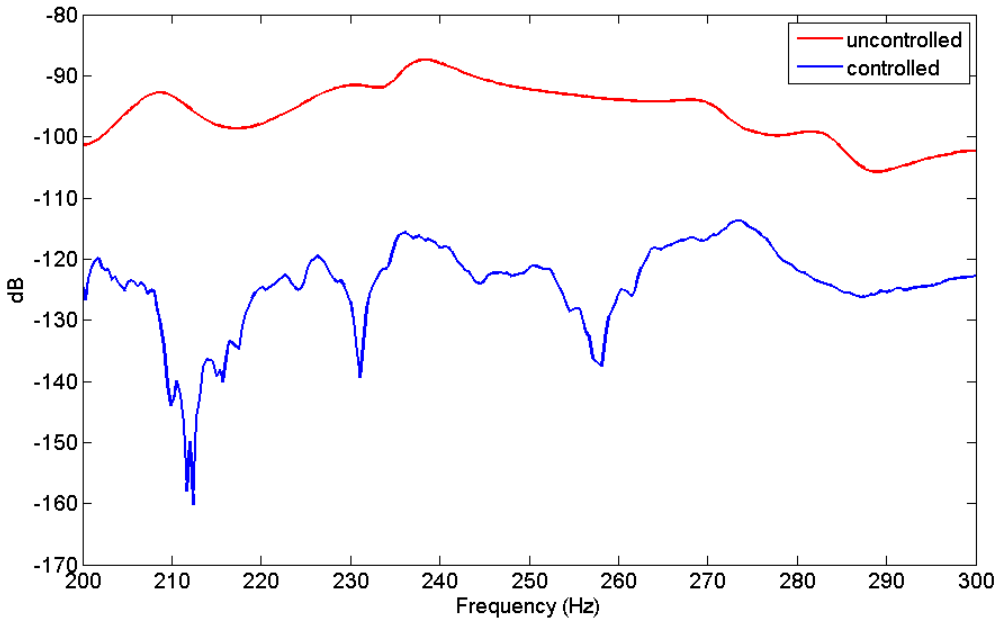

Figure 7.63. Frequency responses to the sine sweep disturbance at accelerometer 1

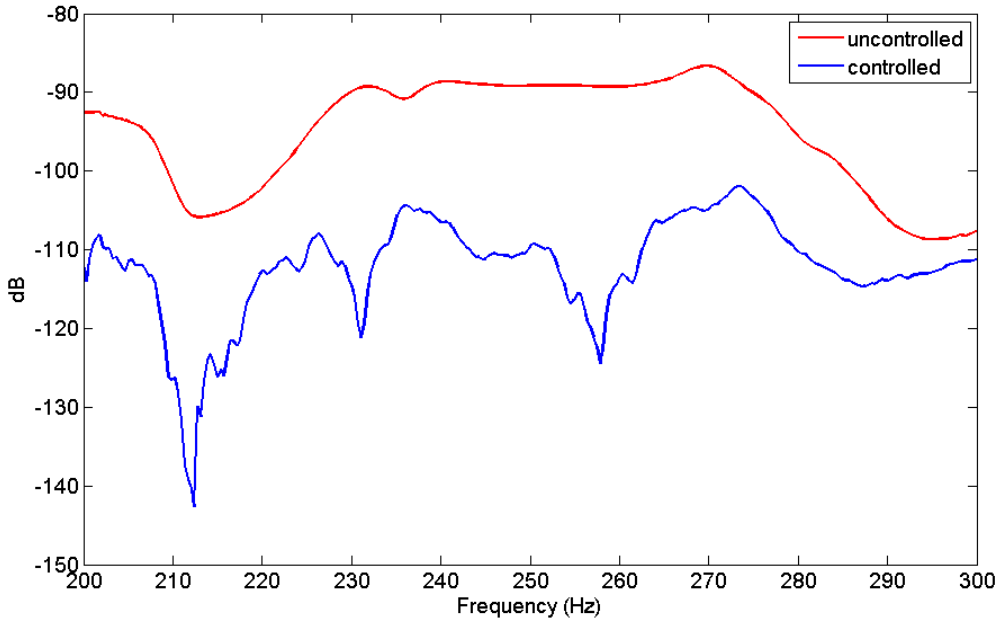

Figure 7.64. Frequency responses to the sine sweep disturbance at accelerometer 2

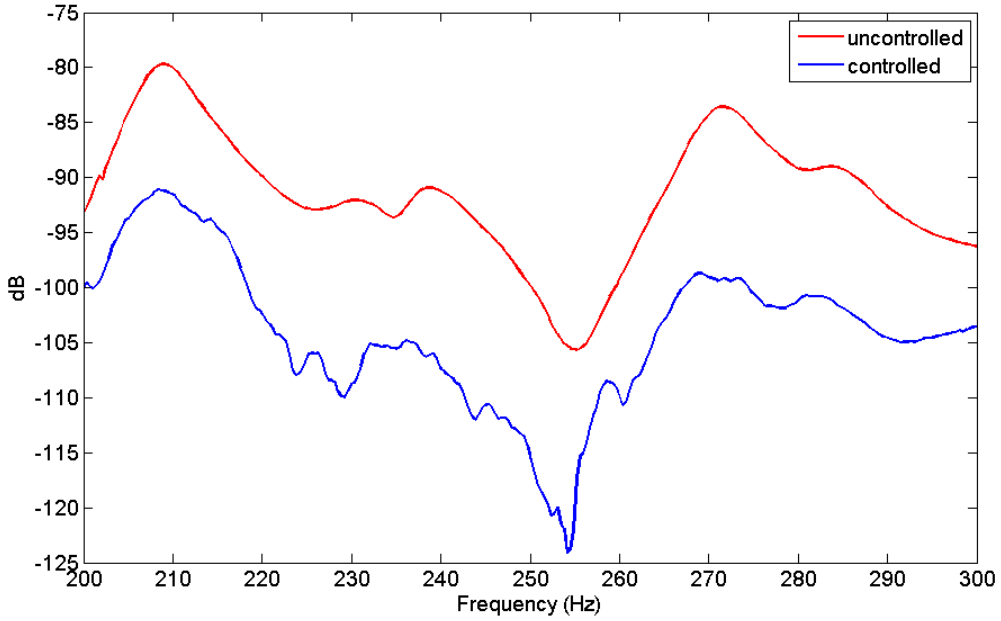

Figure 7.65. Frequency responses to the sine sweep disturbance at accelerometer 3

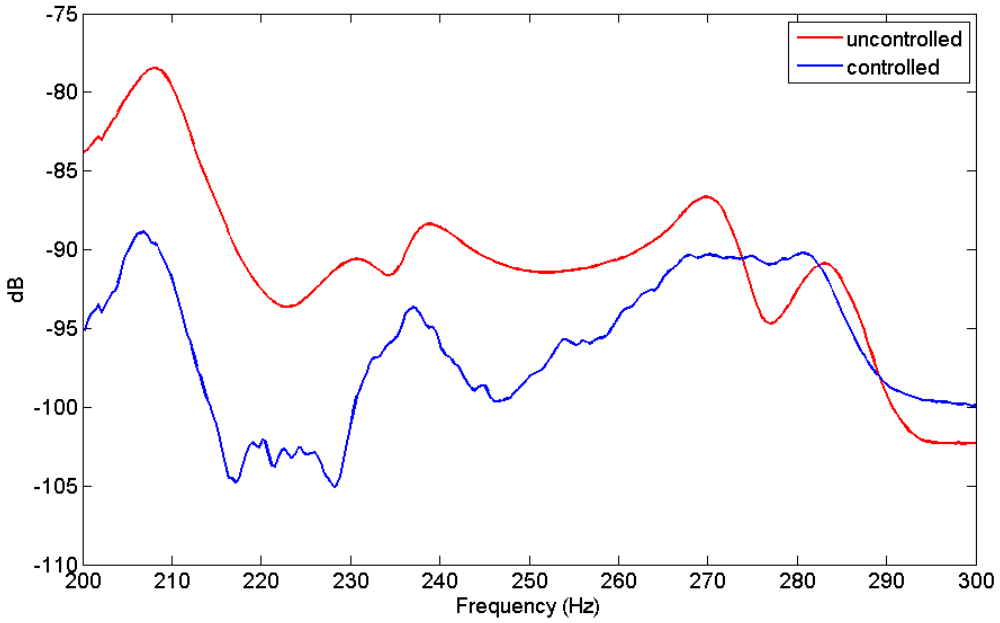

Figure 7.66. Frequency responses to the sine sweep disturbance at accelerometer 4

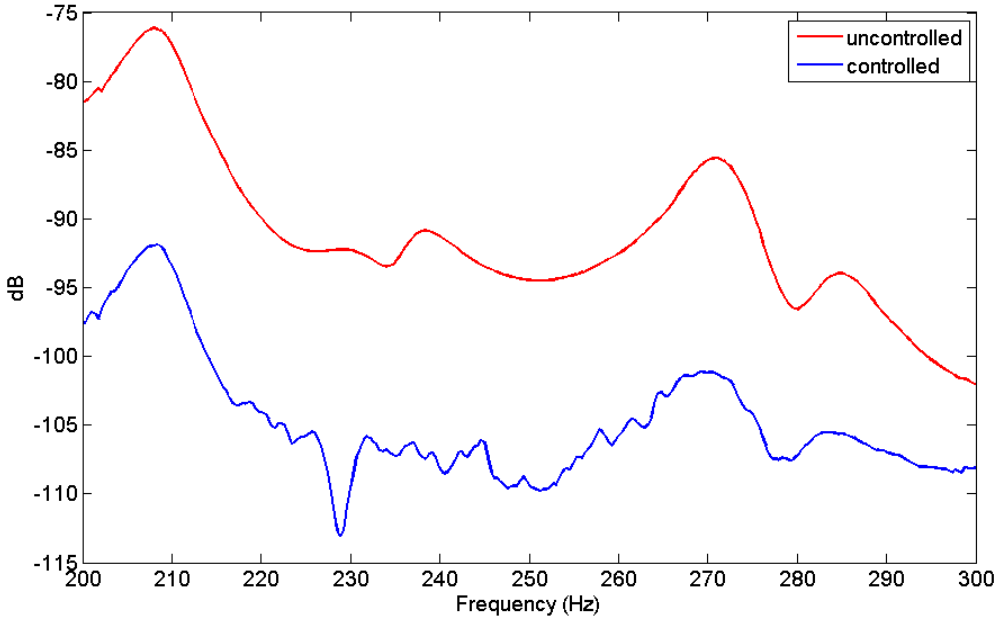

Figure 7.67. Frequency responses to the sine sweep disturbance at accelerometer 5

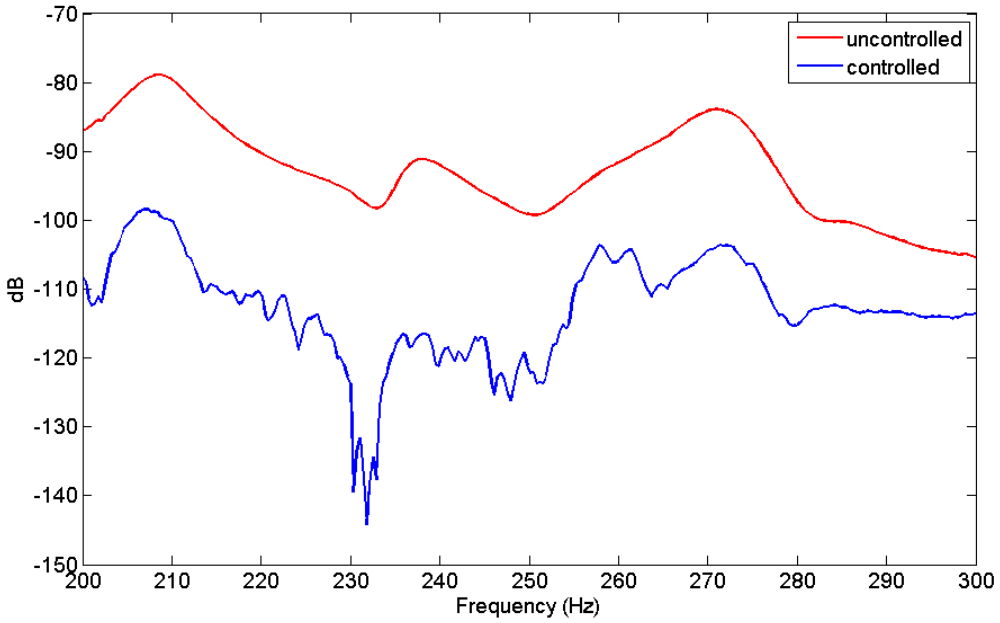

Figure 7.68. Frequency responses to the sine sweep disturbance at accelerometer 6

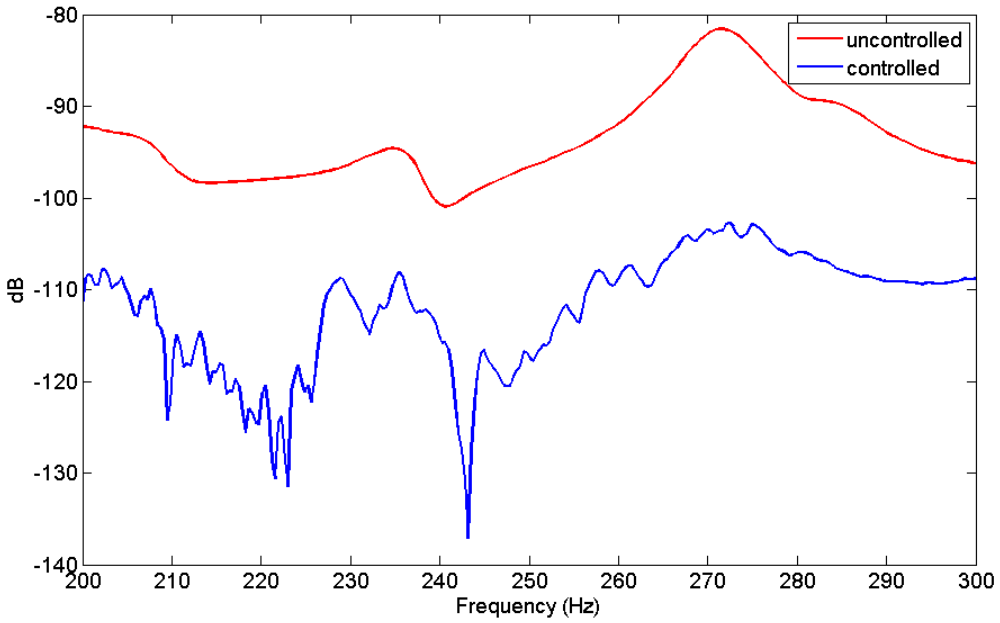

Figure 7.69. Frequency responses to the sine sweep disturbance at accelerometer 7

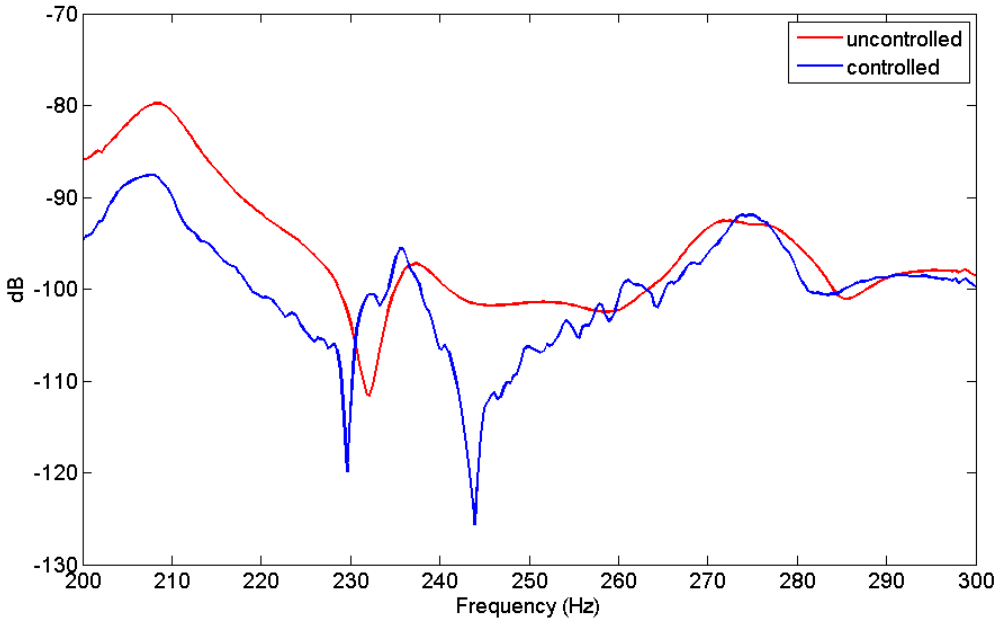

Figure 7.70. Frequency responses to the sine sweep disturbance at accelerometer 8

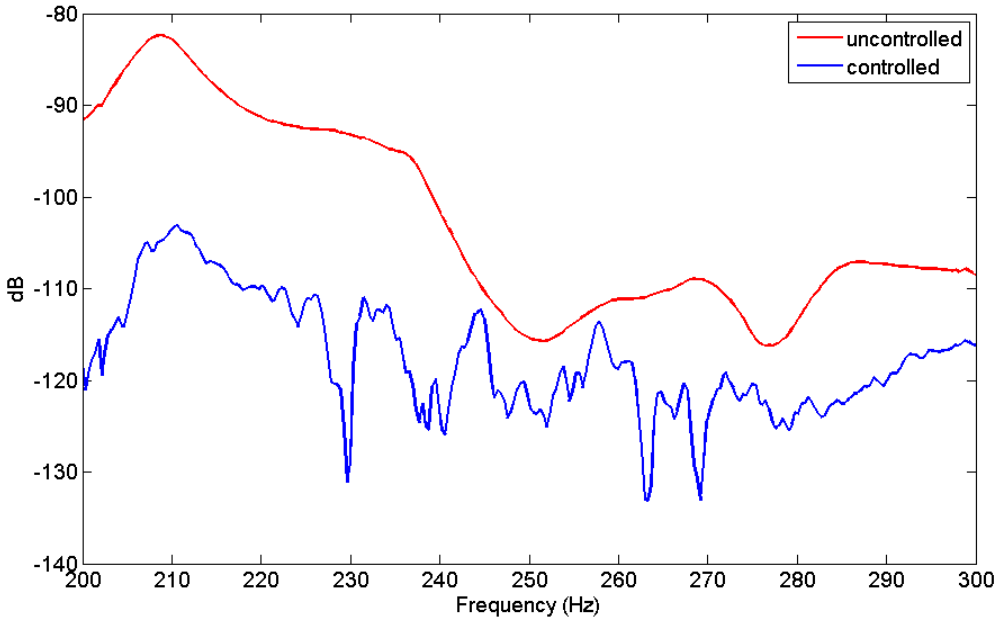

Figure 7.71. Frequency responses to the sine sweep disturbance at accelerometer 9

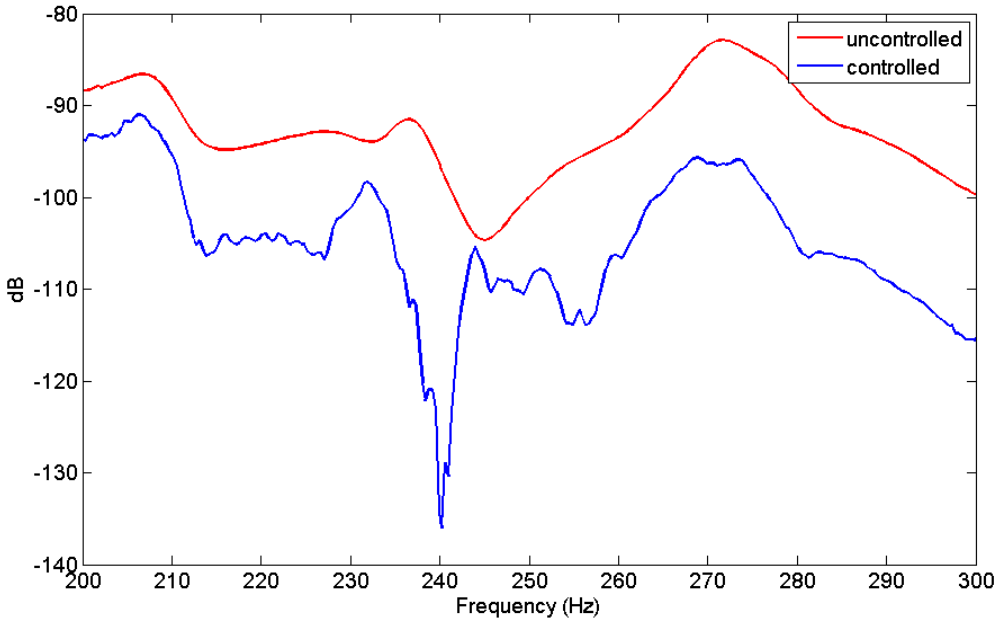

Figure 7.72. Frequency responses to the sine sweep disturbance at accelerometer 10

7.7. Summary

To evaluate the applicability of orthogonal eigenstructure control as an active vibration cancellation method, a test setup was used. The test plate is a steel plate clamped along all edges. An electromagnetic actuator was used as the source of disturbance and two piezoelectric actuators were used for control purposes. A thorough evaluation of the functionality of the test plate was conducted to find the appropriate location of the control actuators based on the mode shapes of the plate. Frequency range of 200-300 Hz was chosen for vibration cancellation of tonal as well as wideband disturbance. Tonal disturbances of 250 Hz and 207 Hz frequencies that coincide with the natural frequencies of the plate were used and the vibration reductions due to orthogonal eigenstructure control were evaluated. Since orthogonal eigenstructure control is a model based control method, state space models of the test setup was estimated at each of the two tonal frequencies. These vibration reductions were noted in the vicinity of the piezoelectric actuators. It was also shown that the control gain determined for tonal disturbance at 250 Hz is able to control the tonal disturbance at 207 Hz. A sine sweep signal was used as a wideband disturbance signal. Large reductions in frequency response at all the

accelerometers occurred. Because of the effect of natural frequency at 277 Hz, vibration cancellation was limited to the range of 200-260 Hz. When the control gain matrix was multiplied by 2, the control of vibration was achieved in almost entire 200-300 Hz frequency range.

Chapter 8

Conclusions

A novel control method, namely orthogonal eigenstructure control, for vibration cancellation in structures was developed. This method is a feedback control method applicable to multiple-input multiple-output linear systems. This control method can automatically determine the feedback control law with minimal experience of controller designer. This new structural vibration control method is able to perform robustly in the presence of a wide variety of disturbances, while significantly reduces the controller development cycle through a mathematically sound approach that can easily be implemented to a broad range of structures in practice.

Orthogonal eigenstructure control eliminates the need for defining the desirable eigenvectors and eigenvalues of the closed-loop system, which are usually needed by other eigenstructure assignment methods. This significantly reduces the amount of time needed for developing a new controller for structural control. Orthogonal eigenstructure control is able to suggest a set of closed-loop systems. For open-loop eigenvectors associated with the operating eigenvalues, this method finds orthogonal vectors within the achievable eigenvector set and substitute them as the associated open-loop eigenvectors. The controller designer can easily determine the most desirable solution by assessing the performance of the results of a number of closed-loop systems for all possible systems. Progressive application of orthogonal eigenstructure control makes the set of suggested closed-loop systems unbounded.

Proper use of design freedom is depended on the experience controller designer. Improper use of this design freedom may cause excessive actuation forces. Orthogonal eigenstructure control reduces those design freedoms that are depended on the designer experience. It limits the design freedom to vectors orthogonal to the eigenvectors of the

system and lets the controller designer to substitute the eigenvectors with vectors that are almost orthogonal to them. Progressive orthogonal eigenstructure control gives an infinite design freedom in more efficient directions.

To address a fail-safe design of a control law in case of components failure, the method is also extended to be applicable to the system with non-collocated actuators and sensors, as well as systems that do not have equal number of actuator and sensors. This makes the control method more readily applicable to real life applications, by better dealing with limitations that happen in case of components failure.

A finite element model of a steel plate was used as an example of a system with large degrees of freedom. It was shown through simulation that application of orthogonal eigenstructure control for vibration cancellation in such systems is relatively straightforward. Also, it was shown that the operating eigenvalues have an important role on the resulting control gains, based on their magnitude. Operating eigenvalues with negative real part farthest from the origin yield more closed-loop systems, for which the stable closed-loop systems converge, because of convergence of their control gain matrices. Large operating eigenvalues lead to decoupled control channels since gain matrices have diagonal elements that are several orders of magnitude larger than the off-diagonal elements. Additionally, it was shown that the controller is robust to the actuators' failure, if the operating eigenvalues are sufficiently large.

A test setup was used to evaluate the application of orthogonal eigenstructure control for active vibration cancellation of a steel plate. Based on the characteristics of the test plate the range of frequency of 200-300 Hz was considered as the frequency range of the interest. The system identification method that has been used is able to identify the system locally in such a way that the response of the identified model to a tonal disturbance and the collected data from the experiment to similar disturbance becomes identical. A thorough investigation was performed using tonal disturbances with frequencies within the range of 200-300 Hz. The control gains for each experiment were found using orthogonal eigenstructure control. It was shown that there is a similarity

between the results for experiment and the simulation of the control through a finite element model of a plate. The actuators choke the vibrational energy and stop them from transferring other areas of the structure. The area close to the disturbance source and in the vicinity of the actuators showed largest confinement of the vibrational energy. The results of the experiments with tonal disturbances showed that the control gain associated with the tonal disturbance 250 Hz is able to cancel vibrations induced by tonal disturbances with different frequencies. Also, the vibration induced by a wideband sine sweep disturbance with frequency range of 200-300 Hz was significantly reduced using this control gain.

8.1. Contribution outlines of this work

The contribution outlines through this research work follows:

1- Orthogonal eigenstructure control as a novel control method for multiple-input multiple-output linear systems is developed that can perform robustly in the presence of a variety of disturbances

2- Orthogonal eigenstructure control provides a significant simplification of the design task while still allowing some experience-based design freedom

3- The control method reduces the design freedom to vectors orthogonal to the eigenvectors of the system and lets the controller designer to substitute the eigenvectors with them in an automatic manner

4- The progressive application of orthogonal eigenstructure control provides an unbounded design freedom in more efficient direction

5- Orthogonal eigenstructure control is extended to be applicable to systems with non-collocated actuators and sensors or different number of sensors and actuators to address the practical issue of components failure

6- This control method can be used as a general control method beyond active vibration control

8.2. Recommendation for future research

In this work, orthogonal eigenstructure control was introduced. Then, it was validated through experiments. The recommendations for the future theoretical improvements and experimental work follows:

1- Based on the number of actuators and sensors, there is a set of closed-loop systems. If orthogonal eigenstructure control is applied progressively, there would be a new set of possible closed-loop systems. The method of determining which closed-loop system is the most desirable one is based on examining the time responses to have minimum standard deviation. A thorough study should be performed to address this issue by finding systematic ways for identifying the most desirable closed-loop system.

2- For both simulation problems and experimental work, the real part of the control gain was used. The effect of imaginary part of control gain matrix need to be studied.

3- The concept of virtual actuators and sensors for extending the applicability of orthogonal eigenstructure control was introduced. This concept may be used for identifying the desirable locations for actuators and sensors.

4- Operating eigenvalues have a major role in finding the set of closed-loop systems. It is shown that they are not required to be the open-loop eigenvalues. The permitted area for choosing the operating eigenvalues on the s-plane should be identified and the possible relationship of this region to the dynamics of the system need to be investigated.

5- A more rigorous system identification algorithm may be used for experimental work that works accurately capable of identifying a system within a frequency range.

6- Different control actuators that are easy to maintain and have longer life should be examined in experimental work. This can address the issues such as cost of the amplifiers, ability to move an actuator, and actuator noise.

References:

1. D'Azzo, J.J. and C.H. Houpis, *Linear Control system Analysis and Design: Conventional and Modern*. 4th ed. 1995: McGraw-Hill, Inc.
2. Moore, B.C., *On the Flexibility Offered by State Feedback in Multivariable Systems Beyond Closed Loop Eigenvalue Assignment.* IEEE Transactions on Automatic Control, 1976: p. 689-692.
3. Wonham, W., *On pole assignment in multi-input controllable linear systems.* IEEE Transactions on Automatic Control, 1967. **12**(6): p. 660- 665.
4. Klein, G. and B.C. Moore, *Eigenvalue-Generalized Eigenvector Assignment with State Feedback.* IEEE Transaction on Automatic Control, 1977. **22**(1): p. 140-141.
5. Srinathkumar, S., *Eigenvalue/eigenvector Assignment Using Output feedback.* IEEE Transactions on Automatic Control, 1978. **23**(1): p. 79-81.
6. Fahmy, M.M. and J. O'Reilly, *On Eigenstructure Assignment in Linear Multivariable Systems.* IEEE Transactions on Automatic Control, 1982. **AC-27**(3): p. 690-693.
7. Fahmy, M.M. and J. Oreilly, *Eigenstructure Assignment in Linear Multivariable Systems - A Parametric Solution.* IEEE Transactions on Automatic Control, 1983. **AC-28**(10): p. 990-994.
8. Andry, A.N., E.Y. Shapiro, and J.C. Chung, *Eigenstructure Assignment for Linear Systems.* IEEE Transaction on Aerospace and Electronic Systems, 1983. **19**(5): p. 711-728.
9. Calvo-Ramon, J.R., *Eigenstructure Assignment by Output Feedback and Residue Analysis.* Transaction on Automatic Control, 1986. **AC-31**(3): p. 247-249.
10. Cunningham, T.B. *Eigenspace Selection Procedures for Closed Loop Response Shaping with Modal Control*. in *Proc. of the 19th IEEE Conference on Decision and Control*. 1980. Albuquerque, New Mexico.
11. Choura, S. and A.S. Yigit, *Confinement and Suppression of Structural Vibrations.* Transactions of the ASME, 2001. **123**: p. 496-501.
12. Bendiksen, O.O., *Mode Localization Phenomena in Large Space Structures.* AIAA Journal, 1987. **25**(9): p. 1241-1248.
13. Hodges, C.H. and J. Woodhouse, *Confinement of vibration by structural irregularity*. Journal of the Acoustical Society of America 1981. **69**(1).
14. Shelley, F.J. and W.W. Clark. *Closed-Loop Mode Localization for Vibration Control in Flexible Structures*. in *American Control Conference*. 1994. Baltimore, Maryland.
15. Pierre, C. and P.D. Cha, *Strong Mode Localization in Nearly Periodic Disordered Structures.* AIAA Journal, 1989. **27**(2): p. 227-241.

16. Shelley, F.J. and W.W. Clark, *Experimental Application of Feedback Control to Localize Vibration.* Journal of Vibration and Acoustics, 2000. **122**: p. 143-150.

17. Song, B. and S. Jayasuriya. *Active vibration control using Eigenvector assignment for mode localization*. in *American Control Conference*. 1993. San Francisco, California.

18. Kwon, B. and M. Youn, *Eigenvalue-Generalized Eigenvector Assignment by Output Feedback.* IEEE Transactions on Automatic Control, 1987. **Ac-32**(5): p. 417-421.

19. Mudge, S.K. and R.J. Patton. *Analysis of the technique of robust eigenstructure assignment with application to aircraft control*. in *IEE*. 1988.

20. Mimins, G., *A Stepwise Approach for the Generalized Eigenstructure Assignment Problem.* SIAM J. Matrix Anal. Appl., 2000. **22**(3): p. 912–924.

21. Choi, J.W. and U.S. Park, *Spillover Suppression via Eigenstructure Assignment in Large Flexible Structures* Journal of Guidance, Control, and Dynamics 2002. **25**(3): p. 599-602.

22. Rew, D.W., J.L. Junkins, and J.N. Juang, *Robust Eigenstructure Assignment by a Projection Method: Applications Using Multiple Optimization Criteria.* J. Guidance, 1989. **12**(3): p. 396-403.

23. Sen, S. and K.B. Datta, *Eigenstructure assignment in high-gain feedback Systems.* IEE Proc. Control Theory Appl., 1991. **138**(2): p. 165-171.

24. Juang, J.-N., K.B. Lim, and J.L. Junkins, *Robust Eigensystem Assignment for Flexible Structures.* Journal of Guidance, 1989. **12**(3): p. 381-387.

25. Liu, G.P. and R.J. Patton. *Parametric State Feedback Design of Multivariable Control Systems Using Eigenstructure Assignment*. in *32nd Conference on Decision and Control*. 1993. San Antonio, Texas.

26. Maghami, P.G., S. Gupta, and S.M. Joshi. *Design of Dissipative Low-Authority Controllers Using an Eigensystem Assignment Technique*. in *American Control Conference*. 1992.

27. Maghami, P.G. and S. Gupta. *On Eigensystem assignment with dissipativity Constraints*. in *American Control Conference*. 1993. San Francisco, California.

28. Maghami, P.G., J.-N. Juang, and K.B. Lim, *On Eigensystem Assignment with Output Feedback.* AIAA 89-3608-CP, 1989.

29. Juang, J.-N. and P.G. Maghami, *Robust Eigensystem Assignment for State Estimators Using Second-Order Models.* Journal of Guidance, Control, and Dynamics, 1992. **15**(4): p. 920-927.

30. Juang, J.-N. and P.G. Maghami. *Robust Eigensystem Assignment for Second-Order Dynamic Systems*. in *AIAA Dynamics Specialists Conference*. 1990. Long Beach, California.

31. Datta, B.N., et al., *Partial Eigenstructure Assignment for the Quadratic Pencil* Journal of Sound and Vibration, 2000. **230**(1): p. 101-110.

32. Keel, L.H., K.B. Lim, and J.-N. Juang, *Robust Eigenvalue Assignment with Maximum Tolerance to System Uncertainties.* Journal of Guidance, 1991. **14**(3): p. 615-620.

33. Schulz, M.J. and D.J. Inman, *Eigenstructure Assignment and Controller Optimization for Mechanical Systems.* IEEE Transaction on Control Systems Technology, 1994. **2**(2): p. 88-100.

34. Shelley, F.J. and W.W. Clark, *Eigenvector Scaling for Mode Localization in Vibrating Systems.* Journal of Guidance, Control, and Dynamics, 1996. **19**(6): p. 1342-1348.

35. Clark, W.W. and F.J. Shelley. *Experiments in Eigenstructure Assignment for Active Mode Localization in A Flexible Beam*. in *American Control Conference*. 1997. Albuquerque, New Mexico.

36. Corr, L.R. and W.W. Clark, *Vibration Confinement Using Piezoelectric Transducers and Eigenstructure Placement.* AIAA-99-1552, 1999.

37. Corr, L.R. and W.W. Clark. *Active and Passive Vibration Confinement using Piezoelectric Transducers and Dynamic Vibration Absorbers*. in *SPIE Conference on Smart Structures and Integrated Systems*. 1999. Newport Beach, California.

38. Shelley, F.J. and W.W. Clark, *Active Mode Localization in Distributed Parameter Systems with Consideration of Limited Actuator Placement, Part 2: Simulations and Experiments.* Journal of Vibration and Acoustics, 2000. **122**: p. 165-168.

39. Tang, J. and K.W. Wang. *A Simultaneous Active-Passive Approach for Structural Vibration Confinement Using Piezoelectric Actuators*. in *44th AIAA/ASME/ ASCE/AHS Structures, Structural Dynamics, and Materials Conferences*. 2003. Norfolk, Virginia.

40. Tang, J. and K.W. Wang, *Vibration Confinement via Optimal Eigenvector Assignment and Piezoelectric Networks.* Journal of Vibration and Acoustics, 2004. **126**: p. 27-36.

41. Wu, T.Y. and K.W. Wang. *Vibration Isolator Design via Energy Confinement through Eigenvector Assignment and Piezoelectric Networking*. in *SPIE, Smart Structures and Materials: Damping and Isolation*. 2004.

42. Choura, S.A. and A.S. Yigit, *Vibration confinement in flexible structures by distributed feedback.* Computers & Structures, 1995. **54**(3): p. 531-540.

43. Yigit, A.S. and S. Choura, *Vibration confinement in flexible structures via alteration of mode shapes by using feedback.* Journal of Sound and Vibration, 1995. **179**(4): p. 553-567.

44. Choura, S., S. EL-Borgi, and A.H. Nayfeh, *Axial Vibration Confinement in Nonhomogenous Rods.* Shock and Vibration, 2005. **12**: p. 177–195.

45. Choura, S. and A.S. Yigit, *Active Control of Linear Time-Varying Structures by Confinement of Vibrations.* Journal of Vibration and Control, 2005. **11**: p. 89–102.

46. Slater, G.L. and Q. Zhang, *Controller Design by Eigenspace Assignment.* AIAA-90-1193-CP, 1990: p. 19-31.

47. Sobel, K.M., S. Banda, and H.H. Yeh. *Structured state space robustness with connection to eigenstructure assignment*. in *American Control Conference*. 1989. Pittsburgh, PA.

48. Yu, W. and K.M. Sobel, *Robust Eigenstructure Assignment with Structured State Space Uncertainty*. J. Guidance, 1991. **14**(3): p. 621-628.

49. Wilson, R.F., J.R. Cloutier, and R.K. Yedavalli. *Control Design for Robust Eigenstructure Assignment in Linear Uncertain Systems*. in *Proc. of Conference on Decision and Control, IEEE Control Systems*. 1992. UK.

50. Wilson, R.F., J.R. Cloutier, and R.K. Yedavalli, *Lyapunov Constrained Eigenstructure Assignment for the Design of the Robust Mode –Decoupled Roll-Yaw Missile Autopilots.* IEEE Transaction on Aerospace and Electronic Systems, 1992: p. 994-999.

51. Patton, R.J. and G.P. Liu. *Robust Control Design Via Eigenstructure Assignment, Genetic Algorithms And Gradient-Based Optimization*. in *IEE Control Theory Appl*. 1994.

52. Triller, M.J. and D.C. Kammer, *Improved Eigenstructure Assignment Controller Design Using a Substructure-Based Coordinate System.* Journal of Guidance, Control, and Dynamics, 1997. **20**(5): p. 941-948.

53. Maghami, P.G. and S. Gupta, *Design of Constant Gain Dissipative Controllers for Eigensystem Assignment in Passive Systems.* Journal of Guidance, Control, and Dynamics, 1997. **20**(4): p. 648-657.

54. Liu, G.P. and R.J. Patton. *Robust Control Design of Descriptor Systems Using Eigenstructure Assignment*. in *UKACC International Conference on Control*. 1998.

55. Liu, G.P. and R.J. Patton, *Robust Eigenstructure Assignment Combining Time- And Frequency-Domain Performance Specifications.* International Journal of Robust and Nonlinear Control, 1998. **8**: p. 61-78.

56. Liu, G.P., G.R. Duan, and R.J. Patton. *Mixed Time- And Frequency-Domain Robust Eigenstructure Assignment*. in *International Journal of Systems Science*. 2000.

57. Duan, G., *Eigenstructure Assignment and Response Analysis in Descriptor Linear Systems with State Feedback Control.* Int. J. Control, 1999. **69**(5): p. 663-694.

58. Duan, G. and R.J. Patton, *Robust Pole Assignment in Descriptor Systems via Proportional Plus Partial Derivative State Feedback.* Int. J. Control, 1999. **72**(13): p. 1193-1203.

59. Cawood, M.E. and C.L. Cox, *Perturbation Analysis For Eigenstructure Assignment Of Linear Multi-Input Systems.* Electronic Transactions On Numerical Analysis, Kent State University, 2000. **11**: p. 25-42.

60. Duan, G. *Parametric Eigenstructure Assignment via State Feedback a Simple Numerically Reliable Approach*. in *Proc. of the 4th World Congress on Intelligent Control and Automation*. 2002. Shanghai, China.

61. Duan, G. *Parametric Eigenstructure Assignment via Output Feedback Based on Singular Value Decompositions*. in *IEE Proc. Control Theory Appl.* 2003.

62. Duan, G. and G. Liu, *Complete Parametric Approach For Eigenstructure Assignment In A Class Of Second-Order Linear Systems.* Automatica, 2002. **38**: p. 725–729.

63. Duan, G., *Parametric Eigenstructure Assignment in Second-Order Descriptor Linear Systems.* IEEE Transactions on Automatic Control, 2004. **49**(10): p. 1789-1795.

64. Duan, G., *Parametric Approaches for Eigenstructure Assignment in High-order Linear Systems.* International Journal of Control, Automation, and Systems, 2005. **3**(3): p. 419-429.

65. Duan, G. *Parametric Approaches for Eigenstructure Assignment in High-order Descriptor Linear Systems*. in *Proc. of the 44th IEEE Conference on Decision and Control, and the European Control Conference*. 2005. Seville, Spain.

66. Duan, G., *Unified Parametric Approaches for Observer Design in Matrix Second-order Linear Systems.* International Journal of Control, Automation, and Systems, 2005. **3**(2): p. 159-165.

67. Duan, G. *Solution to High-order Generalized Sylvester Matrix Equations*. in *Proc. of the 44th IEEE Conference on Decision and Control, and the European Control Conference*. 2005. Seville, Spain.

68. Clarke, T., S.J. Griffin, and J. Ensor, *Output feedback eigenstructure assignment using a new reduced orthogonality condition.* International Journal of Control 2003. **76**(4).

69. Duan, G., *Robust Eigenstructure Assignment via Dynamical Compensators.* Automatica, 1993. **29**(2): p. 469-474.

70. Duan, G. and D. Howe, *Solutions of the Equation AV + BW = W and Their Application to Eigenstructure Assignment in Linear Systems.* IEEE Transactions on Automatic Control, 1993. **38**(2): p. 276-280.

71. Duan, G.R., *Solution to matrix equation AV + BW = EVF and eigenstructure assignment for descriptor systems.* Automatica, 1992. **28**(3): p. 639-642.

72. Duan, G., *Eigenstructure Assignment by Decentralized Output Feedback-A Complete Parametric Approach.* IEEE Transactions on Automatic Control, 1994. **39**(5): p. 1009-1114.

73. Duan, G. *Parametric Approach for Eigenstructure Assignment in Descriptor Systems via Output Feedback*. in *IEE Proc. Control Theory Appl*. 1995.

74. Duan, G., *On the Solution to the Sylvester Matrix Equation AV + BW = EVF*. IEEE Transactions on Automatic Control, 1996. **41**(4): p. 612-614.

75. Duan, G. and R.J. Patton, *Eigenstructure Assignment in Descriptor Systems via Proportional Plus Derivative State Feedback.* Int. J. Control, 1997. **68**(5): p. 1147-1162.

76. Syrmos, V.L. and F.L. Lewis, *Output Feedback Eigenstructure Assignment Using Two Sylvester Equations.* IEEE Transactions on Automatic Control, 1993. **38**(3): p. 495-499.

77. Bottura, C.P. and J.V.d.F. Neto. *Parallel Eigenstructure Assignment via LQR Design and Genetic Algorithms*. in *Proc. of the American Control Conference*. 1999. San Diego, California.

78. Neto, J.V.d.F. and C.P. Bottura. *An Inequalities Method for Multivariable System's Eigenstructure Assignment via Genetic Multi-Objective Optimization*. in *American Control Conference*. 2003. Denver, Colorado.

79. Choi, J.W., et al., *Design of an Effective Controller via Disturbance Accommodating Left Eigenstructure Assignment.* Journal of Guidance, Control, and Dynamics, 1995. **18**(2): p. 347-354.

80. Choi, J.W., *A Simultaneous Assignment Methodology of Right/Left Eigenstructures.* IEEE Transaction on Aerospace and Electronic Systems, 1998. **34**(2): p. 625-634.

81. Shelley, F.J. and W.W. Clark, *Active Mode Localization in Distributed Parameter Systems with Consideration of Limited Actuator Placement, Part 1: Theory*. Journal of Vibration and Acoustics, 2000. **122**: p. 160-164.

82. Golub, G.H. and C.F.V. Loan, *Matrix Computations*. Third ed. 1996: The Johns Hopkins University Press.

83. Hartley, R. and A. Zeisserman, *Multiple View Geometry in Computer Vision*. 2003, Cambridge, UK: Cambridge University Press.

84. Rastgaar, M.A., M. Ahmadian, and S.C. Southward. *Vibration Confinement by Minimum Modal Energy Eigenstructure Assignment. ASME International Design Engineering Technical Conferences, IDETC/CIE 2007*. 2007. Las Vegas, Nevada, USA.

85. Weaver, W. and P.R. Johnston, *Structural Dynamics by Finite Element*. 1987: Prentice-Hall.

86. Jeric, K.M., *An Experimental Evaluation of the Application of Smart Damping Materials for Reducing Structural Noise and Vibrations*, in *Mechanical Engineering*. 1999, Virginia Tech: Blacksburg.

87. Ljung, L., *System Identification: Theory for the User*. 1987, Englewood Cliffs, NJ: Prentice-Hall.

Vita

Mohammad Rastgaar Aagaah was born in Rasht, Iran. He earned his BS degree in mechanical engineering, majored in mechanical design, from Sharif University of Technology in 1995. He received his MS degree in mechanical engineering, majored in solid mechanics, from Tehran Polytechnic in 1998. He held several positions as research engineer, design engineer, and lecturer during 1997 to 2002 in Iran. Then, he moved to the United States to continue his higher education. He received his second master's degree in mechanical engineering form North Dakota State University, working on microfluidics, MEMS, and Nanotechnology. He started his PhD studies at Virginia Tech and joined Center for Vehicle Systems & Safety in July 2005. He earned his PhD on July 2008, working on active vibration cancellation. Publication of more than 10 journal papers and more than 20 conference papers are amongst his accomplishments.